WVMP SAR Reference 3-10

Melter Spout_062614.rad, C. Brandjes, Brandjes, Ameriphysics, LLC, Knoxville, Tennessee, June 26, 2014.

Isotope	Ci	Gm	TBq
C-14	2.217E-03	4.949E-04	8.201E-05
K-40	8.600E-03	1.216E+03	3.182E-04
Mn-54	4.997E-07	6.443E-11	1.849E-08
Co-60	5.467E-03	4.831E-06	2.023E-04
Ni-63	9.799E-02	1.735E-03	3.626E-03
Sr-90	6.332E+01	4.584E-01	2.343E+00
Y-90	6.333E+01	1.165E-04	2.343E+00
Zr-95	3.172E-22	1.476E-26	1.174E-23
Nb-95	6.994E-22	1.779E-26	2.588E-23
Nb-95m	3.631E-24	9.524E-30	1.344E-25
Tc-99	1.570E-02	9.295E-01	5.809E-04
Cs-137	8.566E+02	9.854E+00	3.169E+01
Ba-137m	8.086E+02	1.503E-06	2.992E+01
Eu-154	1.043E-01	3.857E-04	3.858E-03
Hg-206	7.135E-16	6.370E-24	2.640E-17
Tl-206	5.014E-14	2.308E-22	1.855E-15
Tl-207	1.863E-09	9.781E-18	6.893E-11
Tl-208	1.733E-03	5.852E-12	6.412E-05
Tl-209	5.578E-08	1.364E-16	2.064E-09
Tl-210	4.495E-11	6.527E-20	1.663E-12
Pb-209	2.582E-06	5.602E-13	9.555E-08
Pb-210	3.755E-08	4.888E-10	1.390E-09
Pb-211	1.868E-09	7.567E-17	6.911E-11
Pb-212	4.823E-03	3.471E-09	1.785E-04
Pb-214	2.140E-07	6.528E-15	7.919E-09
Bi-209	5.969E-25	6.629E-09	2.208E-26
Bi-210	3.745E-08	3.018E-13	1.385E-09
Bi-211	1.868E-09	4.548E-18	6.911E-11
Bi-212	4.823E-03	3.292E-10	1.785E-04
Bi-213	2.582E-06	1.334E-13	9.554E-08
Bi-214	2.141E-07	4.848E-15	7.921E-09
Bi-215	1.527E-15	1.292E-23	5.648E-17
Po-210	3.454E-08	7.686E-12	1.278E-09
Po-211	5.099E-12	4.921E-23	1.887E-13
Po-212	3.089E-03	1.730E-20	1.143E-04
Po-213	2.527E-06	2.004E-22	9.349E-08
Po-214	2.140E-07	6.646E-22	7.919E-09
Po-215	1.868E-09	6.337E-23	6.911E-11
Po-216	4.823E-03	1.385E-14	1.784E-04
Po-218	2.141E-07	7.689E-16	7.921E-09
At-215	7.472E-15	1.424E-29	2.765E-16
At-217	2.583E-06	1.605E-18	9.555E-08
At-218	4.067E-11	1.179E-21	1.505E-12
At-219	1.574E-15	1.650E-24	5.823E-17
Rn-217	3.099E-10	3.219E-24	1.147E-11
Rn-218	4.067E-14	2.751E-26	1.505E-15
Rn-219	1.868E-09	1.436E-19	6.911E-11
Rn-220	4.823E-03	5.248E-12	1.784E-04
Rn-222	2.141E-07	1.392E-12	7.921E-09

Fr-221	2.583E-06	1.487E-14	9.555E-08
Fr-223	2.623E-11	6.782E-19	9.705E-13
Ra-223	1.868E-09	3.647E-14	6.911E-11
Ra-224	4.823E-03	3.012E-08	1.784E-04
Ra-225	2.591E-06	6.607E-11	9.585E-08
Ra-226	2.143E-07	2.168E-07	7.930E-09
Ra-228	3.409E-05	1.250E-07	1.261E-06
Ac-225	2.583E-06	4.451E-11	9.555E-08
Ac-227	1.901E-09	2.628E-11	7.033E-11
Ac-228	3.409E-05	1.525E-11	1.261E-06
Th-227	1.854E-09	6.035E-14	6.861E-11
Th-228	4.822E-03	5.883E-06	1.784E-04
Th-229	2.602E-06	1.224E-05	9.629E-08
Th-230	3.892E-05	1.888E-03	1.440E-06
Th-231	3.950E-05	7.432E-11	1.462E-06
Th-232	4.340E-05	3.958E+02	1.606E-06
Th-234	2.410E-04	1.041E-08	8.917E-06
Pa-231	1.066E-08	2.258E-07	3.946E-10
Pa-233	7.086E-04	3.414E-08	2.622E-05
Pa-234	3.615E-07	1.830E-13	1.337E-08
Pa-234m	2.410E-04	3.510E-13	8.917E-06
U-232	4.660E-03	2.111E-04	1.724E-04
U-233	2.160E-03	2.242E-01	7.992E-05
U-234	1.034E-03	1.664E-01	3.827E-05
U-235	3.950E-05	1.828E+01	1.462E-06
U-235m	3.007E-02	9.774E-10	1.113E-03
U-236	1.190E-04	1.862E+00	4.403E-06
U-237	4.556E-06	5.583E-11	1.686E-07
U-238	2.410E-04	7.170E+02	8.917E-06
Np-237	7.086E-04	1.005E+00	2.622E-05
Np-239	4.545E-03	1.959E-08	1.681E-04
Pu-238	1.139E-01	6.653E-03	4.215E-03
Pu-239	3.009E-02	4.852E-01	1.113E-03
Pu-240	2.294E-02	1.011E-01	8.488E-04
Pu-241	1.850E-01	1.787E-03	6.844E-03
Am-241	3.804E-01	1.110E-01	1.408E-02
Am-243	4.545E-03	2.276E-02	1.681E-04
Cm-242	1.047E-11	3.164E-15	3.876E-13
Cm-243	1.854E-03	3.781E-05	6.860E-05
Cm-244	4.067E-02	4.998E-04	1.505E-03

WVMP SAR Reference 3-11

"Nuclear Decay Data for Dosimetric Calculations," Ann. ICRP, 38(3), 1-96, 2008, ICRP Paper 107, International Commission on Radiation Protection.

Annex A. Radionuclides of the ICRP-07 Collection

ANNEX A. RADIONUCLIDES OF THE ICRP-07 COLLECTION

(A1) The 1252 radionuclides of the ICRP-07 collection are listed in Table A.1 in order of atomic number. Indented on the line following the radionuclide is the identity of the daughter nuclide formed by the nuclear transformation (nt) of the parent, along with the fraction of the parent's transformation creating the daughter. If the daughter nucleus is stable then it is shown in italics. The half-life, decay mode, and energy emitted per nuclear transformation are also shown.

(A2) The units of the half-life are abbreviated as: μs - microsecond, ms - millisecond, s - second, m - minute, d - day, and y - year. The decay modes are abbreviated as: A - alpha, B– - beta minue, B+ - beta minus, EC - electron capture, IT - isomeric transition, SF-spontaneous fission. The contribution of fission fragments and neutrons associated with spontaneous fission are included in the total energy.

Table A.1 Properties of the radionuclides of the ICRP-07 collection.

					Emitted energy (MeV/nt)			
Z	Element	Nuclide	Half-life	Decay mode	Alpha	Electron	Photon	Total
1	Hydrogen	H-3	12.32 y	B-	–	0.005	–	0.0057
			He-3	1.00				
4	Beryllium	Be-7	53.22 d	EC	–	<E-04	0.0499	0.0499
			Li-7	1.00				
		Be-10	1.51E+6 y	B-	–	0.2525	–	0.2525
			B-10	1.00				
6	Carbon	C-10	19.255 s	ECB+	–	0.8087	1.7443	2.5531
			B-10	1.00				
		C-11	20.39 m	ECB+	–	0.3847	1.0196	1.4043
			B-11	1.00				
		C-14	5.70E+3 y	B-	–	0.0495	–	0.0495
			N-14	1.00				
7	Nitrogen	N-13	9.965 m	ECB+	–	0.4909	1.0200	1.5109
			C-13	1.00				
		N-16	7.13 s	B-	–	2.7646	4.4932	7.2579
			O-16	1.00				
8	Oxygen	O-14	70.606 s	ECB+	–	0.7763	3.3201	4.0965
			N-14	1.00				
		O-15	122.24 s	ECB+	–	0.7347	1.0210	1.7557
			N-15	1.00				
		O-19	26.464 s	B-	–	1.7608	0.9397	2.7006
			F-19	1.00				
9	Fluorine	F-17	64.49 s	ECB+	–	0.7385	1.0208	1.7593
			O-17	1.00				
		F-18	109.77 m	ECB+	–	0.2416	0.9886	1.2302
			O-18	1.00				
10	Neon	Ne-19	17.22 s	ECB+	–	0.9624	1.0210	1.9834
			F-19	1.00				
		Ne-24	3.38 m	B-	–	0.8035	0.5419	1.3455
			Na-24	1.00				

Table A.1 continued

Z	Element	Nuclide	Half-life	Decay mode	Emitted energy (MeV/nt)			
					Alpha	Electron	Photon	Total
11	Sodium	Na-22	2.6019 y	ECB+	–	0.1941	2.1926	2.3866
			Ne-22	1.00				
		Na-24	14.9590 h	B-	–	0.5538	4.1232	4.6770
			Mg-24	1.00				
12	Magnesium	Mg-27	9.458 m	B-	–	0.7021	0.8912	1.5933
			Al-27	1.00				
		Mg-28	20.915 h	B-	–	0.1610	1.3700	1.5310
			Al-28	1.00				
13	Aluminium	Al-26	7.17E+5 y	ECB+	–	0.4444	2.6751	3.1195
			Mg-26	1.00				
		Al-28	2.2414 m	B-	–	1.2417	1.7789	3.0205
			Si-28	1.00				
		Al-29	6.56 m	B-	–	0.9764	1.3794	2.3558
			Si-29	1.00				
14	Silicon	Si-31	157.3 m	B-	–	0.5949	0.0009	0.5957
			P-31	1.00				
		Si-32	132 y	B-	–	0.0686	–	0.0686
			P-32	1.00				
15	Phosphorus	P-30	2.498 m	ECB+	–	1.4389	1.0222	2.4610
			Si-30	1.00				
		P-32	14.263 d	B-	–	0.6948	–	0.6948
			S-32	1.00				
		P-33	25.34 d	B-	–	0.0764	–	0.0764
			S-33	1.00				
16	Sulphur	S-35	87.51 d	B-	–	0.0487	–	0.0487
			Cl-35	1.00				
		S-37	5.05 m	B-	–	0.7998	2.9311	3.7309
			Cl-37	1.00				
		S-38	170.3 m	B-	–	0.4898	1.6953	2.1851
			Cl-38	1.00				
17	Chlorine	Cl-34	1.5264 s	ECB+	–	2.0508	1.0212	3.0720
			S-34	1.00				
		Cl-34m	32.00 m	ECB+IT	–	0.4596	2.1127	2.5722
			Cl-34	4.4600E-01				
			S-34	5.5400E-01				
		Cl-36	3.01E+5 y	B-ECB+	–	0.2732	0.0001	0.2733
			Ar-36	9.8100E-01				
			S-36	1.9000E-02				
		Cl-38	37.24 m	B-	–	1.5504	1.4430	2.9934
			Ar-38	1.00				
		Cl-39	55.6 m	B-	–	0.8246	1.4509	2.2755
			Ar-39	1.00				
		Cl-40	1.35 m	B-	–	1.5265	4.0821	5.6085
			Ar-40	1.00				
18	Argon	Ar-37	35.04 d	EC	–	0.0023	0.0003	0.0025
			Cl-37	1.00				
		Ar-39	269 y	B-	–	0.2188	–	0.2188
			K-39	1.00				

Table A.1 continued

Z	Element	Nuclide	Half-life	Decay mode	Emitted energy (MeV/nt)			
					Alpha	Electron	Photon	Total
		Ar-41	109.61 m	B-	–	0.4637	1.2836	1.7474
			K-41	1.00				
		Ar-42	32.9 y	B-	–	0.2325	–	0.2325
			K-42	1.00				
		Ar-43	5.37 m	B-	–	1.3570	1.5352	2.8921
			K-43	1.00				
		Ar-44	11.87 m	B-	–	0.5245	1.9376	2.4621
			K-44	1.00				
19	Potassium	K-38	7.636 m	ECB+	–	1.2107	3.1867	4.3974
			Ar-38	1.00				
		K-40	1.251E+9 y	B-ECB+	–	0.5218	0.1567	0.6785
			Ca-40	8.9140E-01				
			Ar-40	1.0860E-01				
		K-42	12.360 h	B-	–	1.4303	0.2787	1.7090
			Ca-42	1.00				
		K-43	22.3 h	B-	–	0.3097	0.9641	1.2739
			Ca-43	1.00				
		K-44	22.13 m	B-	–	1.4567	2.3846	3.8413
			Ca-44	1.00				
		K-45	17.3 m	B-	–	0.9959	1.8360	2.8319
			Ca-45	1.00				
		K-46	105 s	B-	–	2.3161	2.8710	5.1871
			Ca-46	1.00				
20	Calcium	Ca-41	1.02E+5 y	EC	–	0.0027	0.0005	0.0032
			K-41	1.00				
		Ca-45	162.67 d	B-	–	0.0772	<E-04	0.0772
			Sc-45	1.00				
		Ca-47	4.536 d	B-	–	0.3521	1.0521	1.4042
			Sc-47	1.00				
		Ca-49	8.718 m	B-	–	0.8693	3.1675	4.0369
			Sc-49	1.00				
21	Scandium	Sc-42m	62.0 s	ECB+	–	1.2565	4.2042	5.4607
			Ca-42	1.00				
		Sc-43	3.891 h	ECB+	–	0.4195	0.9841	1.4035
			Ca-43	1.00				
		Sc-44	3.97 h	ECB+	–	0.5961	2.1369	2.7330
			Ca-44	1.00				
		Sc-44m	58.61 h	ITEC	–	0.0328	0.2743	0.3071
			Sc-44	9.8800E-01				
			Ca-44	1.2000E-02				
		Sc-46	83.79 d	B-	–	0.1121	2.0096	2.1217
			Ti-46	1.00				
		Sc-47	3.3492 d	B-	–	0.1624	0.1089	0.2713
			Ti-47	1.00				
		Sc-48	43.67 h	B-	–	0.2216	3.3529	3.5744
			Ti-48	1.00				

(*continued on next page*)

Table A.1 continued

Z	Element	Nuclide	Half-life	Decay mode	Emitted energy (MeV/nt)			
					Alpha	Electron	Photon	Total
		Sc-49	57.2 m	B-	–	0.8177	0.0010	0.8188
			Ti-49	1.00				
		Sc-50	102.5 s	B-	–	1.6362	3.2022	4.8384
			Ti-50	1.00				
22	Titanium	Ti-44	60.0 y	EC	–	0.0108	0.1396	0.1504
			Sc-44	1.00				
		Ti-45	184.8 m	ECB+	–	0.3728	0.8703	1.2431
			Sc-45	1.00				
		Ti-51	5.76 m	B-	–	0.8692	0.3692	1.2383
			V-51	1.00				
		Ti-52	1.7 m	B-	–	0.7530	0.1282	0.8812
			V-52	1.00				
23	Vanadium	V-47	32.6 m	ECB+	–	0.8027	0.9951	1.7978
			Ti-47	1.00				
		V-48	15.9735 d	ECB+	–	0.1526	2.9140	3.0666
			Ti-48	1.00				
		V-49	330 d	EC	–	0.0035	0.0009	0.0045
			Ti-49	1.00				
		V-50	1.50E+17 y	ECB-	–	0.0158	1.4235	1.4393
			Ti-50	8.3000E-01				
			Cr-50	1.7000E-01				
		V-52	3.743 m	B-	–	1.0684	1.4449	2.5133
			Cr-52	1.00				
		V-53	1.61 m	B-	–	1.0048	1.0382	2.0430
			Cr-53	1.00				
24	Chromium	Cr-48	21.56 h	ECB+	–	0.0086	0.4363	0.4449
			V-48	1.00				
		Cr-49	42.3 m	ECB+	–	0.6047	1.0538	1.6584
			V-49	1.00				
		Cr-51	27.7025 d	EC	–	0.0038	0.0329	0.0367
			V-51	1.00				
		Cr-55	3.497 m	B-	–	1.1007	0.0007	1.1013
			Mn-55	1.00				
		Cr-56	5.94 m	B-	–	0.6083	0.0918	0.7000
			Mn-56	1.00				
25	Manganese	Mn-50m	1.75 m	ECB+	–	1.5243	4.6397	6.1640
			Cr-50	1.00				
		Mn-51	46.2 m	ECB+	–	0.9344	0.9977	1.9321
			Cr-51	1.00				
		Mn-52m	21.1 m	ECB+IT	–	1.1321	2.4086	3.5407
			Mn-52	1.7500E-02				
			Cr-52	9.8250E-01				
		Mn-52	5.591 d	ECB+	–	0.0750	3.4585	3.5335
			Cr-52	1.00				
		Mn-53	3.7E+6 y	EC	–	0.0040	0.0014	0.0053
			Cr-53	1.00				

Table A.1 continued

Z	Element	Nuclide	Half-life	Decay mode	Emitted energy (MeV/nt)			
					Alpha	Electron	Photon	Total
		Mn-54	312.12 d	ECB+B-	–	0.0042	0.8360	0.8402
			Cr-54	1.00				
			Fe-54	2.9000E-06				
		Mn-56	2.5789 h	B-	–	0.8299	1.6916	2.5215
			Fe-56	1.00				
		Mn-57	85.4 s	B-	–	1.1013	0.0996	1.2009
			Fe-57	1.00				
		Mn-58m	65.2 s	B-	–	1.7443	2.3854	4.1297
			Fe-58	1.00				
26	Iron	Fe-52	8.275 h	ECB+	–	0.1917	0.7405	0.9322
			Mn-52m	1.00				
		Fe-53	8.51 m	ECB+	–	1.1013	1.1782	2.2795
			Mn-53	1.00				
		Fe-53m	2.526 m	IT	–	0.0023	3.0547	3.0570
			Fe-53	1.00				
		Fe-55	2.737 y	EC	–	0.0042	0.0017	0.0058
			Mn-55	1.00				
		Fe-59	44.495 d	B-	–	0.1179	1.1883	1.3062
			Co-59	1.00				
		Fe-60	1.5E+6 y	B-	–	0.0647	–	0.0647
			Co-60m	1.00				
		Fe-61	5.98 m	B-	–	1.0934	1.3910	2.4844
			Co-61	1.00				
		Fe-62	68 s	B-	–	0.8258	0.5061	1.3319
			Co-62	1.00				
27	Cobalt	Co-54m	1.48 m	ECB+	–	2.0484	3.9306	5.9790
			Fe-54	1.00				
		Co-55	17.53 h	ECB+	–	0.4312	1.9960	2.4272
			Fe-55	1.00				
		Co-56	77.23 d	ECB+	–	0.1198	3.6404	3.7602
			Fe-56	1.00				
		Co-57	271.74 d	EC	–	0.0186	0.1252	0.1439
			Fe-57	1.00				
		Co-58	70.86 d	ECB+	–	0.0340	0.9749	1.0089
			Fe-58	1.00				
		Co-58m	9.04 h	IT	–	0.0229	0.0020	0.0249
			Co-58	1.00				
		Co-60	5.2713 y	B-	–	0.0969	2.5038	2.6007
			Ni-60	1.00				
		Co-60m	10.467 m	ITB-	–	0.0565	0.0067	0.0632
			Co-60	9.9760E-01				
			Ni-60	2.4000E-03				
		Co-61	1.650 h	B-	–	0.4664	0.0970	0.5634
			Ni-61	1.00				
		Co-62	1.50 m	B-	–	1.6336	1.6050	3.2386
			Ni-62	1.00				

(*continued on next page*)

Table A.1 continued

Z	Element	Nuclide	Half-life	Decay mode	Emitted energy (MeV/nt)			
					Alpha	Electron	Photon	Total
		Co-62m	13.91 m	B-	–	1.0974	2.6923	3.7897
			Ni-62	1.00				
28	Nickel	Ni-56	6.075 d	ECB+	–	0.0073	1.7207	1.7280
			Co-56	1.00				
		Ni-57	35.60 h	ECB+	–	0.1571	1.9382	2.0953
			Co-57	1.00				
		Ni-59	1.01E+5 y	ECB+	–	0.0045	0.0024	0.0069
			Co-59	1.00				
		Ni-63	100.1 y	B-	–	0.0174	–	0.0174
			Cu-63	1.00				
		Ni-65	2.51719 h	B-	–	0.6277	0.5583	1.1860
			Cu-65	1.00				
		Ni-66	54.6 h	B-	–	0.0734	–	0.0734
			Cu-66	1.00				
29	Copper	Cu-57	0.1963 s	ECB+	–	3.5987	1.1407	4.7394
			Ni-57	1.00				
		Cu-59	81.5 s	ECB+	–	1.4892	1.4451	2.9342
			Ni-59	1.00				
		Cu-60	23.7 m	ECB+	–	0.8975	3.9111	4.8087
			Ni-60	1.00				
		Cu-61	3.333 h	ECB+	–	0.3090	0.8237	1.1327
			Ni-61	1.00				
		Cu-62	9.673 m	ECB+	–	1.2843	1.0069	2.2912
			Ni-62	1.00				
		Cu-64	12.700 h	ECB+B-	–	0.1248	0.1855	0.3102
			Ni-64	6.1000E-01				
			Zn-64	3.9000E-01				
		Cu-66	5.120 m	B-	–	1.0664	0.0978	1.1642
			Zn-66	1.00				
		Cu-67	61.83 h	B-	–	0.1504	0.1154	0.2657
			Zn-67	1.00				
		Cu-69	2.85 m	B-	–	0.8863	0.5284	1.4147
			Zn-69	1.00				
30	Zinc	Zn-60	2.38 m	ECB+	–	1.1301	1.5282	2.6584
			Cu-60	1.00				
		Zn-61	89.1 s	ECB+	–	1.8571	1.5327	3.3898
			Cu-61	1.00				
		Zn-62	9.186 h	ECB+	–	0.0326	0.4431	0.4757
			Cu-62	1.00				
		Zn-63	38.47 m	ECB+	–	0.9204	1.0967	2.0171
			Cu-63	1.00				
		Zn-65	244.06 d	ECB+	–	0.0069	0.5819	0.5888
			Cu-65	1.00				
		Zn-69m	13.76 h	ITB-	–	0.0226	0.4162	0.4388
			Zn-69	9.9967E-01				
			Ga-69	3.3000E-04				
		Zn-69	56.4 m	B-	–	0.3216	<E-04	0.3216
			Ga-69	1.00				

Table A.1 continued

Z	Element	Nuclide	Half-life	Decay mode	Emitted energy (MeV/nt)			
					Alpha	Electron	Photon	Total
		Zn-71m	3.96 h	B-	–	0.5430	1.5606	2.1037
			Ga-71	1.00				
		Zn-71	2.45 m	B-	–	1.0474	0.3150	1.3624
			Ga-71	1.00				
		Zn-72	46.5 h	B-	–	0.1021	0.1519	0.2541
			Ga-72	1.00				
31	Gallium	Ga-64	2.627 m	ECB+	–	1.7031	3.3726	5.0756
			Zn-64	1.00				
		Ga-65	15.2 m	ECB+	–	0.8158	1.1650	1.9808
			Zn-65	1.00				
		Ga-66	9.49 h	ECB+	–	0.9634	2.4944	3.4577
			Zn-66	1.00				
		Ga-67	3.2612 d	EC	–	0.0363	0.1595	0.1959
			Zn-67	1.00				
		Ga-68	67.71 m	ECB+	–	0.7379	0.9487	1.6866
			Zn-68	1.00				
		Ga-70	21.14 m	B-EC	–	0.6441	0.0073	0.6514
			Ge-70	9.9590E-01				
			Zn-70	4.1000E-03				
		Ga-72	14.10 h	B-	–	0.5060	2.7071	3.2131
			Ge-72	1.00				
		Ga-73	4.86 h	B-	–	0.4999	0.3520	0.8519
			Ge-73	1.00				
		Ga-74	8.12 m	B-	–	0.9945	3.1540	4.1486
			Ge-74	1.00				
32	Germanium	Ge-66	2.26 h	ECB+	–	0.0984	0.6780	0.7764
			Ga-66	1.00				
		Ge-67	18.9 m	ECB+	–	1.1688	1.4254	2.5942
			Ga-67	1.00				
		Ge-68	270.95 d	EC	–	0.0050	0.0041	0.0091
			Ga-68	1.00				
		Ge-69	39.05 h	ECB+	–	0.1203	0.9505	1.0708
			Ga-69	1.00				
		Ge-71	11.43 d	EC	–	0.0050	0.0042	0.0092
			Ga-71	1.00				
		Ge-75	82.78 m	B-	–	0.4206	0.0352	0.4558
			As-75	1.00				
		Ge-77	11.30 h	B-	–	0.6493	1.0787	1.7280
			As-77	1.00				
		Ge-78	88 m	B-	–	0.2273	0.2781	0.5053
			As-78	1.00				
33	Arsenic	As-68	151.6 s	ECB+	–	1.9985	3.7113	5.7097
			Ge-68	1.00				
		As-69	15.23 m	ECB+	–	1.2182	1.1431	2.3613
			Ge-69	1.00				
		As-70	52.6 m	ECB+	–	0.8799	4.2528	5.1327
			Ge-70	1.00				

(*continued on next page*)

Table A.1 continued

Z	Element	Nuclide	Half-life	Decay mode	Emitted energy (MeV/nt)			
					Alpha	Electron	Photon	Total
		As-71	65.28 h	ECB+	–	0.1167	0.5765	0.6932
			Ge-71	1.00				
		As-72	26.0 h	ECB+	–	1.0409	1.7832	2.8240
			Ge-72	1.00				
		As-73	80.30 d	EC	–	0.0606	0.0159	0.0765
			Ge-73	1.00				
		As-74	17.77 d	ECB+B-	–	0.2658	0.7582	1.0241
			Ge-74	6.6000E-01				
			Se-74	3.4000E-01				
		As-76	1.0778 d	B-	–	1.0670	0.4166	1.4836
			Se-76	1.00				
		As-77	38.83 h	B-	–	0.2258	0.0083	0.2342
			Se-77	1.00				
		As-78	90.7 m	B-	–	1.2460	1.3066	2.5525
			Se-78	1.00				
		As-79	9.01 m	B-	–	0.8771	0.0338	0.9109
			Se-79m	9.7188E-01				
			Se-79	2.8121E-02				
34	Selenium	Se-70	41.1 m	ECB+	–	0.2375	0.7211	0.9586
			As-70	1.00				
		Se-71	4.74 m	ECB+	–	1.3844	1.6056	2.9900
			As-71	1.00				
		Se-72	8.40 d	EC	–	0.0228	0.0343	0.0571
			As-72	1.00				
		Se-73	7.15 h	ECB+	–	0.3871	1.0924	1.4795
			As-73	1.00				
		Se-73m	39.8 m	ITECB+	–	0.1642	0.2633	0.4275
			Se-73	7.2600E-01				
			As-73	2.7400E-01				
		Se-75	119.779 d	EC	–	0.0144	0.3890	0.4034
			As-75	1.00				
		Se-77m	17.36 s	IT	–	0.0737	0.0888	0.1625
			Se-77	1.00				
		Se-79	2.95E+5 y	B-	–	0.0529	–	0.0529
			Br-79	1.00				
		Se-79m	3.92 m	ITB-	–	0.0820	0.0138	0.0957
			Se-79	9.9944E-01				
			Br-79	5.6000E-04				
		Se-81	18.45 m	B-	–	0.6108	0.0080	0.6188
			Br-81	1.00				
		Se-81m	57.28 m	ITB-	–	0.0871	0.0183	0.1054
			Se-81	9.9948E-01				
			Br-81	5.2000E-04				
		Se-83	22.3 m	B-	–	0.4528	2.6254	3.0782
			Br-83	1.00				
		Se-83m	70.1 s	B-	–	1.2570	0.9849	2.2419
			Br-83	1.00				

Table A.1 continued

Z	Element	Nuclide	Half-life	Decay mode	Emitted energy (MeV/nt)			
					Alpha	Electron	Photon	Total
		Se-84	3.1 m	B-	–	0.5499	0.4202	0.9701
			Br-84	1.00				
35	Bromine	Br-72	78.6 s	ECB+	–	2.7880	2.9624	5.7504
			Se-72	1.00				
		Br-73	3.4 m	ECB+	–	1.3434	1.4331	2.7765
			Se-73m	9.9881E-01				
			Se-73	1.1920E-03				
		Br-74	25.4 m	ECB+	–	1.0616	4.6130	5.6746
			Se-74	1.00				
		Br-74m	46 m	ECB+	–	1.2747	4.1467	5.4214
			Se-74	1.00				
		Br-75	96.7 m	ECB+	–	0.5283	1.1981	1.7263
			Se-75	1.00				
		Br-76	16.2 h	ECB+	–	0.6497	2.7933	3.4430
			Se-76	1.00				
		Br-76m	1.31 s	ITECB+	–	0.0690	0.0433	0.1123
			Br-76	9.9700E-01				
			Se-76	3.0000E-03				
		Br-77	57.036 h	ECB+	–	0.0094	0.3209	0.3303
			Se-77	1.00				
		Br-77m	4.28 m	IT	–	0.0876	0.0197	0.1073
			Br-77	1.00				
		Br-78	6.46 m	ECB+B-	–	1.0235	1.0336	2.0571
			Se-78	9.9990E-01				
			Kr-78	1.0000E-04				
		Br-80	17.68 m	B-ECB+	–	0.7247	0.0761	0.8007
			Kr-80	9.1700E-01				
			Se-80	8.3000E-02				
		Br-80m	4.4205 h	IT	–	0.0617	0.0242	0.0859
			Br-80	1.00				
		Br-82	35.30 h	B-	–	0.1454	2.6389	2.7844
			Kr-82	1.00				
		Br-82m	6.13 m	ITB-	–	0.0704	0.0081	0.0785
			Br-82	9.7600E-01				
			Kr-82	2.4000E-02				
		Br-83	2.40 h	B-	–	0.3258	0.0069	0.3326
			Kr-83m	9.9845E-01				
			Kr-83	1.5519E-03				
		Br-84	31.80 m	B-	–	1.2364	1.7595	2.9959
			Kr-84	1.00				
		Br-84m	6.0 m	B-	–	0.8983	2.7684	3.6667
			Kr-84	1.00				
		Br-85	2.90 m	B-	–	1.0384	0.0660	1.1045
			Kr-85m	9.9779E-01				
			Kr-85	2.2112E-03				

(*continued on next page*)

Table A.1 continued

Z	Element	Nuclide	Half-life	Decay mode	Emitted energy (MeV/nt)			
					Alpha	Electron	Photon	Total
36	Krypton	Kr-74	11.50 m	ECB+	–	0.6006	1.0579	1.6585
			Br-74	1.00				
		Kr-75	4.29 m	ECB+	–	1.5430	1.2800	2.8230
			Br-75	1.00				
		Kr-76	14.8 h	EC	–	0.0154	0.4276	0.4430
			Br-76	9.9189E-01				
			Br-76m	8.1144E-03				
		Kr-77	74.4 m	ECB+	–	0.6744	1.0384	1.7128
			Br-77	9.0386E-01				
			Br-77m	9.6135E-02				
		Kr-79	35.04 h	ECB+	–	0.0237	0.2549	0.2786
			Br-79	1.00				
		Kr-81	2.29E+5 y	EC	–	0.0052	0.0072	0.0124
			Br-81	1.00				
		Kr-81m	13.10 s	ITEC	–	0.0596	0.1309	0.1905
			Kr-81	9.9998E-01				
			Br-81	2.5000E-05				
		Kr-83m	1.83 h	IT	–	0.0388	0.0028	0.0416
			Kr-83	1.00				
		Kr-85	10.756 y	B-	–	0.2507	0.0022	0.2529
			Rb-85	1.00				
		Kr-85m	4.480 h	B-IT	–	0.2549	0.1574	0.4123
			Kr-85	2.1400E-01				
			Rb-85	7.8600E-01				
		Kr-87	76.3 m	B-	–	1.3281	0.7919	2.1201
			Rb-87	1.00				
		Kr-88	2.84 h	B-	–	0.3689	1.9538	2.3227
			Rb-88	1.00				
		Kr-89	3.15 m	B-	–	1.3705	1.9313	3.3018
			Rb-89	1.00				
37	Rubidium	Rb-77	3.77 m	ECB+	–	1.6865	1.5452	3.2318
			Kr-77	1.00				
		Rb-78	17.66 m	ECB+	–	1.2889	4.0918	5.3808
			Kr-78	1.00				
		Rb-78m	5.74 m	ECB+IT	–	1.4992	3.2149	4.7141
			Rb-78	1.0000E-01				
			Kr-78	9.0000E-01				
		Rb-79	22.9 m	ECB+	–	0.8099	1.4493	2.2592
			Kr-79	1.00				
		Rb-80	33.4 s	ECB+	–	2.0455	1.1900	3.2355
			Kr-80	1.00				
		Rb-81	4.576 h	ECB+	–	0.1222	0.5081	0.6304
			Kr-81m	9.5691E-01				
			Kr-81	4.3091E-02				
		Rb-81m	30.5 m	ITECB+	–	0.0817	0.0303	0.1120
			Rb-81	9.7600E-01				
			Kr-81	2.3786E-02				
			Kr-81m	2.1355E-04				

Table A.1 continued

Z	Element	Nuclide	Half-life	Decay mode	Emitted energy (MeV/nt)			
					Alpha	Electron	Photon	Total
		Rb-82	1.273 m	ECB+	–	1.4112	1.1083	2.5195
			Kr-82	1.00				
		Rb-82m	6.472 h	ECB+	–	0.0935	2.9212	3.0147
			Kr-82	1.00				
		Rb-83	86.2 d	EC	–	0.0083	0.4914	0.4997
			Kr-83m	7.4292E-01				
			Kr-83	2.5708E-01				
		Rb-84	32.77 d	ECB+B-	–	0.1633	0.9077	1.0710
			Kr-84	9.6200E-01				
			Sr-84	3.8000E-02				
		Rb-84m	20.26 m	IT	–	0.0813	0.3831	0.4644
			Rb-84	1.00				
		Rb-86	18.642 d	B-EC	–	0.6680	0.0930	0.7610
			Sr-86	9.9995E-01				
			Kr-86	5.2000E-05				
		Rb-86m	1.017 m	IT	–	0.0100	0.5461	0.5561
			Rb-86	1.00				
		Rb-87	4.923E10 y	B-	–	0.1154	–	0.1154
			Sr-87	1.00				
		Rb-88	17.78 m	B-	–	2.0720	0.6370	2.7089
			Sr-88	1.00				
		Rb-89	15.15 m	B-	–	0.9528	2.2430	3.1959
			Sr-89	1.00				
		Rb-90	158 s	B-	–	2.0443	2.0286	4.0729
			Sr-90	1.00				
		Rb-90m	258 s	B-IT	–	1.4104	3.2406	4.6510
			Sr-90	9.7400E-01				
			Rb-90	2.6000E-02				
38	Strontium	Sr-79	2.25 m	ECB+	–	1.8572	1.1801	3.0373
			Rb-79	1.00				
		Sr-80	106.3 m	ECB+	–	0.0418	0.4371	0.4789
			Rb-80	1.00				
		Sr-81	22.3 m	ECB+	–	0.9743	1.3866	2.3609
			Rb-81	9.9856E-01				
			Rb-81m	1.4422E-03				
		Sr-82	25.36 d	EC	–	0.0054	0.0079	0.0132
			Rb-82	1.00				
		Sr-83	32.41 h	ECB+	–	0.1604	0.8213	0.9817
			Rb-83	1.00				
		Sr-85	64.84 d	EC	–	0.0089	0.5001	0.5090
			Rb-85	1.00				
		Sr-85m	67.63 m	ITECB+	–	0.0130	0.2177	0.2307
			Sr-85	8.6600E-01				
			Rb-85	1.3400E-01				
		Sr-87m	2.815 h	ITEC	–	0.0672	0.3202	0.3874
			Rb-87	3.0000E-03				
			Sr-87	9.9700E-01				

(*continued on next page*)

Table A.1 continued

Z	Element	Nuclide	Half-life	Decay mode	Emitted energy (MeV/nt)			
					Alpha	Electron	Photon	Total
		Sr-89	50.53 d	B-	–	0.5845	<E-04	0.5846
			Y-89	1.00				
		Sr-90	28.79 y	B-	–	0.1957	–	0.1957
			Y-90	1.00				
		Sr-91	9.63 h	B-	–	0.6549	0.7072	1.3621
			Y-91m	5.8247E-01				
			Y-91	4.1753E-01				
		Sr-92	2.66 h	B-	–	0.2025	1.3368	1.5393
			Y-92	1.00				
		Sr-93	7.423 m	B-	–	0.8094	2.2637	3.0731
			Y-93	1.00				
		Sr-94	75.3 s	B-	–	0.8381	1.4270	2.2651
			Y-94	1.00				
39	Yttrium	Y-81	70.4 s	ECB+	–	1.9658	1.1702	3.1360
			Sr-81	1.00				
		Y-83	7.08 m	ECB+	–	1.3138	1.3458	2.6596
			Sr-83	1.00				
		Y-83m	2.85 m	ECB+IT	–	0.8177	0.8370	1.6546
			Sr-83	6.0000E-01				
			Y-83	4.0000E-01				
		Y-84m	39.5 m	ECB+	–	1.2253	3.9751	5.2003
			Sr-84	1.00				
		Y-85	2.68 h	ECB+	–	0.4881	1.0795	1.5676
			Sr-85m	1.00				
		Y-85m	4.86 h	ECB+	–	0.5765	1.3242	1.9007
			Sr-85	9.6000E-01				
			Sr-85m	3.9998E-02				
		Y-86	14.74 h	ECB+	–	0.2179	3.5777	3.7956
			Sr-86	1.00				
		Y-86m	48 m	ITECB+	–	0.0243	0.2203	0.2446
			Y-86	9.9310E-01				
			Sr-86	6.9000E-03				
		Y-87	79.8 h	ECB+	–	0.0072	0.4462	0.4534
			Sr-87m	1.00				
		Y-87m	13.37 h	ITECB+	–	0.0794	0.3072	0.3866
			Y-87	9.8430E-01				
			Sr-87	1.5700E-02				
		Y-88	106.65 d	ECB+	–	0.0067	2.6950	2.7017
			Sr-88	1.00				
		Y-89m	15.663 s	IT	–	0.0077	0.9014	0.9091
			Y-89	1.00				
		Y-90	64.10 h	B-	–	0.9331	<E-04	0.9331
			Zr-90	1.00				
		Y-90m	3.19 h	ITB-	–	0.0470	0.6354	0.6823
			Y-90	9.9998E-01				
			Zr-90	1.8000E-05				
		Y-91	58.51 d	B-	–	0.6032	0.0031	0.6063
			Zr-91	1.00				

Table A.1 continued

Z	Element	Nuclide	Half-life	Decay mode	Emitted energy (MeV/nt)			
					Alpha	Electron	Photon	Total
		Y-91m	49.71 m	IT	–	0.0279	0.5283	0.5562
			Y-91	1.00				
		Y-92	3.54 h	B-	–	1.4494	0.2517	1.7011
			Zr-92	1.00				
		Y-93	10.18 h	B-	–	1.1721	0.0961	1.2682
			Zr-93	1.00				
		Y-94	18.7 m	B-	–	1.8133	0.7725	2.5858
			Zr-94	1.00				
		Y-95	10.3 m	B-	–	1.4288	1.1080	2.5368
			Zr-95	1.00				
40	Zirconium	Zr-85	7.86 m	ECB+	–	1.3252	1.4718	2.7970
			Y-85m	9.6841E-01				
			Y-85	3.1588E-02				
		Zr-86	16.5 h	ECB+	–	0.0310	0.2952	0.3263
			Y-86	1.00				
		Zr-87	1.68 h	ECB+	–	0.8218	0.9271	1.7488
			Y-87m	9.9704E-01				
			Y-87	2.9636E-03				
		Zr-88	83.4 d	EC	–	0.0160	0.3918	0.4078
			Y-88	1.00				
		Zr-89	78.41 h	ECB+	–	0.1019	1.1581	1.2600
			Y-89	1.00				
		Zr-89m	4.161 m	ITECB+	–	0.0318	0.6344	0.6662
			Zr-89	9.3770E-01				
			Y-89	6.2300E-02				
		Zr-93	1.53E+6 y	B-	–	0.0194	–	0.0194
			Nb-93m	9.7500E-01				
			Nb-93	2.5000E-02				
		Zr-95	64.032 d	B-	–	0.1185	0.7321	0.8506
			Nb-95	9.8920E-01				
			Nb-95m	1.0802E-02				
		Zr-97	16.744 h	B-	–	0.7212	0.8792	1.6004
			Nb-97	1.00				
41	Niobium	Nb-87	3.75 m	ECB+	–	1.7709	1.2202	2.9911
			Zr-87	1.00				
		Nb-88	14.5 m	ECB+	–	1.4555	4.2188	5.6743
			Zr-88	1.00				
		Nb-88m	7.78 m	ECB+	–	1.4589	4.1063	5.5652
			Zr-88	1.00				
		Nb-89	2.03 h	ECB+	–	1.0859	1.3668	2.4527
			Zr-89	9.8772E-01				
			Zr-89m	1.2278E-02				
		Nb-89m	66 m	ECB+	–	0.7855	1.3058	2.0913
			Zr-89m	1.00				
		Nb-90	14.60 h	ECB+	–	0.4032	4.2135	4.6167
			Zr-90	1.00				

(*continued on next page*)

Table A.1 continued

Z	Element	Nuclide	Half-life	Decay mode	Emitted energy (MeV/nt)			
					Alpha	Electron	Photon	Total
		Nb-91	680 y	ECB+	–	0.0058	0.0118	0.0176
			Zr-91	1.00				
		Nb-91m	60.86 d	ITECB+	–	0.0963	0.0340	0.1303
			Nb-91	9.6600E-01				
			Zr-91	3.4000E-02				
		Nb-92	3.47E+7 y	EC	–	0.0079	1.5055	1.5133
			Zr-92	1.00				
		Nb-92m	10.15 d	ECB+	–	0.0065	0.9689	0.9753
			Zr-92	1.00				
		Nb-93m	16.13 y	IT	–	0.0294	0.0020	0.0314
			Nb-93	1.00				
		Nb-94	2.03E+4 y	B-	–	0.1684	1.5581	1.7265
			Mo-94	1.00				
		Nb-94m	6.263 m	ITB-	–	0.0356	0.0117	0.0473
			Nb-94	9.9500E-01				
			Mo-94	5.0000E-03				
		Nb-95	34.991 d	B-	–	0.0446	0.7645	0.8091
			Mo-95	1.00				
		Nb-95m	3.61 d	ITB-	–	0.1800	0.0697	0.2497
			Nb-95	9.4400E-01				
			Mo-95	5.6000E-02				
		Nb-96	23.35 h	B-	–	0.2534	2.4614	2.7149
			Mo-96	1.00				
		Nb-97	72.1 m	B-	–	0.4683	0.6650	1.1333
			Mo-97	1.00				
		Nb-98m	51.3 m	B-	–	0.7636	2.8177	3.5813
			Mo-98	1.00				
		Nb-99	15.0 s	B-	–	1.5132	0.1743	1.6875
			Mo-99	1.00				
		Nb-99m	2.6 m	B-IT	–	1.4148	0.7567	2.1714
			Mo-99	9.8000E-01				
			Nb-99	2.0000E-02				
42	Molybdenum	Mo-89	2.11 m	ECB+	–	1.9620	1.2173	3.1793
			Nb-89	1.00				
		Mo-90	5.56 h	ECB+	–	0.2107	0.8331	1.0438
			Nb-90	1.00				
		Mo-91	15.49 m	ECB+	–	1.4510	0.9773	2.4283
			Nb-91	9.9966E-01				
			Nb-91m	3.4232E-04				
		Mo-91m	64.6 s	ECB+IT	–	0.5559	1.3857	1.9416
			Nb-91m	5.0000E-01				
			Mo-91	5.0000E-01				
		Mo-93	4.0E+3 y	EC	–	0.0056	0.0107	0.0163
			Nb-93m	8.8000E-01				
			Nb-93	1.2000E-01				

Table A.1 continued

Z	Element	Nuclide	Half-life	Decay mode	Emitted energy (MeV/nt)			
					Alpha	Electron	Photon	Total
		Mo-93m	6.85 h	ITEC	–	0.1045	2.3183	2.4228
			Mo-93	9.9880E-01				
			Nb-93	1.2000E-03				
		Mo-99	65.94 h	B-	–	0.3929	0.1484	0.5413
			Tc-99m	8.7730E-01				
			Tc-99	1.2270E-01				
		Mo-101	14.61 m	B-	–	0.5524	1.4706	2.0230
			Tc-101	1.00				
		Mo-102	11.3 m	B-	–	0.3509	0.0185	0.3694
			Tc-102	1.00				
43	Technetium	Tc-91	3.14 m	ECB+	–	1.6985	2.4847	4.1832
			Mo-91	9.9302E-01				
			Mo-91m	6.9789E-03				
		Tc-91m	3.3 m	ECB+	–	1.8871	1.4231	3.3102
			Mo-91m	9.7976E-01				
			Mo-91	2.0245E-02				
		Tc-92	4.25 m	ECB+	–	1.7984	3.8278	5.6263
			Mo-92	1.00				
		Tc-93	2.75 h	ECB+	–	0.0436	1.5686	1.6122
			Mo-93	1.00				
		Tc-93m	43.5 m	ITECB+	–	0.1015	0.9522	1.0537
			Tc-93	7.6600E-01				
			Mo-93	2.3400E-01				
		Tc-94	293 m	ECB+	–	0.0475	2.6608	2.7083
			Mo-94	1.00				
		Tc-94m	52.0 m	ECB+	–	0.7543	1.9567	2.7110
			Mo-94	1.00				
		Tc-95	20.0 h	EC	–	0.0069	0.7965	0.8033
			Mo-95	1.00				
		Tc-95m	61 d	ECB+IT	–	0.0154	0.6887	0.7042
			Tc-95	3.8800E-02				
			Mo-95	9.6120E-01				
		Tc-96	4.28 d	EC	–	0.0089	2.5032	2.5121
			Mo-96	1.00				
		Tc-96m	51.5 m	ITECB+	–	0.0269	0.0480	0.0749
			Tc-96	9.8000E-01				
			Mo-96	2.0000E-02				
		Tc-97	2.6E+6 y	EC	–	0.0055	0.0114	0.0169
			Mo-97	1.00				
		Tc-97m	90.1 d	IT	–	0.0869	0.0096	0.0964
			Tc-97	1.00				
		Tc-98	4.2E+6 y	B-	–	0.1415	1.4127	1.5542
			Ru-98	1.00				
		Tc-99	2.111E+5 y	B-	–	0.1013	<E-04	0.1013
			Ru-99	1.00				

(*continued on next page*)

Table A.1 continued

Z	Element	Nuclide	Half-life	Decay mode	Emitted energy (MeV/nt)			
					Alpha	Electron	Photon	Total
		Tc-99m	6.015 h	ITB-	–	0.0162	0.1266	0.1428
			Tc-99	9.9996E-01				
			Ru-99	3.7000E-05				
		Tc-101	14.2 m	B-	–	0.4725	0.3367	0.8092
			Ru-101	1.00				
		Tc-102	5.28 s	B-	–	1.9441	0.0808	2.0249
			Ru-102	1.00				
		Tc-102m	4.35 m	B-IT	–	0.7902	2.4744	3.2646
			Tc-102	2.0000E-02				
			Ru-102	9.8000E-01				
		Tc-104	18.3 m	B-	–	1.6014	2.2453	3.8467
			Ru-104	1.00				
		Tc-105	7.6 m	B-	–	1.2708	0.7981	2.0690
			Ru-105	1.00				
44	Ruthenium	Ru-92	3.65 m	ECB+	–	0.7939	2.0844	2.8783
			Tc-92	1.00				
		Ru-94	51.8 m	ECB+	–	0.0085	0.5197	0.5282
			Tc-94m	1.00				
		Ru-95	1.643 h	ECB+	–	0.0831	1.2419	1.3249
			Tc-95	9.7387E-01				
			Tc-95m	2.6131E-02				
		Ru-97	2.9 d	EC	–	0.0132	0.2408	0.2540
			Tc-97	9.9958E-01				
			Tc-97m	4.2179E-04				
		Ru-103	39.26 d	B-	–	0.0660	0.4962	0.5622
			Rh-103m	9.8755E-01				
			Rh-103	1.2453E-02				
		Ru-105	4.44 h	B-	–	0.4406	0.7480	1.1886
			Rh-105	1.00				
		Ru-106	373.59 d	B-	–	0.0100	–	0.0100
			Rh-106	1.00				
		Ru-107	3.75 m	B-	–	1.0704	0.3453	1.4157
			Rh-107	1.00				
		Ru-108	4.55 m	B-	–	0.4803	0.0626	0.5429
			Rh-108	1.00				
45	Rhodium	Rh-94	70.6 s	ECB+	–	2.9012	3.7634	6.6645
			Ru-94	1.00				
		Rh-95	5.02 m	ECB+	–	0.8973	2.5603	3.4576
			Ru-95	1.00				
		Rh-95m	1.96 m	ITECB+	–	0.1822	0.8973	1.0794
			Rh-95	8.8000E-01				
			Ru-95	1.2000E-01				
		Rh-96	9.90 m	ECB+	–	0.7419	3.9266	4.6685
			Ru-96	1.00				
		Rh-96m	1.51 m	ITECB+	–	0.5673	1.2819	1.8492
			Rh-96	6.0000E-01				
			Ru-96	4.0000E-01				

Table A.1 continued

Z	Element	Nuclide	Half-life	Decay mode	Emitted energy (MeV/nt)			
					Alpha	Electron	Photon	Total
		Rh-97	30.7 m	ECB+	–	0.5211	1.4448	1.9660
			Ru-97	1.00				
		Rh-97m	46.2 m	ECB+IT	–	0.1992	2.2017	2.4009
			Ru-97	9.4400E-01				
			Rh-97	5.6000E-02				
		Rh-98	8.7 m	ECB+	–	1.3371	1.8115	3.1486
			Ru-98	1.00				
		Rh-99	16.1 d	ECB+	–	0.0611	0.5627	0.6238
			Ru-99	1.00				
		Rh-99m	4.7 h	ECB+	–	0.0367	0.6511	0.6878
			Ru-99	1.00				
		Rh-100	20.8 h	ECB+	–	0.0494	2.7425	2.7920
			Ru-100	1.00				
		Rh-100m	4.6 m	ITECB+	–	0.0802	0.0637	0.1439
			Rh-100	9.8300E-01				
			Ru-100	1.7000E-02				
		Rh-101	3.3 y	EC	–	0.0267	0.2878	0.3145
			Ru-101	1.00				
		Rh-101m	4.34 d	ECIT	–	0.0199	0.2877	0.3076
			Rh-101	6.4000E-02				
			Ru-101	9.3600E-01				
		Rh-102	207 d	ECB+B-	–	0.1717	0.5060	0.6777
			Ru-102	7.8000E-01				
			Pd-102	2.2000E-01				
		Rh-102m	3.742 y	ECB+IT	–	0.0125	2.1536	2.1661
			Rh-102	2.3300E-03				
			Ru-102	9.9767E-01				
		Rh-103m	56.114 m	IT	–	0.0377	0.0017	0.0394
			Rh-103	1.00				
		Rh-104	42.3 s	B-EC	–	0.9823	0.0124	0.9947
			Pd-104	9.9550E-01				
			Ru-104	4.5000E-03				
		Rh-104m	4.34 m	ITB-	–	0.0846	0.0441	0.1287
			Rh-104	9.9870E-01				
			Pd-104	1.3000E-03				
		Rh-105	35.36 h	B-	–	0.1533	0.0773	0.2306
			Pd-105	1.00				
		Rh-106	29.80 s	B-	–	1.4111	0.2061	1.6172
			Pd-106	1.00				
		Rh-106m	131 m	B-	–	0.3492	2.8526	3.2018
			Pd-106	1.00				
		Rh-107	21.7 m	B-	–	0.4407	0.3133	0.7539
			Pd-107	1.00				
		Rh-108	16.8 s	B-	–	1.8209	0.3172	2.1381
			Pd-108	1.00				
		Rh-109	80 s	B-	–	0.9320	0.2995	1.2315
			Pd-109	1.00				

(*continued on next page*)

Table A.1 continued

Z	Element	Nuclide	Half-life	Decay mode	Emitted energy (MeV/nt)			
					Alpha	Electron	Photon	Total
46	Palladium	Pd-96	122 s	ECB+	–	0.2257	1.4403	1.6660
			Rh-96m	1.00				
		Pd-97	3.10 m	ECB+	–	0.7524	2.3813	3.1337
			Rh-97	9.8838E-01				
			Rh-97m	1.1622E-02				
		Pd-98	17.7 m	ECB+	–	0.0455	0.4154	0.4609
			Rh-98	1.00				
		Pd-99	21.4 m	ECB+	–	0.4499	1.2833	1.7331
			Rh-99m	9.6647E-01				
			Rh-99	3.3529E-02				
		Pd-100	3.63 d	EC	–	0.0455	0.1231	0.1686
			Rh-100	1.00				
		Pd-101	8.47 h	ECB+	–	0.0328	0.3518	0.3846
			Rh-101m	9.9730E-01				
			Rh-101	2.7000E-03				
		Pd-103	16.991 d	EC	–	0.0058	0.0146	0.0204
			Rh-103m	9.9875E-01				
			Rh-103	1.2512E-03				
		Pd-107	6.5E+6 y	B-	–	0.0096	–	0.0096
			Ag-107	1.00				
		Pd-109	13.7012 h	B-	–	0.4380	0.0118	0.4497
			Ag-109	1.00				
		Pd-109m	4.69 m	IT	–	0.0777	0.1112	0.1889
			Pd-109	1.00				
		Pd-111	23.4 m	B-	–	0.8409	0.0478	0.8887
			Ag-111m	9.9756E-01				
			Ag-111	2.4368E-03				
		Pd-112	21.03 h	B-	–	0.0900	0.0051	0.0951
			Ag-112	1.00				
		Pd-114	2.42 m	B-	–	0.5317	0.0259	0.5576
			Ag-114	1.00				
47	Silver	Ag-99	124 s	ECB+	–	1.3076	2.3092	3.6168
			Pd-99	1.00				
		Ag-100m	2.24 m	ECB+	–	1.9068	2.8248	4.7316
			Pd-100	1.00				
		Ag-101	11.1 m	ECB+	–	0.8396	1.5703	2.4099
			Pd-101	1.00				
		Ag-102	12.9 m	ECB+	–	0.8430	3.4092	4.2522
			Pd-102	1.00				
		Ag-102m	7.7 m	ECB+IT	–	0.3964	1.9933	2.3897
			Ag-102	4.9000E-01				
			Pd-102	5.1000E-01				
		Ag-103	65.7 m	ECB+	–	0.1973	0.8440	1.0412
			Pd-103	1.00				
		Ag-104	69.2 m	ECB+	–	0.0917	2.7066	2.7982
			Pd-104	1.00				

Table A.1 continued

Z	Element	Nuclide	Half-life	Decay mode	Emitted energy (MeV/nt)			
					Alpha	Electron	Photon	Total
		Ag-104m	33.5 m	ECB+IT	–	0.7331	1.8047	2.5377
			Ag-104	7.0000E-04				
			Pd-104	9.9930E-01				
		Ag-105	41.29 d	EC	–	0.0192	0.5138	0.5330
			Pd-105	1.00				
		Ag-105m	7.23 m	ITECB+	–	0.0252	0.0013	0.0265
			Ag-105	9.9660E-01				
			Pd-105	3.4000E-03				
		Ag-106	23.96 m	ECB+B-	–	0.4967	0.6996	1.1963
			Pd-106	9.9000E-01				
			Cd-106	1.0000E-02				
		Ag-106m	8.28 d	EC	–	0.0131	2.8091	2.8222
			Pd-106	1.00				
		Ag-108	2.37 m	B-ECB+	–	0.6071	0.0186	0.6256
			Cd-108	9.7150E-01				
			Pd-108	2.8500E-02				
		Ag-108m	418 y	ECIT	–	0.0159	1.6209	1.6368
			Ag-108	8.7000E-02				
			Pd-108	9.1300E-01				
		Ag-109m	39.6 s	IT	–	0.0770	0.0111	0.0880
			Ag-109	1.00				
		Ag-110	24.6 s	B-EC	–	1.1812	0.0307	1.2119
			Cd-110	9.9700E-01				
			Pd-110	3.0000E-03				
		Ag-110m	249.76 d	B-IT	–	0.0758	2.7606	2.8363
			Ag-110	1.3600E-02				
			Cd-110	9.8640E-01				
		Ag-111	7.45 d	B-	–	0.3539	0.0265	0.3804
			Cd-111	1.00				
		Ag-111m	64.8 s	ITB-	–	0.0568	0.0079	0.0646
			Ag-111	9.9300E-01				
			Cd-111	7.0000E-03				
		Ag-112	3.130 h	B-	–	1.3540	0.6905	2.0445
			Cd-112	1.00				
		Ag-113	5.37 h	B-	–	0.7614	0.0719	0.8333
			Cd-113	9.8261E-01				
			Cd-113m	1.7388E-02				
		Ag-113m	68.7 s	ITB-	–	0.2278	0.2134	0.4412
			Ag-113	6.4000E-01				
			Cd-113	3.6000E-01				
		Ag-114	4.6 s	B-	–	2.1091	0.2589	2.3681
			Cd-114	1.00				
		Ag-115	20.0 m	B-	–	1.0928	0.4831	1.5760
			Cd-115	9.4210E-01				
			Cd-115m	5.7870E-02				
		Ag-116	2.68 m	B-	–	1.7540	2.1473	3.9014
			Cd-116	1.00				

(continued on next page)

Table A.1 continued

Z	Element	Nuclide	Half-life	Decay mode	Emitted energy (MeV/nt)			
					Alpha	Electron	Photon	Total
		Ag-117	73.6 s	B-	–	1.2813	1.3028	2.5841
			Cd-117	8.4703E-01				
			Cd-117m	1.5297E-01				
48	Cadmium	Cd-101	1.36 m	ECB+	–	1.0685	2.4853	3.5538
			Ag-101	1.00				
		Cd-102	5.5 m	ECB+	–	0.0756	0.8380	0.9136
			Ag-102m	9.4624E-01				
			Ag-102	5.3762E-02				
		Cd-103	7.3 m	ECB+	–	0.3636	2.0891	2.4527
			Ag-103	1.00				
		Cd-104	57.7 m	EC	–	0.0306	0.2513	0.2819
			Ag-104m	1.00				
		Cd-105	55.5 m	ECB+	–	0.2167	1.2995	1.5161
			Ag-105m	8.2963E-01				
			Ag-105	1.7037E-01				
		Cd-107	6.50 h	ECB+	–	0.0870	0.0337	0.1207
			Ag-107	1.00				
		Cd-109	461.4 d	EC	–	0.0827	0.0265	0.1092
			Ag-109	1.00				
		Cd-111m	48.50 m	IT	–	0.1066	0.2843	0.3908
			Cd-111	1.00				
		Cd-113	7.7E+15 y	B-	–	0.0926	–	0.0926
			In-113	1.00				
		Cd-113m	14.1 y	B-IT	–	0.1847	<E-04	0.1848
			Cd-113	1.4000E-03				
			In-113	9.9860E-01				
		Cd-115	53.46 h	B-	–	0.3182	0.1926	0.5107
			In-115m	1.00				
		Cd-115m	44.6 d	B-	–	0.6045	0.0329	0.6374
			In-115	9.9989E-01				
			In-115m	1.0578E-04				
		Cd-117	2.49 h	B-	–	0.4379	1.0796	1.5175
			In-117m	9.1507E-01				
			In-117	8.4933E-02				
		Cd-117m	3.36 h	B-	–	0.2279	2.0437	2.2716
			In-117	9.9002E-01				
			In-117m	9.9831E-03				
		Cd-118	50.3 m	B-	–	0.1614	–	0.1614
			In-118	1.00				
		Cd-119	2.69 m	B-	–	0.8186	1.6380	2.4566
			In-119m	9.0091E-01				
			In-119	9.9092E-02				
		Cd-119m	2.20 m	B-	–	0.6898	2.3021	2.9919
			In-119	9.9787E-01				
			In-119m	2.1328E-03				

Table A.1 continued

Z	Element	Nuclide	Half-life	Decay mode	Emitted energy (MeV/nt)			
					Alpha	Electron	Photon	Total
49	Indium	In-103	60 s	ECB+	–	1.5404	2.7528	4.2932
			Cd-103	1.00				
		In-105	5.07 m	ECB+	–	1.0358	1.9307	2.9666
			Cd-105	1.00				
		In-106m	5.2 m	ECB+	–	1.5889	2.8243	4.4132
			Cd-106	1.00				
		In-106	6.2 m	ECB+	–	1.0844	3.5541	4.6385
			Cd-106	1.00				
		In-107	32.4 m	ECB+	–	0.3263	1.5307	1.8570
			Cd-107	1.00				
		In-108m	39.6 m	ECB+	–	0.7021	2.7655	3.4675
			Cd-108	1.00				
		In-108	58.0 m	ECB+	–	0.1620	3.9164	4.0784
			Cd-108	1.00				
		In-109m	1.34 m	IT	–	0.0416	0.6085	0.6501
			In-109	1.00				
		In-109	4.2 h	ECB+	–	0.0334	0.6441	0.6775
			Cd-109	1.00				
		In-110m	69.1 m	ECB+	–	0.6282	1.5782	2.2065
			Cd-110	1.00				
		In-110	4.9 h	ECB+	–	0.0122	3.0972	3.1094
			Cd-110	1.00				
		In-111m	7.7 m	IT	–	0.0675	0.4706	0.5380
			In-111	1.00				
		In-111	2.8047 d	EC	–	0.0348	0.4061	0.4409
			Cd-111m	4.9998E-05				
			Cd-111	9.9995E-01				
		In-112m	20.56 m	IT	–	0.1217	0.0347	0.1564
			In-112	1.00				
		In-112	14.97 m	ECB+B-	–	0.2452	0.2675	0.5127
			Cd-112	5.6000E-01				
			Sn-112	4.4000E-01				
		In-113m	1.6579 h	IT	–	0.1361	0.2606	0.3967
			In-113	1.00				
		In-114m	49.51 d	ITEC	–	0.1450	0.0804	0.2254
			In-114	9.6750E-01				
			Cd-114	3.2500E-02				
		In-114	71.9 s	B-ECB+	–	0.7740	0.0023	0.7764
			Sn-114	9.9500E-01				
			Cd-114	5.0000E-03				
		In-115m	4.486 h	ITB-	–	0.1748	0.1627	0.3376
			In-115	9.5000E-01				
			Sn-115	5.0000E-02				
		In-115	4.41E+14 y	B-	–	0.1526	–	0.1526
			Sn-115	1.00				
		In-116m	54.41 m	B-	–	0.3128	2.4691	2.7819
			Sn-116	1.00				

(*continued on next page*)

Table A.1 continued

Z	Element	Nuclide	Half-life	Decay mode	Emitted energy (MeV/nt)			
					Alpha	Electron	Photon	Total
		In-117m	116.2 m	B-IT	–	0.4344	0.0910	0.5254
			In-117	4.7100E-01				
			Sn-117	5.2900E-01				
		In-117	43.2 m	B-	–	0.2673	0.6939	0.9612
			Sn-117m	3.5321E-03				
			Sn-117	9.9647E-01				
		In-118m	4.364 m	B-	–	0.6708	2.7765	3.4473
			Sn-118	1.00				
		In-118	5.0 s	B-	–	1.8792	0.0778	1.9570
			Sn-118	1.00				
		In-119m	18.0 m	B-IT	–	1.0221	0.0660	1.0882
			In-119	5.6000E-02				
			Sn-119	9.4400E-01				
		In-119	2.4 m	B-	–	0.6148	0.7701	1.3849
			Sn-119m	9.4773E-03				
			Sn-119	9.9052E-01				
		In-121m	3.88 m	B-IT	–	1.5288	0.0635	1.5922
			Sn-121	9.8800E-01				
			In-121	1.2000E-02				
		In-121	23.1 s	B-	–	0.9869	0.9266	1.9135
			Sn-121	8.8650E-01				
			Sn-121m	1.1350E-01				
50	Tin	Sn-106	1.92 m	ECB+	–	0.1279	1.2091	1.3370
			In-106m	1.00				
		Sn-108	10.30 m	ECB+	–	0.0269	0.6847	0.7117
			In-108m	1.00				
		Sn-109	18.0 m	ECB+	–	0.0571	2.2063	2.2634
			In-109	7.1734E-01				
			In-109m	2.8266E-01				
		Sn-110	4.11 h	EC	–	0.0152	0.2918	0.3070
			In-110m	1.00				
		Sn-111	35.3 m	ECB+	–	0.1915	0.4903	0.6818
			In-111	9.9793E-01				
			In-111m	2.0745E-03				
		Sn-113m	21.4 m	ITEC	–	0.0588	0.0137	0.0725
			Sn-113	9.1100E-01				
			In-113	8.9000E-02				
		Sn-113	115.09 d	EC	–	0.0063	0.0237	0.0300
			In-113m	9.9998E-01				
			In-113	2.2352E-05				
		Sn-117m	13.76 d	IT	–	0.1616	0.1581	0.3197
			Sn-117	1.00				
		Sn-119m	293.1 d	IT	–	0.0781	0.0151	0.0932
			Sn-119	1.00				
		Sn-121m	43.9 y	ITB-	–	0.0354	0.0052	0.0405
			Sn-121	7.7600E-01				
			Sb-121	2.2400E-01				

Table A.1 continued

Z	Element	Nuclide	Half-life	Decay mode	Emitted energy (MeV/nt)			
					Alpha	Electron	Photon	Total
		Sn-121	27.03 h	B-	–	0.1156	–	0.1156
			Sb-121	1.00				
		Sn-123m	40.06 m	B-	–	0.4788	0.1407	0.6196
			Sb-123	1.00				
		Sn-123	129.2 d	B-	–	0.5227	0.0069	0.5296
			Sb-123	1.00				
		Sn-125m	9.52 m	B-	–	0.8070	0.3464	1.1534
			Sb-125	1.00				
		Sn-125	9.64 d	B-	–	0.8037	0.3346	1.1383
			Sb-125	1.00				
		Sn-126	2.30E+5 y	B-	–	0.1380	0.0569	0.1949
			Sb-126m	1.00				
		Sn-127m	4.13 m	B-	–	1.1140	0.5686	1.6826
			Sb-127	1.00				
		Sn-127	2.10 h	B-	–	0.5199	1.9075	2.4274
			Sb-127	1.00				
		Sn-128	59.07 m	B-	–	0.2457	0.6041	0.8498
			Sb-128m	1.00				
		Sn-129	2.23 m	B-	–	1.2576	1.0081	2.2657
			Sb-129	1.00				
		Sn-130m	1.7 m	B-	–	1.4040	0.8861	2.2901
			Sb-130	8.6005E-01				
			Sb-130m	1.3995E-01				
		Sn-130	3.72 m	B-	–	0.4612	0.9372	1.3984
			Sb-130m	1.00				
51	Antimony	Sb-111	75 s	ECB+	–	1.3640	1.4859	2.8499
			Sn-111	1.00				
		Sb-113	6.67 m	ECB+	–	0.7203	1.2683	1.9886
			Sn-113	7.7569E-01				
			Sn-113m	2.2431E-01				
		Sb-114	3.49 m	ECB+	–	1.2184	2.6893	3.9077
			Sn-114	1.00				
		Sb-115	32.1 m	ECB+	–	0.2342	0.8894	1.1236
			Sn-115	1.00				
		Sb-116	15.8 m	ECB+	–	0.5138	2.2788	2.7926
			Sn-116	1.00				
		Sb-116m	60.3 m	ECB+	–	0.1408	3.1029	3.2437
			Sn-116	1.00				
		Sb-117	2.80 h	ECB+	–	0.0298	0.1864	0.2162
			Sn-117	1.00				
		Sb-118	3.6 m	ECB+	–	0.8730	0.8039	1.6769
			Sn-118	1.00				
		Sb-118m	5.00 h	ECB+	–	0.0374	2.6130	2.6504
			Sn-118	1.00				
		Sb-119	38.19 h	EC	–	0.0258	0.0234	0.0492
			Sn-119	1.00				

(*continued on next page*)

Table A.1 continued

Z	Element	Nuclide	Half-life	Decay mode	Emitted energy (MeV/nt)			
					Alpha	Electron	Photon	Total
		Sb-120	15.89 m	ECB+	–	0.3077	0.4521	0.7599
			Sn-120	1.00				
		Sb-120m	5.76 d	EC	–	0.0449	2.4663	2.5112
			Sn-120	1.00				
		Sb-122	2.7238 d	B-ECB+	–	0.5618	0.4453	1.0072
			Te-122	9.7590E-01				
			Sn-122	2.4100E-02				
		Sb-122m	4.191 m	IT	–	0.0937	0.0707	0.1644
			Sb-122	1.00				
		Sb-124	60.20 d	B-	–	0.3831	1.8531	2.2362
			Te-124	1.00				
		Sb-124m	93 s	ITB-	–	0.1157	0.4401	0.5558
			Sb-124	7.5000E-01				
			Te-124	2.5000E-01				
		Sb-124n	20.2 m	IT	–	0.0256	0.0004	0.0260
			Sb-124m	1.00				
		Sb-125	2.75856 y	B-	–	0.1010	0.4373	0.5383
			Te-125m	2.3136E-01				
			Te-125	7.6864E-01				
		Sb-126	12.35 d	B-	–	0.3545	2.7552	3.1097
			Te-126	1.00				
		Sb-126m	19.15 m	B-IT	–	0.6322	1.5483	2.1805
			Sb-126	1.4000E-01				
			Te-126	8.6000E-01				
		Sb-127	3.85 d	B-	–	0.3160	0.6934	1.0094
			Te-127	8.2320E-01				
			Te-127m	1.7680E-01				
		Sb-128	9.01 h	B-	–	0.4999	3.0934	3.5934
			Te-128	1.00				
		Sb-128m	10.4 m	B-IT	–	0.9580	1.9063	2.8643
			Sb-128	3.6000E-02				
			Te-128	9.6400E-01				
		Sb-129	4.40 h	B-	–	0.3953	1.4601	1.8553
			Te-129	7.7381E-01				
			Te-129m	2.2619E-01				
		Sb-130	39.5 m	B-	–	0.7579	3.2724	4.0303
			Te-130	1.00				
		Sb-130m	6.3 m	B-	–	1.0290	2.7077	3.7367
			Te-130	1.00				
		Sb-131	23.03 m	B-	–	0.5867	2.0733	2.6601
			Te-131	9.1793E-01				
			Te-131m	8.2067E-02				
		Sb-133	2.5 m	B-	–	0.6785	2.7434	3.4219
			Te-133	8.2662E-01				
			Te-133m	1.7338E-01				

Table A.1 continued

Z	Element	Nuclide	Half-life	Decay mode	Emitted energy (MeV/nt)			
					Alpha	Electron	Photon	Total
52	Tellurium	Te-113	1.7 m	ECB+	–	1.7023	2.2208	3.9231
			Sb-113	1.00				
		Te-114	15.2 m	ECB+	–	0.1551	1.2817	1.4368
			Sb-114	1.00				
		Te-115	5.8 m	ECB+	–	0.8124	2.2449	3.0572
			Sb-115	1.00				
		Te-115m	6.7 m	ECB+	–	0.6939	2.6041	3.2980
			Sb-115	1.00				
		Te-116	2.49 h	ECB+	–	0.0618	0.1122	0.1740
			Sb-116	1.00				
		Te-117	62 m	ECB+	–	0.2139	1.5492	1.7631
			Sb-117	1.00				
		Te-118	6.00 d	EC	–	0.0061	0.0199	0.0260
			Sb-118	1.00				
		Te-119	16.05 h	ECB+	–	0.0143	0.7679	0.7822
			Sb-119	1.00				
		Te-119m	4.70 d	ECB+	–	0.0180	1.5059	1.5239
			Sb-119	1.00				
		Te-121	19.16 d	EC	–	0.0098	0.5775	0.5872
			Sb-121	1.00				
		Te-121m	154 d	ITEC	–	0.0817	0.2176	0.2993
			Te-121	8.8600E-01				
			Sb-121	1.1400E-01				
		Te-123	6.00E+14 y	EC	–	0.0028	0.0004	0.0031
			Sb-123	1.00				
		Te-123m	119.25 d	IT	–	0.0990	0.1477	0.2467
			Te-123	1.00				
		Te-125m	57.40 d	IT	–	0.1091	0.0360	0.1451
			Te-125	1.00				
		Te-127	9.35 h	B-	–	0.2246	0.0049	0.2294
			I-127	1.00				
		Te-127m	109 d	ITB-	–	0.0824	0.0113	0.0937
			Te-127	9.7600E-01				
			I-127	2.4000E-02				
		Te-129	69.6 m	B-	–	0.5436	0.0625	0.6061
			I-129	1.00				
		Te-129m	33.6 d	ITB-	–	0.2709	0.0376	0.3085
			Te-129	6.3000E-01				
			I-129	3.7000E-01				
		Te-131	25.0 m	B-	–	0.7122	0.4200	1.1322
			I-131	1.00				
		Te-131m	30 h	B-IT	–	0.1870	1.4545	1.6415
			I-131	7.7800E-01				
			Te-131	2.2200E-01				
		Te-132	3.204 d	B-	–	0.1108	0.2344	0.3453
			I-132	1.00				

(*continued on next page*)

Table A.1 continued

Z	Element	Nuclide	Half-life	Decay mode	Emitted energy (MeV/nt)			
					Alpha	Electron	Photon	Total
		Te-133	12.5 m	B-	–	0.6897	1.2007	1.8904
			I-133	1.00				
		Te-133m	55.4 m	B-IT	–	0.3880	1.8597	2.2477
			I-133	8.2500E-01				
			Te-133	1.7500E-01				
		Te-134	41.8 m	B-	–	0.2266	0.8714	1.0980
			I-134	1.00				
53	Iodine	I-118	13.7 m	ECB+	–	1.9645	2.0163	3.9809
			Te-118	1.00				
		I-118m	8.5 m	ECB+	–	1.1055	3.7513	4.8567
			Te-118	1.00				
		I-119	19.1 m	ECB+	–	0.5116	0.9110	1.4227
			Te-119	9.9046E-01				
			Te-119m	9.5421E-03				
		I-120	81.6 m	ECB+	–	1.1680	2.6611	3.8291
			Te-120	1.00				
		I-120m	53 m	ECB+	–	0.9070	3.5248	4.4318
			Te-120	1.00				
		I-121	2.12 h	ECB+	–	0.0665	0.3995	0.4660
			Te-121	9.9714E-01				
			Te-121m	2.8631E-03				
		I-122	3.63 m	ECB+	–	1.1055	0.9619	2.0674
			Te-122	1.00				
		I-123	13.27 h	EC	–	0.0282	0.1730	0.2012
			Te-123	9.9996E-01				
			Te-123m	4.4420E-05				
		I-124	4.1760 d	ECB+	–	0.1943	1.1132	1.3075
			Te-124	1.00				
		I-125	59.400 d	EC	–	0.0192	0.0428	0.0621
			Te-125	1.00				
		I-126	12.93 d	ECB+B-	–	0.1606	0.4354	0.5959
			Te-126	5.2700E-01				
			Xe-126	4.7300E-01				
		I-128	24.99 m	B-ECB+	–	0.7463	0.0676	0.8139
			Xe-128	9.3100E-01				
			Te-128	6.9000E-02				
		I-129	1.57E+7 y	B-	–	0.0651	0.0252	0.0902
			Xe-129	1.00				
		I-130	12.36 h	B-	–	0.2786	2.1372	2.4158
			Xe-130	1.00				
		I-130m	8.84 m	ITB-	–	0.1778	0.1097	0.2875
			I-130	8.4000E-01				
			Xe-130	1.6000E-01				
		I-131	8.02070 d	B-	–	0.1918	0.3828	0.5746
			Xe-131m	1.1759E-02				
			Xe-131	9.8824E-01				
		I-132	2.295 h	B-	–	0.4930	2.2645	2.7575
			Xe-132	1.00				

Table A.1 continued

Z	Element	Nuclide	Half-life	Decay mode	Emitted energy (MeV/nt)			
					Alpha	Electron	Photon	Total
		I-132m	1.387 h	ITB-	–	0.1614	0.3403	0.5018
			I-132	8.6000E-01				
			Xe-132	1.4000E-01				
		I-133	20.8 h	B-	–	0.4142	0.6120	1.0262
			Xe-133	9.7115E-01				
			Xe-133m	2.8846E-02				
		I-134	52.5 m	B-	–	0.5776	2.5953	3.1729
			Xe-134	1.00				
		I-134m	3.60 m	ITB-	–	0.0913	0.2887	0.3800
			I-134	9.7700E-01				
			Xe-134	2.3000E-02				
		I-135	6.57 h	B-	–	0.3465	1.5815	1.9280
			Xe-135	8.3432E-01				
			Xe-135m	1.6568E-01				
54	Xenon	Xe-120	40 m	ECB+	–	0.0461	0.4015	0.4476
			I-120	1.00				
		Xe-121	40.1 m	ECB+	–	0.5819	1.4720	2.0539
			I-121	1.00				
		Xe-122	20.1 h	EC	–	0.0100	0.0684	0.0784
			I-122	1.00				
		Xe-123	2.08 h	ECB+	–	0.1875	0.6411	0.8286
			I-123	1.00				
		Xe-125	16.9 h	ECB+	–	0.0350	0.2723	0.3074
			I-125	1.00				
		Xe-127	36.4 d	EC	–	0.0325	0.2806	0.3131
			I-127	1.00				
		Xe-127m	69.2 s	IT	–	0.1293	0.1685	0.2978
			Xe-127	1.00				
		Xe-129m	8.88 d	IT	–	0.1844	0.0517	0.2362
			Xe-129	1.00				
		Xe-131m	11.84 d	IT	–	0.1470	0.0206	0.1676
			Xe-131	1.00				
		Xe-133	5.243 d	B-	–	0.1379	0.0474	0.1854
			Cs-133	1.00				
		Xe-133m	2.19 d	IT	–	0.1924	0.0410	0.2333
			Xe-133	1.00				
		Xe-135	9.14 h	B-	–	0.3208	0.2483	0.5691
			Cs-135	1.00				
		Xe-135m	15.29 m	ITB-	–	0.1008	0.4249	0.5257
			Xe-135	9.9400E-01				
			Cs-135	6.0000E-03				
		Xe-137	3.818 m	B-	–	1.6952	0.1908	1.8859
			Cs-137	1.00				
		Xe-138	14.08 m	B-	–	0.6596	1.1222	1.7818
			Cs-138	1.00				

(*continued on next page*)

Table A.1 continued

Z	Element	Nuclide	Half-life	Decay mode	Emitted energy (MeV/nt)			
					Alpha	Electron	Photon	Total
55	Caesium	Cs-121	155 s	ECB+	–	1.7391	1.1733	2.9123
			Xe-121	1.00				
		Cs-121m	122 s	ECB+IT	–	1.3475	1.1821	2.5296
			Xe-121	8.3000E-01				
			Cs-121	1.7000E-01				
		Cs-123	5.88 m	ECB+	–	0.9509	1.0860	2.0369
			Xe-123	1.00				
		Cs-124	30.8 s	ECB+	–	1.9908	1.1607	3.1515
			Xe-124	1.00				
		Cs-125	45 m	ECB+	–	0.3524	0.7550	1.1075
			Xe-125	1.00				
		Cs-126	1.64 m	ECB+	–	1.3193	1.1545	2.4738
			Xe-126	1.00				
		Cs-127	6.25 h	ECB+	–	0.0293	0.4334	0.4627
			Xe-127	1.00				
		Cs-128	3.640 m	ECB+	–	0.8735	0.8917	1.7651
			Xe-128	1.00				
		Cs-129	32.06 h	ECB+	–	0.0175	0.2802	0.2977
			Xe-129	1.00				
		Cs-130	29.21 m	ECB+B-	–	0.3869	0.5026	0.8894
			Xe-130	9.8400E-01				
			Ba-130	1.6000E-02				
		Cs-130m	3.46 m	ITEC	–	0.0937	0.0737	0.1674
			Cs-130	9.9840E-01				
			Xe-130	1.6000E-03				
		Cs-131	9.689 d	EC	–	0.0064	0.0232	0.0295
			Xe-131	1.00				
		Cs-132	6.479 d	ECB+B-	–	0.0143	0.7151	0.7294
			Xe-132	9.8130E-01				
			Ba-132	1.8700E-02				
		Cs-134	2.0648 y	B-EC	–	0.1639	1.5551	1.7190
			Ba-134	1.00				
			Xe-134	3.0000E-06				
		Cs-134m	2.903 h	IT	–	0.1122	0.0273	0.1394
			Cs-134	1.00				
		Cs-135	2.3E+6 y	B-	–	0.0894	–	0.0894
			Ba-135	1.00				
		Cs-135m	53 m	IT	–	0.0361	1.5972	1.6333
			Cs-135	1.00				
		Cs-136	13.16 d	B-	–	0.1449	2.1283	2.2732
			Ba-136	1.00				
		Cs-137	30.1671 y	B-	–	0.1884	<E-04	0.1884
			Ba-137m	9.4399E-01				
			Ba-137	5.6005E-02				
		Cs-138	33.41 m	B-	–	1.2462	2.3611	3.6073
			Ba-138	1.00				

Table A.1 continued

Z	Element	Nuclide	Half-life	Decay mode	Emitted energy (MeV/nt)			
					Alpha	Electron	Photon	Total
		Cs-138m	2.91 m	ITB-	–	0.3201	0.4149	0.7350
			Cs-138	8.1000E-01				
			Ba-138	1.9000E-01				
		Cs-139	9.27 m	B-	–	1.6598	0.3030	1.9629
			Ba-139	1.00				
		Cs-140	63.7 s	B-	–	1.9361	1.7692	3.7054
			Ba-140	1.00				
56	Barium	Ba-124	11.0 m	ECB+	–	0.1743	0.5728	0.7471
			Cs-124	1.00				
		Ba-126	100 m	ECB+	–	0.0178	0.5803	0.5981
			Cs-126	1.00				
		Ba-127	12.7 m	ECB+	–	0.5971	0.7282	1.3253
			Cs-127	1.00				
		Ba-128	2.43 d	EC	–	0.0086	0.0665	0.0751
			Cs-128	1.00				
		Ba-129	2.23 h	ECB+	–	0.1270	0.3331	0.4601
			Cs-129	1.00				
		Ba-129m	2.16 h	ECB+	–	0.0419	1.5833	1.6252
			Cs-129	1.00				
		Ba-131	11.50 d	EC	–	0.0455	0.4763	0.5219
			Cs-131	1.00				
		Ba-131m	14.6 m	IT	–	0.1102	0.0773	0.1875
			Ba-131	1.00				
		Ba-133	10.52 y	EC	–	0.0553	0.4030	0.4583
			Cs-133	1.00				
		Ba-133m	38.9 h	ITEC	–	0.2259	0.0686	0.2945
			Ba-133	9.9990E-01				
			Cs-133	9.6000E-05				
		Ba-135m	28.7 h	IT	–	0.2080	0.0602	0.2682
			Ba-135	1.00				
		Ba-137m	2.552 m	IT	–	0.0653	0.5963	0.6617
			Ba-137	1.00				
		Ba-139	83.06 m	B-	–	0.9012	0.0457	0.9470
			La-139	1.00				
		Ba-140	12.752 d	B-	–	0.3202	0.1826	0.5029
			La-140	1.00				
		Ba-141	18.27 m	B-	–	0.9624	0.9271	1.8895
			La-141	1.00				
		Ba-142	10.6 m	B-	–	0.4141	1.0469	1.4610
			La-142	1.00				
57	Lanthanum	La-128	5.18 m	ECB+	–	1.3340	2.8283	4.1623
			Ba-128	1.00				
		La-129	11.6 m	ECB+	–	0.6135	0.9212	1.5347
			Ba-129	9.2384E-01				
			Ba-129m	7.6164E-02				
		La-130	8.7 m	ECB+	–	1.1113	2.2324	3.3438
			Ba-130	1.00				

(*continued on next page*)

Table A.1 continued

Z	Element	Nuclide	Half-life	Decay mode	Emitted energy (MeV/nt)			
					Alpha	Electron	Photon	Total
		La-131	59 m	ECB+	–	0.1963	0.6633	0.8596
			Ba-131	1.00				
		La-132	4.8 h	ECB+	–	0.5693	1.9952	2.5645
			Ba-132	1.00				
		La-132m	24.3 m	ITECB+	–	0.1126	0.6706	0.7832
			La-132	7.6000E-01				
			Ba-132	2.4000E-01				
		La-133	3.912 h	ECB+	–	0.0503	0.1605	0.2108
			Ba-133	1.00				
		La-134	6.45 m	ECB+	–	0.7647	0.7196	1.4844
			Ba-134	1.00				
		La-135	19.5 h	ECB+	–	0.0067	0.0361	0.0428
			Ba-135	1.00				
		La-136	9.87 m	ECB+	–	0.2941	0.4070	0.7011
			Ba-136	1.00				
		La-137	6.0E+4 y	EC	–	0.0065	0.0250	0.0315
			Ba-137	1.00				
		La-138	1.02E+11 y	ECB-	–	0.0377	1.2316	1.2693
			Ba-138	6.6400E-01				
			Ce-138	3.3600E-01				
		La-140	1.6781 d	B-	–	0.5346	2.3084	2.8429
			Ce-140	1.00				
		La-141	3.92 h	B-	–	0.9876	0.0268	1.0144
			Ce-141	1.00				
		La-142	91.1 m	B-	–	0.8697	2.3738	3.2435
			Ce-142	1.00				
		La-143	14.2 m	B-	–	1.2995	0.2631	1.5625
			Ce-143	1.00				
58	Cerium	Ce-130	22.9 m	ECB+	–	0.0738	0.5003	0.5741
			La-130	1.00				
		Ce-131	10.2 m	ECB+	–	0.6153	1.6267	2.2420
			La-131	1.00				
		Ce-132	3.51 h	EC	–	0.0180	0.2727	0.2908
			La-132	1.00				
		Ce-133	97 m	ECB+	–	0.3817	0.5430	0.9247
			La-133	1.00				
		Ce-133m	4.9 h	ECB+	–	0.0739	1.7373	1.8112
			La-133	1.00				
		Ce-134	3.16 d	EC	–	0.0072	0.0281	0.0353
			La-134	1.00				
		Ce-135	17.7 h	ECB+	–	0.0296	0.8237	0.8533
			La-135	1.00				
		Ce-137	9.0 h	ECB+	–	0.0165	0.0388	0.0553
			La-137	1.00				
		Ce-137m	34.4 h	ITEC	–	0.2067	0.0558	0.2625
			Ce-137	9.9220E-01				
			La-137	7.8000E-03				

Table A.1 continued

Z	Element	Nuclide	Half-life	Decay mode	Emitted energy (MeV/nt)			
					Alpha	Electron	Photon	Total
		Ce-139	137.641 d	EC	–	0.0355	0.1599	0.1954
			La-139	1.00				
		Ce-141	32.508 d	B-	–	0.1710	0.0768	0.2478
			Pr-141	1.00				
		Ce-143	33.039 h	B-	–	0.4364	0.2796	0.7159
			Pr-143	1.00				
		Ce-144	284.91 d	B-	–	0.0916	0.0194	0.1110
			Pr-144	9.9023E-01				
			Pr-144m	9.7699E-03				
		Ce-145	3.01 m	B-	–	0.6794	0.8142	1.4937
			Pr-145	1.00				
59	Praseodymium	Pr-134	11 m	ECB+	–	1.0801	3.1504	4.2305
			Ce-134	1.00				
		Pr-134m	17 m	ECB+	–	1.5274	2.3101	3.8375
			Ce-134	1.00				
		Pr-135	24 m	ECB+	–	0.5793	0.8741	1.4534
			Ce-135	1.00				
		Pr-136	13.1 m	ECB+	–	0.7545	2.1458	2.9003
			Ce-136	1.00				
		Pr-137	1.28 h	ECB+	–	0.1947	0.3693	0.5640
			Ce-137	1.00				
		Pr-138	1.45 m	ECB+	–	1.1617	0.8153	1.9770
			Ce-138	1.00				
		Pr-138m	2.12 h	ECB+	–	0.2208	2.4776	2.6984
			Ce-138	1.00				
		Pr-139	4.41 h	ECB+	–	0.0478	0.1298	0.1777
			Ce-139	1.00				
		Pr-140	3.39 m	ECB+	–	0.5516	0.5467	1.0983
			Ce-140	1.00				
		Pr-142	19.12 h	B-EC	–	0.8098	0.0581	0.8679
			Nd-142	9.9984E-01				
			Ce-142	1.6400E-04				
		Pr-142m	14.6 m	IT	–	0.0036	0.0001	0.0037
			Pr-142	1.00				
		Pr-143	13.57 d	B-	–	0.3150	<E-04	0.3150
			Nd-143	1.00				
		Pr-144	17.28 m	B-	–	1.2084	0.0289	1.2373
			Nd-144	1.00				
		Pr-144m	7.2 m	ITB-	–	0.0475	0.0134	0.0608
			Pr-144	9.9930E-01				
			Nd-144	7.0000E-04				
		Pr-145	5.984 h	B-	–	0.6757	0.0186	0.6943
			Nd-145	1.00				
		Pr-146	24.15 m	B-	–	1.3277	1.0105	2.3382
			Nd-146	1.00				
		Pr-147	13.4 m	B-	–	0.8896	0.4887	1.3784
			Nd-147	1.00				

(*continued on next page*)

Table A.1 continued

Z	Element	Nuclide	Half-life	Decay mode	Emitted energy (MeV/nt)			
					Alpha	Electron	Photon	Total
		Pr-148	2.29 m	B-	–	1.6637	0.9905	2.6542
			Nd-148	1.00				
		Pr-148m	2.01 m	B-	–	1.6807	0.9337	2.6144
			Nd-148	1.00				
60	Neodymium	Nd-134	8.5 m	ECB+	–	0.1728	0.5421	0.7149
			Pr-134m	1.00				
		Nd-135	12.4 m	ECB+	–	1.0551	1.2617	2.3168
			Pr-135	1.00				
		Nd-136	50.65 m	ECB+	–	0.0805	0.2793	0.3598
			Pr-136	1.00				
		Nd-137	38.5 m	ECB+	–	0.3247	1.1789	1.5036
			Pr-137	1.00				
		Nd-138	5.04 h	EC	–	0.0082	0.0438	0.0520
			Pr-138	1.00				
		Nd-139	29.7 m	ECB+	–	0.2084	0.4431	0.6515
			Pr-139	1.00				
		Nd-139m	5.50 h	ECB+IT	–	0.0795	1.5852	1.6647
			Pr-139	8.8200E-01				
			Nd-139	1.1800E-01				
		Nd-140	3.37 d	EC	–	0.0069	0.0287	0.0357
			Pr-140	1.00				
		Nd-141	2.49 h	ECB+	–	0.0165	0.0765	0.0930
			Pr-141	1.00				
		Nd-141m	62.0 s	ITECB+	–	0.0622	0.6947	0.7569
			Nd-141	9.9968E-01				
			Pr-141	3.2000E-04				
		Nd-144	2.29E+15 y	A	1.9052	–	–	1.9052
			Ce-140	1.00				
		Nd-147	10.98 d	B-	–	0.2702	0.1408	0.4109
			Pm-147	1.00				
		Nd-149	1.728 h	B-	–	0.5042	0.3713	0.8756
			Pm-149	1.00				
		Nd-151	12.44 m	B-	–	0.6195	0.8518	1.4712
			Pm-151	1.00				
		Nd-152	11.4 m	B-	–	0.3314	0.1644	0.4957
			Pm-152	1.00				
61	Promethium	Pm-136	107 s	ECB+	–	2.1436	2.7178	4.8614
			Nd-136	1.00				
		Pm-137m	2.4 m	ECB+	–	1.1120	1.7835	2.8955
			Nd-137	1.00				
		Pm-139	4.15 m	ECB+	–	1.0416	0.9390	1.9807
			Nd-139	1.00				
		Pm-140	9.2 s	ECB+	–	2.0432	1.0506	3.0937
			Nd-140	1.00				
		Pm-140m	5.95 m	ECB+	–	0.9932	3.0324	4.0256
			Nd-140	1.00				

Table A.1 continued

Z	Element	Nuclide	Half-life	Decay mode	Emitted energy (MeV/nt)			
					Alpha	Electron	Photon	Total
		Pm-141	20.90 m	ECB+	–	0.6054	0.7349	1.3403
			Nd-141	9.9833E-01				
			Nd-141m	1.6651E-03				
		Pm-142	40.5 s	ECB+	–	1.3122	0.8561	2.1683
			Nd-142	1.00				
		Pm-143	265 d	EC	–	0.0083	0.3157	0.3240
			Nd-143	1.00				
		Pm-144	363 d	EC	–	0.0171	1.5631	1.5802
			Nd-144	1.00				
		Pm-145	17.7 y	ECA	<E-04	0.0126	0.0315	0.0441
			Nd-145	1.00				
			Pr-141	2.8000E-09				
		Pm-146	5.53 y	ECB-	–	0.0941	0.7512	0.8453
			Sm-146	3.4000E-01				
			Nd-146	6.6000E-01				
		Pm-147	2.6234 y	B-	–	0.0619	<E-04	0.0619
			Sm-147	1.00				
		Pm-148	5.368 d	B-	–	0.7284	0.5743	1.3028
			Sm-148	1.00				
		Pm-148m	41.29 d	B-IT	–	0.1699	1.9916	2.1615
			Sm-148	9.5800E-01				
			Pm-148	4.2000E-02				
		Pm-149	53.08 h	B-	–	0.3650	0.0119	0.3769
			Sm-149	1.00				
		Pm-150	2.68 h	B-	–	0.8101	1.4705	2.2806
			Sm-150	1.00				
		Pm-151	28.40 h	B-	–	0.3048	0.3289	0.6337
			Sm-151	1.00				
		Pm-152	4.12 m	B-	–	1.3283	0.2866	1.6149
			Sm-152	1.00				
		Pm-152m	7.52 m	B-	–	0.9055	1.5189	2.4244
			Sm-152	1.00				
		Pm-153	5.25 m	B-	–	0.6881	0.0764	0.7645
			Sm-153	1.00				
		Pm-154	1.73 m	B-	–	0.8706	1.7933	2.6638
			Sm-154	1.00				
		Pm-154m	2.68 m	B-	–	0.9492	1.7996	2.7488
			Sm-154	1.00				
62	Samarium	Sm-139	2.57 m	ECB+	–	1.0871	1.4540	2.5410
			Pm-139	1.00				
		Sm-140	14.82 m	ECB+	–	0.1710	0.5677	0.7387
			Pm-140	1.00				
		Sm-141	10.2 m	ECB+	–	0.7126	1.4089	2.1215
			Pm-141	1.00				
		Sm-141m	22.6 m	ECB+IT	–	0.3995	1.9494	2.3489
			Pm-141	9.9690E-01				
			Sm-141	3.1000E-03				

(*continued on next page*)

Table A.1 continued

Z	Element	Nuclide	Half-life	Decay mode	Emitted energy (MeV/nt)			
					Alpha	Electron	Photon	Total
		Sm-142	72.49 m	ECB+	–	0.0446	0.1105	0.1551
			Pm-142	1.00				
		Sm-143	8.75 m	ECB+	–	0.4978	0.5289	1.0267
			Pm-143	1.00				
		Sm-143m	66 s	ITECB+	–	0.0720	0.6844	0.7564
			Sm-143	9.9760E-01				
			Pm-143	2.4000E-03				
		Sm-145	340 d	EC	–	0.0307	0.0642	0.0950
			Pm-145	1.00				
		Sm-146	1.03E+8 y	A	2.5290	–	–	2.5290
			Nd-142	1.00				
		Sm-147	1.060E11 y	A	2.3105	–	–	2.3105
			Nd-143	1.00				
		Sm-148	7E+15 y	A	1.9860	–	–	1.9860
			Nd-144	1.00				
		Sm-151	90 y	B-	–	0.0200	<E-04	0.0200
			Eu-151	1.00				
		Sm-153	46.50 h	B-	–	0.2699	0.0643	0.3341
			Eu-153	1.00				
		Sm-155	22.3 m	B-	–	0.5674	0.1029	0.6703
			Eu-155	1.00				
		Sm-156	9.4 h	B-	–	0.2093	0.1150	0.3242
			Eu-156	1.00				
		Sm-157	8.03 m	B-	–	0.8750	0.4142	1.2892
			Eu-157	1.00				
63	Europium	Eu-142	2.34 s	ECB+	–	2.7670	1.1970	3.9641
			Sm-142	1.00				
		Eu-142m	1.223 m	ECB+	–	1.7683	3.4305	5.1987
			Sm-142	1.00				
		Eu-143	2.59 m	ECB+	–	1.3676	1.1227	2.4903
			Sm-143	9.9879E-01				
			Sm-143m	1.2069E-03				
		Eu-144	10.2 s	ECB+	–	2.0761	1.0917	3.1678
			Sm-144	1.00				
		Eu-145	5.93 d	ECB+	–	0.0254	1.2798	1.3052
			Sm-145	1.00				
		Eu-146	4.61 d	ECB+	–	0.0455	2.4007	2.4462
			Sm-146	1.00				
		Eu-147	24.1 d	ECB+A	<E-04	0.0431	0.4721	0.5152
			Sm-147	9.9998E-01				
			Pm-143	2.2000E-05				
		Eu-148	54.5 d	ECB+A	<E-04	0.0224	2.2287	2.2511
			Sm-148	1.00				
			Pm-144	9.4000E-09				
		Eu-149	93.1 d	EC	–	0.0241	0.0661	0.0902
			Sm-149	1.00				
		Eu-150	36.9 y	ECB+	–	0.0285	1.5554	1.5839
			Sm-150	1.00				

Table A.1 continued

Z	Element	Nuclide	Half-life	Decay mode	Emitted energy (MeV/nt)			
					Alpha	Electron	Photon	Total
		Eu-150m	12.8 h	B-ECB+	–	0.3122	0.0494	0.3615
			Gd-150	8.9000E-01				
			Sm-150	1.1000E-01				
		Eu-152	13.537 y	ECB+B-	–	0.1286	1.1759	1.3045
			Gd-152	2.7900E-01				
			Sm-152	7.2100E-01				
		Eu-152m	9.3116 h	B-ECB+	–	0.5060	0.2963	0.8023
			Gd-152	7.2000E-01				
			Sm-152	2.8000E-01				
		Eu-152n	96 m	IT	–	0.0666	0.0753	0.1419
			Eu-152	1.00				
		Eu-154	8.593 y	B-EC	–	0.2730	1.2493	1.5223
			Gd-154	9.9980E-01				
			Sm-154	2.0000E-04				
		Eu-154m	46.0 m	IT	–	0.0745	0.0706	0.1451
			Eu-154	1.00				
		Eu-155	4.7611 y	B-	–	0.0647	0.0612	0.1259
			Gd-155	1.00				
		Eu-156	15.19 d	B-	–	0.4579	1.2342	1.6920
			Gd-156	1.00				
		Eu-157	15.18 h	B-	–	0.3961	0.2930	0.6891
			Gd-157	1.00				
		Eu-158	45.9 m	B-	–	0.8920	1.2978	2.1898
			Gd-158	1.00				
		Eu-159	18.1 m	B-	–	0.8923	0.3032	1.1954
			Gd-159	1.00				
64	Gadolinium	Gd-142	70.2 s	ECB+	–	0.7390	1.0432	1.7822
			Eu-142	1.00				
		Gd-143m	110.0 s	ECB+	–	1.2854	2.1211	3.4065
			Eu-143	1.00				
		Gd-144	4.47 m	ECB+	–	0.5858	0.9086	1.4944
			Eu-144	1.00				
		Gd-145	23.0 m	ECB+	–	0.3456	2.4236	2.7692
			Eu-145	1.00				
		Gd-145m	85 s	ITECB+	–	0.1927	0.6814	0.8741
			Gd-145	9.4300E-01				
			Eu-145	5.7000E-02				
		Gd-146	48.27 d	EC	–	0.1274	0.2526	0.3800
			Eu-146	1.00				
		Gd-147	38.1 h	ECB+	–	0.0617	1.4030	1.4647
			Eu-147	1.00				
		Gd-148	74.6 y	A	3.2712	–	–	3.2712
			Sm-144	1.00				
		Gd-149	9.28 d	ECB+	–	0.0686	0.5292	0.5978
			Eu-149	1.00				
		Gd-150	1.79E+6 y	A	2.8090	–	–	2.8090
			Sm-146	1.00				

(*continued on next page*)

Table A.1 continued

Z	Element	Nuclide	Half-life	Decay mode	Emitted energy (MeV/nt)			
					Alpha	Electron	Photon	Total
		Gd-151	124 d	ECA	<E-04	0.0394	0.0708	0.1102
			Sm-147	1.0000E-08				
			Eu-151	1.0000E+00				
		Gd-152	1.08E+14 y	A	2.2046	–	–	2.2046
			Sm-148	1.00				
		Gd-153	240.4 d	EC	–	0.0438	0.1057	0.1494
			Eu-153	1.00				
		Gd-159	18.479 h	B-	–	0.3096	0.0539	0.3635
			Tb-159	1.00				
		Gd-162	8.4 m	B-	–	0.3387	0.4170	0.7557
			Tb-162	1.00				
65	Terbium	Tb-146	23 s	ECB+	–	1.4644	3.6256	5.0900
			Gd-146	1.00				
		Tb-147	1.64 h	ECB+	–	0.2810	2.1845	2.4655
			Gd-147	1.00				
		Tb-147m	1.87 m	ECB+	–	0.3196	1.9116	2.2312
			Gd-147	1.00				
		Tb-148	60 m	ECB+	–	0.8411	2.3590	3.2001
			Gd-148	1.00				
		Tb-148m	2.20 m	ECB+	–	0.3106	3.1390	3.4495
			Gd-148	1.00				
		Tb-149	4.118 h	ECB+A	0.6810	0.0871	1.3612	2.1292
			Gd-149	8.3300E-01				
			Eu-145	1.6700E-01				
		Tb-149m	4.16 m	ECB+A	0.0009	0.2091	1.3748	1.5847
			Gd-149	9.9978E-01				
			Eu-145	2.2000E-04				
		Tb-150	3.48 h	ECB+A	<E-04	0.2890	2.4403	2.7293
			Gd-150	1.00				
			Eu-146	7.0000E-06				
		Tb-150m	5.8 m	ECB+	–	0.1267	2.5202	2.6470
			Gd-150	1.00				
		Tb-151	17.609 h	ECB+A	0.0003	0.0800	0.9941	1.0744
			Gd-151	1.00				
			Eu-147	9.5000E-05				
		Tb-151m	25 s	ITECB+	–	0.0793	0.0808	0.1601
			Tb-151	9.3400E-01				
			Gd-151	6.6000E-02				
		Tb-152	17.5 h	ECB+	–	0.2503	1.4932	1.7436
			Gd-152	1.00				
		Tb-152m	4.2 m	ITECB+	–	0.1520	0.7619	0.9139
			Tb-152	7.8800E-01				
			Gd-152	2.1200E-01				
		Tb-153	2.34 d	ECB+	–	0.0481	0.3318	0.3800
			Gd-153	1.00				
		Tb-154	21.5 h	ECB+	–	0.0681	2.2831	2.3512
			Gd-154	1.00				

Table A.1 continued

Z	Element	Nuclide	Half-life	Decay mode	Emitted energy (MeV/nt)			
					Alpha	Electron	Photon	Total
		Tb-155	5.32 d	EC	–	0.0434	0.1777	0.2211
			Gd-155	1.00				
		Tb-156	5.35 d	EC	–	0.0835	1.9371	2.0206
			Gd-156	1.00				
		Tb-156m	24.4 h	IT	–	0.0171	0.0370	0.0540
			Tb-156	1.00				
		Tb-156n	5.3 h	IT	–	0.0874	0.0048	0.0922
			Tb-156	1.00				
		Tb-157	71 y	EC	–	0.0057	0.0057	0.0114
			Gd-157	1.00				
		Tb-158	180 y	ECB-	–	0.1117	0.8048	0.9165
			Gd-158	8.3400E-01				
			Dy-158	1.6600E-01				
		Tb-160	72.3 d	B-	–	0.2593	1.1264	1.3856
			Dy-160	1.00				
		Tb-161	6.906 d	B-	–	0.2025	0.0365	0.2390
			Dy-161	1.00				
		Tb-162	7.60 m	B-	–	0.5327	1.1066	1.6393
			Dy-162	1.00				
		Tb-163	19.5 m	B-	–	0.3597	0.7887	1.1484
			Dy-163	1.00				
		Tb-164	3.0 m	B-	–	0.8249	2.4455	3.2704
			Dy-164	1.00				
		Tb-165	2.11 m	B-	–	0.8966	0.8363	1.7330
			Dy-165m	8.9028E-01				
			Dy-165	1.0972E-01				
66	Dysprosium	Dy-148	3.3 m	ECB+	–	0.0278	0.7170	0.7448
			Tb-148	1.00				
		Dy-149	4.20 m	ECB+	–	0.1120	1.6222	1.7342
			Tb-149	5.6682E-01				
			Tb-149m	4.3318E-01				
		Dy-150	7.17 m	ECB+A	1.5664	0.0070	0.2785	1.8519
			Tb-150	6.4000E-01				
			Gd-146	3.6000E-01				
		Dy-151	17.9 m	ECB+A	0.2341	0.0653	1.3723	1.6717
			Tb-151	5.3377E-01				
			Tb-151m	4.1023E-01				
			Gd-147	5.6000E-02				
		Dy-152	2.38 h	ECA	0.0037	0.0130	0.2867	0.3034
			Tb-152	9.9900E-01				
			Gd-148	1.0000E-03				
		Dy-153	6.4 h	ECB+A	0.0003	0.0901	0.8746	0.9651
			Tb-153	1.00				
			Gd-149	9.4000E-05				
		Dy-154	3.0E+6 y	A	2.9470	–	–	2.9470
			Gd-150	1.00				

(*continued on next page*)

Table A.1 continued

Z	Element	Nuclide	Half-life	Decay mode	Emitted energy (MeV/nt)			
					Alpha	Electron	Photon	Total
		Dy-155	9.9 h	ECB+	–	0.0272	0.6687	0.6959
			Tb-155	1.00				
		Dy-157	8.14 h	EC	–	0.0138	0.3472	0.3610
			Tb-157	1.00				
		Dy-159	144.4 d	EC	–	0.0131	0.0456	0.0587
			Tb-159	1.00				
		Dy-165	2.334 h	B-	–	0.4473	0.0267	0.4740
			Ho-165	1.00				
		Dy-165m	1.257 m	ITB-	–	0.1049	0.0192	0.1240
			Dy-165	9.7760E-01				
			Ho-165	2.2400E-02				
		Dy-166	81.6 h	B-	–	0.1667	0.0433	0.2100
			Ho-166	1.00				
		Dy-167	6.20 m	B-	–	0.7262	0.5326	1.2589
			Ho-167	1.00				
		Dy-168	8.7 m	B-	–	0.4332	0.3948	0.8280
			Ho-168	1.00				
67	Holmium	Ho-150	76.8 s	ECB+	–	1.9857	1.8843	3.8701
			Dy-150	1.00				
		Ho-153	2.01 m	ECB+A	0.0020	0.5387	1.0281	1.5689
			Dy-153	9.9949E-01				
			Tb-149m	5.1000E-04				
		Ho-153m	9.3 m	ECB+A	0.0074	0.6952	1.0618	1.7644
			Dy-153	9.9820E-01				
			Tb-149	1.8000E-03				
		Ho-154	11.76 m	ECB+A	0.0008	1.0927	1.8817	2.9752
			Dy-154	9.9981E-01				
			Tb-150	1.9000E-04				
		Ho-154m	3.10 m	ECB+A	<E-04	0.5434	2.4367	2.9801
			Dy-154	1.00				
			Tb-150m	1.0000E-05				
		Ho-155	48 m	ECB+	–	0.2176	0.6142	0.8318
			Dy-155	1.00				
		Ho-156	56 m	ECB+	–	0.6655	2.1064	2.7719
			Dy-156	1.00				
		Ho-157	12.6 m	ECB+	–	0.0929	0.5835	0.6764
			Dy-157	1.00				
		Ho-159	33.05 m	ECB+	–	0.0576	0.3857	0.4433
			Dy-159	1.00				
		Ho-160	25.6 m	ECB+	–	0.0703	1.6950	1.7653
			Dy-160	1.00				
		Ho-161	2.48 h	EC	–	0.0336	0.0582	0.0918
			Dy-161	1.00				
		Ho-162	15.0 m	ECB+	–	0.0598	0.1640	0.2239
			Dy-162	1.00				
		Ho-162m	67.0 m	ITECB+	–	0.0739	0.5614	0.6353
			Ho-162	6.2000E-01				
			Dy-162	3.8000E-01				

Table A.1 continued

Z	Element	Nuclide	Half-life	Decay mode	Emitted energy (MeV/nt)			
					Alpha	Electron	Photon	Total
		Ho-163	4570 y	EC	–	0.0005	<E-04	0.0006
			Dy-163	1.00				
		Ho-164	29 m	ECB-	–	0.1470	0.0297	0.1768
			Dy-164	6.0000E-01				
			Er-164	4.0000E-01				
		Ho-164m	38.0 m	IT	–	0.0926	0.0472	0.1399
			Ho-164	1.00				
		Ho-166	26.80 h	B-	–	0.6963	0.0301	0.7264
			Er-166	1.00				
		Ho-166m	1.20E+3 y	B-	–	0.1497	1.6249	1.7746
			Er-166	1.00				
		Ho-167	3.1 h	B-	–	0.2329	0.3661	0.5990
			Er-167	1.00				
		Ho-168	2.99 m	B-	–	0.8138	0.8762	1.6901
			Er-168	1.00				
		Ho-168m	132 s	IT	–	0.0518	0.0073	0.0590
			Ho-168	1.00				
		Ho-170	2.76 m	B-	–	0.8366	1.7041	2.5407
			Er-170	1.00				
68	Erbium	Er-154	3.73 m	ECB+A	0.0201	0.0376	0.0759	0.1336
			Ho-154	9.9530E-01				
			Dy-150	4.7000E-03				
		Er-156	19.5 m	EC	–	0.0943	0.0678	0.1621
			Ho-156	1.00				
		Er-159	36 m	ECB+	–	0.0738	0.9635	1.0373
			Ho-159	1.00				
		Er-161	3.21 h	ECB+	–	0.0522	0.9905	1.0427
			Ho-161	1.00				
		Er-163	75.0 m	ECB+	–	0.0081	0.0403	0.0484
			Ho-163	1.00				
		Er-165	10.36 h	EC	–	0.0080	0.0379	0.0459
			Ho-165	1.00				
		Er-167m	2.269 s	IT	–	0.1111	0.0967	0.2078
			Er-167	1.00				
		Er-169	9.40 d	B-	–	0.1035	<E-04	0.1035
			Tm-169	1.00				
		Er-171	7.516 h	B-	–	0.4205	0.3731	0.7936
			Tm-171	1.00				
		Er-172	49.3 h	B-	–	0.1387	0.5166	0.6552
			Tm-172	1.00				
		Er-173	1.434 m	B-	–	0.7213	0.8313	1.5526
			Tm-173	1.00				
69	Thulium	Tm-161	30.2 m	ECB+	–	0.2308	1.2992	1.5300
			Er-161	1.00				
		Tm-162	21.70 m	ECB+	–	0.5648	1.9155	2.4803
			Er-162	1.00				

(*continued on next page*)

Table A.1 continued

Z	Element	Nuclide	Half-life	Decay mode	Emitted energy (MeV/nt)			
					Alpha	Electron	Photon	Total
		Tm-163	1.810 h	ECB+	–	0.0716	1.3200	1.3916
			Er-163	1.00				
		Tm-164	2.0 m	ECB+	–	0.5994	0.7760	1.3754
			Er-164	1.00				
		Tm-165	30.06 h	ECB+	–	0.0637	0.5625	0.6262
			Er-165	1.00				
		Tm-166	7.70 h	ECB+	–	0.0892	1.9768	2.0660
			Er-166	1.00				
		Tm-167	9.25 d	EC	–	0.1332	0.1482	0.2814
			Er-167	1.00				
		Tm-168	93.1 d	ECB+B-	–	0.0847	1.2432	1.3279
			Er-168	9.9990E-01				
			Yb-168	1.0000E-04				
		Tm-170	128.6 d	B-EC	–	0.3280	0.0041	0.3321
			Yb-170	9.9869E-01				
			Er-170	1.3100E-03				
		Tm-171	1.92 y	B-	–	0.0255	0.0006	0.0261
			Yb-171	1.00				
		Tm-172	63.6 h	B-	–	0.5327	0.4744	1.0072
			Yb-172	1.00				
		Tm-173	8.24 h	B-	–	0.3103	0.3885	0.6988
			Yb-173	1.00				
		Tm-174	5.4 m	B-	–	0.5129	1.7787	2.2915
			Yb-174	1.00				
		Tm-175	15.2 m	B-	–	0.5196	1.0848	1.6044
			Yb-175	1.00				
		Tm-176	1.85 m	B-	–	0.9972	1.9682	2.9654
			Yb-176	1.00				
70	Ytterbium	Yb-162	18.87 m	ECB+	–	0.0374	0.2519	0.2893
			Tm-162	1.00				
		Yb-163	11.05 m	ECB+	–	0.2718	0.7277	0.9996
			Tm-163	1.00				
		Yb-164	75.8 m	EC	–	0.0095	0.0542	0.0637
			Tm-164	1.00				
		Yb-165	9.9 m	ECB+	–	0.1518	0.3390	0.4908
			Tm-165	1.00				
		Yb-166	56.7 h	EC	–	0.0417	0.0868	0.1285
			Tm-166	1.00				
		Yb-167	17.5 m	ECB+	–	0.0952	0.2696	0.3648
			Tm-167	1.00				
		Yb-169	32.026 d	EC	–	0.1471	0.3302	0.4773
			Tm-169	1.00				
		Yb-175	4.185 d	B-	–	0.1308	0.0391	0.1699
			Lu-175	1.00				
		Yb-177	1.911 h	B-	–	0.4358	0.1952	0.6309
			Lu-177	1.00				
		Yb-178	74 m	B-	–	0.1925	0.0381	0.2306
			Lu-178	1.00				

Table A.1 continued

Z	Element	Nuclide	Half-life	Decay mode	Emitted energy (MeV/nt)			
					Alpha	Electron	Photon	Total
		Yb-179	8.0 m	B-	–	0.7093	0.9743	1.6836
			Lu-179	1.00				
71	Lutetium	Lu-165	10.74 m	ECB+	–	0.3751	1.1102	1.4853
			Yb-165	1.00				
		Lu-167	51.5 m	ECB+	–	0.1109	1.6920	1.8030
			Yb-167	1.00				
		Lu-169	34.06 h	ECB+	–	0.0477	1.3166	1.3643
			Yb-169	1.00				
		Lu-169m	160 s	IT	–	0.0274	0.0017	0.0290
			Lu-169	1.00				
		Lu-170	2.012 d	ECB+	–	0.0585	2.5636	2.6220
			Yb-170	1.00				
		Lu-171	8.24 d	ECB+	–	0.0928	0.6503	0.7431
			Yb-171	1.00				
		Lu-171m	79 s	IT	–	0.0691	0.0021	0.0711
			Lu-171	1.00				
		Lu-172	6.70 d	ECB+	–	0.1154	1.9565	2.0718
			Yb-172	1.00				
		Lu-172m	3.7 m	IT	–	0.0404	0.0015	0.0419
			Lu-172	1.00				
		Lu-173	1.37 y	EC	–	0.0526	0.1834	0.2360
			Yb-173	1.00				
		Lu-174	3.31 y	ECB+	–	0.0458	0.1163	0.1621
			Yb-174	1.00				
		Lu-174m	142 d	ITEC	–	0.1188	0.0626	0.1814
			Lu-174	9.9380E-01				
			Yb-174	6.2000E-03				
		Lu-176	3.85E+10 y	B-	–	0.3026	0.4799	0.7825
			Hf-176	1.00				
		Lu-176m	3.635 h	B-EC	–	0.4783	0.0146	0.4929
			Hf-176	9.9905E-01				
			Yb-176	9.5000E-04				
		Lu-177	6.647 d	B-	–	0.1479	0.0351	0.1830
			Hf-177	1.00				
		Lu-177m	160.4 d	B-IT	–	0.2687	1.0005	1.2692
			Lu-177	2.1700E-01				
			Hf-177	7.8300E-01				
		Lu-178	28.4 m	B-	–	0.7561	0.1256	0.8817
			Hf-178	1.00				
		Lu-178m	23.1 m	B-	–	0.4907	1.0481	1.5389
			Hf-178	1.00				
		Lu-179	4.59 h	B-	–	0.4869	0.0298	0.5167
			Hf-179	1.00				
		Lu-180	5.7 m	B-	–	0.6352	1.5148	2.1499
			Hf-180	1.00				
		Lu-181	3.5 m	B-	–	0.8512	0.5740	1.4252
			Hf-181	1.00				

(*continued on next page*)

Table A.1 continued

Z	Element	Nuclide	Half-life	Decay mode	Emitted energy (MeV/nt)			
					Alpha	Electron	Photon	Total
72	Hafnium	Hf-167	2.05 m	ECB+	–	0.4952	0.6171	1.1123
			Lu-167	1.00				
		Hf-169	3.24 m	ECB+	–	0.1309	0.6416	0.7725
			Lu-169	9.6904E-01				
			Lu-169m	3.0960E-02				
		Hf-170	16.01 h	EC	–	0.0687	0.4403	0.5090
			Lu-170	1.00				
		Hf-172	1.87 y	EC	–	0.0828	0.1062	0.1890
			Lu-172m	1.00				
		Hf-173	23.6 h	ECB+	–	0.0524	0.3970	0.4494
			Lu-173	1.00				
		Hf-174	2.0E+15 y	A	2.4948	–	–	2.4948
			Yb-170	1.00				
		Hf-175	70 d	EC	–	0.0450	0.3534	0.3984
			Lu-175	1.00				
		Hf-177m	51.4 m	IT	–	0.5078	2.2864	2.7941
			Hf-177	1.00				
		Hf-178m	31 y	IT	–	0.2113	2.2383	2.4496
			Hf-178	1.00				
		Hf-179m	25.05 d	IT	–	0.1897	0.9207	1.1104
			Hf-179	1.00				
		Hf-180m	5.5 h	ITB-	–	0.1437	0.9884	1.1321
			Hf-180	9.9700E-01				
			Ta-180m	3.0000E-03				
		Hf-181	42.39 d	B-	–	0.2052	0.5324	0.7377
			Ta-181	1.00				
		Hf-182	9E+6 y	B-	–	0.0632	0.2397	0.3030
			Ta-182	1.00				
		Hf-182m	61.5 m	B-IT	–	0.2441	0.9135	1.1575
			Ta-182	4.9070E-01				
			Hf-182	4.2000E-01				
			Ta-182m	8.9280E-02				
		Hf-183	1.067 h	B-	–	0.4478	0.7749	1.2227
			Ta-183	1.00				
		Hf-184	4.12 h	B-	–	0.4787	0.2387	0.7174
			Ta-184	1.00				
73	Tantalum	Ta-170	6.76 m	ECB+	–	1.6049	1.0602	2.6652
			Hf-170	1.00				
		Ta-172	36.8 m	ECB+	–	0.5513	1.6967	2.2480
			Hf-172	1.00				
		Ta-173	3.14 h	ECB+	–	0.1686	0.5824	0.7510
			Hf-173	1.00				
		Ta-174	1.14 h	ECB+	–	0.4670	0.9767	1.4438
			Hf-174	1.00				
		Ta-175	10.5 h	ECB+	–	0.0663	1.1126	1.1790
			Hf-175	1.00				
		Ta-176	8.09 h	ECB+	–	0.0849	2.2322	2.3171
			Hf-176	1.00				

Table A.1 continued

Z	Element	Nuclide	Half-life	Decay mode	Emitted energy (MeV/nt)			
					Alpha	Electron	Photon	Total
		Ta-177	56.56 h	EC	–	0.0240	0.0678	0.0917
			Hf-177	1.00				
		Ta-178	9.31 m	ECB+	–	0.0391	0.1218	0.1609
			Hf-178	1.00				
		Ta-178m	2.36 h	EC	–	0.1616	1.1558	1.3174
			Hf-178	1.00				
		Ta-179	1.82 y	EC	–	0.0078	0.0256	0.0334
			Hf-179	1.00				
		Ta-180	8.152 h	ECB-	–	0.0565	0.0482	0.1048
			Hf-180	8.6000E-01				
			W-180	1.4000E-01				
		Ta-182	114.43 d	B-	–	0.2105	1.2918	1.5023
			W-182	1.00				
		Ta-182m	15.84 m	IT	–	0.2665	0.2659	0.5324
			Ta-182	1.00				
		Ta-183	5.1 d	B-	–	0.3537	0.2963	0.6499
			W-183	1.00				
		Ta-184	8.7 h	B-	–	0.5426	1.5727	2.1152
			W-184	1.00				
		Ta-185	49.4 m	B-	–	0.7416	0.1547	0.8963
			W-185	1.00				
		Ta-186	10.5 m	B-	–	1.0710	1.4202	2.4912
			W-186	1.00				
74	Tungsten	W-177	132 m	ECB+	–	0.0970	0.9185	1.0155
			Ta-177	1.00				
		W-178	21.6 d	EC	–	0.0075	0.0164	0.0239
			Ta-178	1.00				
		W-179	37.05 m	EC	–	0.0326	0.0554	0.0880
			Ta-179	1.00				
		W-179m	6.40 m	ITEC	–	0.1661	0.0561	0.2221
			W-179	9.9720E-01				
			Ta-179	2.8000E-03				
		W-181	121.2 d	EC	–	0.0129	0.0404	0.0533
			Ta-181	1.00				
		W-185	75.1 d	B-	–	0.1270	<E-04	0.1270
			Re-185	1.00				
		W-185m	1.597 m	IT	–	0.1738	0.0287	0.2025
			W-185	1.00				
		W-187	23.72 h	B-	–	0.2995	0.4483	0.7478
			Re-187	1.00				
		W-188	69.78 d	B-	–	0.0997	0.0019	0.1016
			Re-188	1.00				
		W-190	30.0 m	B-	–	0.4771	0.1511	0.6282
			Re-190	1.00				
75	Rhenium	Re-178	13.2 m	ECB+	–	0.6192	1.7085	2.3277
			W-178	1.00				

(continued on next page)

Table A.1 continued

Z	Element	Nuclide	Half-life	Decay mode	Emitted energy (MeV/nt)			
					Alpha	Electron	Photon	Total
		Re-179	19.5 m	ECB+	–	0.0668	1.0841	1.1509
			W-179	7.6079E-01				
			W-179m	2.3921E-01				
		Re-180	2.44 m	ECB+	–	0.1720	1.2028	1.3748
			W-180	1.00				
		Re-181	19.9 h	ECB+	–	0.1360	0.8044	0.9404
			W-181	1.00				
		Re-182	64.0 h	EC	–	0.2045	1.7982	2.0027
			W-182	1.00				
		Re-182m	12.7 h	ECB+	–	0.0922	1.2214	1.3136
			W-182	1.00				
		Re-183	70.0 d	EC	–	0.1093	0.1575	0.2667
			W-183	1.00				
		Re-184	38.0 d	ECB+	–	0.0562	0.8919	0.9481
			W-184	1.00				
		Re-184m	169 d	ITEC	–	0.1413	0.3836	0.5249
			Re-184	7.5400E-01				
			W-184	2.4600E-01				
		Re-186	3.7183 d	B-EC	–	0.3362	0.0208	0.3570
			Os-186	9.2530E-01				
			W-186	7.4700E-02				
		Re-186m	2.00E+5 y	IT	–	0.1267	0.0207	0.1474
			Re-186	1.00				
		Re-187	4.12E+10 y	B-	–	0.0006	–	0.0006
			Os-187	1.00				
		Re-188	17.0040 h	B-	–	0.7793	0.0613	0.8406
			Os-188	1.00				
		Re-188m	18.59 m	IT	–	0.0976	0.0715	0.1692
			Re-188	1.00				
		Re-189	24.3 h	B-	–	0.3260	0.0556	0.3816
			Os-189m	1.2211E-01				
			Os-189	8.7789E-01				
		Re-190	3.1 m	B-	–	0.6863	1.3376	2.0239
			Os-190	1.00				
		Re-190m	3.2 h	B-IT	–	0.4456	0.9257	1.3714
			Re-190	4.5600E-01				
			Os-190	5.4400E-01				
76	Osmium	Os-180	21.5 m	ECB+	–	0.0298	0.1265	0.1564
			Re-180	1.00				
		Os-181	105 m	ECB+	–	0.0918	1.3835	1.4753
			Re-181	1.00				
		Os-182	22.10 h	EC	–	0.0565	0.4317	0.4882
			Re-182m	1.00				
		Os-183	13.0 h	ECB+	–	0.0792	0.6288	0.7081
			Re-183	1.00				
		Os-183m	9.9 h	ECB+IT	–	0.0416	1.0062	1.0478
			Re-183	8.5000E-01				
			Os-183	1.5000E-01				

Table A.1 continued

Z	Element	Nuclide	Half-life	Decay mode	Emitted energy (MeV/nt)			
					Alpha	Electron	Photon	Total
		Os-185	93.6 d	EC	–	0.0184	0.6917	0.7101
			Re-185	1.00				
		Os-186	2.0E+15 y	A	2.8220	–	–	2.8220
			W-182	1.00				
		Os-189m	5.8 h	IT	–	0.0286	0.0023	0.0309
			Os-189	1.00				
		Os-190m	9.9 m	IT	–	0.1166	1.5894	1.7059
			Os-190	1.00				
		Os-191	15.4 d	B-	–	0.1372	0.0843	0.2215
			Ir-191	1.00				
		Os-191m	13.10 h	IT	–	0.0664	0.0080	0.0744
			Os-191	1.00				
		Os-193	30.11 h	B-	–	0.3797	0.0674	0.4471
			Ir-193m	3.4757E-03				
			Ir-193	9.9652E-01				
		Os-194	6.0 y	B-	–	0.0453	0.0045	0.0498
			Ir-194	1.00				
		Os-196	34.9 m	B-	–	0.3807	0.0805	0.4612
			Ir-196	1.00				
77	Iridium	Ir-180	1.5 m	ECB+	–	1.2439	1.5955	2.8394
			Os-180	1.00				
		Ir-182	15 m	ECB+	–	1.0474	1.4121	2.4595
			Os-182	1.00				
		Ir-183	58 m	ECB+	–	0.1516	1.1889	1.3404
			Os-183m	7.0972E-01				
			Os-183	2.9028E-01				
		Ir-184	3.09 h	ECB+	–	0.3194	1.9644	2.2838
			Os-184	1.00				
		Ir-185	14.4 h	ECB+	–	0.1228	0.8581	0.9809
			Os-185	1.00				
		Ir-186	16.64 h	ECB+	–	0.1453	1.6651	1.8104
			Os-186	1.00				
		Ir-186m	1.92 h	ECB+IT	–	0.1103	1.2523	1.3626
			Os-186	7.5000E-01				
			Ir-186	2.5000E-01				
		Ir-187	10.5 h	ECB+	–	0.0568	0.3325	0.3892
			Os-187	1.00				
		Ir-188	41.5 h	ECB+	–	0.0508	2.0974	2.1483
			Os-188	1.00				
		Ir-189	13.2 d	EC	–	0.0458	0.0793	0.1251
			Os-189m	7.4264E-02				
			Os-189	9.2574E-01				
		Ir-190	11.78 d	EC	–	0.0746	1.4768	1.5514
			Os-190	1.00				
		Ir-190m	1.120 h	IT	–	0.0240	0.0024	0.0264
			Ir-190	1.00				

(*continued on next page*)

Table A.1 continued

Z	Element	Nuclide	Half-life	Decay mode	Emitted energy (MeV/nt)			
					Alpha	Electron	Photon	Total
		Ir-190n	3.087 h	ECIT	–	0.0289	0.0577	0.0867
			Os-190m	9.1400E-01				
			Ir-190	8.6000E-02				
		Ir-191m	4.94 s	IT	–	0.0971	0.0764	0.1735
			Ir-191	1.00				
		Ir-192	73.827 d	B-EC	–	0.2177	0.8165	1.0342
			Pt-192	9.5130E-01				
			Os-192	4.8700E-02				
		Ir-192m	1.45 m	ITB-	–	0.0540	0.0029	0.0569
			Ir-192	9.9983E-01				
			Pt-192	1.7500E-04				
		Ir-192n	241 y	IT	–	0.1617	0.0066	0.1682
			Ir-192	1.00				
		Ir-193m	10.53 d	IT	–	0.0776	0.0027	0.0803
			Ir-193	1.00				
		Ir-194	19.28 h	B-	–	0.8105	0.0911	0.9015
			Pt-194	1.00				
		Ir-194m	171 d	B-	–	0.1422	2.3339	2.4761
			Pt-194	1.00				
		Ir-195	2.5 h	B-	–	0.3803	0.0593	0.4397
			Pt-195	1.00				
		Ir-195m	3.8 h	B-IT	–	0.2606	0.3766	0.6372
			Pt-195m	4.3692E-01				
			Ir-195	5.0000E-02				
			Pt-195	5.1308E-01				
		Ir-196	52 s	B-	–	1.1738	0.2322	1.4060
			Pt-196	1.00				
		Ir-196m	1.40 h	B-	–	0.3844	2.4677	2.8522
			Pt-196	1.00				
78	Platinum	Pt-184	17.3 m	ECB+A	<E-04	0.2004	0.7266	0.9271
			Ir-184	1.00				
			Os-180	1.7000E-05				
		Pt-186	2.08 h	ECA	<E-04	0.0451	0.6844	0.7296
			Ir-186m	8.1942E-01				
			Ir-186	1.8058E-01				
			Os-182	1.0000E-06				
		Pt-187	2.35 h	ECB+	–	0.1549	0.6183	0.7732
			Ir-187	1.00				
		Pt-188	10.2 d	ECA	<E-04	0.0823	0.2055	0.2878
			Ir-188	1.00				
			Os-184	2.9000E-07				
		Pt-189	10.87 h	ECB+	–	0.0996	0.4870	0.5867
			Ir-189	1.00				
		Pt-190	6.50E+11 y	A	3.2490	–	–	3.2490
			Os-186	1.00				
		Pt-191	2.802 d	EC	–	0.0749	0.2960	0.3709
			Ir-191	1.00				

Table A.1 continued

Z	Element	Nuclide	Half-life	Decay mode	Emitted energy (MeV/nt)			
					Alpha	Electron	Photon	Total
		Pt-193	50 y	EC	–	0.0071	0.0026	0.0097
			Ir-193	1.00				
		Pt-193m	4.33 d	IT	–	0.1377	0.0132	0.1510
			Pt-193	1.00				
		Pt-195m	4.02 d	IT	–	0.1845	0.0772	0.2617
			Pt-195	1.00				
		Pt-197	19.8915 h	B-	–	0.2552	0.0256	0.2809
			Au-197	1.00				
		Pt-197m	95.41 m	ITB-	–	0.3250	0.0839	0.4089
			Pt-197	9.6700E-01				
			Au-197	3.3000E-02				
		Pt-199	30.80 m	B-	–	0.5455	0.1995	0.7450
			Au-199	1.00				
		Pt-200	12.5 h	B-	–	0.2321	0.0605	0.2926
			Au-200	1.00				
		Pt-202	44 h	B-	–	0.6537	–	0.6537
			Au-202	1.00				
79	Gold	Au-186	10.7 m	ECB+	–	1.0751	1.4983	2.5735
			Pt-186	1.00				
		Au-187	8.4 m	ECB+A	0.0001	0.1360	1.0652	1.2014
			Pt-187	1.00				
			Ir-183	3.0000E-05				
		Au-190	42.8 m	ECB+	–	0.2129	2.3807	2.5936
			Pt-190	1.00				
		Au-191	3.18 h	ECB+	–	0.0865	0.5946	0.6811
			Pt-191	1.00				
		Au-192	4.94 h	ECB+	–	0.0904	1.9392	2.0296
			Pt-192	1.00				
		Au-193	17.65 h	EC	–	0.0575	0.1673	0.2249
			Pt-193	1.00				
		Au-193m	3.9 s	ITEC	–	0.0904	0.1979	0.2883
			Au-193	9.9970E-01				
			Pt-193m	3.0000E-04				
		Au-194	38.02 h	ECB+	–	0.0421	1.0386	1.0806
			Pt-194	1.00				
		Au-195	186.098 d	EC	–	0.0520	0.0839	0.1359
			Pt-195	1.00				
		Au-195m	30.5 s	IT	–	0.1172	0.2014	0.3186
			Au-195	1.00				
		Au-196	6.183 d	ECB-	–	0.0372	0.4734	0.5105
			Pt-196	9.2800E-01				
			Hg-196	7.2000E-02				
		Au-196m	9.6 h	IT	–	0.3760	0.2473	0.6233
			Au-196	1.00				
		Au-198	2.69517 d	B-	–	0.3277	0.4029	0.7306
			Hg-198	1.00				

(*continued on next page*)

Table A.1 continued

Z	Element	Nuclide	Half-life	Decay mode	Emitted energy (MeV/nt)			
					Alpha	Electron	Photon	Total
		Au-198m	2.27 d	IT	–	0.2748	0.5332	0.8080
			Au-198	1.00				
		Au-199	3.139 d	B-	–	0.1451	0.0961	0.2412
			Hg-199	1.00				
		Au-200	48.4 m	B-	–	0.7303	0.2737	1.0041
			Hg-200	1.00				
		Au-200m	18.7 h	B-IT	–	0.2433	1.9843	2.2276
			Au-200	1.8000E-01				
			Hg-200	8.2000E-01				
		Au-201	26 m	B-	–	0.4259	0.0346	0.4605
			Hg-201	1.00				
		Au-202	28.8 s	B-	–	1.0749	0.1720	1.2469
			Hg-202	1.00				
80	Mercury	Hg-190	20.0 m	ECB+	–	0.0539	0.2018	0.2557
			Au-190	1.00				
		Hg-191m	50.8 m	ECB+	–	0.1378	1.4895	1.6273
			Au-191	1.00				
		Hg-192	4.85 h	EC	–	0.0636	0.2749	0.3385
			Au-192	1.00				
		Hg-193	3.80 h	ECB+	–	0.0740	0.8377	0.9117
			Au-193	9.6459E-01				
			Au-193m	3.5408E-02				
		Hg-193m	11.8 h	ECB+IT	–	0.0470	1.0239	1.0709
			Au-193m	8.9197E-01				
			Hg-193	7.1000E-02				
			Au-193	3.7027E-02				
		Hg-194	440 y	EC	–	0.0078	0.0027	0.0106
			Au-194	1.00				
		Hg-195	10.53 h	ECB+	–	0.0650	0.2008	0.2658
			Au-195	1.00				
		Hg-195m	41.6 h	ITECB+	–	0.1480	0.2047	0.3527
			Hg-195	5.4200E-01				
			Au-195	4.5800E-01				
		Hg-197	64.94 h	EC	–	0.0702	0.0740	0.1442
			Au-197	1.00				
		Hg-197m	23.8 h	ITEC	–	0.2170	0.0977	0.3148
			Hg-197	9.1400E-01				
			Au-197	8.6000E-02				
		Hg-199m	42.66 m	IT	–	0.3487	0.1836	0.5323
			Hg-199	1.00				
		Hg-203	46.612 d	B-	–	0.0990	0.2380	0.3370
			Tl-203	1.00				
		Hg-205	5.2 m	B-	–	0.5390	0.0053	0.5444
			Tl-205	1.00				
		Hg-206	8.15 m	B-	–	0.4211	0.1215	0.5426
			Tl-206	1.00				
		Hg-207	2.9 m	B-	–	0.8262	2.6614	3.4876
			Tl-207	1.00				

Table A.1 continued

Z	Element	Nuclide	Half-life	Decay mode	Emitted energy (MeV/nt)			
					Alpha	Electron	Photon	Total
81	Thallium	Tl-190	2.6 m	ECB+	–	1.5288	1.2914	2.8202
			Hg-190	1.00				
		Tl-190m	3.7 m	ECB+	–	0.7985	2.4550	3.2535
			Hg-190	1.00				
		Tl-194	33.0 m	ECB+	–	0.5972	0.9143	1.5115
			Hg-194	1.00				
		Tl-194m	32.8 m	ECB+	–	0.3037	2.5218	2.8255
			Hg-194	1.00				
		Tl-195	1.16 h	ECB+	–	0.0740	1.2250	1.2991
			Hg-195	9.9656E-01				
			Hg-195m	3.4358E-03				
		Tl-196	1.84 h	ECB+	–	0.1782	1.8734	2.0516
			Hg-196	1.00				
		Tl-197	2.84 h	ECB+	–	0.0544	0.4587	0.5130
			Hg-197	1.00				
		Tl-198	5.3 h	ECB+	–	0.0414	2.0108	2.0522
			Hg-198	1.00				
		Tl-198m	1.87 h	ECB+IT	–	0.2006	1.2168	1.4175
			Tl-198	4.6000E-01				
			Hg-198	5.4000E-01				
		Tl-199	7.42 h	ECB+	–	0.0600	0.2520	0.3120
			Hg-199	1.00				
		Tl-200	26.1 h	ECB+	–	0.0408	1.3106	1.3514
			Hg-200	1.00				
		Tl-201	72.912 h	EC	–	0.0447	0.0938	0.1385
			Hg-201	1.00				
		Tl-202	12.23 d	EC	–	0.0233	0.4658	0.4891
			Hg-202	1.00				
		Tl-204	3.78 y	B-EC	–	0.2372	0.0013	0.2385
			Pb-204	9.7100E-01				
			Hg-204	2.9000E-02				
		Tl-206	4.200 m	B-	–	0.5398	0.0001	0.5399
			Pb-206	1.00				
		Tl-206m	3.74 m	IT	–	0.2003	2.4192	2.6195
			Tl-206	1.00				
		Tl-207	4.77 m	B-	–	0.4952	0.0024	0.4975
			Pb-207	1.00				
		Tl-208	3.053 m	B-	–	0.6113	3.3603	3.9716
			Pb-208	1.00				
		Tl-209	2.161 m	B-	–	0.6875	2.1426	2.8302
			Pb-209	1.00				
		Tl-210	1.30 m	B-	–	1.2699	2.7632	4.0331
			Pb-210	1.00				
82	Lead	Pb-194	12.0 m	ECB+A	<E-04	0.0844	1.0832	1.1677
			Tl-194	1.00				
			Hg-190	7.3000E-08				

(*continued on next page*)

Table A.1 continued

Z	Element	Nuclide	Half-life	Decay mode	Emitted energy (MeV/nt)			
					Alpha	Electron	Photon	Total
		Pb-195m	15 m	ECB+	–	0.3167	1.6547	1.9714
			Tl-195	1.00				
		Pb-196	37 m	ECB+	–	0.0969	0.4940	0.5909
			Tl-196	1.00				
		Pb-197	8 m	ECB+	–	0.0818	1.5319	1.6137
			Tl-197	1.00				
		Pb-197m	43 m	ECB+IT	–	0.2477	1.1732	1.4209
			Tl-197	8.1000E-01				
			Pb-197	1.9000E-01				
		Pb-198	2.4 h	EC	–	0.0781	0.4385	0.5166
			Tl-198	1.00				
		Pb-199	90 m	ECB+	–	0.0584	1.0394	1.0978
			Tl-199	1.00				
		Pb-200	21.5 h	EC	–	0.0997	0.2086	0.3083
			Tl-200	1.00				
		Pb-201	9.33 h	ECB+	–	0.0594	0.7562	0.8156
			Tl-201	1.00				
		Pb-201m	61 s	IT	–	0.2633	0.3658	0.6291
			Pb-201	1.00				
		Pb-202	5.25E+4 y	ECA	0.0260	0.0061	0.0025	0.0346
			Tl-202	9.9000E-01				
			Hg-198	1.0000E-02				
		Pb-202m	3.53 h	ITEC	–	0.1321	1.9925	2.1246
			Pb-202	9.0500E-01				
			Tl-202	9.5000E-02				
		Pb-203	51.873 h	EC	–	0.0530	0.3143	0.3672
			Tl-203	1.00				
		Pb-204m	67.2 m	IT	–	0.1030	2.0634	2.1664
			Pb-204	1.00				
		Pb-205	1.53E+7 y	EC	–	0.0062	0.0025	0.0087
			Tl-205	1.00				
		Pb-209	3.253 h	B-	–	0.1974	–	0.1974
			Bi-209	1.00				
		Pb-210	22.20 y	B-A	<E-04	0.0404	0.0053	0.0457
			Bi-210	1.00				
			Hg-206	1.9000E-08				
		Pb-211	36.1 m	B-	–	0.4543	0.0644	0.5187
			Bi-211	1.00				
		Pb-212	10.64 h	B-	–	0.1766	0.1450	0.3217
			Bi-212	1.00				
		Pb-214	26.8 m	B-	–	0.2948	0.2533	0.5481
			Bi-214	1.00				
83	Bismuth	Bi-197	9.3 m	ECB+	–	0.2887	1.6992	1.9879
			Pb-197	5.6103E-01				
			Pb-197m	4.3897E-01				
		Bi-200	36.4 m	ECB+	–	0.2469	2.4355	2.6825
			Pb-200	1.00				

Table A.1 continued

Z	Element	Nuclide	Half-life	Decay mode	Emitted energy (MeV/nt)			
					Alpha	Electron	Photon	Total
		Bi-201	108 m	ECB+	–	0.0612	1.7304	1.7916
			Pb-201	5.4833E-01				
			Pb-201m	4.5167E-01				
		Bi-202	1.72 h	ECB+	–	0.1515	2.7561	2.9076
			Pb-202	1.00				
		Bi-203	11.76 h	ECB+	–	0.0809	2.3850	2.4659
			Pb-203	1.00				
		Bi-204	11.22 h	ECB+	–	0.0807	2.9162	2.9968
			Pb-204m	9.8525E-02				
			Pb-204	9.0148E-01				
		Bi-205	15.31 d	ECB+	–	0.0346	1.6913	1.7259
			Pb-205	1.00				
		Bi-206	6.243 d	ECB+	–	0.1379	3.2796	3.4175
			Pb-206	1.00				
		Bi-207	32.9 y	ECB+	–	0.1193	1.5370	1.6563
			Pb-207	1.00				
		Bi-208	3.68E+5 y	EC	–	0.0144	2.6460	2.6604
			Pb-208	1.00				
		Bi-210	5.013 d	B-A	<E-04	0.3889	<E-04	0.3889
			Po-210	1.00				
			Tl-206	1.3200E-06				
		Bi-210m	3.04E+6 y	A	5.0064	0.0475	0.2607	5.3146
			Tl-206	1.00				
		Bi-211	2.14 m	A B-	6.6757	0.0100	0.0473	6.7330
			Tl-207	9.9724E-01				
			Po-211	2.7600E-03				
		Bi-212	60.55 m	B-A	2.2164	0.5046	0.1038	2.8247
			Po-212	6.4060E-01				
			Tl-208	3.5940E-01				
		Bi-212n	7.0 m	B-	–	0.5351	–	0.5351
			Po-212m	1.00				
		Bi-213	45.59 m	B-A	0.1245	0.4440	0.1277	0.6963
			Po-213	9.7910E-01				
			Tl-209	2.0900E-02				
		Bi-214	19.9 m	B-A	0.0012	0.6631	1.4793	2.1436
			Po-214	9.9979E-01				
			Tl-210	2.1000E-04				
		Bi-215	7.6 m	B-	–	0.6694	0.2534	0.9228
			Po-215	1.00				
		Bi-216	2.17 m	B-	–	1.3295	0.7385	2.0680
			Po-216	1.00				
84	Polonium	Po-203	36.7 m	ECB+A	0.0060	0.1672	1.6348	1.8080
			Bi-203	9.9890E-01				
			Pb-199	1.1000E-03				
		Po-204	3.53 h	ECA	0.0362	0.1839	1.1650	1.3850
			Bi-204	9.9340E-01				
			Pb-200	6.6000E-03				

(*continued on next page*)

Table A.1 continued

Z	Element	Nuclide	Half-life	Decay mode	Emitted energy (MeV/nt)			
					Alpha	Electron	Photon	Total
		Po-205	1.66 h	ECB+A	0.0021	0.0660	1.5846	1.6527
			Bi-205	9.9900E-01				
			Pb-201	4.0000E-04				
		Po-206	8.8 d	ECA	0.2903	0.1655	1.1928	1.6486
			Bi-206	9.4550E-01				
			Pb-202	5.4500E-02				
		Po-207	5.80 h	ECB+A	0.0011	0.0490	1.2847	1.3347
			Bi-207	9.9979E-01				
			Pb-203	2.1000E-04				
		Po-208	2.898 y	AEC	5.2154	<E-04	<E-04	5.2154
			Bi-208	2.2300E-05				
			Pb-204	9.9998E-01				
		Po-209	102 y	AEC	4.9529	0.0030	0.0063	4.9622
			Pb-205	9.9520E-01				
			Bi-209	4.8000E-03				
		Po-210	138.376 d	A	5.4075	<E-04	<E-04	5.4075
			Pb-206	1.00				
		Po-211	0.516 s	A	7.5860	0.0002	0.0082	7.5944
			Pb-207	1.00				
		Po-212	2.99E-7 s	A	8.9541	–	–	8.9541
			Pb-208	1.00				
		Po-212m	45.1 s	A	11.7755	0.0004	0.0792	11.8551
			Pb-208	9.9930E-01				
		Po-213	4.2E-6 s	A	8.5370	<E-04	<E-04	8.5370
			Pb-209	1.00				
		Po-214	1.643E-4 s	A	7.8334	<E-04	<E-04	7.8335
			Pb-210	1.00				
		Po-215	1.781E-3 s	A	7.5261	<E-04	0.0002	7.5263
			Pb-211	1.00				
		Po-216	0.145 s	A	6.9064	<E-04	<E-04	6.9064
			Pb-212	1.00				
		Po-218	3.10 m	A B-	6.1134	<E-04	–	6.1135
			Pb-214	9.9980E-01				
			At-218	2.0000E-04				
85	Astatine	At-204	9.2 m	ECB+A	0.2307	0.4485	2.3234	3.0025
			Po-204	9.6200E-01				
			Bi-200	3.8000E-02				
		At-205	26.2 m	ECB+A	0.6021	0.2575	1.1444	2.0039
			Po-205	9.0000E-01				
			Bi-201	1.0000E-01				
		At-206	30.6 m	ECB+A	0.0517	0.3324	2.4807	2.8647
			Po-206	9.9110E-01				
			Bi-202	8.9000E-03				
		At-207	1.80 h	ECB+A	0.5049	0.1298	2.0136	2.6483
			Po-207	9.1400E-01				
			Bi-203	8.6000E-02				

Table A.1 continued

Z	Element	Nuclide	Half-life	Decay mode	Emitted energy (MeV/nt)			
					Alpha	Electron	Photon	Total
		At-208	1.63 h	ECB+A	0.0316	0.1598	3.0408	3.2322
			Po-208	9.9450E-01				
			Bi-204	5.5000E-03				
		At-209	5.41 h	ECB+A	0.2360	0.1172	2.2846	2.6378
			Po-209	9.5900E-01				
			Bi-205	4.1000E-02				
		At-210	8.1 h	ECB+A	0.0097	0.0796	2.9622	3.0515
			Po-210	9.9825E-01				
			Bi-206	1.7500E-03				
		At-211	7.214 h	ECA	2.4998	0.0059	0.0367	2.5424
			Po-211	5.8200E-01				
			Bi-207	4.1800E-01				
		At-215	1.00E-4 s	A	8.1778	<E-04	0.0002	8.1780
			Bi-211	1.00				
		At-216	3.00E-4 s	A	7.9407	0.0013	0.0025	7.9446
			Bi-212	1.00				
		At-217	3.23E-2 s	A	7.2008	<E-04	0.0002	7.2011
			Bi-213	9.9988E-01				
		At-218	1.5 s	A B-	6.8042	0.0011	–	6.8053
			Bi-214	9.9900E-01				
			Rn-218	1.0000E-03				
		At-219	56 s	A	6.1343	–	–	6.1343
			Bi-215	9.7000E-01				
		At-220	3.71 m	B-A	0.4842	1.2130	0.4497	2.1469
			Rn-220	9.2000E-01				
			Bi-216	8.0000E-02				
86	Radon	Rn-207	9.25 m	ECB+A	1.3126	0.2197	0.9854	2.5177
			At-207	7.9000E-01				
			Po-203	2.1000E-01				
		Rn-209	28.5 m	ECB+A	1.0466	0.1167	1.1953	2.3586
			At-209	8.3000E-01				
			Po-205	1.7000E-01				
		Rn-210	2.4 h	AEC	5.9121	0.0091	0.0610	5.9821
			Po-206	9.6000E-01				
			At-210	4.0000E-02				
		Rn-211	14.6 h	ECB+A	1.6205	0.0663	1.8727	3.5595
			At-211	7.2600E-01				
			Po-207	2.7400E-01				
		Rn-212	23.9 m	A	6.3847	<E-04	0.0003	6.3850
			Po-208	1.00				
		Rn-215	2.30 us	A	8.8390	–	–	8.8390
			Po-211	1.00				
		Rn-216	4.5E-5 s	A	8.2000	–	–	8.2000
			Po-212	1.00				
		Rn-217	5.40E-4 s	A	7.8856	–	–	7.8856
			Po-213	1.00				

(*continued on next page*)

Table A.1 continued

Z	Element	Nuclide	Half-life	Decay mode	Emitted energy (MeV/nt)			
					Alpha	Electron	Photon	Total
		Rn-218	3.5E-2 s	A	7.2618	<E-04	0.0008	7.2626
			Po-214	1.00				
		Rn-219	3.96 s	A	6.8801	0.0068	0.0586	6.9456
			Po-215	1.00				
		Rn-220	55.6 s	A	6.4040	<E-04	0.0006	6.4047
			Po-216	1.00				
		Rn-222	3.8235 d	A	5.5899	<E-04	0.0004	5.5903
			Po-218	1.00				
		Rn-223	24.3 m	B-	–	0.6282	0.3444	0.9726
			Fr-223	1.00				
87	Francium	Fr-212	20.0 m	ECB+A	2.7731	0.1294	1.1415	4.0440
			Rn-212	5.7000E-01				
			At-208	4.3000E-01				
		Fr-219	2.0E-2 s	A	7.4437	0.0004	0.0036	7.4477
			At-215	1.00				
		Fr-220	27.4 s	A B-	6.7413	0.0163	0.0105	6.7680
			At-216	9.9650E-01				
			Ra-220	3.5000E-03				
		Fr-221	4.9 m	A	6.4199	0.0089	0.0294	6.4582
			At-217	1.00				
		Fr-222	14.2 m	B-	–	0.7145	0.1806	0.8951
			Ra-222	1.00				
		Fr-223	22.00 m	B-A	0.0003	0.3829	0.0583	0.4415
			Ra-223	1.00				
			At-219	6.0000E-05				
		Fr-224	3.33 m	B-	–	0.8751	0.5523	1.4274
			Ra-224	1.00				
		Fr-227	2.47 m	B-	–	0.7967	0.4499	1.2466
			Ra-227	1.00				
88	Radium	Ra-219	10 ms	A	7.9071	0.0600	0.1702	8.1372
			Rn-215	1.00				
		Ra-220	1.79E-2 s	A	7.5904	0.0002	0.0047	7.5952
			Rn-216	1.00				
		Ra-221	28 s	A	6.7915	0.0690	0.0390	6.8995
			Rn-217	1.00				
		Ra-222	38.0 s	A	6.6710	0.0009	0.0092	6.6811
			Rn-218	1.00				
		Ra-223	11.43 d	A	5.7702	0.0781	0.1413	5.9895
			Rn-219	1.00				
		Ra-224	3.66 d	A	5.7766	0.0023	0.0104	5.7893
			Rn-220	1.00				
		Ra-225	14.9 d	B-	–	0.1050	0.0145	0.1194
			Ac-225	1.00				
		Ra-226	1600 y	A	4.8603	0.0039	0.0074	4.8716
			Rn-222	1.00				
		Ra-227	42.2 m	B-	–	0.4511	0.1508	0.6019
			Ac-227	1.00				

Table A.1 continued

Z	Element	Nuclide	Half-life	Decay mode	Emitted energy (MeV/nt)			
					Alpha	Electron	Photon	Total
		Ra-228	5.75 y	B-	–	0.0132	0.0031	0.0163
			Ac-228	1.00				
		Ra-230	93 m	B-	–	0.2201	0.0794	0.2995
			Ac-230	1.00				
89	Actinium	Ac-223	2.10 m	A	6.6721	0.0254	0.0190	6.7165
			Fr-219	9.9000E-01				
		Ac-224	2.78 h	ECA	0.5662	0.0490	0.2325	0.8477
			Ra-224	9.0900E-01				
			Fr-220	9.1000E-02				
		Ac-225	10.0 d	A	5.8920	0.0248	0.0171	5.9338
			Fr-221	1.00				
		Ac-226	29.37 h	B-ECA	0.0003	0.2914	0.1327	0.4245
			Th-226	8.3000E-01				
			Ra-226	1.7000E-01				
			Fr-222	6.0000E-05				
		Ac-227	21.772 y	B-A	0.0693	0.0150	0.0011	0.0853
			Th-227	9.8620E-01				
			Fr-223	1.3800E-02				
		Ac-228	6.15 h	B-	–	0.4495	0.8671	1.3166
			Th-228	1.00				
		Ac-230	122 s	B-	–	0.9229	0.5440	1.4668
			Th-230	1.00				
		Ac-231	7.5 m	B-	–	0.6361	0.4190	1.0550
			Th-231	1.00				
		Ac-232	119 s	B-	–	0.9707	1.1528	2.1235
			Th-232	1.00				
		Ac-233	145 s	B-	–	0.8355	0.4993	1.3348
			Th-233	1.00				
90	Thorium	Th-223	0.60 s	A	7.4134	0.0575	0.0754	7.5463
			Ra-219	1.00				
		Th-224	1.05 s	A	7.2635	0.0129	0.0232	7.2996
			Ra-220	1.00				
		Th-226	30.57 m	A	6.4219	0.0211	0.0089	6.4519
			Ra-222	1.00				
		Th-227	18.68 d	A	5.9883	0.0755	0.1317	6.1955
			Ra-223	1.00				
		Th-228	1.9116 y	A	5.4956	0.0210	0.0036	5.5202
			Ra-224	1.00				
		Th-229	7.34E+3 y	A	4.9584	0.1217	0.0971	5.1772
			Ra-225	1.00				
		Th-230	7.538E+4 y	A	4.7538	0.0146	0.0018	4.7702
			Ra-226	1.00				
		Th-231	25.52 h	B-	–	0.1622	0.0269	0.1891
			Pa-231	1.00				
		Th-232	1.405E10 y	A	4.0688	0.0126	0.0015	4.0829
			Ra-228	1.00				

(*continued on next page*)

Table A.1 continued

Z	Element	Nuclide	Half-life	Decay mode	Emitted energy (MeV/nt)			
					Alpha	Electron	Photon	Total
		Th-233	22.3 m	B-	–	0.4140	0.0375	0.4515
			Pa-233	1.00				
		Th-234	24.10 d	B-	–	0.0622	0.0105	0.0728
			Pa-234m	1.00				
		Th-235	7.1 m	B-	–	0.6713	0.0537	0.7251
			Pa-235	1.00				
		Th-236	37.5 m	B-	–	0.3671	0.0346	0.4017
			Pa-236	1.00				
91	Protactinium	Pa-227	38.3 m	AEC	5.5650	0.0226	0.0234	5.6110
			Ac-223	8.5000E-01				
			Th-227	1.5000E-01				
		Pa-228	22 h	ECB+A	0.1217	0.1320	1.3694	1.6230
			Th-228	9.8000E-01				
			Ac-224	2.0000E-02				
		Pa-229	1.50 d	ECA	0.0274	0.0131	0.0666	0.1071
			Th-229	9.9520E-01				
			Ac-225	4.8000E-03				
		Pa-230	17.4 d	ECB-A	0.0002	0.0668	0.6708	0.7377
			Th-230	9.1600E-01				
			U-230	8.4000E-02				
			Ac-226	3.2000E-05				
		Pa-231	3.276E+4 y	A	5.0592	0.0538	0.0450	5.1580
			Ac-227	1.00				
		Pa-232	1.31 d	B-EC	–	0.1738	0.9393	1.1131
			U-232	1.00				
			Th-232	3.0000E-05				
		Pa-233	26.967 d	B-	–	0.2151	0.2229	0.4380
			U-233	1.00				
		Pa-234	6.70 h	B-	–	0.4037	1.4718	1.8755
			U-234	1.00				
		Pa-234m	1.17 m	B-IT	–	0.8171	0.0162	0.8334
			U-234	9.9840E-01				
			Pa-234	1.6000E-03				
		Pa-235	24.5 m	B-	–	0.4886	0.0008	0.4894
			U-235m	9.9990E-01				
			U-235	1.0109E-04				
		Pa-236	9.1 m	B-	–	0.8049	0.9148	1.7197
			U-236	1.00				
		Pa-237	8.7 m	B-	–	0.5780	0.6095	1.1875
			U-237	1.00				
92	Uranium	U-227	1.1 m	A	6.9984	0.0960	0.1199	7.2143
			Th-223	1.00				
		U-228	9.1 m	A	6.6046	0.0231	0.0056	6.6333
			Th-224	9.7500E-01				
		U-230	20.8 d	A	5.9681	0.0216	0.0032	5.9929
			Th-226	1.00				

Table A.1 continued

Z	Element	Nuclide	Half-life	Decay mode	Emitted energy (MeV/nt)			
					Alpha	Electron	Photon	Total
		U-231	4.2 d	ECA	0.0002	0.0847	0.0896	0.1745
			Pa-231	1.00				
			Th-227	4.0000E-05				
		U-232	68.9 y	A	5.3948	0.0164	0.0023	5.4135
			Th-228	1.00				
		U-233	1.592E+5 y	A	4.9013	0.0059	0.0013	4.9085
			Th-229	1.00				
		U-234	2.455E+5 y	A	4.8430	0.0137	0.0020	4.8587
			Th-230	1.00				
		U-235	7.04E+8 y	A	4.4693	0.0530	0.1669	4.6891
			Th-231	1.00				
		U-235m	26 m	IT	–	<E-04	<E-04	<E-04
			U-235	1.00				
		U-236	2.342E+7 y	A	4.5592	0.0114	0.0018	4.5723
			Th-232	1.00				
		U-237	6.75 d	B-	–	0.1991	0.1442	0.3433
			Np-237	1.00				
		U-238	4.468E+9 y	ASF	4.2584	0.0092	0.0014	4.2691
			Th-234	1.00				
			SF	5.4500E-07				
		U-239	23.45 m	B-	–	0.4108	0.0519	0.4626
			Np-239	1.00				
		U-240	14.1 h	B-	–	0.1276	0.0099	0.1374
			Np-240m	1.00				
		U-242	16.8 m	B-	–	0.3859	0.0413	0.4272
			Np-242	1.00				
93	Neptunium	Np-232	14.7 m	ECB+	–	0.1073	1.1969	1.3042
			U-232	1.00				
		Np-233	36.2 m	ECA	<E-04	0.0144	0.0911	0.1055
			U-233	1.00				
			Pa-229	1.0000E-05				
		Np-234	4.4 d	ECB+	–	0.0574	1.1086	1.1660
			U-234	1.00				
		Np-235	396.1 d	ECA	0.0001	0.0105	0.0071	0.0178
			U-235	9.9598E-01				
			U-235m	3.9933E-03				
			Pa-231	2.6000E-05				
		Np-236	1.54E+5 y	ECB-A	0.0074	0.2372	0.1594	0.4039
			U-236	8.7300E-01				
			Pu-236	1.2500E-01				
			Pa-232	1.6000E-03				
		Np-236m	22.5 h	ECB-	–	0.0880	0.0507	0.1387
			U-236	5.2000E-01				
			Pu-236	4.8000E-01				
		Np-237	2.144E+6 y	A	4.8499	0.0681	0.0350	4.9529
			Pa-233	1.00				

(*continued on next page*)

Table A.1 continued

Z	Element	Nuclide	Half-life	Decay mode	Emitted energy (MeV/nt)			
					Alpha	Electron	Photon	Total
		Np-238	2.117 d	B-	–	0.2519	0.5879	0.8398
			Pu-238	1.00				
		Np-239	2.3565 d	B-	–	0.2623	0.1846	0.4469
			Pu-239	1.00				
		Np-240	61.9 m	B-	–	0.5095	1.0538	1.5632
			Pu-240	1.00				
		Np-240m	7.22 m	B-IT	–	0.6779	0.3225	1.0004
			Pu-240	9.9890E-01				
			Np-240	1.1000E-03				
		Np-241	13.9 m	B-	–	0.4341	0.0395	0.4736
			Pu-241	1.00				
		Np-242	2.2 m	B-	–	0.9027	0.2654	1.1681
			Pu-242	1.00				
		Np-242m	5.5 m	B-	–	0.7551	0.9194	1.6744
			Pu-242	1.00				
94	Plutonium	Pu-232	33.7 m	ECA	1.5402	0.0087	0.0633	1.6122
			Np-232	7.7000E-01				
			U-228	2.3000E-01				
		Pu-234	8.8 h	ECA	0.3776	0.0114	0.0693	0.4583
			Np-234	9.4000E-01				
			U-230	6.0000E-02				
		Pu-235	25.3 m	ECA	0.0002	0.0228	0.0957	0.1187
			Np-235	9.9997E-01				
			U-231	2.7000E-05				
		Pu-236	2.858 y	ASF	5.8524	0.0128	0.0022	5.8674
			U-232	1.00				
			SF	1.3700E-09				
		Pu-237	45.2 d	ECA	0.0002	0.0171	0.0537	0.0710
			Np-237	1.00				
			U-233	4.2000E-05				
		Pu-238	87.7 y	ASF	5.5803	0.0107	0.0021	5.5930
			U-234	1.00				
			SF	1.8500E-09				
		Pu-239	2.411E+4 y	A	5.2357	0.0075	0.0011	5.2442
			U-235m	9.9940E-01				
			U-235	6.0000E-04				
		Pu-240	6564 y	ASF	5.2434	0.0105	0.0019	5.2559
			U-236	1.00				
			SF	5.7500E-08				
		Pu-241	14.35 y	B-A	0.0001	0.0052	<E-04	0.0054
			Am-241	9.9998E-01				
			U-237	2.4500E-05				
		Pu-242	3.75E+5 y	ASF	4.9738	0.0090	0.0017	4.9855
			U-238	1.00				
			SF	5.5400E-06				
		Pu-243	4.956 h	B-	–	0.1729	0.0259	0.1988
			Am-243	1.00				

Table A.1 continued

Z	Element	Nuclide	Half-life	Decay mode	Emitted energy (MeV/nt)			
					Alpha	Electron	Photon	Total
		Pu-244	8.00E+7 y	ASF	4.6513	0.0197	0.0211	4.9094
			U-240	9.9879E-01				
			SF	1.2100E-03				
		Pu-245	10.5 h	B-	–	0.3190	0.4027	0.7217
			Am-245	1.00				
		Pu-246	10.84 d	B-	–	0.1159	0.1431	0.2590
			Am-246m	1.00				
95	Americium	Am-237	73.0 m	ECA	0.0015	0.0802	0.3714	0.4531
			Pu-237	9.9975E-01				
			Np-233	2.5000E-04				
		Am-238	98 m	ECB+A	<E-04	0.0485	0.9023	0.9509
			Pu-238	1.00				
			Np-234	1.0000E-06				
		Am-239	11.9 h	ECA	0.0006	0.1709	0.2436	0.4150
			Pu-239	9.9990E-01				
			Np-235	1.0000E-04				
		Am-240	50.8 h	ECA	<E-04	0.0758	1.0355	1.1112
			Pu-240	1.00				
			Np-236	1.9000E-06				
		Am-241	432.2 y	A	5.5712	0.0373	0.0293	5.6379
			Np-237	1.00				
		Am-242	16.02 h	B-EC	–	0.1806	0.0188	0.1994
			Cm-242	8.2700E-01				
			Pu-242	1.7300E-01				
		Am-242m	141 y	ITA	0.0238	0.0439	0.0056	0.0734
			Am-242	9.9550E-01				
			Np-238	4.5000E-03				
		Am-243	7.37E+3 y	A	5.3583	0.0234	0.0585	5.4402
			Np-239	1.00				
		Am-244	10.1 h	B-	–	0.3330	0.8052	1.1382
			Cm-244	1.00				
		Am-244m	26 m	B-	–	0.5187	0.0172	0.5359
			Cm-244	9.9960E-01				
		Am-245	2.05 h	B-	–	0.2874	0.0324	0.3198
			Cm-245	1.00				
		Am-246	39 m	B-	–	0.7241	0.7498	1.4739
			Cm-246	1.00				
		Am-246m	25.0 m	B-	–	0.5033	0.9799	1.4832
			Cm-246	1.00				
		Am-247	23.0 m	B-	–	0.5683	0.1348	0.7031
			Cm-247	1.00				
96	Curium	Cm-238	2.4 h	ECA	0.2537	0.0117	0.0829	0.3482
			Am-238	9.6160E-01				
			Pu-234	3.8400E-02				
		Cm-239	2.9 h	ECB+	–	0.0291	0.2593	0.2883
			Am-239	1.00				

(*continued on next page*)

Table A.1 continued

Z	Element	Nuclide	Half-life	Decay mode	Emitted energy (MeV/nt)			
					Alpha	Electron	Photon	Total
		Cm-240	27 d	ASF	6.3650	0.0108	0.0022	6.3781
			Pu-236	9.9700E-01				
			SF	3.9000E-08				
		Cm-241	32.8 d	ECA	0.0603	0.1342	0.5034	0.6979
			Am-241	9.9000E-01				
			Pu-237	1.0000E-02				
		Cm-242	162.8 d	ASF	6.2041	0.0096	0.0020	6.2156
			Pu-238	1.00				
			SF	6.3700E-08				
		Cm-243	29.1 y	AEC	5.8929	0.1342	0.1353	6.1624
			Pu-239	9.9760E-01				
			Am-243	2.4000E-03				
		Cm-244	18.10 y	ASF	5.8915	0.0079	0.0017	5.9014
			Pu-240	1.00				
			SF	1.3710E-06				
		Cm-245	8.5E+3 y	ASF	5.4474	0.0824	0.1084	5.6382
			Pu-241	1.00				
			SF	6.1000E-09				
		Cm-246	4.76E+3 y	ASF	5.4654	0.0085	0.0050	5.5285
			Pu-242	9.9974E-01				
			SF	2.6300E-04				
		Cm-247	1.56E+7 y	A	5.0292	0.0114	0.3138	5.3544
			Pu-243	1.00				
		Cm-248	3.48E+5 y	ASF	4.7212	0.7716	1.3127	22.5608
			Pu-244	9.1610E-01				
			SF	8.3900E-02				
		Cm-249	64.15 m	B-	–	0.2835	0.0200	0.3035
			Bk-249	1.00				
		Cm-250	8300 y	AB-SF	0.9283	8.4270	13.3167	161.287
			Pu-246	1.8000E-01				
			Bk-250	8.0000E-02				
			SF	7.4000E-01				
		Cm-251	16.8 m	B-	–	0.4545	0.1112	0.5657
			Bk-251	1.00				
97	Berkelium	Bk-245	4.94 d	ECA	0.0075	0.1326	0.2352	0.3752
			Cm-245	9.9880E-01				
			Am-241	1.2000E-03				
		Bk-246	1.80 d	EC	–	0.0554	0.8546	0.9101
			Cm-246	1.00				
		Bk-247	1.38E+3 y	A	5.7031	0.0691	0.1468	5.9190
			Am-243	1.00				
		Bk-248m	23.7 h	B-EC	–	0.1910	0.0559	0.2470
			Cf-248	7.0000E-01				
			Cm-248	3.0000E-01				
		Bk-249	330 d	B-A	<E-04	0.0324	<E-04	0.0325
			Cf-249	1.00				
			Am-245	1.4500E-05				

Table A.1 continued

Z	Element	Nuclide	Half-life	Decay mode	Emitted energy (MeV/nt)			
					Alpha	Electron	Photon	Total
		Bk-250	3.212 h	B-	–	0.2949	0.8983	1.1932
			Cf-250	1.00				
		Bk-251	55.6 m	B-	–	0.3693	0.0915	0.4608
			Cf-251	1.00				
98	Californium	Cf-244	19.4 m	A	7.3196	0.0075	0.0020	7.3291
			Cm-240	1.00				
		Cf-246	35.7 h	ASF	6.8527	0.0060	0.0014	6.8606
			Cm-242	1.00				
			SF	2.5000E-06				
		Cf-247	3.11 h	ECA	0.0022	0.0463	0.1050	0.1536
			Bk-247	9.9965E-01				
			Cm-243	3.5000E-04				
		Cf-248	334 d	ASF	6.3518	0.0075	0.0020	6.3670
			Cm-244	9.9997E-01				
			SF	2.9000E-05				
		Cf-249	351 y	ASF	5.9262	0.0399	0.3282	6.2944
			Cm-245	1.00				
			SF	5.0200E-09				
		Cf-250	13.08 y	ASF	6.1168	0.0103	0.0111	6.2897
			Cm-246	9.9923E-01				
			SF	7.7000E-04				
		Cf-251	900 y	A	5.8803	0.1705	0.1245	6.1754
			Cm-247	1.00				
		Cf-252	2.645 y	ASF	6.0177	0.2516	0.4572	12.8107
			Cm-248	9.6908E-01				
			SF	3.0920E-02				
		Cf-253	17.81 d	B-A	0.0188	0.0908	0.0048	0.1144
			Es-253	9.9690E-01				
			Cm-249	3.1000E-03				
		Cf-254	60.5 d	ASF	0.0183	10.0442	16.8399	222.890
			Cm-250	3.1000E-03				
			SF	9.9690E-01				
		Cf-255	85 m	B-	–	0.2178	–	0.2178
			Es-255	1.00				
99	Einsteinium	Es-249	102.2 m	ECB+A	0.0392	0.0437	0.4129	0.4958
			Cf-249	9.9430E-01				
			Bk-245	5.7000E-03				
		Es-250	8.6 h	EC	–	0.3281	1.2235	1.5516
			Cf-250	9.8500E-01				
		Es-250m	2.22 h	ECB+	–	0.0343	0.5549	0.5892
			Cf-250	1.00				
		Es-251	33 h	ECA	0.0329	0.0522	0.1016	0.1868
			Cf-251	9.9500E-01				
			Bk-247	5.0000E-03				
		Es-253	20.47 d	ASF	6.7335	0.0022	0.0008	6.7366
			Bk-249	1.00				
			SF	8.9000E-08				

(continued on next page)

Table A.1 continued

Z	Element	Nuclide	Half-life	Decay mode	Emitted energy (MeV/nt)			
					Alpha	Electron	Photon	Total
		Es-254	275.7 d	A B-SF	6.5244	0.0727	0.0208	6.6179
			Bk-250	1.00				
			Fm-254	1.7400E-06				
			SF	3.0000E-08				
		Es-254m	39.3 h	B-AECSF	0.0208	0.2408	0.4757	0.8269
			Fm-254	9.8000E-01				
			Bk-250	3.2000E-03				
			Cf-254	7.6000E-04				
			SF	4.5000E-04				
		Es-255	39.8 d	B-ASF	0.5117	0.0737	0.0007	0.5950
			Fm-255	9.2000E-01				
			Bk-251	8.0000E-02				
			SF	4.5000E-05				
		Es-256	25.4 m	B-	–	0.5822	0.0032	0.5854
			Fm-256	1.00				
100	Fermium	Fm-251	5.30 h	ECB+A	0.1252	0.0337	0.1588	0.3176
			Es-251	9.8200E-01				
			Cf-247	1.8000E-02				
		Fm-252	25.39 h	ASF	7.1449	0.0064	0.0018	7.1578
			Cf-248	9.9998E-01				
			SF	2.3000E-05				
		Fm-253	3.00 d	ECA	0.8352	0.1084	0.0713	1.0150
			Es-253	8.8000E-01				
			Cf-249	1.2000E-01				
		Fm-254	3.240 h	ASF	7.2956	0.0095	0.0086	7.4339
			Cf-250	9.9941E-01				
			SF	5.9200E-04				
		Fm-255	20.07 h	ASF	7.1292	0.0954	0.0170	7.2417
			Cf-251	1.00				
			SF	2.3000E-07				
		Fm-256	157.6 m	ASF	0.5686	6.3116	12.4371	205.496
			Cf-252	8.1000E-02				
			SF	9.1900E-01				
		Fm-257	100.5 d	ASF	6.6154	0.1471	0.1521	7.3388
			Cf-253	9.9790E-01				
			SF	2.1000E-03				

WVMP SAR Reference 3-12

Materials and Design Experience in a Slurry-Fed Electric Glass Melter, Barnes, S.M. and D. E. Larsen, PNL-3959, UC-70, Pacific Northwest Laboratory, Richland Washington, August 1981.

PNL-3959
UC-70

Materials and Design Experience in a Slurry-Fed Electric Glass Melter

S. M. Barnes
D. E. Larson

August 1981

Prepared for the U.S. Department of Energy
under Contract DE-AC06-76RLO 1830

Pacific Northwest Laboratory
Operated for the U.S. Department of Energy
by Battelle Memorial Institute

Battelle

PNL-3959

PACIFIC NORTHWEST LABORATORY
operated by
BATTELLE
for the
UNITED STATES DEPARTMENT OF ENERGY
Under Contract DE-AC06-76RLO 1830

Printed in the United States of America
Available from
National Technical Information Service
United States Department of Commerce
5285 Port Royal Road
Springfield, Virginia 22151

Price: Printed Copy $_____*; Microfiche $3.00

*Pages	NTIS Selling Price
001-025	$4.00
026-050	$4.50
051-075	$5.25
076-100	$6.00
101-125	$6.50
126-150	$7.25
151-175	$8.00
176-200	$9.00
201-225	$9.25
226-250	$9.50
251-275	$10.75
276-300	$12.00

PNL-3959
UC-70

MATERIALS AND DESIGN EXPERIENCE IN A SLURRY-FED ELECTRIC GLASS MELTER

S. M. Barnes
D. E. Larson

August 1981

Prepared for
the U.S. Department of Energy
under Contract DE-AC06-76RLO 1830

Pacific Northwest Laboratory
Richland, Washington 99352

ACKNOWLEDGMENTS

The authors appreciate the efforts of the numerous individuals who made this report possible.

The following staff contributed needed technical information and analyses for the melter examination:

- Structural Analysis
  E. M. Patten
- Sample Analysis
  P. L. Koehmstedt
  J. E. Coleman
  F. T. Hara

The following staff members made valuable suggestions to improve the document quality:

W. J. Bjorklund
W. F. Bonner
J. L. Buelt
J. R. Divine
G. B. Mellinger
E. M. Patten
L. T. Lakey

Substantial assistance and effort have been given in the editing, word processing, and production of this report:

G. B. Long, Editor
M. A. Eierdam, Word Processor.

ABSTRACT

The design of a slurry-fed electric gas melter and an examination of the performance and condition of the construction materials were completed. The joule-heated, ceramic-lined melter was constructed to test the applicability of materials and processes for high-level waste vitrification. The developmental Liquid-Fed Ceramic Melter (LFCM) was operated for three years with simulated high-level waste and was subjected to conditions more severe than those expected for a nuclear waste vitrification plant.

The melter examination and analyses resulted in the following conclusions:

- Inconel 690® is an excellent material for the electrodes (corrosion rate ≤0.11 cm/yr).
- The Monofrax K-3® glass containment refractory developed moderate cracking, but this cracking did not produce a marked increase in refractory corrosion. The refractory cracking could be largely eliminated with improved design techniques. Monofrax K-3 wall corrosion was ≤0.85 cm/yr.
- The Alfrax 66® insulating refractory exhibited cracking caused by an excessive initial heat-up rate and by thermal expansion stresses of the melter refractory differential. No significant refractory corrosion was noted.
- The Zirmul® backup refractory was in excellent condition.
- The melter lid and cover plate were warped during the operating period as a result of materials differential thermal expansion.

® Inconel is a registered trademark of the International Nickel Co., Huntington, West Virginia.
® Monofrax is a registered trademark of the Carborundum Co., Falconer, New York.
® Alfrax is a registered trademark of the Carborundum Co., Falconer, New York.
® Zirmul is a registered trademark of the Charles Taylor Sons Co., Cincinnati, Ohio.

This deformation created some air inleakage problems. Increased thermal expansion allowance will reduce this concern. Several metal components, attached to the lid and exposed to process offgas (for which the metals were not selected), exhibited significant corrosion.

Thus, the melter materials were in generally good condition after the three-year operating period. Design modifications to this experimental melter can significantly extend the service life of a vitrification system to longer operating periods. All of the major glass containment refractories displayed very good resistance to glass corrosion and are recommended for future designs.

SUMMARY

An electric glass-melting furnace designed to vitrify simulated high-level waste was operated for three years at the Pacific Northwest Laboratory. This report documents the analysis of the melter undertaken to study the effects of long-term operation on the construction materials.

The Pacific Northwest Laboratory has been developing joule-heated, ceramic-lined glass melters since 1973 under the sponsorship of the U.S. Department of Energy. An experimental, full-scale electric melter began operation in February 1977. This melter was designed to vitrify simulated high-level waste at a rate compatible with that of waste slurry feed produced by a 5 MTU/d commercial nuclear-fuel reprocessing plant. This melter operated from February 1977 to February 1980 and processed both slurry and dry feeds (representative of a coupled spray-calciner/ceramic-melter system). A pool of molten glass at operating temperature was maintained in the melter for the entire operating period. The details of the individual glass-production tests are presented in Appendix B. The Liquid-Fed Ceramic Melter (LFCM) produced about 80 tonnes of glass from 54 tonnes of calcine plus glass formers, and 19,000 L of slurry feed. The feed was nonradioactive synthetic wastes representative of reprocessed defense and commercial nuclear fuels.

The melter was shut down and examined in detail to determine the construction materials' performance and to evaluate the LFCM design. The melter was methodically dismantled, physical dimensions of the construction materials were measured, and selected materials were analyzed in the laboratory. Also, a stress analysis, based on the LFCM refractory design, was performed to predict refractory stress levels in the idling (melter at temperature, but not processing glass) and liquid-feeding modes.

The Monofrax K-3 glass contact refractory was uniformly cracked throughout the melter. The Monofrax K-3 refractory along the two-electrode and north melting cavity walls was in good condition (especially considering the severity of service the LFCM was exposed to relative to a production glass melter), but pieces in the south (drain) wall Monofrax K-3 refractory had

detached from the wall and fallen to the floor. The refractory cracking causing detachment was caused by the arrangement of thermal profiles in the melting cavity wall. The temperature profiles in all but the south wall produced thermal cracking perpendicular to the glass contact face; thus, the cracked refractories remained in position. The south wall thermal pattern, however, induced cracks that were inclined with respect to the glass contact face. These nonperpendicular cracks allowed the damaged refractory sections to fall from the wall. The general Monofrax K-3 corrosion rate was calculated to be ~0.85 cm/yr.

The Alfrax 66 and Zirmul backup refractories were very resistant to glass corrosion, but numerous glass-filled cracks were found in the Alfrax 66 castable refractory. These cracks were the result of the rapid temperature changes in the LFCM startup, thermal expansion differences between the refractory materials, and tensile thermal stresses in the castable refractory regions.

The melter containment box and lid were largely unaffected by the corrosive conditions present during the three-year operating period, but the lid and one of the coolant channels were warped during service. Stress analysis showed that lid warpage can be reduced by designing increased thermal expansion freedom. The coolant channel distortion is thought to be caused by the high pressure developed by steam formation in the channel.

The Inconel 690 electrodes were in excellent condition; in fact, marks from the original machining operations were visible on the LFCM secondary electrode faces following the three-year exposure to the glass. The maximum corrosion rate of the electrodes was 0.11 cm/yr.

Evidence of sulfidation attack (corrosion by sulfur compounds and halides) was detected on an auxiliary heater and offgas bellows attached to the melter lid. Recent work with a modified slurry-fed melter indicates that this corrosion mechanism can affect components that demonstrated good corrosion resistance in the LFCM (e.g., lid, offgas ducting). This evidence suggests that use of alloys in contact with melter offgas need be considered for corrosion resistance for specific feeds.

The melter operating performance and the corrosion resistance of the Monofrax K-3 are not affected by the cracked refractory if the refractory remains in position. The materials selected for the LFCM generally performed as expected for the three-year period and are recommended for future use in melters operated under similar corrosive conditions. The majority of the refractory cracking and containment box warpage can be prevented by allowing additional design accommodation for the thermal expansion and contraction properties of the construction materials.

CONTENTS

FIGURES

TABLES

GLOSSARY

A	amp
® Alfrax	a registered trademark of the Carborundum Co., Falconer, New York.
CFCM	Calcine-Fed Ceramic Melter
cm	Centimeter
^{o}C	Degree centigrade
d	Day
DOE	Department of Energy
^{o}F	Degree Fahrenheit
h	Hour
HEPA	High Efficiency Particulate Air
HLW	High-Level Waste
in.	Inch
INEL	Idaho National Engineering Laboratory
® Inconel	a registered trademark of the International Nickel Co., Huntington, West Virginia.
K	Kelvin
kg	Kilogram
KVA	Thousand Volt Amps
L	Liter
LFCM	Liquid-Fed Ceramic Melter
mm	Millimeter
mo	Month
® Monofrax	a registered trademark of the Carborundum Co., Falconer, New York.
MPa	Pascal x 10^6

MTU	Metric Tonne Uranium
NC	Normally Closed
NO	Normally Open
PNL	Pacific Northwest Laboratory
s	second
SCR	Silicon-Controlled Rectifier
SEM	Scanning Electron Microscope
psi	Pounds per Square Inch
® Zirmul	a registered trademark of the Charles Taylor Sons Co., Cincinnati, Ohio.

1.0 INTRODUCTION

Pacific Northwest Laboratory (PNL) has been developing technology for the immobilization of high-level radioactive waste (HLW) under the sponsorship of the Department of Energy (DOE) and its predecessors for over 20 years. For the last 15 years, emphasis has been placed on the vitrification of HLW. One of the processes being developed at PNL for HLW vitrification is the slurry-fed electric melter process (Brouns et al. 1980; Dierks 1980; Buelt et al. 1979). The electric melter process has been under development at PNL since 1973. As of March 1981, nine electric melters (excluding laboratory melters) have been constructed and tested for process development. These have produced 130 tonnes of glass.

The largest of the PNL melters, the Liquid Fed Ceramic Melter (LFCM), pictured in Figure 1, was placed in service in February 1977. The LFCM was scaled to process simulated HLW at a rate compatible with that generated by a 5 MTU/d spent-nuclear-fuel processing facility. During the operating life of the melter, slurry and calcine feeds (which represent both commercial and defense wastes) have been processed. Most recently, the LFCM has been used for full-scale development studies in support of the Defense Waste Processing Facility at the Savannah River Plant. The melter has demonstrated processing slurry feeds of 100 L/h with only joule heating and up to 150 L/h with additional process energy input (e.g., ionic boosting, lid heaters). Calcined or dry feeds have been vitrified at rates of 160 kg/h.

During the three-year service, the LFCM was used to develop ceramic-lined melter technology, establish melter operating parameters, and study the processing characteristics of the glass formulations (presented in Appendix B). Modifications to the melting system, as well as processing experiments required to perform these studies frequently subjected the LFCM to conditions more extreme than those expected in a plant HLW vitrification system. In February 1980, the melter was shut down. Following the final draining, a comprehensive investigation was undertaken to determine the condition and performance of the construction materials and to assess the adequacy of the melter design.

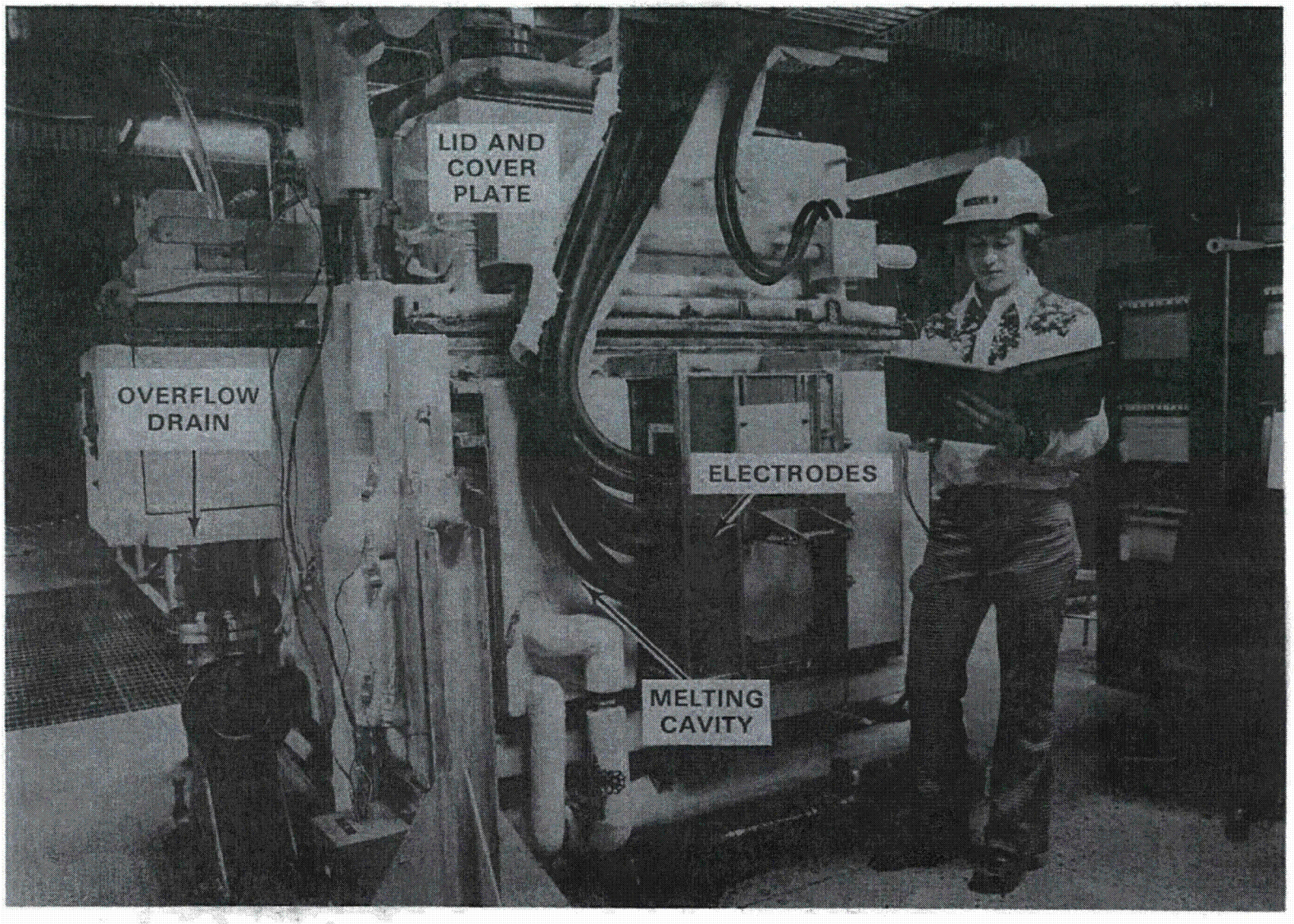

FIGURE 1. Liquid-Fed Ceramic Melter

This report documents the materials and design experience of the LFCM so the knowledge developed may be used to construct reliable, long-life electric melters for radioactive waste immobilization in a plant. This report provides the context for interpreting the LFCM experiences by describing the LFCM vitrification system (Sections 1.0 through 4.0), documenting the effects of the operating period on the construction materials (Section 5.0), and interpreting the findings of the detailed examination of the melter and components (Sections 6.0 and 7.0).

In addition, comparisons are made with observations concerning the calcine-fed ceramic melter materials experience (Dierks et al. 1980), which was investigated in 1980. Results and conclusions are presented, and recommendations are made to provide guidance for future melter design.

2.0 CONCLUSIONS AND RECOMMENDATIONS

Conclusions and recommendations drawn from the LFCM examination and analyses are found in this section

2.1 GENERAL

The design of the LFCM and the performance of the structural materials were generally good. The corrosion performance of the glass containment refractories (Monofrax K-3, Zirmul, and Alfrax 66) was excellent. The melter operation was not affected by cracked primary or secondary refractories, provided the cracked refractory remained in place. Corrosion of the glass contact refractory, Monofrax K-3, was not enhanced by the refractory cracking. Future melter designs should consider the melter temperature and stress patterns in the ceramics to minimize the cracking and thus reduce the likelihood of failed refractory sections falling from the walls.

Only minor corrosion of the melter metallic materials was observed, with the exception of ionic booster system components and a section of flexible offgas ducting. In both of these cases, the corrosion was due to service under conditions for which they were not originally intended. The corrosion of these components can be alleviated by specifying alloys designed to resist the mixture of volatile sulfur and halogen compounds produced by recently tested waste-glass formulations.

The analyses performed on the LFCM indicate that the service life of ceramic-lined, waste-glass melters can be increased beyond the three years demonstrated by this melter. The most important factor for extended melter service is adequate accommodation of the thermal expansion properties of the construction materials.

2.2 MELTER CONTAINMENT BOX AND LID

Type 304L stainless steel is adequate for service in the melter containment box where contact with glass vapors and molten glass is not normally expected. This stainless steel, normally resistant to attack by sulfur

compounds, will corrode rapidly at elevated temperatures in sulfur atmospheres also containing halides and water vapor. Typical 18-8 stainless steels should not be used in sulfur-halide atmospheres above 200°C. Selection of the proper alloy for exposure to these conditions requires further characterization of the melter offgases to determine the concentration of the corroding species (NaCl, HCl, Na_2SO_4, SO_2, SO_3, etc.). The Inconel 601 LFCM lid was protected from sulfidation (high temperature halide and sulfur corrosion) by the external insulation. This insulation maintained the lid in the 850°C to 950°C temperature range during idling and (roughly) in the 100°C to 400°C range during operation. These temperatures are too hot and cold, respectively, for sulfidation to occur.

The thermal cycling inherent to externally insulated lids, however, produced the warpage and tearing detected in the lid following the melter shutdown. This damage was primarily due to the restriction of free thermal expansion of the heated lid by the water cooled containment box. Improved design to reduce the induced thermal stresses at the containment box-lid junction will produce an effective, inherently corrosion-resistant melter containment method.

The current trend to increase slurry feed processing rates by heating the "cold cap" from above will increase the operating temperature of an externally insulated lid into the sulfidation temperature range. In this case, an alternative insulation method or an alloy other than Inconel 601 may be needed to produce extended service life.

The warpage of the containment-box cooling channel was probably caused by a pressurization in the channel as residual water was converted to steam following the elimination of water cooling to this region. This damage can be avoided in the future by insuring that the coolant channels are either actively used or are dry and isolated from the coolant drain.

2.3 MELTING CAVITY REFRACTORY

Monofrax K-3, Zirmul, and Alfrax 66 demonstrated excellent corrosion resistance during the three-year operating period. Very little refractory

corrosion (<0.85 cm/yr) was observed in this melter examination. The Monofrax K-3 cracking did not increase the corrosion rate of this material.

The cracking of the Alfrax 66 observed during the LFCM disassembly was due to the rapid (∿22 h) initial melter startup period, differences in thermal expansion between the Alfrax 66 and the Monofrax K-3, and thermal stresses developed in the Alfrax 66 region. The rapid melter startup would not have permitted sufficient time for the residual water from refractory mixing (both excess water and water of hydration) to diffuse through the refractory and escape. This water would generate steam within the refractory and create damaging tensile stresses. This startup schedule heats the refractory much faster than the manufacturer recommends (presented in Section 5.3.2). Second, the Alfrax 66 has significantly different thermal-expansion characteristics than the Monofrax K-3. The Alfrax 66 tends to maintain roughly the same dimensions during the curing process whereas the Monofrax K-3 would be thermally expanding. As the Alfrax is cast surrounding the Monofrax K-3, this also would result in tensile stresses in the Alfrax 66 layer. Finally, the thermal-stress analyses of the LFCM refractory design presume tensile stresses as high as 83 MPa in the Alfrax 66 layer under the assumed liquid-feeding boundary conditions. This exceeds the Alfrax 66 tensile rupture strength by ∿30 times. Therefore, to reduce the magnitude of the Alfrax 66 cracking observed, the initial curing temperature schedule should be followed and the refractory installation should be designed to allow slippage along Alfrax 66-Monofrax K-3 joints, as well as to reduce the general thermal stress patterns. Following these suggestions, the Alfrax 66 cracking, and thus the number of glass penetrations through the Alfrax 66 layer, will be reduced.

Most of the Monofrax K-3 cracking can probably be prevented in future melters by allowing sufficient space for refractory thermal expansion, reducing the thermal gradients in the refractory by increasing refractory wall thickness, and reducing the severity of thermal transients such as startup and liquid-feeding initiation. The damage to the Monofrax K-3 refractory of the south wall (where cracked refractory pieces were missing) can be eliminated by modifying the temperature profile in the drain region.

2.4 ELECTRODES

The Inconel 690 electrodes demonstrated excellent corrosion resistance and no structural deformation. Similar good performance was noted in all of the other applications of this alloy. The electrode corrosion rate was calculated to be ≤0.11 cm/yr.

2.5 GLASS DISCHRAGE SECTION

The monolithic Monofrax K-3 riser block exhibited enlargement of the melter cavity inlet nozzle, about 0.32 cm (0.1 cm/y) horizontally and 5.7 cm (1.9 cm/y) vertically). Corrosion of the riser inlet was expected to be larger than the general refractory-face corrosion rate because: the velocity of the glass flow through the riser is higher than the velocity produced by convection currents in the melting cavity (slag buildup on the melter floor produces a smaller glass-flow area at the riser inlet, leading to even higher velocity); the riser leaves the melter at $10^{o}24'$ angle from the horizontal, resulting in a thin refractory section at the top of the riser inlet which is surrounded by hot glass; and melter refractory temperatures are greatest in this region because of the glass in the riser and the overflow drain heaters.

3.0 PROCESS AND EQUIPMENT DESCRIPTION

The LFCM processes and melter equipment are described in this section. Following a general description of the melter, process flowsheets representative of the LFCM operating conditions are presented. Completing this section is a detailed description of the melter subassemblies.

The LFCM may be characterized as a ceramic-lined melting cavity containing two sets of electrodes. Melter heat is primarily supplied by the joule-heating effect created by passing an alternating current through the glass between the electrodes. Feed and glass-forming materials enter the melter from the top and drop onto the molten glass pool. Unreacted feed materials accumulated on the glass surface are known as a "cold cap." As the feed and glass-forming materials are converted into vitrified oxides, moisture and other decomposition products are converted into a process offgas. These effluents are routed to an offgas treatment system for removal of water, particulates, volatile radionuclides, and toxic volatile chemicals. The vitrified molten product is emptied from the melter into a canister where it solidifies. The overall melter assembly is illustrated in Figure 2.

The LFCM is composed of the subassemblies indicated below and shown in the schematic in Figure 3.

Assembly	Function
Refractory	Glass containment and thermal insulation
Containment Box	Surrounds melter refractory providing cooling and controlled atmosphere
Lid	Covers melter containment box to house nozzles for melter-cavity access and to contain decomposition effluents and volatile species
Power Electrodes and Control	Main power source for cavity heat supply
Overflow Section	Melter section designed to transfer the molten glass product to the storage canister

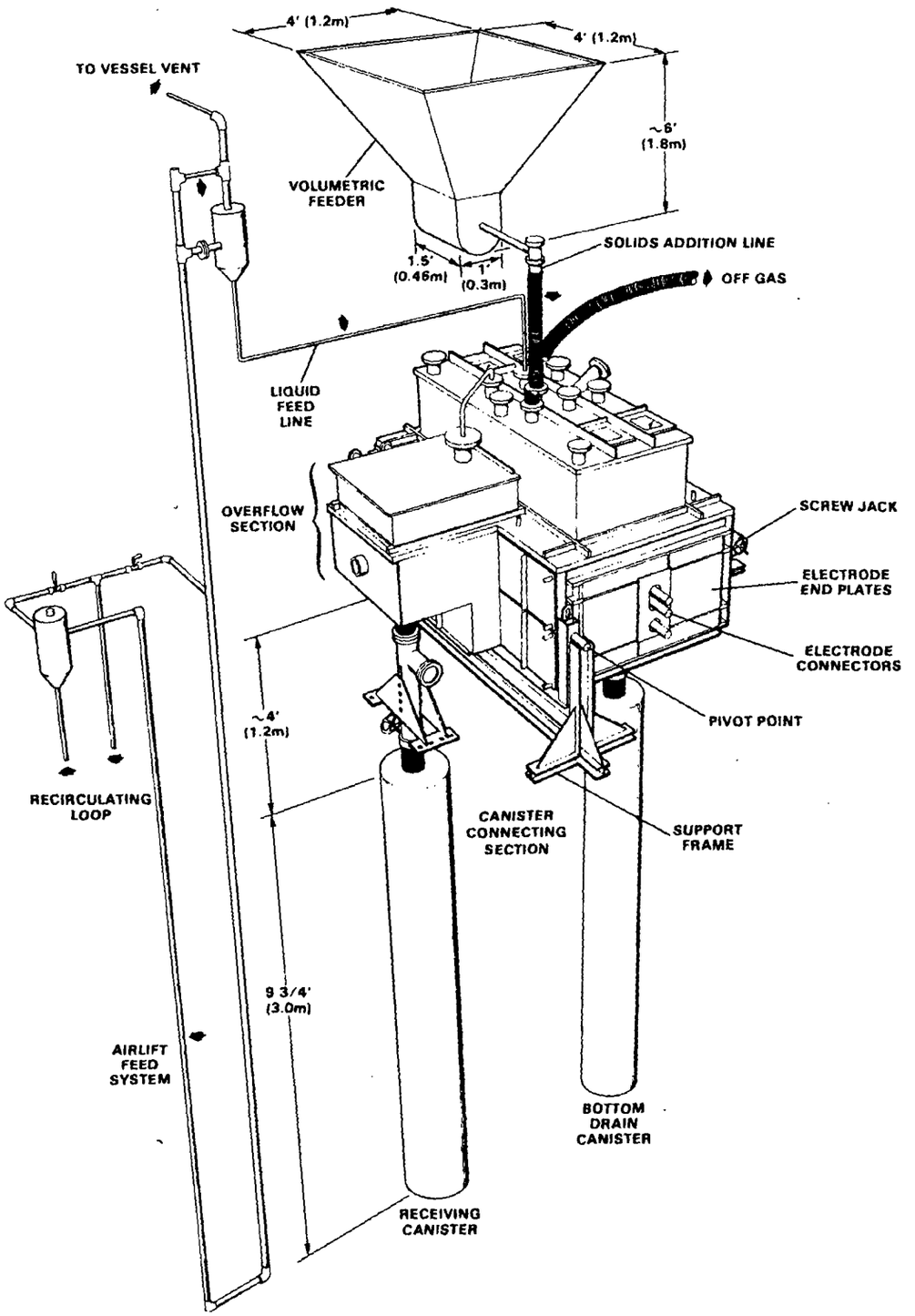

FIGURE 2. Liquid-Fed Ceramic Melter System Assembly

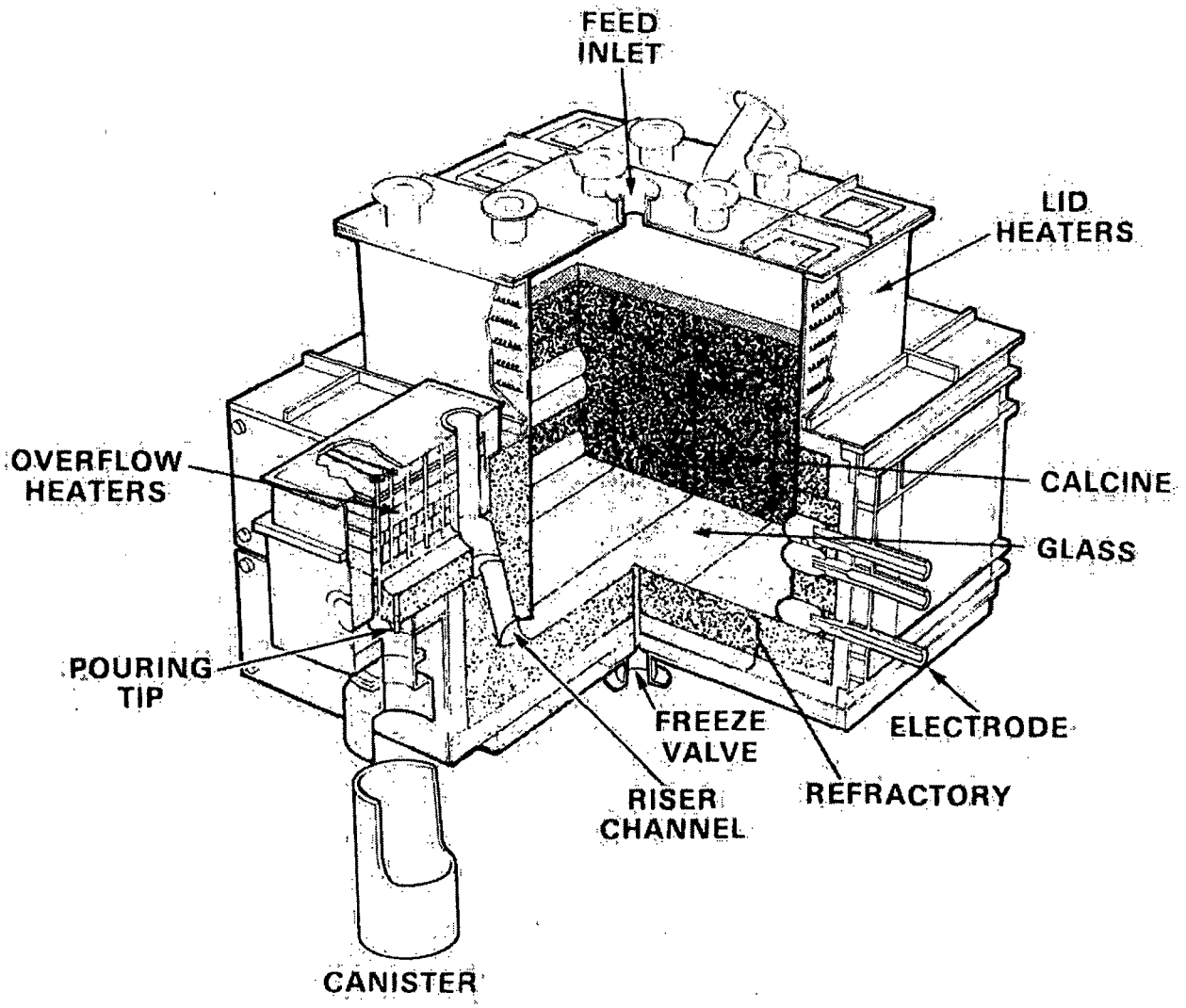

FIGURE 3. Liquid-Fed Ceramic Melter Cutaway

Assembly	Function
Auxiliary Power Systems	Three additional power systems are used in the LFCM: 1) glass-overflow section heaters, 2) lid heaters, 3) bottom drain heaters
Lid Heaters	Provide heat source for melter startup and boosting
Ionic Booster Electrodes and Control	Provide power for increased liquid feed evaporation capacity by directly heating aqueous "cold cap"

Assembly	Function
Bottom Drain	Molten glass drain for melter cavity draining
Instrumentation	Process monitoring and control
Feed Systems	Provide aqueous and calcined feed together with glass-forming materials to melter
Offgas System	Melter offgas handling and treatment

3.1 PROCESS FLOWSHEET DESCRIPTION

The LFCM has processed a variety of nonradioactive waste feeds. The principal melter feeds have been synthetic, commercial acid-waste slurry, defense-waste slurry, and defense-waste calcine (dry feed materials representative of a coupled spray-calciner/ceramic-melter system). Other minor feed materials generally consisted of a variety of frits. The general method of melter operation, representative flowsheets, and typical melter thermal conditions are discussed in this section.

The LFCM was operated in two predominant modes--slurry feeding and calcine feeding. In the liquid-fed process, the glass formers are premixed with simulated liquid waste before feeding the waste slurry to the melter. Normally, a crust of solid, partially reacted feed materials forms in the melting cavity separating the slurry and the molten glass. This solid crust and the boiling slurry above are known as the "cold cap." Heat from the molten glass is transferred through the crust to evaporate the slurry. This process continually generates new crust materials to replace the feed reacting to form glass at the molten interface. Supplementary heat may be supplied to the feed materials in the cold cap by radiation from lid heaters or electrodes placed in the slurry pool (ionic boosting). As the crust melts into the glass, additional gases are generated by the final decomposition stages. The steam and gases are collected in the plenum above the melting surface. This region is maintained at a slightly negative pressure relative to ambient conditions (-250 mm of water). From here, the effluents pass through the offgas treatment system. Particulates and volatiles collected in this system are recycled to the melter as required. The waste glass product is drained continuously into a receiving canister.

The slurry-feeding process is characterized by two operating modes based on the volume of liquid feed maintained in the cold cap. These operating styles are termed "fully flooded" and "nonflooded." In the fully flooded mode, the feed slurry covers the entire melting cavity surface. Maximum vitrification rates are achieved with fully flooded cold caps. The gases generated by the final decomposition stages of the feed forming the crust must, however, vent through the crust. Release of these decomposition gases results in local crust fractures and momentary contact of feed slurry and molten glass. The contact with the molten glass results in rapid heat transfer to the slurry and increased offgas flow (roughly three times the average steady-state effluents flowrate--Brouns et al. 1980). This phenomenon occurs regularly every few minutes and is depicted in Figure 4.

The nonflooded cold cap is shown in Figure 5. In this mode, the feedrate is deliberately maintained below the maximum processing capability of the melter. This results in more stable melter operation with fewer offgas flow peaks as the decomposition gases are released around the cold cap periphery. The

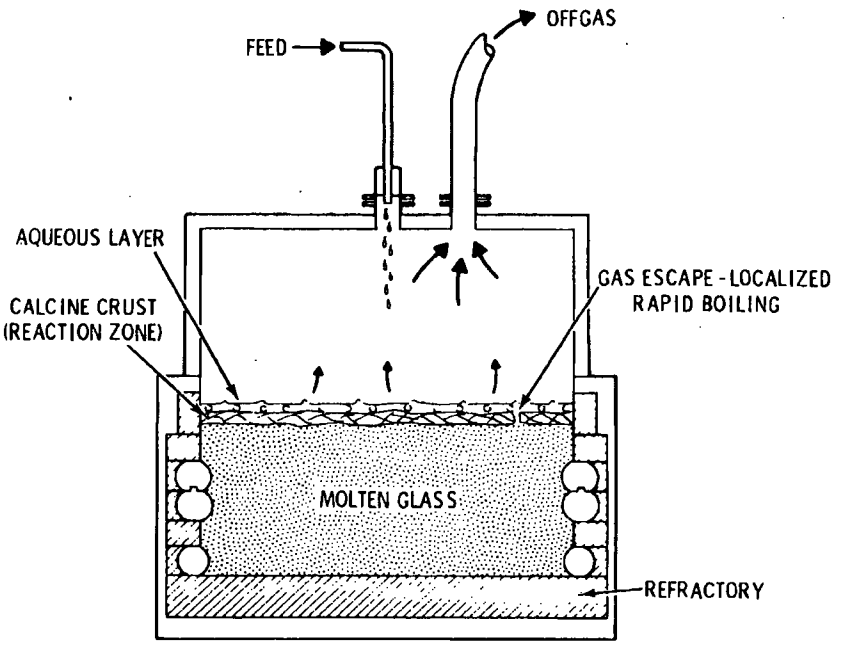

FIGURE 4. Fully Flooded Liquid-Fed Cold Cap

offgas surges in this mode take place as the result of the feed slurry pouring over the edge of the crust onto the glass surface.

The slurry processing capabilities of the melter can be enhanced (or boosted) by using auxiliary heating systems. The primary boosting technique demonstrated to date is heating the cold cap from above with the lid heaters (see Section 3.2.9) and the ionic booster system. The ionic boosters, shown in Figure 6, are metal electrodes that are immersed in the aqueous slurry pool in the cold cap. An alternating electric current, in the same phasing as the power electrodes in the glass, is passed between the ionic booster electrodes creating joule-heat generation in the slurry. The ionic boosting system has increased the capacity of a melter by 50% (Buelt and Chapman 1979), and higher rates are anticipated. The boosters must be water-cooled to prevent film boiling at the slurry-electrode interface. Water-cooling also extends booster life by reducing the electrode temperature, and thereby the corrosion rate, during melter idling periods. The water-cooled ionic booster electrodes can

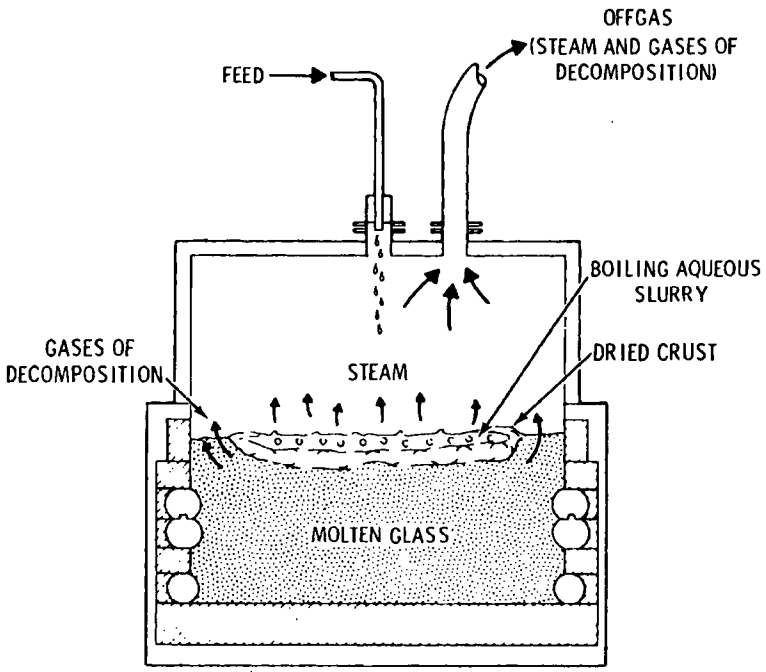

FIGURE 5. Nonflooded Liquid-Fed Cold Cap

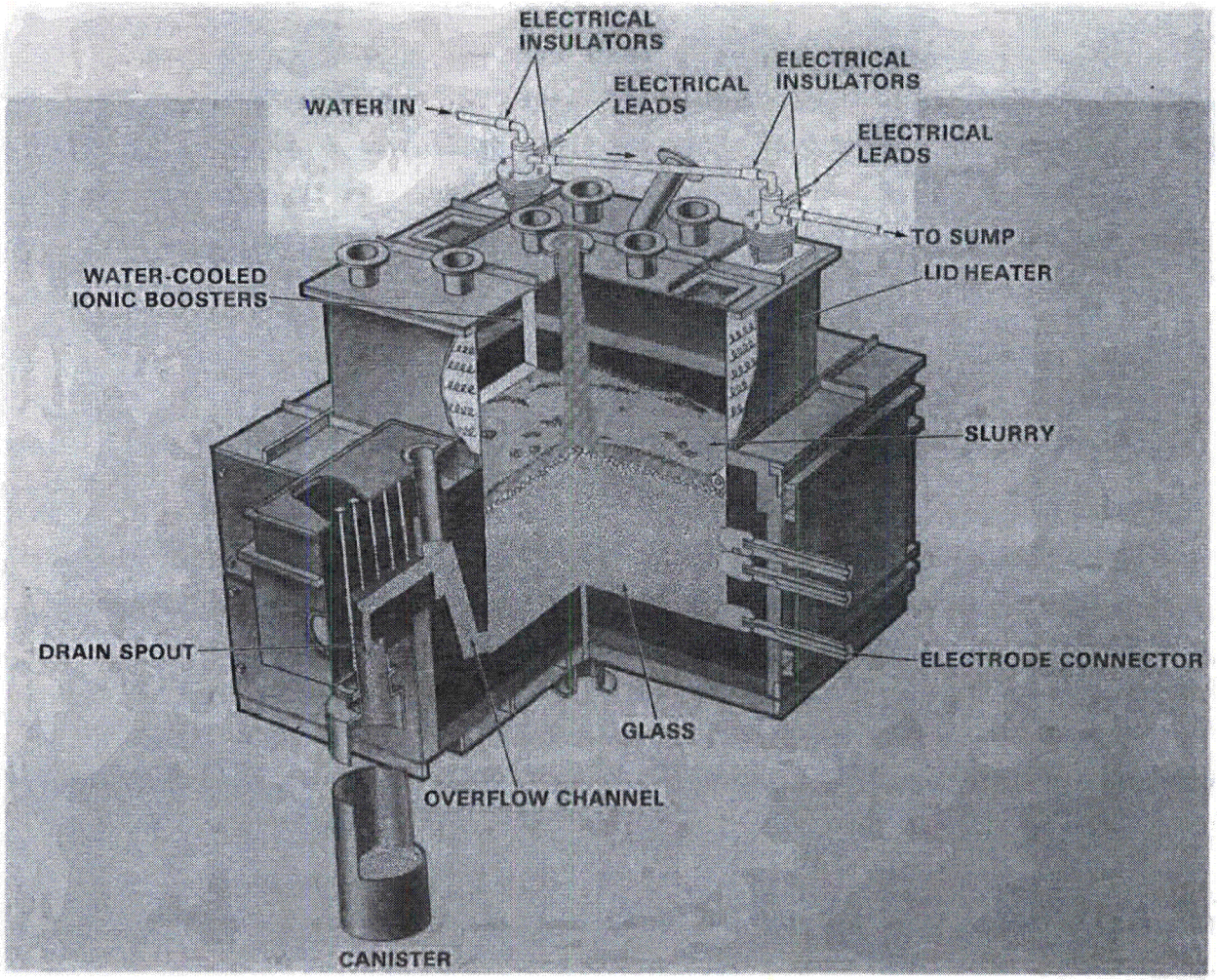

FIGURE 6. LFCM Ionic Booster Electrodes and Lid Heaters

also reduce the melter operating capacity up to 25% during slurry feeding if they are not used. This capacity reduction is the result of the electrodes acting as reflux condensers in the melting cavity.

In the LFCM calcine-feeding mode, the calcine and feed materials are premixed and added to the melter as a single stream. This mixture enters the top of the melter and drops onto the cold cap of solids floating on the molten glass in the melter cavity. Melter operation with calcine feeding is similar to that with slurry feeding, except that there is much less gas generation and a more uniform offgas generation rate without the pressure surges.

Typical flowsheets for the major processing modes are shown in Figures 7 and 8 for defense-waste slurry and defense-waste calcine. Heat balances for typical slurry and calcine feed modes are shown in Figures 9 and 10, respectively. The calculated temperature distributions (based on thermocouple measurements) within the melter during liquid feeding and the idling modes of operation are provided in Section 6.2.

3.2 MELTER DESCRIPTION

The melter components are described below (Buelt and Chapman 1978).

3.2.1 Containment Box

To contain gaseous effluents generated during the vitrification process, an air-tight box encompasses the entire ceramic melter. This is illustrated in Figures 11 and 12. The construction material for the LFCM container is 1/4-in. 304L stainless steel for the container box and 1/4-in. Inconel 601 for the lid. The lower part of the shell, which contains the refractory components, is lined with cooling baffles. Each of these zones can be controlled independently, with either water, steam, or air as the cooling fluid. Aside from keeping the refractories cool, the cooling is intended to solidify the glass as it approaches the outer wall and acts as a second barrier for preventing glass leakage through cracks in the refractory.

3.2.2 Lid

The upper section of the melter container, termed the lid (Figures 11 and 12), provides for de-entrainment of dust or aerosol vapors from the melter effluents. The lid is surrounded by plate heaters, which can be used for melting built-up material that accumulates during liquid feeding. The lid heaters are controlled manually, automatically by temperature control, or are ramped for heatup and cooldown. The cover plate of the lid has various access ports for feeding, viewing, and acquiring data.

3.2.3 Refractory

The molten glass in the LFCM is contained by high-temperature refractories constructed of two basic layers. First, the glass-contact refractory maintains

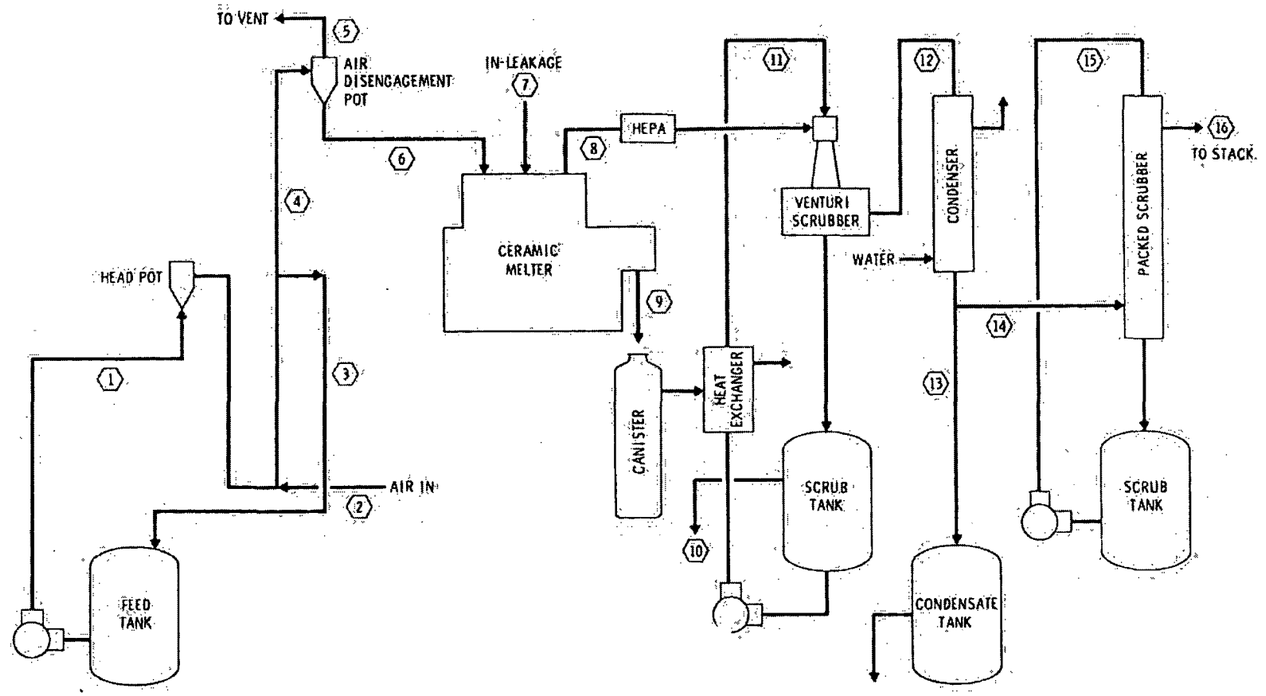

STREAM NUMBER	1	2	3	4	5	6	7	8	9	10	11	12	13	14	15	16
	FEED TO HEAD POT (3)	AIR INLET	RECYCLE	AIRLIFT	AIR OUTLET	LIQUID FEED	IN-LEAKAGE (3)	GAS FLOW	GLASS	SCRUB TANK OVERFLOW	VENTURI SCRUB SOLUTION	VENTURI OUTLET	CONDENSATE	PACKED SCRUB INLET	PACKED SCRUB SOLUTION	OFFGAS TO STACK (5)
LIQUID FLOW (L/h)	300		200	100		100			36.4	35.6	9 E5		0.4		2 E3	
MASS FLOW H_2O (kg/h)	249	NEG.	166	83	NEG.	83	0.42	86.0		85.3	9 E5	0.4	0.4	0.03	2 E3	0.02
MASS FLOW O_2 (kg/h)		0.036		0.036	0.036		6.4	2.22		NEG.	NEG.	2.22	NEG.	2.22	NEG.	2.22
MASS FLOW N_2 (kg/h)		0.12		0.12	0.12		32.4	0.540		NEG.	NEG.	0.540	NEG.	0.540	NEG.	0.540
MASS FLOW CO_x (kg/h) (1)								0.712		NEG.	NEG.	42.7	NEG.	42.7	NEG.	42.7
MASS FLOW NO_x (kg/h) (2)								8.76		2.64	2 E6	6.12	NEG.	6.12	VAR.	6.12

1. ASSUMED 50 mole % CO, 50 mole % CO_2
2. ASSUMED 50 mole % NO, 50 mole % NO_2
3. ASSUMED 20 SCFM
4. ASSUMED DF[(a)] = 2 FOR NO_2, DF = 1 FOR NO
5. ASSUMES DF = 10 FOR NO_2, DF = 1 FOR NO

(a) DECONTAMINATION FACTOR

FIGURE 7. Defense-Waste Slurry Flowsheet

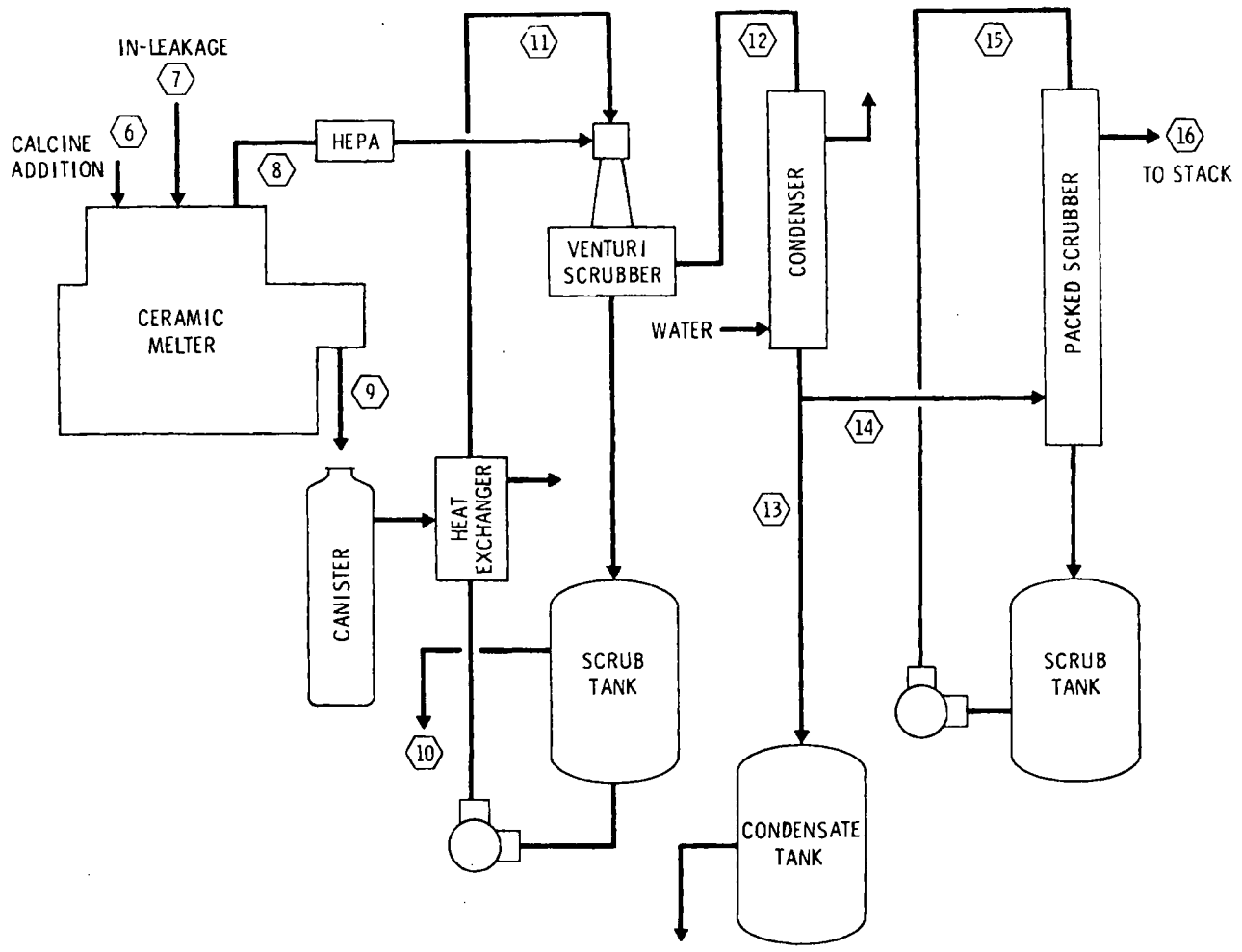

STREAM NUMBER	1	2	3	4	5	6	7	8	9	10	11
	CALCINE FEED (1)	IN-LEAKAGE (2)	GAS FLOW	GLASS	SCRUB TANK OVERFLOW	VENTURI SCRUB SOLUTION	VENTURI OUTLET (3)	CONDENSATE	PACKED SCRUB INLET	PACKED SCRUB SOLUTION	OFFGAS TO STACK (4)
CALCINE ADDITION (kg/h)	109.6										
LIQUID FLOW (L/h)		0.82	8.53	38.6	7.74	9E5	0.79	NEG.	8.79	2E3	0.79
MASS FLOW H_2O (kg/h)		0.82	8.53			9E3				2E3	
MASS FLOW O_2 (kg/h)		2.07	2.77		NEG.	NEG.	2.77	NEG.	2.77	NEG.	7.77
MASS FLOW N_2 (kg/h)		6.77	6.77		NEG.	NEG.	6.77	NEG.	6.77	NEG.	6.77
MASS FLOW CO_2 (kg/h)		NEG.	0.79		NEG.	NEG.	0.79	NEG.	0.79	NEG.	0.79
MASS FLOW NO_2 (kg/h)		NEG.	0.88		0.44	5E4	0.44	NEG.	0.44		0.04

1. SEE TABLE A2 - SRL-13 FOR FEED COMPOSITION
2. ASSUMED 4 SCFM
3. ASSUMED $DF^{(a)}$ = 2 FOR NO_2
4. ASSUMES DF = 10 FOR NO_2

(a) DECONTAMINATION FACTOR

(b) 100 kg/h

FIGURE 8. Defense-Waste Calcine Flowsheet

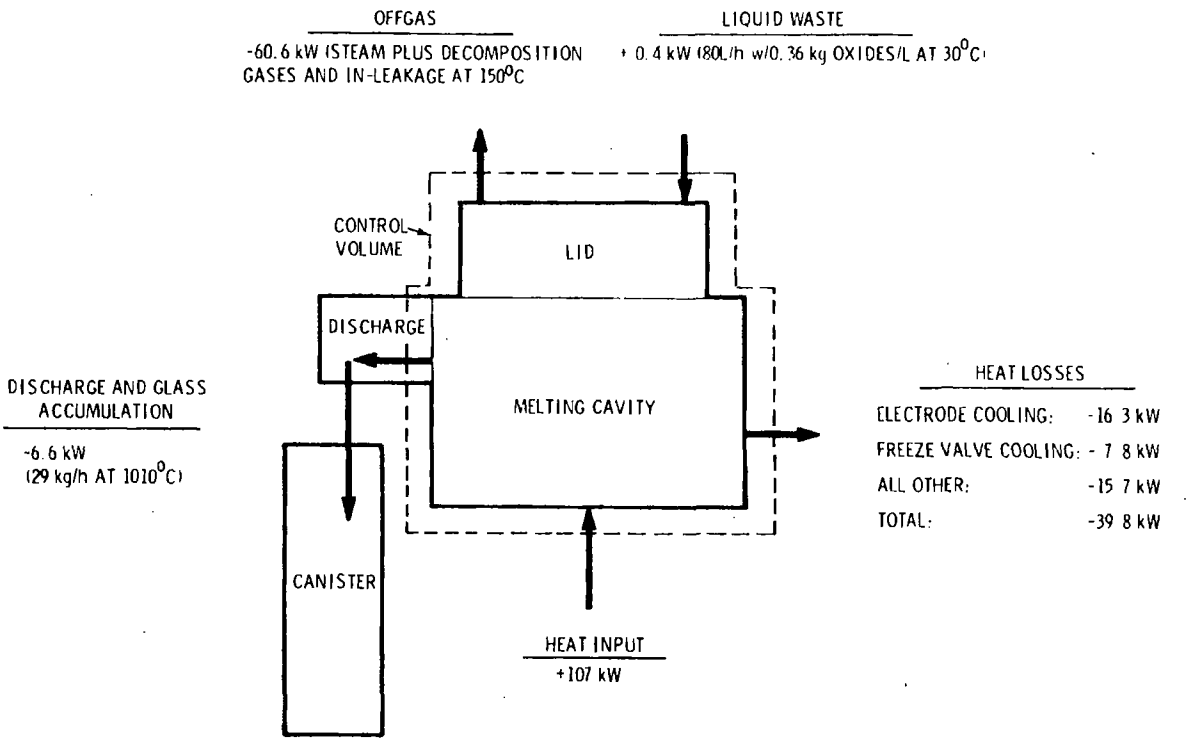

FIGURE 9. LFCM Liquid-Fed Heat Balance

the highest resistance to corrosive attack and contains the molten glass directly. A backup layer of insulating refractory provides higher thermally insulative properties, yet still maintains good corrosive resistance.

The glass contact refractory, shown in Figures 13 and 14, must be:

- resistant to corrosion over long periods of time at operating temperatures (1200°C)
- more electrically resistive than the molten glass to avoid electrical shorting
- thermally insulative
- resistant to thermal shock.

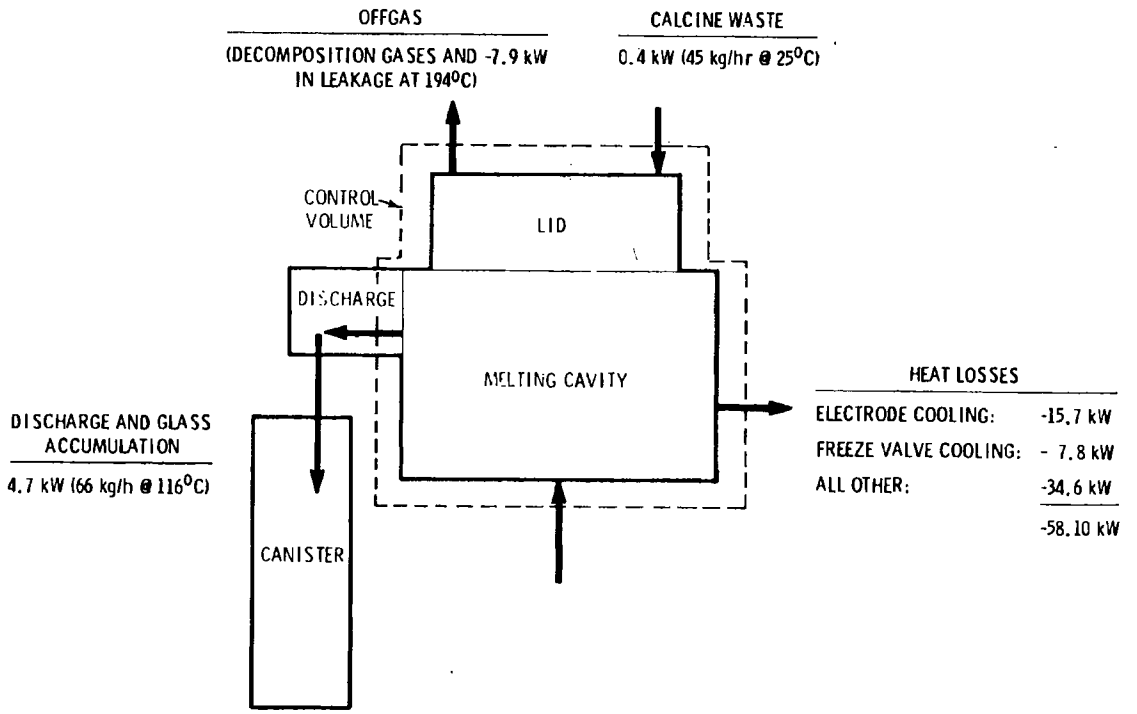

FIGURE 10. LFCM Calcine-Fed Heat Balance

High chromia refractories have excellent resistance to corrosion; however, chromia refractories also have high electrical conductivity properties. For the refractory lining in the LFCM, Monofrax K-3, which contains about 30% chromia and 60% alumina was chosen. The chemical composition and physical properties of the Monofrax K-3 bricks are shown in Table A.1. Typical brick dimensions are 15.2 cm by 30.5 cm by 45.7 cm, although many custom sizes were installed.

Because the Monofrax K-3 is fused-cast, it is very dense and has a fairly high thermal conductivity. Therefore, the walls are backed with 7.62 cm of Alfrax 66 castable refractory (see Figure 15). The chemical composition and properties of the Alfrax 66 are provided in Tables A.1 and A.2. The floor is insulated with a dense Zirmul brick, which has better insulative properties than Monofrax K-3 but still maintains good resistance to molten glass attack. Zirmul brick is also used as the backup refractory behind the electrodes. The chemical composition and physical properties of the Zirmul bricks are provided

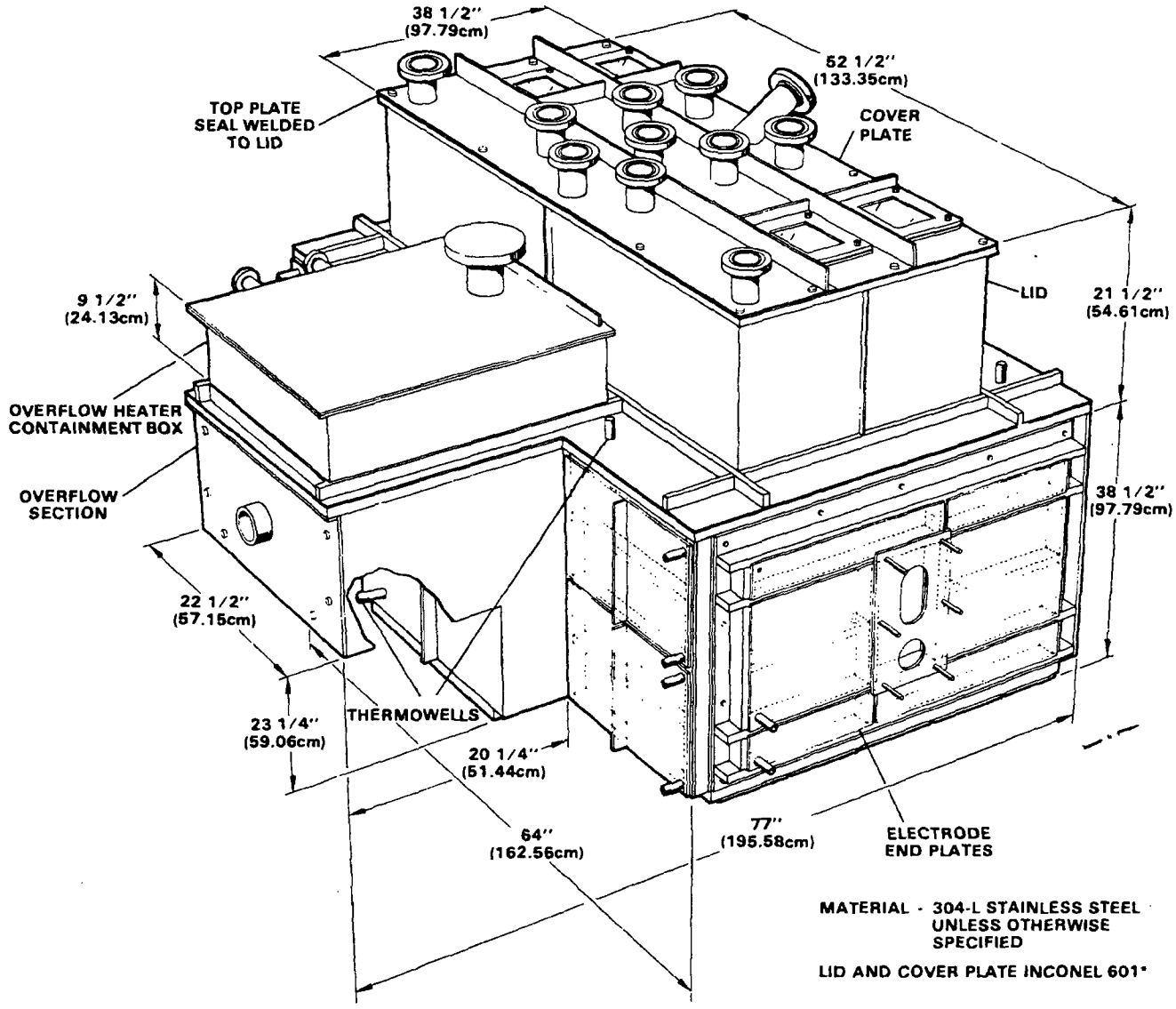

FIGURE 11. Containment Box and Lid, Southeast View

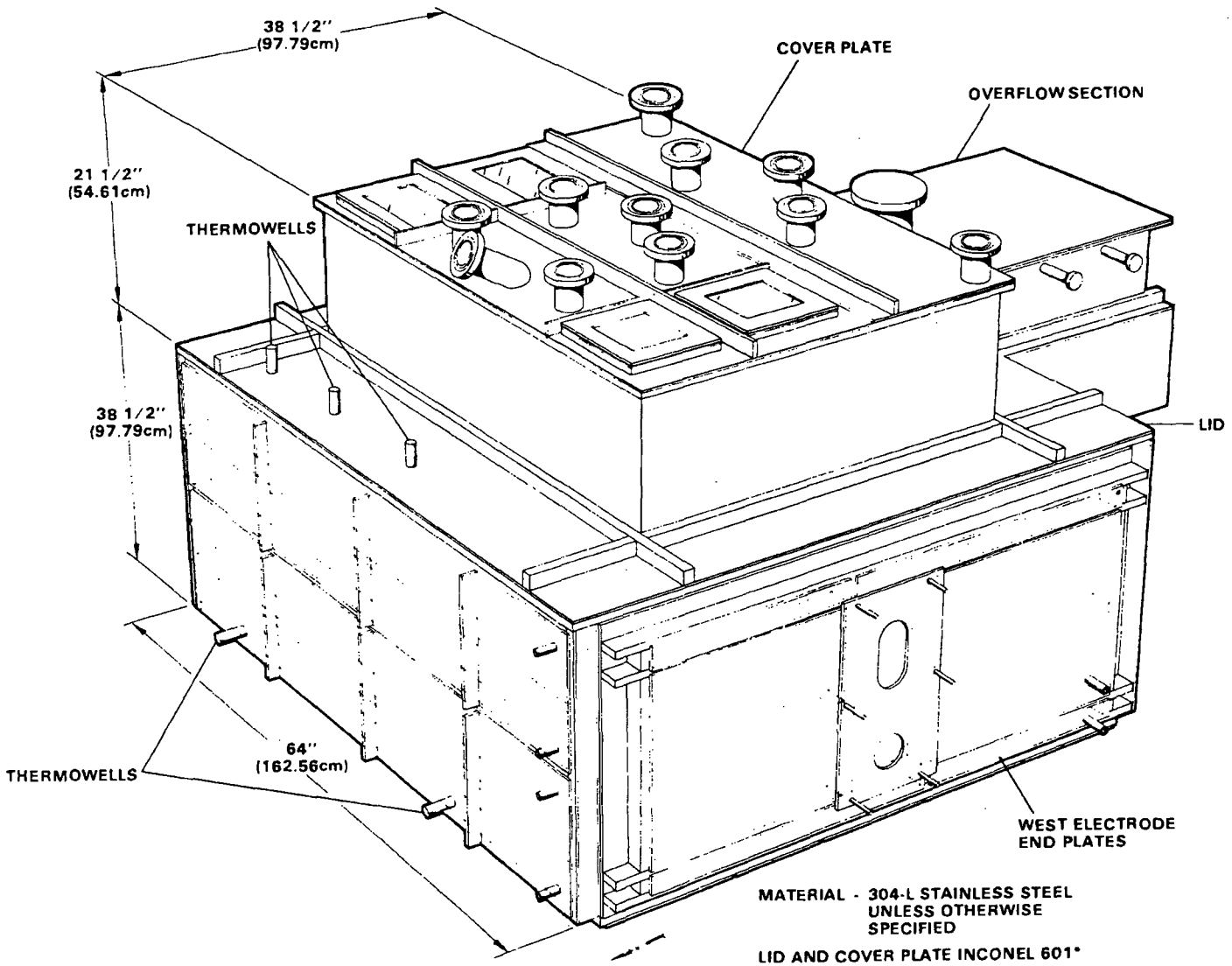

FIGURE 12. Containment Box and Lid, Northwest View

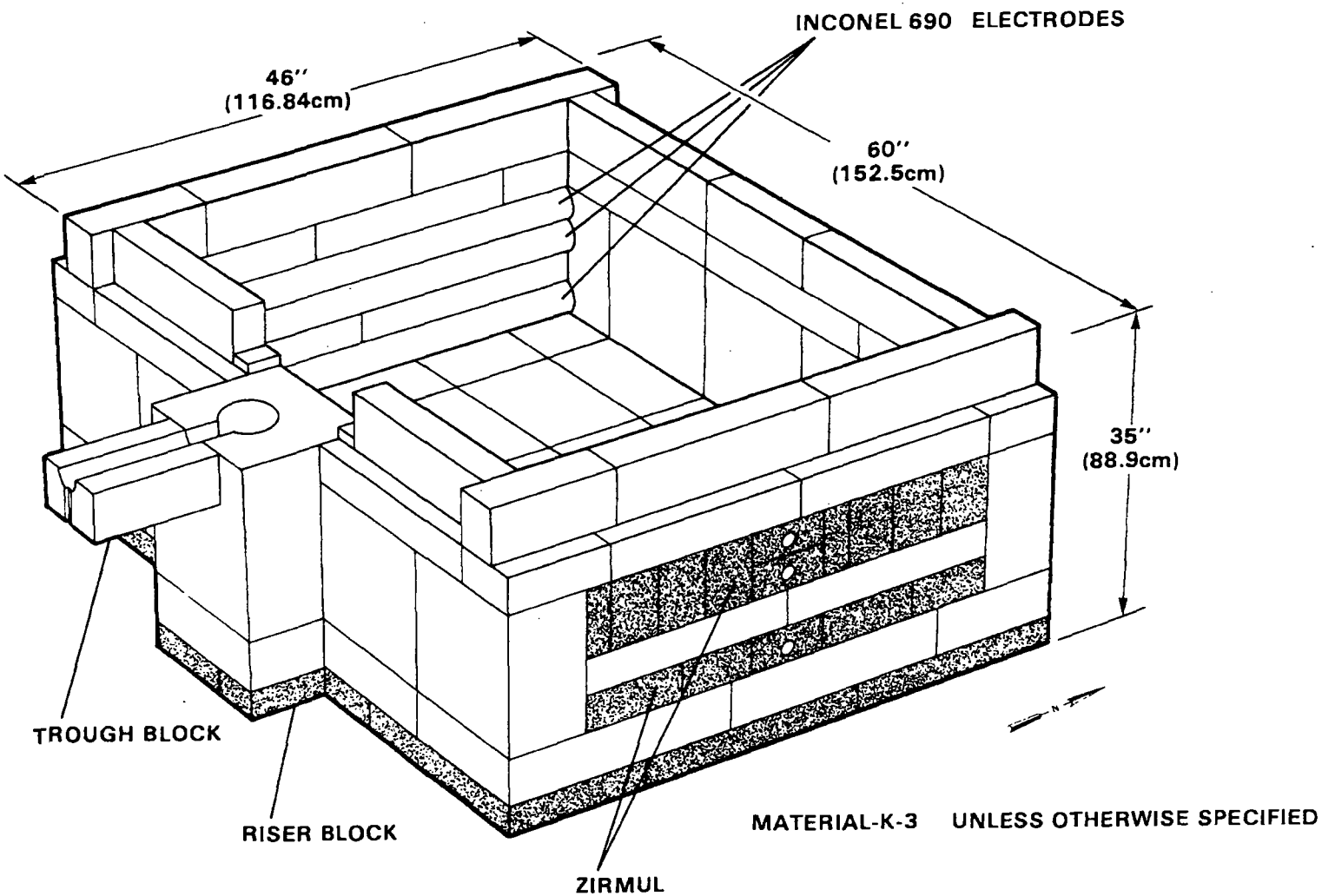

FIGURE 13. Glass Contact Refractory, Southeast View

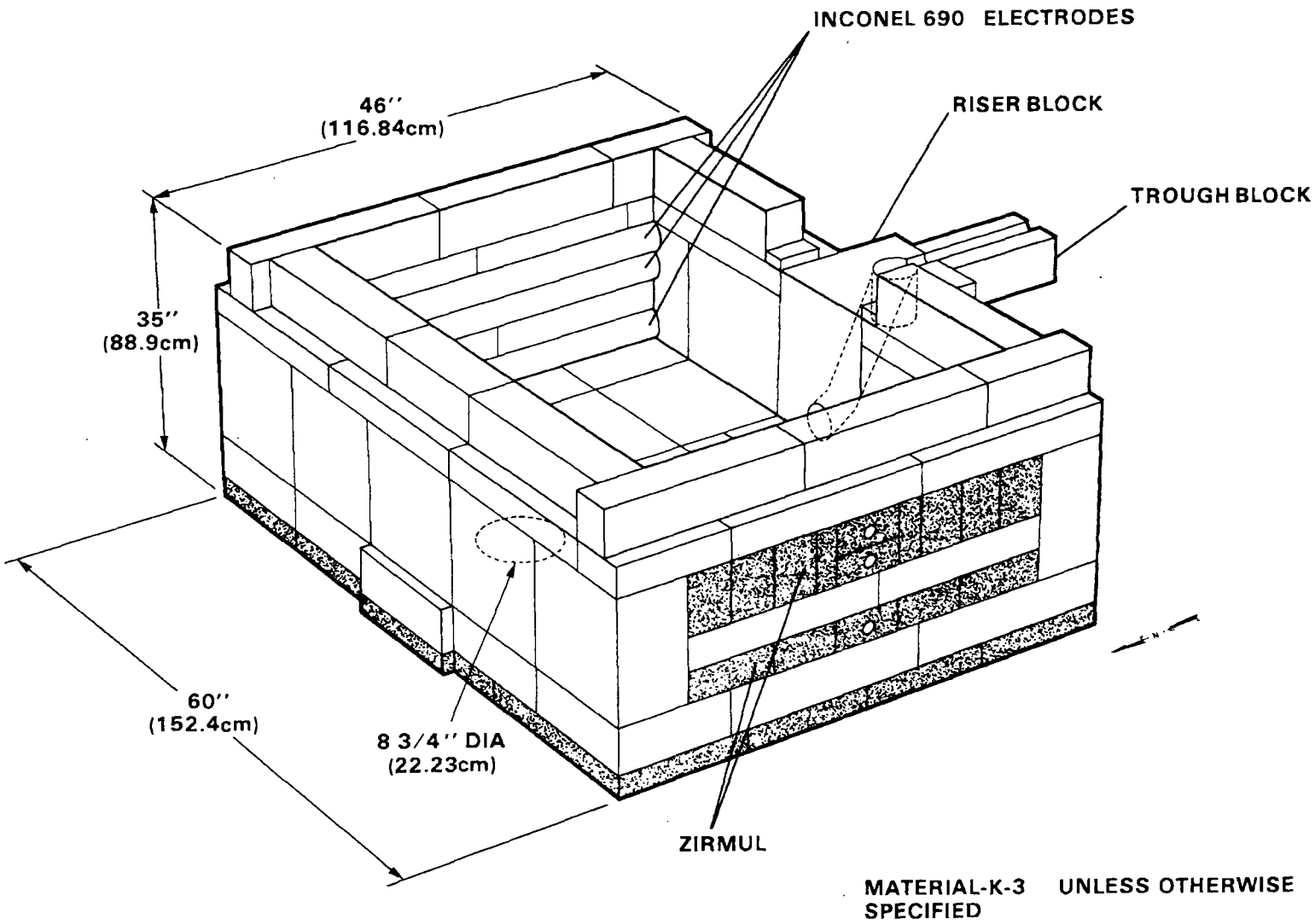

FIGURE 14. Glass Contact Refractory, Northwest View

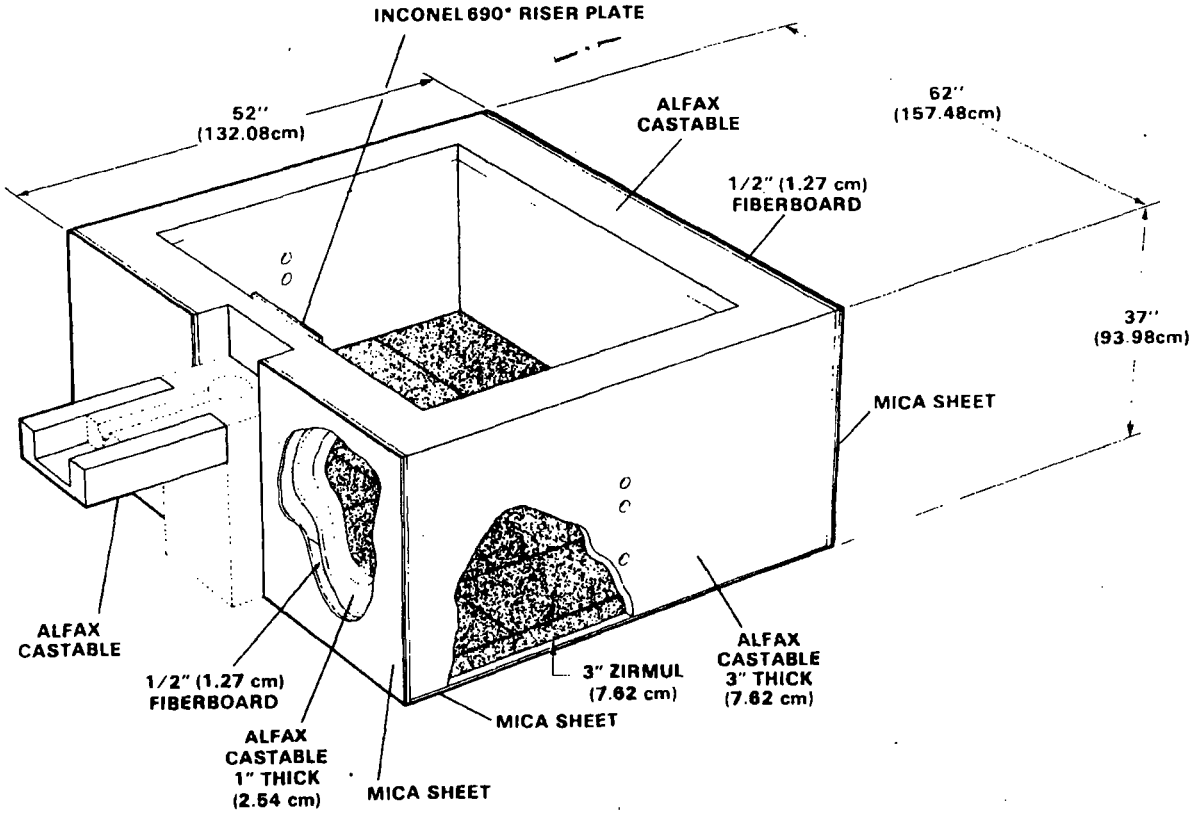

FIGURE 15. Backup and Insulating Refractory Detail

in Tables A.1 and A.2. Typical brick dimensions used were 30.5 cm by 7.6 cm by 45.7 cm. The floor and walls are surrounded by sheets of mica for added electrical protection. Crushable fiberboard, 1.3 cm thick, was placed between the refractory walls and containment box to accommodate the thermal expansion of the refractory during heatup.

3.2.4 Overflow Drain

During operation, the glass flows from near the melting cavity floor, through a riser block, over a trough, and into a receiving canister. The glass drainage is controlled by a tilting mechanism (screw jack), shown in Figure 2. This tilting mechanism operates much the same way as a tea kettle. When the screw jack is raised or lowered, the melter tilts about the pivot point, allowing the glass to drain. Molten glass falls from a pouring spout

made of Inconel 690 through an airtight spool piece into the canister below. More than 100 kg of the glass reservior maintained in the melting cavity may be drained with an $\sim 2^{o}$ tilt angle with this melter.

The overflow section must be heated externally so the glass will remain fluid enough for pouring. The LFCM uses three separately controlled zones of silicon carbide heaters. Each of these zones is controlled independently, either manually or by automatic temperature control. The riser block also has two zones of plate-type heaters located outside the containment box.

3.2.5 Power Electrodes and Control

Inconel 690 was chosen for the LFCM electrodes based on prior good experience with this alloy in other melters. The electrode positions are shown in Figure 16. The electrodes, which were machined out of 5-in.-dia Inconel ingot, are imbedded in the opposing electrode walls. For additional control of glass tank temperatures, the electrodes are arranged in a dual electrode system consisting of an upper and lower set of electrodes, as shown in Figure 16.

The upper electrodes receive their power from a multitapped, 250-KVA, single-phase transformer. The power can be controlled by a manual constant-current or constant-power signal feedback loop. Since electrical resistivity of glass decreases with temperature, constant-current control offers a desirable self-regulating feature because the voltage, and thus power, decreases as the temperature rises. The electrodes can also be controlled by constant temperature, which is read by an internal thermocouple in the electrodes or by an infrared optical pyrometer. The lower electrodes can either be controlled manually or by a ratio of the current feedback signal from the upper electrodes. The actual power to the electrodes is regulated by silicon-controlled rectifiers (SCRs). Figure 17 shows the overall power system component schematic.

3.2.6 Ionic Booster System

The ionic booster system is designed to increase slurry feed throughput by heating the slurry pool directly with the joule effect. The system

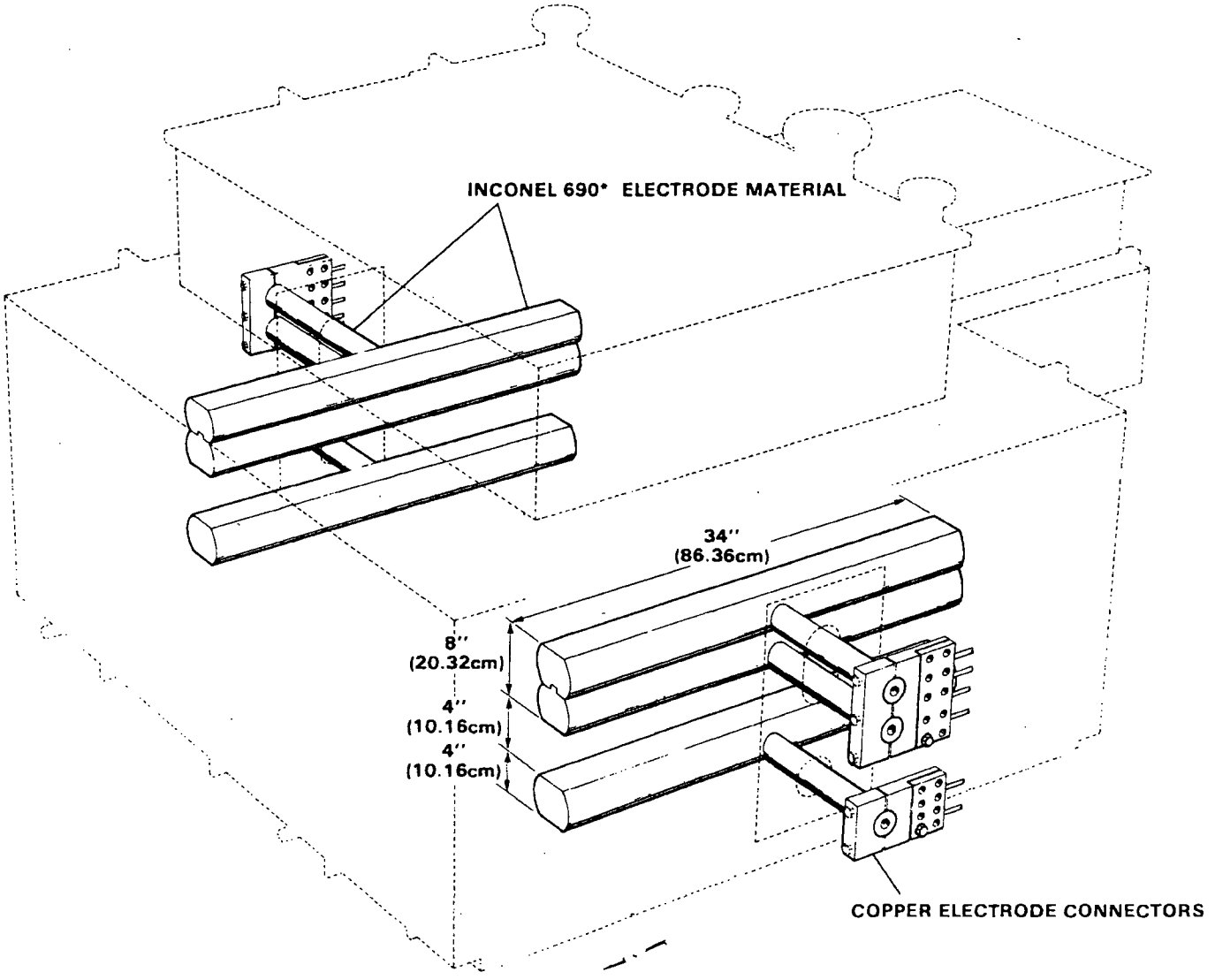

FIGURE 16. Electrode Arrangement

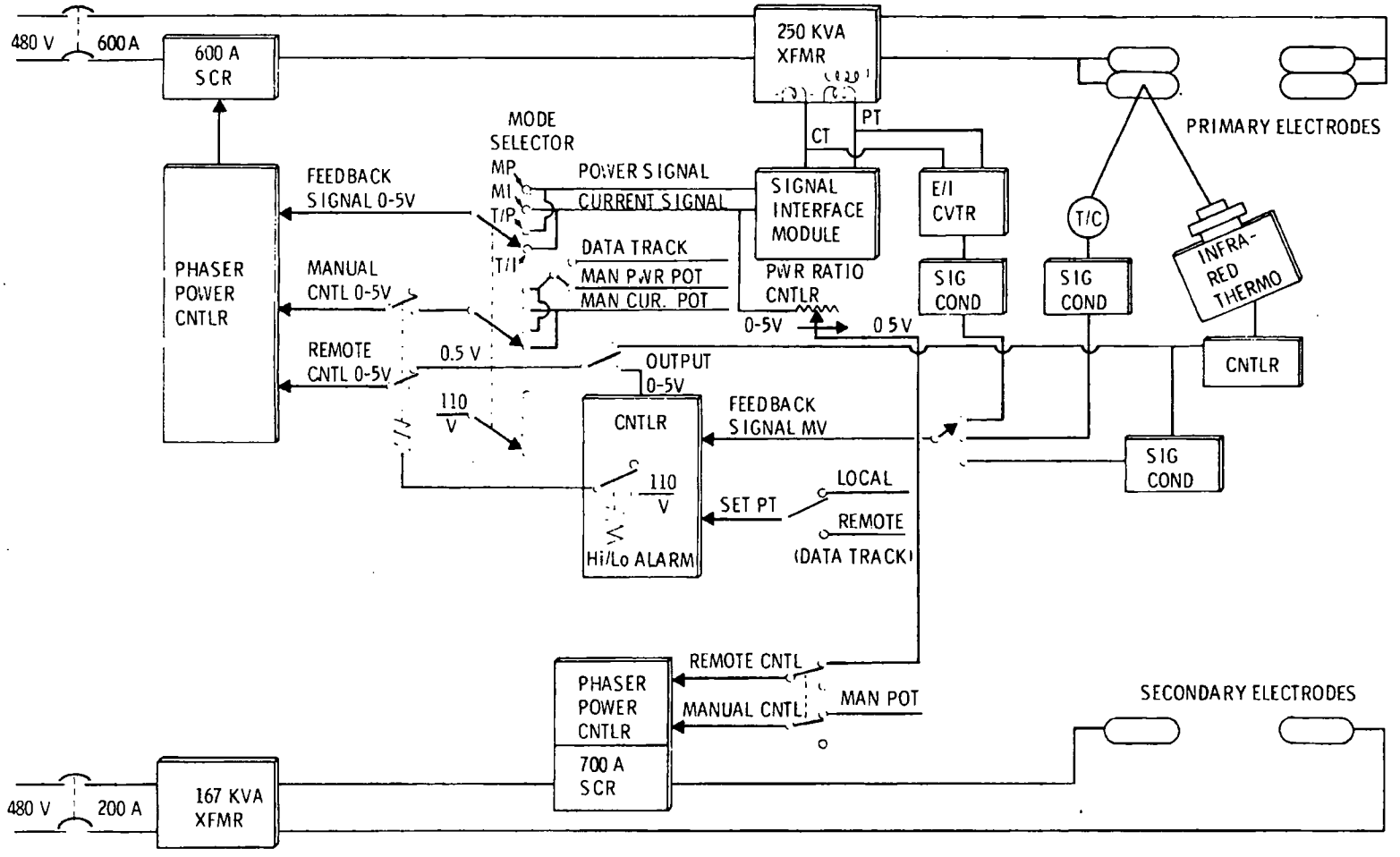

FIGURE 17. Liquid-Fed Melter Electrode Power Control Systems

comprises two water-cooled, stainless steel 304L electrodes with an associated power supply and control system. An electrode is installed at the east and west ends of the melter above the glass, as shown in Figure 6. The ionic booster electrodes are placed in contact with the slurry, and an alternating electric current, in the same phasing as the electrodes in the glass, is passed between them. This generates joule heating directly in the slurry feed.

The electrodes are constructed of 5-cm, schedule-40 pipe. The water coolant passes through the electrodes in series with electrical isolators between the electrodes. Provisions were made for stopping the cooling water flow in the event of a melter pressurization (a possible result of a leak in the ionic booster cooling design, among other causes). The electrodes were designed to be vertically mobile with flexible metal bellows sealing the system to the melter containment.

3.2.7 Offgas System

The gases generated from the vitrification process first pass through a venturi scrubber and then through a packed-column scrubber for removal of nitrates and other effluents. The noncondensibles are then exhausted through a blower to the atmosphere. Figure 18 shows the offgas system used for the LFCM. Vacuum in the melter is controlled by a valve upstream from the offgas blower.

3.2.8 Freeze Valve

A bottom drain was incorporated into the design of the LFCM as an auxiliary drain system and as a method of completely removing the glass from the melter for shutdown purposes. For hot-cell use, the drain must operate remotely. This type of technology is not available in the commercial glass industry. A schematic of the freeze valve is shown in Figure 19.

The freeze valve is an annulus 0.5-cm wide. The annulus is provided with cooling jackets on both the internal and external sides and is also supplied with a heat source. When not in operation, there is a solidified glass plug in the annulus, preventing any glass from flowing. When glass drainage is

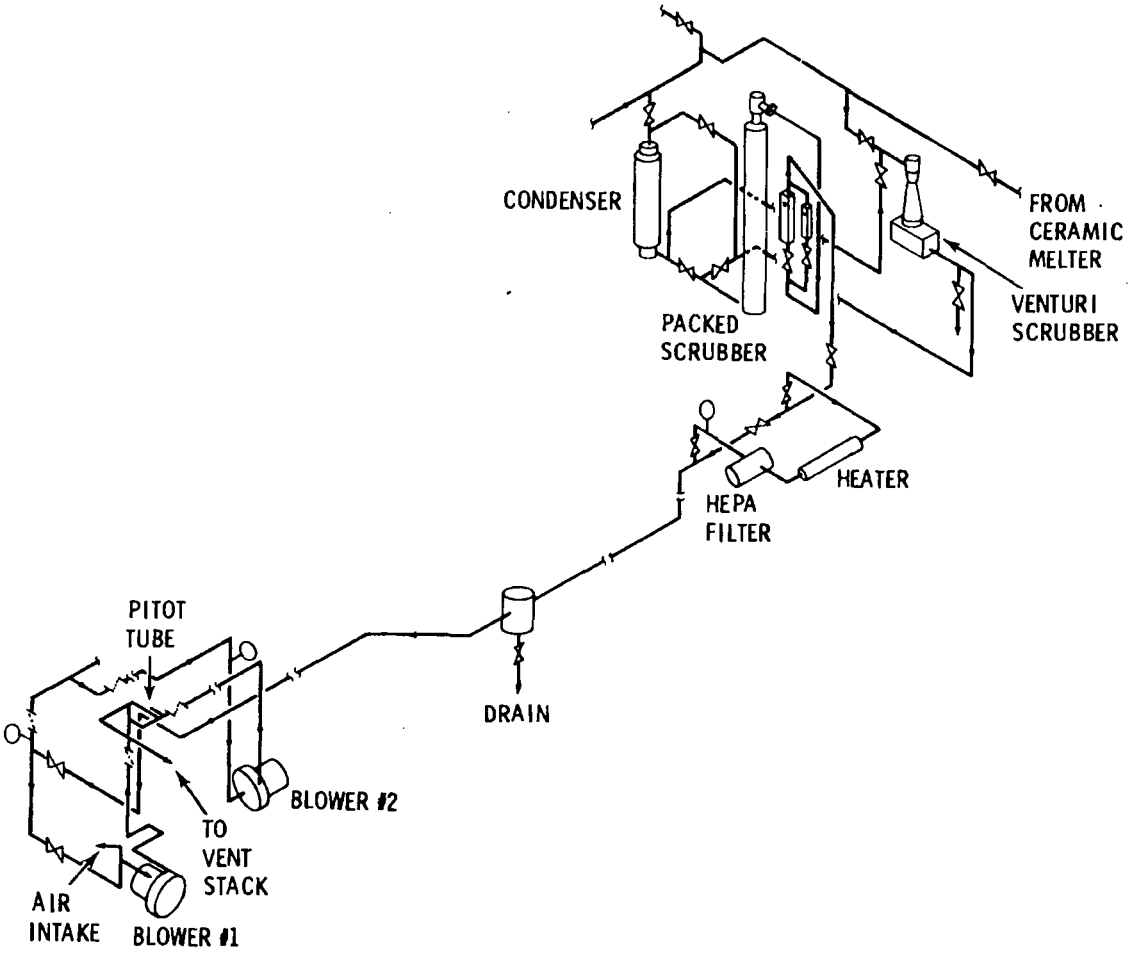

FIGURE 18. Offgas Treatment System

desired, the cooling is turned off and heat is applied. This thaws the solid glass plug and allows the glass to drain. Glass drainage can be controlled and stopped if a cooling fluid is introduced in the cooling jacket. This fluid can be water, steam, or air.

3.2.9 Auxiliary Power Systems

As discussed earlier, certain sections of the LFCM require heat generation in addition to the energy supplied by the power electrodes. The heaters

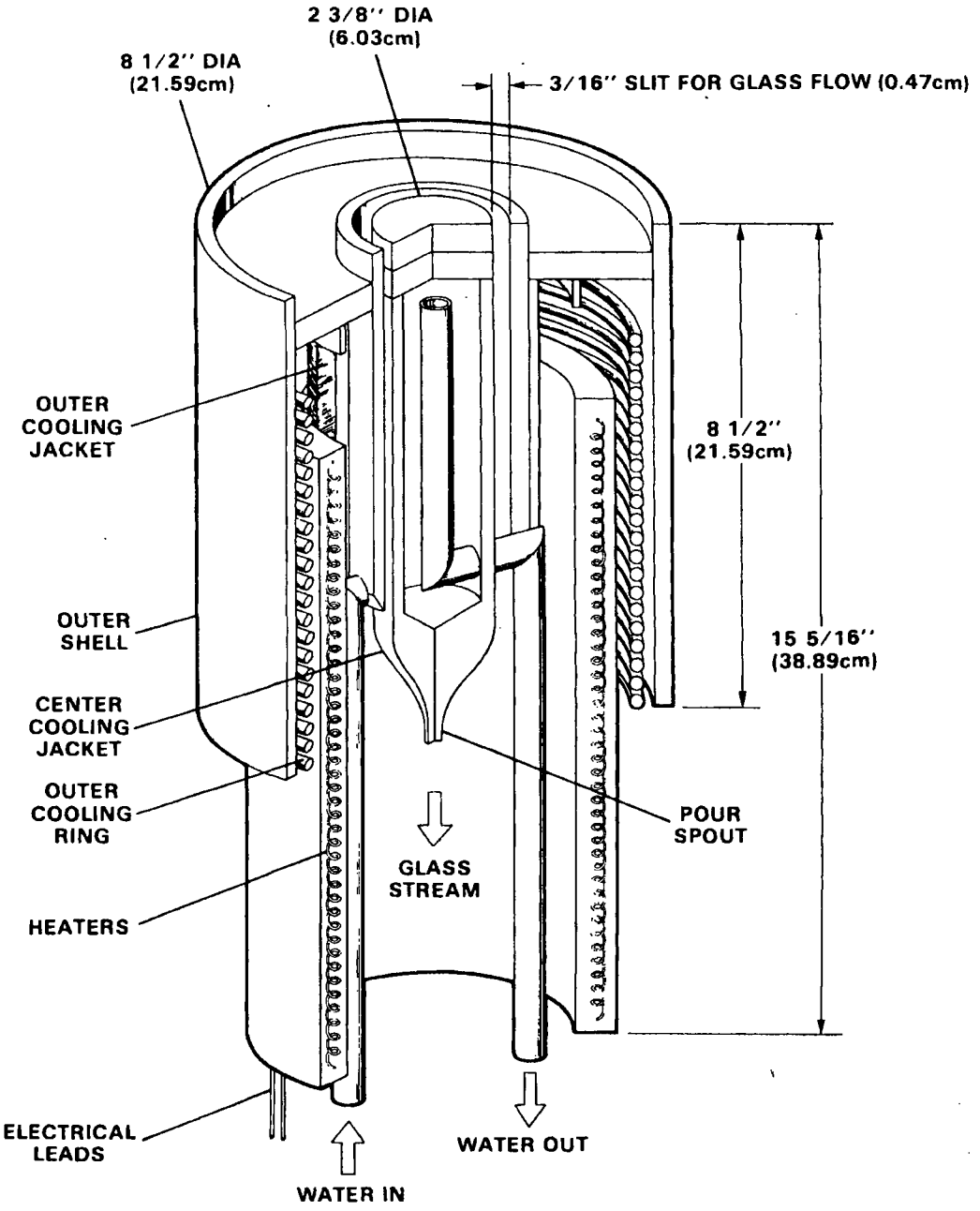

FIGURE 19. LFCM Freeze Valve Detail

are either ceramic plate heaters with resistance heating wire as the heating element, or silicon carbide resistance heaters. Their locations and type are shown in Figure 20 and are identified below:

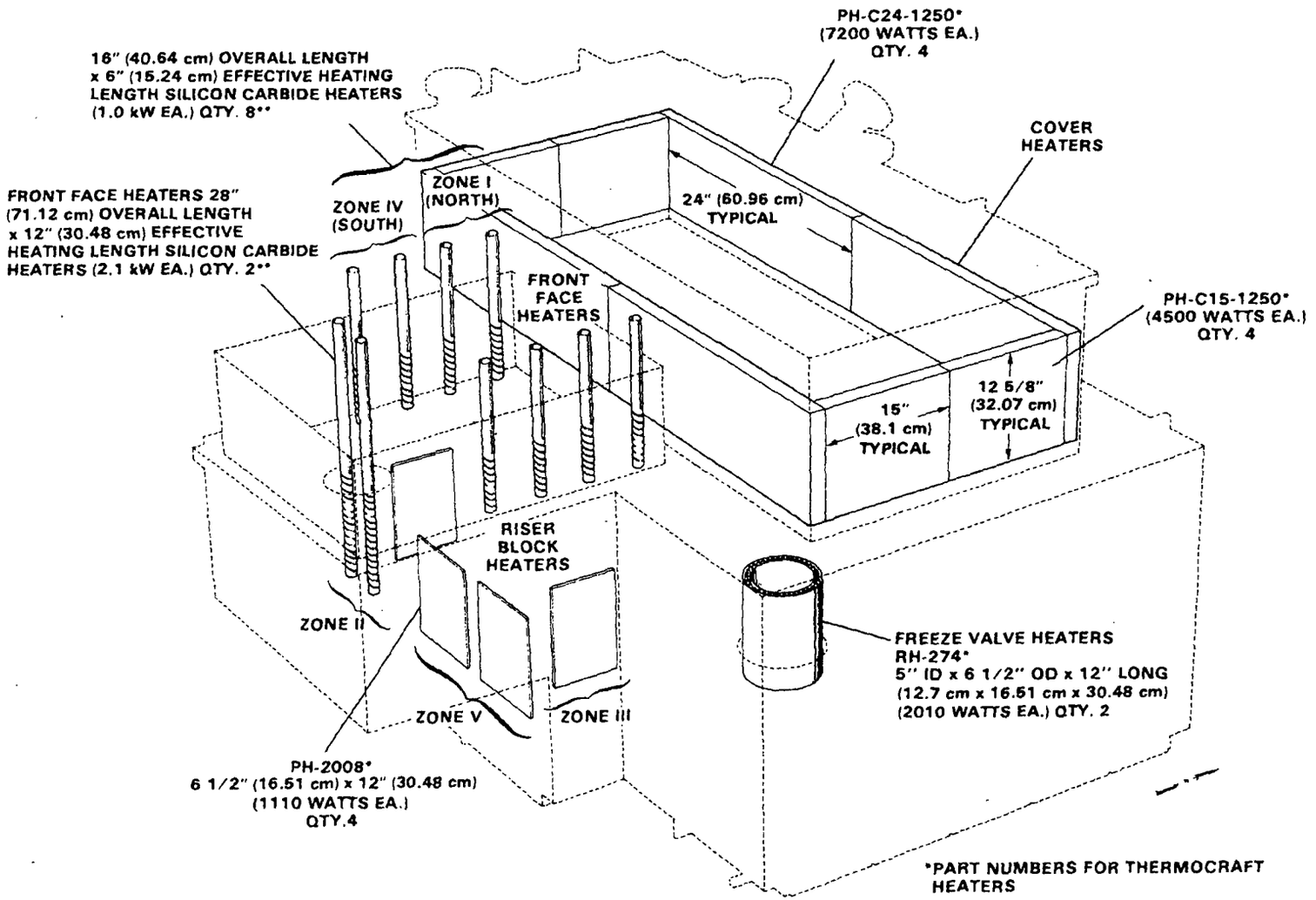

FIGURE 20. Auxiliary Heating Systems

- overflow heaters, Zones I, II, and IV
- riser block heaters, Zones III and V
- lid heaters
- bottom drain heaters.

The lid heaters were used for the initial melter startup and could be used to improve the slurry-fed glass production rate by radiative heating of the cold cap from above.

3.2.10 Instrumentation

The LFCM has been constructed with instrumentation for extensive data acquisition. Temperatures are continually monitored and recorded for the electrodes, for various locations within the refractory floor and walls, amid the auxiliary heaters in the overflow, on the lid, and on the riser section. Thermocouples are also located in the bottom drain and on the receiving canisters. Cooling flow to the various sections of the melter is also monitored for temperature and flowrate. In addition, the gross canister weight is continually recorded for monitoring the glass-production rates.

3.2.11 Feed Systems

Because of the different operating modes of this melter, both liquid and calcine feeding systems are required. Simulated liquid waste is metered by an air lift from a head tank pot up to an air/liquid disengagement chamber. From that chamber, the liquid flows by gravity to the melter, as shown in Figure 21.

During calcine feeding, solids are fed from a volumetric feeder through a central flange in the cover plate of the melter. During the early tests with the LFCM, solids were introduced near the rear wall of the melter and were distributed over the entire surface with a batch distributor (Chapman et al. 1979). This distributor system process was eliminated to reduce the amount of moving parts in the calcine-fed mode.

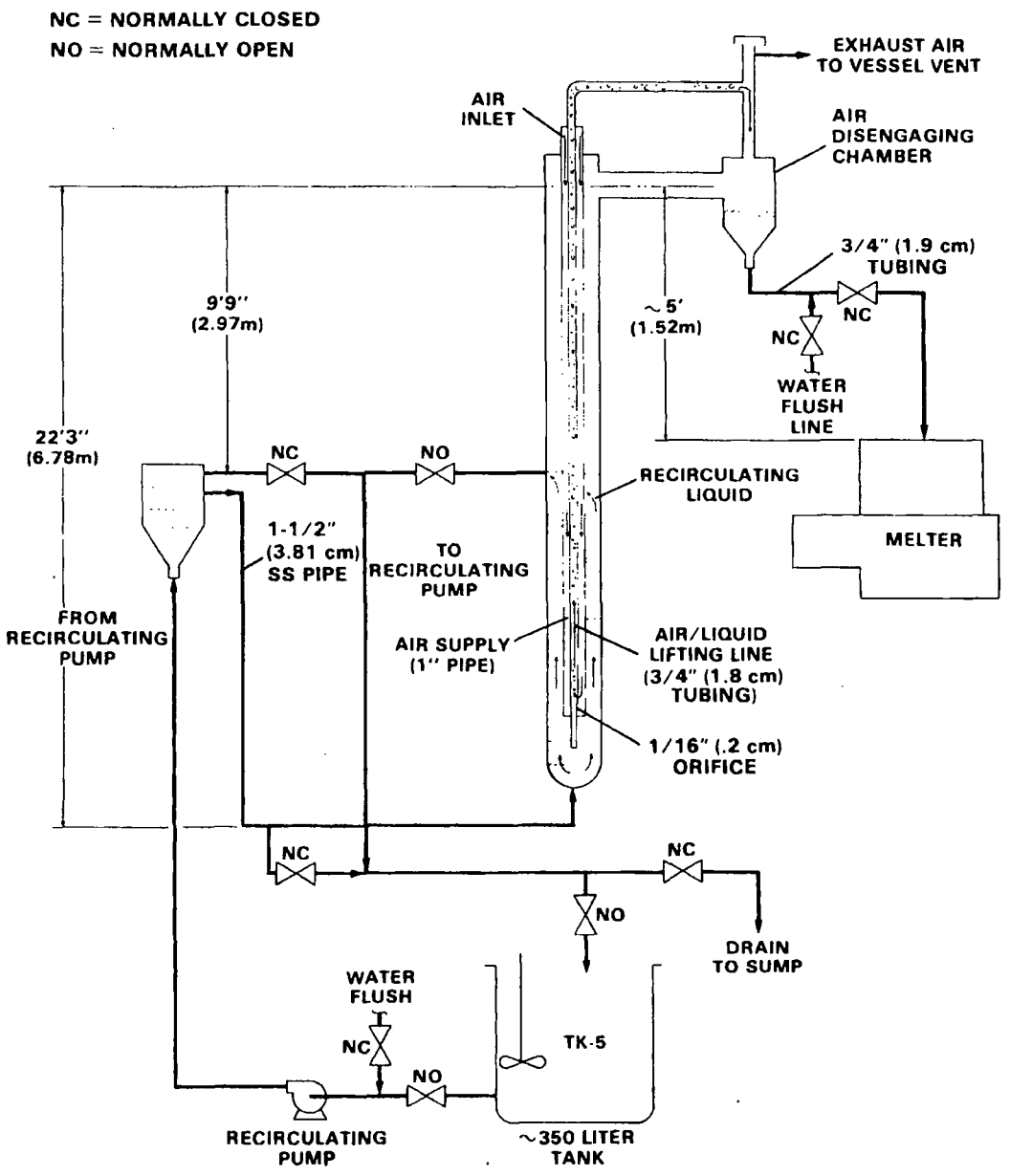

FIGURE 21. Liquid Feed System

4.0 OPERATING EXPERIENCE

Construction of the LFCM was completed in February 1977. The melter was started up by filling it with premelted glass granules (cullet). Using the lid heaters to melt sodium hydroxide placed on the cullet surface, joule-heating was initiated. The melter was heated to operating temperature over a 22-h period and was operated continuously, either in the processing or idling mode, until it was shut down in February 1980 for modifications and examination. Thus, the melter was in operation for about three years.

During its operating life, 19,000 L of slurry and 54,000 kg of calcine with glass formers were fed to the melter. This produced 80 tonnes of glass with about 780 operating hours under feeding conditions. A summary of the melter operation is presented in Appendix B.

Specific operating characteristics of the LFCM (and ceramic melters in general) during glass-production testing has been well documented in earlier reports, and is beyond the scope of this report. The documents by Brouns et al. (1980) and Chapman et al. (1979) are recommended for the reader interested in specific melter operational data.

The following are significant events that occurred during the operating life of the melter that may have affected the condition of the melter, or are notable from a design/operation viewpoint:

- rapid initial startup--The LFCM was initially brought to operating status in about 22 h. This rapid heatup rate exceeds the recommended temperature-increase rate for the refractories and probably produced excessive thermal stresses in the refractory layers.
- overflow-drain section rapid heatup--The overflow-drain refractory was also heated rapidly to operating temperature on several occasions following the replacement of failed silicon carbide heating elements. As above, rapid temperature changes can produce damaging thermal stresses.

- foaming events--The melter refractory also was exposed to thermal shock conditions during periods of glass-foam generation. Although glass foam is generated by several mechanisms (Blair and Lukacs 1980), foam generation following stable cold-cap development would expose the cool Monofrax K-3 refractory above the cold cap to high-temperature glass. Depending on the initial Monofrax K-3 surface temperature, this could produce refractory heating much faster than the $<40^{o}C/h$ recommended by the Monofrax K-3 manufacturer.

- slurry feed initiation transients--Typical melting-cavity temperature decreases of $150^{o}C/h$ have been measured during slurry feeding initiation, and maximum rates of $\sim 300^{o}C/h$ have been recorded. Audible cracking has been reported at these high rates of refractory temperature change.

- power outages--The LFCM operating power was suspended for many short periods, and two extended power outages (maximum of 17 h) were encountered. On each occasion, the melter was returned to operating status by joule-heat generation in the melting cavity by the electrodes.

- elimination of melter containment-box cooling--The melter-containment-shell water cooling was discontinued (with the exception of the electrode walls) in August 1979. The temperature profile changes in the refractory may have affected the refractory cracking and produced the bowing observed in one of the coolant channels (Section 5.1).

- coolant interruptions of the ionic booster electrodes--The coolant for the ionic booster electrodes was interrupted on two occasions, producing $200^{o}C$ higher plenum temperatures than normal. These elevated temperatures may have increased the warpage of the melter lid and cover plate.

- melting cavity pressurization--The melting cavity pressure varies during glass production testing because of changing offgas production, especially during slurry feeding. Routine minor pressure variations were observed, and one event produced ∿3.7 MPa melting cavity pressure. Large pressure variations may affect the mechanical deformation of the melter lid.

5.0 MELTER EXAMINATION

The following sections discuss the observations made of the melter condition during dismantling. The mechanisms producing the observed corrosion of the Monofrax K-3, Alfrax 66, electrodes, ionic booster electrodes and offgas piping are presented in Section 7.0.

5.1 CONTAINMENT BOX AND LID

Following the melter draining, the external insulation was removed from the stainless steel containment box. The melter box was found to be in generally good condition, with a few discolored areas from exposure to elevated temperatures. The areas of discoloration were found primarily in the overflow drain section where the internal insulation was at a minimum. The only physical distortion of the containment box was bowing of the lower south-east cooling jacket. This deflection, shown in Figure 22, was probably the result of the elimination of the water coolant flow in the lower cooling jackets. This change was intended to increase the operating temperature of the refractory near the melter floor to minimize the deposition of precipitates from the glass. Following the coolant shut off, sufficient steam pressure to cause the bowing could have occurred as residual water in the jacket began to boil. Also, if the melter drain system pressurized, water could have been injected into the cooling jacket producing the same results. Minor changes in the cooling system design to reduce the coolant flow restrictions can eliminate this problem.

The lid assembly was more seriously affected by the melter operating cycles. Figure 23 shows the melter lid following removal. The photograph illustrates the bowing of the assembly's vertical surfaces, tears in the flanges where the lid is joined to the melter box, and the warpage of the cover plate.

The difference in the condition of the lid and melter box was expected as the containment box was protected by substantial internal insulation, whereas the lid assembly was insulated only externally. The lid, therefore, experienced the full effects of the thermal cycling induced during the operation of the melter.

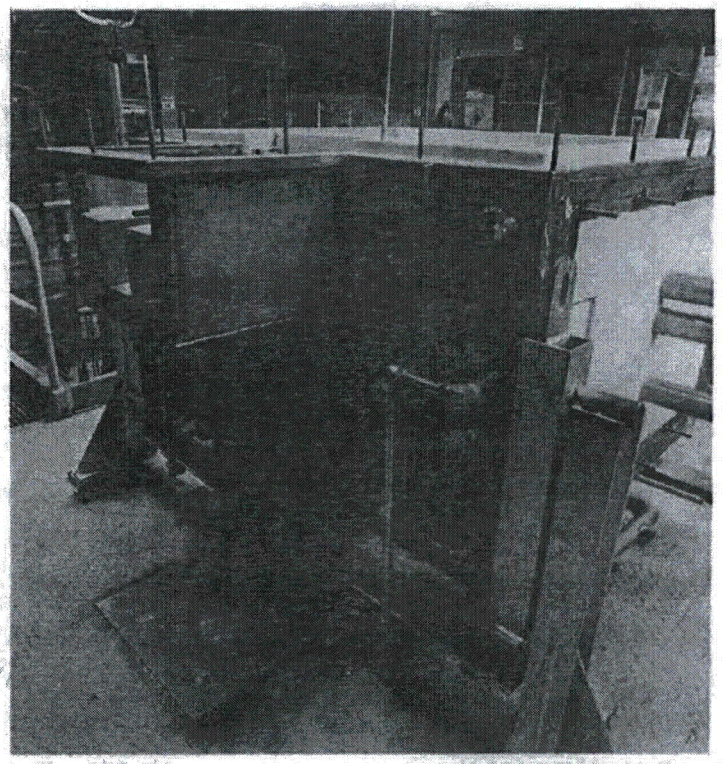

APPEARANCE OF COOLING JACKETS DURING CONSTRUCTION

DISTORTED COOLING JACKET

FIGURE 22. Distortion of Lower Southeast Containment Box Cooling Jacket

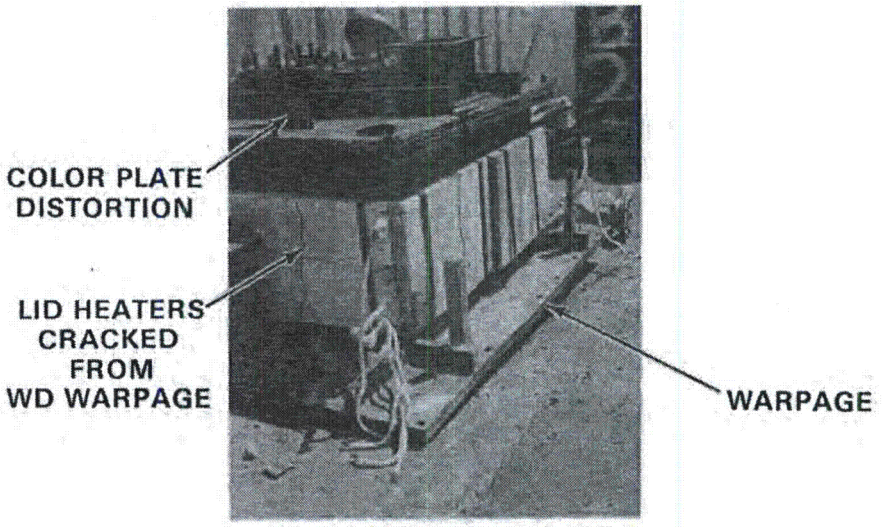

VIEW FROM SOUTHEAST

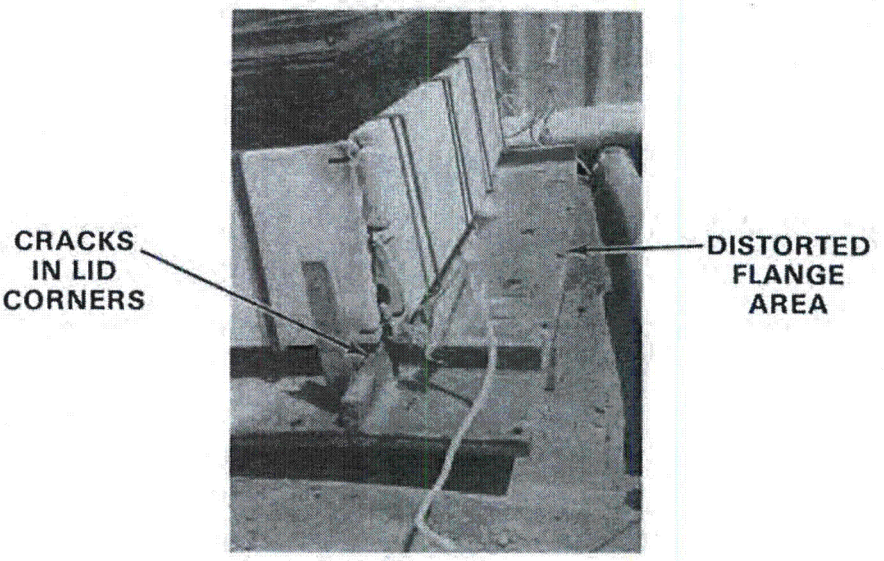

VIEW ALONG NORTH SIDE

FIGURE 23. Melter Lid Assembly Following Removal

Because lid heaters were installed on the exterior surface of the lid, it also served as a radiative heat source during the melter startup and on other occasions when the external lid heaters were employed. The thermal cycling caused by normal operations, combined with periods of lid heater use resulted in the lid warpage. In some locations, the lid warpage was sufficient to crack the lid heaters, as shown in Figure 23.

The tears in the lid, which developed in each of the corners, are also the result of temperature cycling. Free thermal expansion of the lid was restrained by the water-cooled melter box. This restricted thermal expansion, combined with the different thermal expansion coefficient for the stainless steel and Inconel 601 components, caused the lid weld failures.

The operating temperature cycles and stress concentrations from the numerous penetrations, welds, and dissimilar construction metals account for the severe warpage of the cover plate. The cover plate deformation explains air inleakage experienced early in the operating life of the melter. The distortion of the cover plate, combined with the high-temperature degradation of the asbestos gasketing material initially used to seal the cover plate to the lid assembly, forced the removal of the asbestos rope and the welding of the cover plate to the lid assembly to seal the melter.

5.2 RESIDUAL GLASS AND SLAG

The melting cavity contained significant quantities of residual glass and precipitated crystals (slag) after the melter was drained, as pictured in Figure 24. The slag in this photograph covers approximately the bottom 7.5 cm

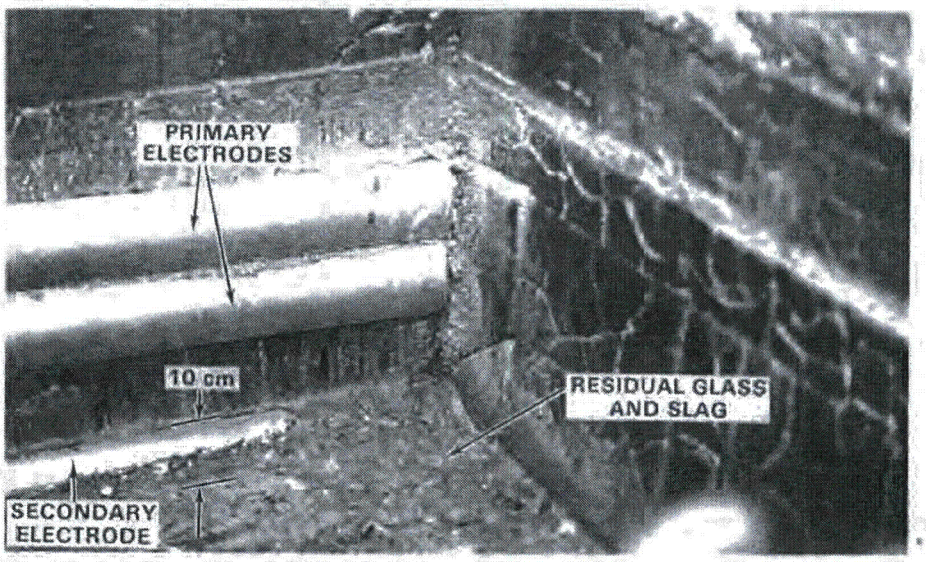

FIGURE 24. Slag and Residual Glass Remaining on Melter Floor Following Shutdown

of the 10.2-cm secondary electrode. Figure 25 is a contour plot of the melter floor showing the depth of slag deposits in centimeters. The empty area in the figure is an area on the melter floor where the slag deposits were disturbed in an early effort to determine the condition of the riser inlet nozzle. Thus, accurate measurement of the slag deposit depth in this region could not be determined.

From Figure 25 it is apparent that there is a slag depth gradient from the electrode walls down to the center. Also, the deposits in the corners of the north wall are deeper than the corresponding corners of the south wall. This pattern is the result of the corners and edges being the coldest locations along the melter floor (thereby tending to precipitate crystalline phases), and of the two convection cells that are present in the melter. These major convection cells were predicted by melter modeling (Quigley and Kreid 1979). The convection cells rise along the melter's east-west

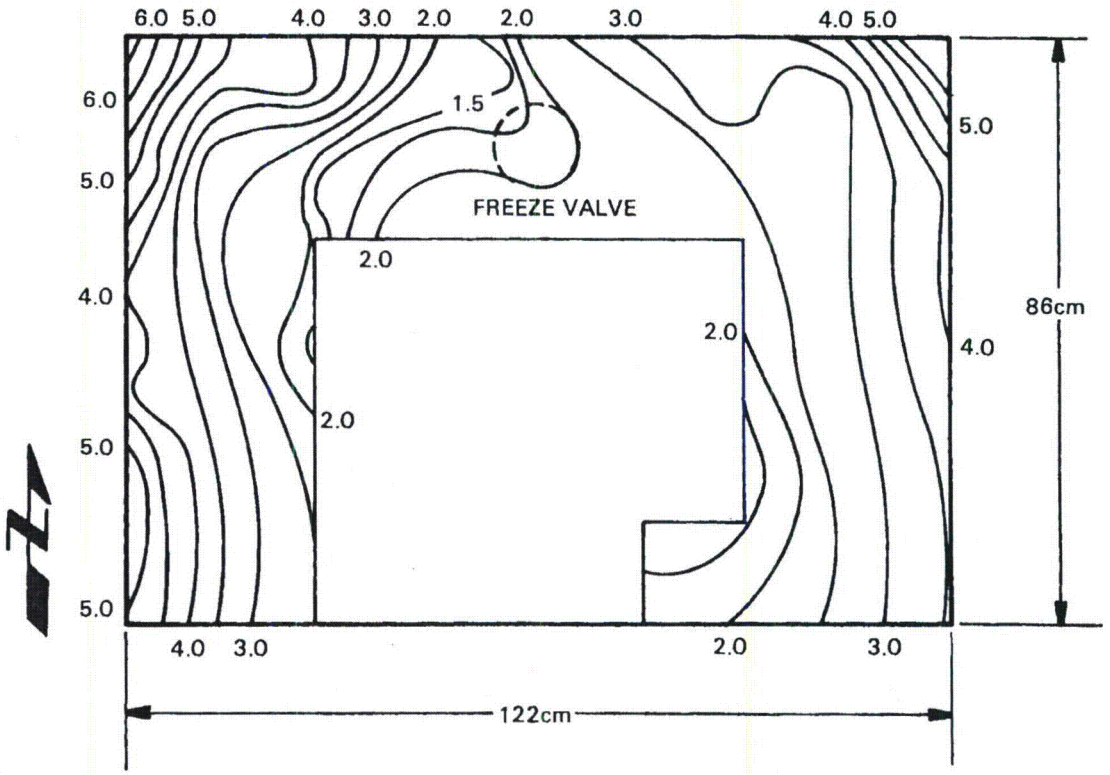

FIGURE 25. Depth at Slag Deposits in LFCM (cm)

centerline, flow toward the electrode walls, and sweep across the electrodes and the melter floor, producing slag accumulations in the relatively stagnant zones at the base of the electrodes.

The fact that the deposits are deepest along the north wall suggests that the slag has a tendency to accumulate on the north side because of the sloping of the melter floor during the idling periods. Typically, when the melter idles, the LFCM is oriented with a 2^{o} tilt from horizontal toward the north. Also, the north wall would be generally cooler than the south wall because the overflow drain heading would affect the south wall temperature profiles. The two major operational concerns about the slag layer were whether the slag would grow deep enough to block the riser drain inlet nozzle or prevent the freeze valve from functioning. The slag deposits on the LFCM floor did not interfere with either of these melter operations.

One of the objectives of this investigation was to determine if the concentration of any of the feed chemicals in the slag was greater at one location than at another. This was accomplished by systematically excavating the slag deposit by grids. The grid pattern is shown in Figure 26. Samples were

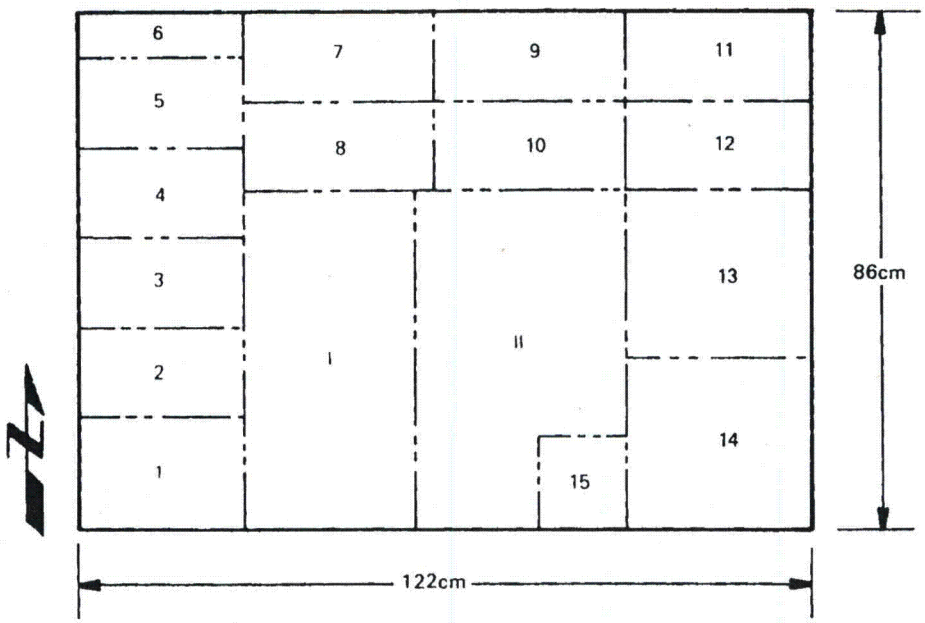

FIGURE 26. Slag Excavation Grid Pattern on LFCM Floor

removed from the various grids and examined by x-ray fluorescence to determine the composition. The results of the analysis are presented in Figures 27 and 28. The results are inconclusive becuase the elemental concentrations were not found to be constant among the samples removed from a particular grid. However, two findings are apparent from this data. First, the samples containing relatively large concentrations of cerium oxide were removed from areas of the melter floor containing the deepest deposits. This was expected because cerium was a feed component only in the early melter tests and therefore should be found in the older, deeper slag deposits.

Second, a relationship between the concentrations of two groups of elements in the slag was observed. The concentration of Ce, Cr, and Zn vary inversely with the concentration of Fe, Mn, and Ni for all of the locations on the melter floor. This relationship is a result of the time that the slag was formed. The data indicate that the slags formed during the early processing tests were cerium oxide, Zn-Cr spinel, and chromium oxide. These chemicals were common components of the early feeds. Also, the release of Cr_2O_3 from the Monofrax K-3 corrosion would be expected to be maximum during the early tests before the spinel layers on the refractory were fully developed. The more recent process test feeds, however, contained substantial quantities of iron, manganese, and nickel, and would tend to form (Mn, Ni) Fe_2O_4 spinels. Therefore, the variation in the slag composition is a result of the operating period during which they were formed.

The appearance of the slag is pictured in Figure 29. The samples pictured here were removed from the upper layers of the slag. The composition of the material was shown to be primarily a spinel, $[(Fe,Mn,Ni)(Fe,Cr)_2O_4]$, with sporadic appearances of other crystalline phases. In general, the slag was found to be a complex mixture of glass compositions, Mn-Ni-Fe-Cr spinels, Cr-Fe-Zr crystals, CeO_2 deposits, Al_2O_3 nodules, Ru phases, and trace quantities of all of the other feed components. Additionally, a metallic nickel alloy with small quantities of chromium and iron was found in the slag.

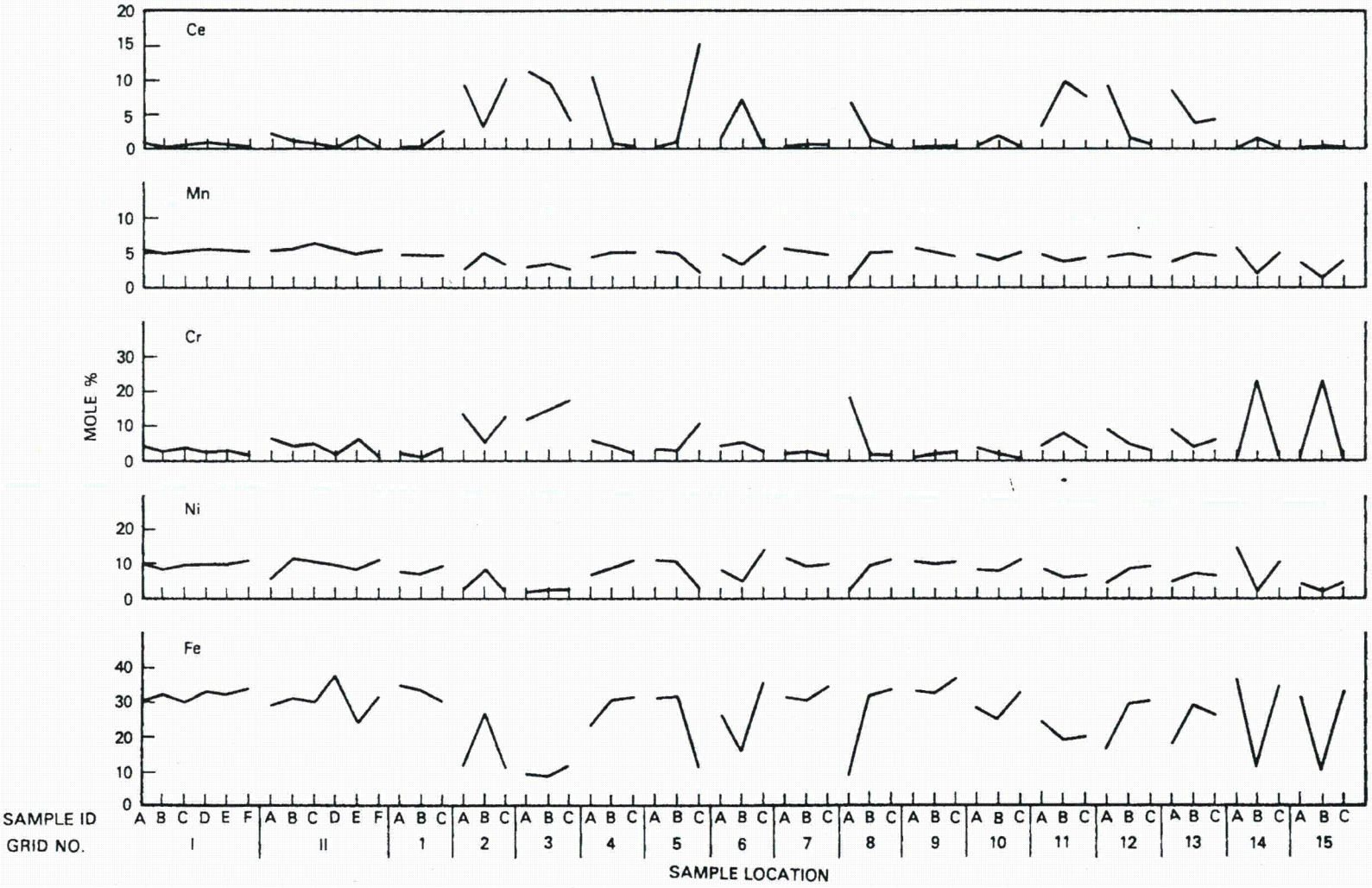

FIGURE 27. Metal Concentrations for Samples Removed from the LFCM Slag, by Grid Number

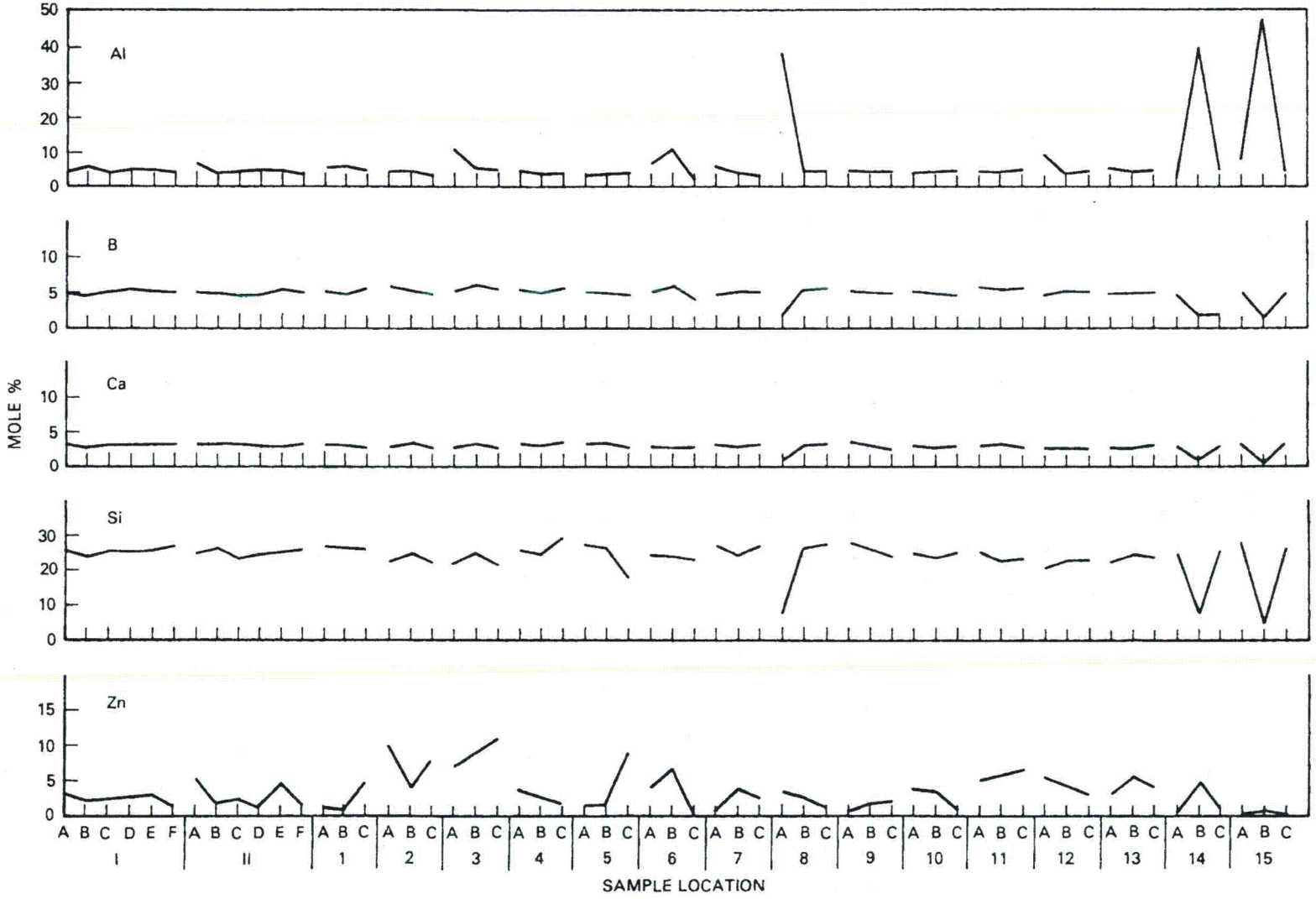

FIGURE 28. Chemical Concentrations for Samples Removed from the LFCM Slag, by Grid Number

FIGURE 29. Enlargement of Slag Sample Removed from Grid Sector II

5.3 MELTING CAVITY REFRACTORY

The following section discusses the condition of the various melter refractory components.

5.3.1 Monofrax K-3

The Monofrax K-3 refractory following the melter shut down is pictured in Figures 30, 31, and 32. The most apparent features are the general uniformity of the cracking present in the bricks and the intact cold wall (wall opposite

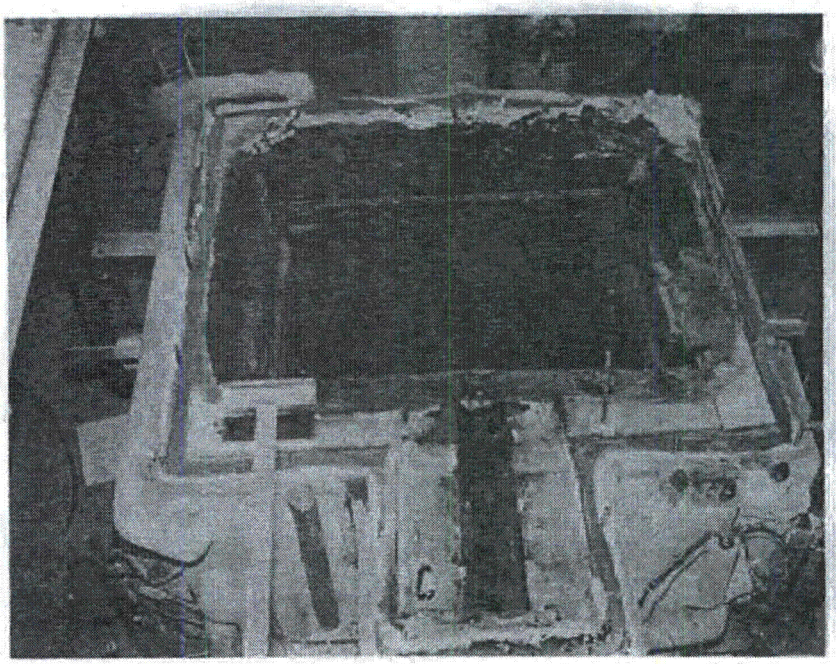

FIGURE 30. Melting Cavity North Monofrax K-3 Wall

the melting cavity drain), whereas several large brick pieces have fallen from the hot wall (south wall). The difference between these refractory walls can also be seen by comparing Figures 33 and 34. These figures are representative of the wall contours. The contours were measured in centimeters from a plane set at an arbitrary distance from the wall. The numbers reported are the distances from this plane to the wall. Because the contour numbers reported for a particular wall are based on a common plane, the changes in the surface characteristics from one point to another are obtained by subtracting the contour magnitudes at the points of interest.

The photographs and respective contour plots display the difference between the conditions of the north and south walls. The mechanisms for crack formation in the Monofrax K-3 is discussed in detail in the stress analysis section of this report (Section 6.0). Briefly, the Monofrax K-3 cracking is due to excessive stresses developed by thermal expansion, and thermal shocking of the refractory during liquid-feed initiation.

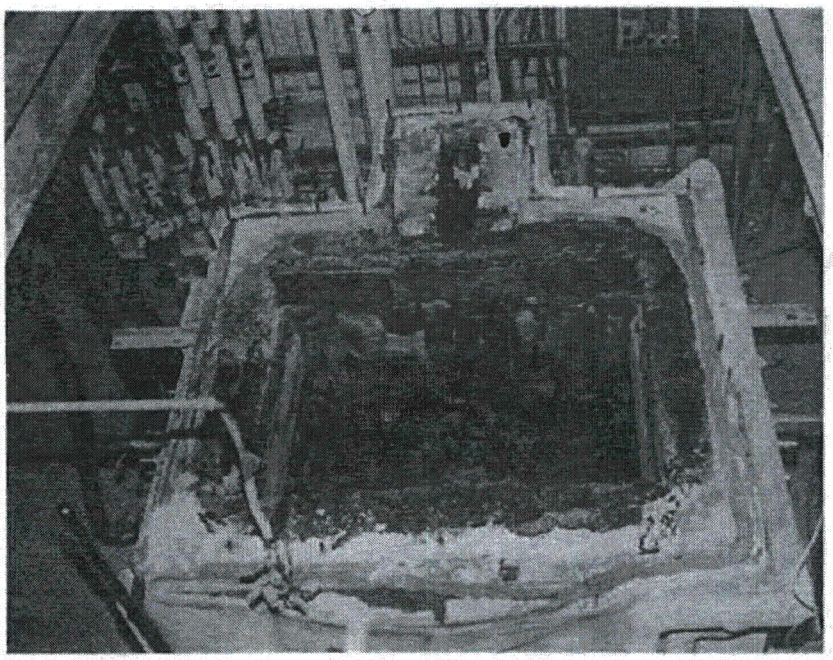

FIGURE 31. Melting Cavity South Monofrax K-3 Wall

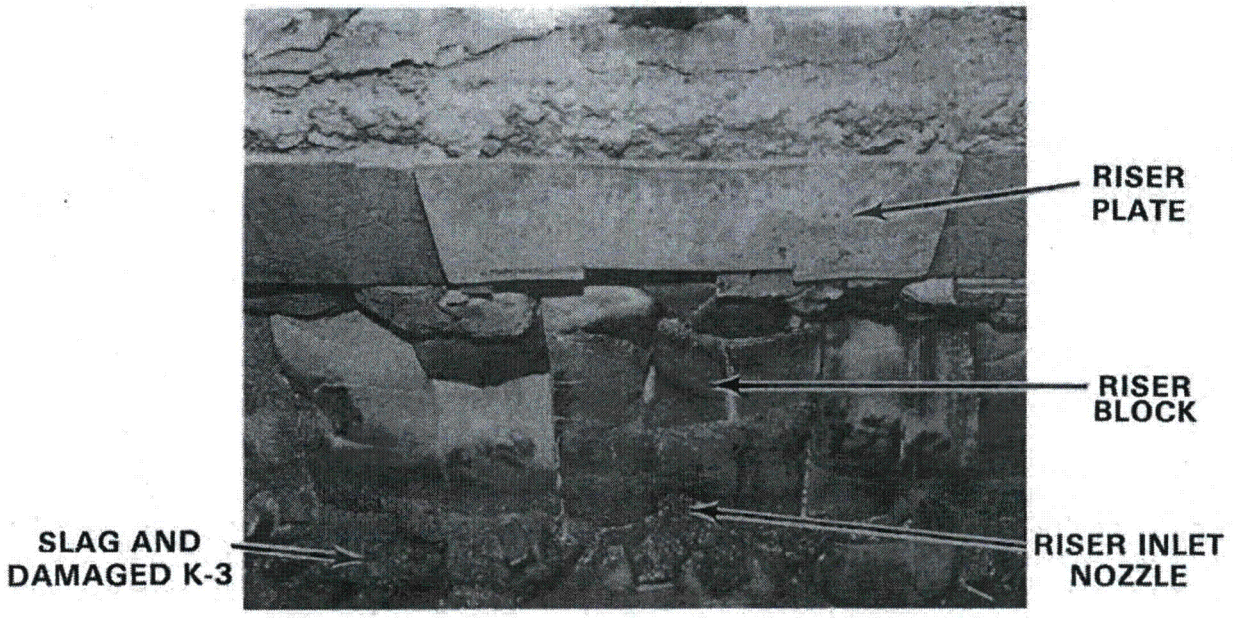

FIGURE 32. Cracking Around LFCM Riser Block

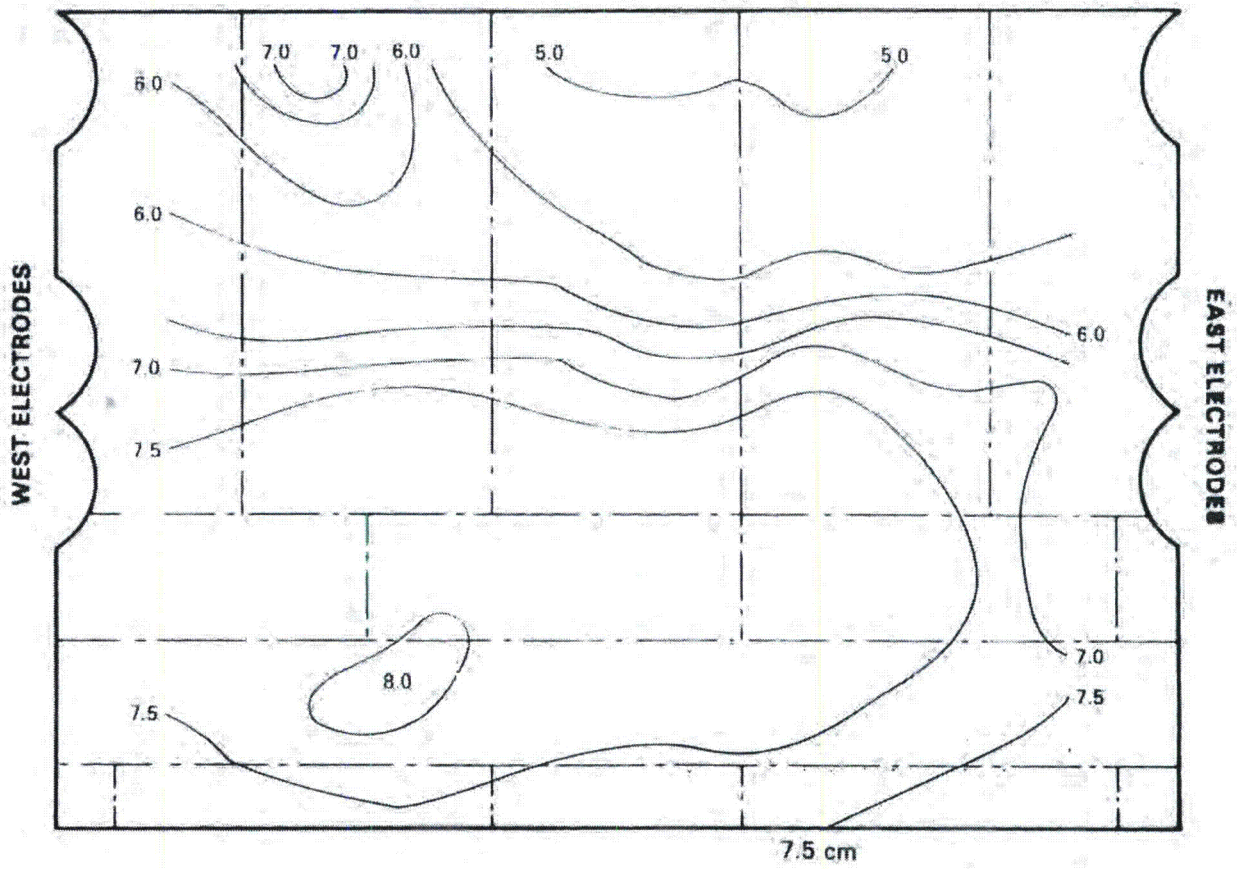

FIGURE 33. Contour Plot of Melting Cavity North Wall Following Drainage

Although both refractory walls are severely cracked, the cold wall remains intact because the cracks are oriented perpendicularly to the glass contact face. This is due to the characteristics of the temperature distribution in the wall. However, the thermal gradients present in the hot wall are oriented such that the cracks are inclined with respect to the glass contact face. Therefore, the cracked portions of the north wall remain in place, but the damaged south wall refractory tended to slough off onto the floor.

Another indication that high refractory stresses are present can be seen in the photograph and contour plot of the east electrode wall, Figures 35 and 36. The refractory above the primary electrodes has bowed toward the melting

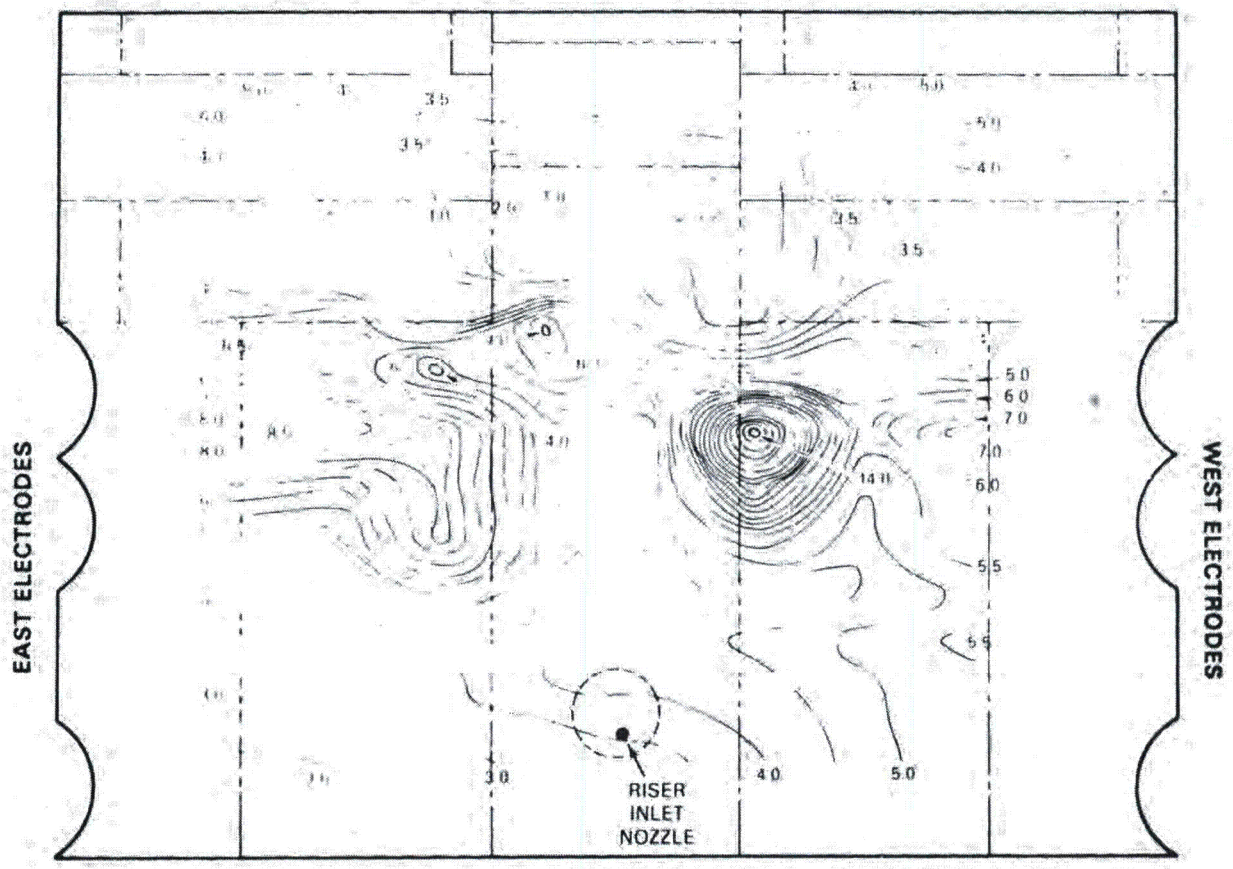

FIGURE 34. Contour Plot of Refractory South Wall Following Drainage

cavity to relieve the thermal expansion stresses. Similar refractory displacement was produced in the west melting cavity wall.

In general, the Monofrax K-3 was found to be highly corrosion resistant. The north wall underwent a generally uniform corrosion, with the maximum loss of roughly 2.5 cm at the center. The flat corrosion profile of this refractory is established very near the electrodes, as can be seen in Figure 37. The riser drain is another example of the applicability of Monofrax K-3. Figures 38 and 39 are photographs of the drain. The riser inlet has grown during service (original size of inlet shown in Figure 38) as the slag built up, yet the riser itself remains circular and in good condition (Figure 39). The

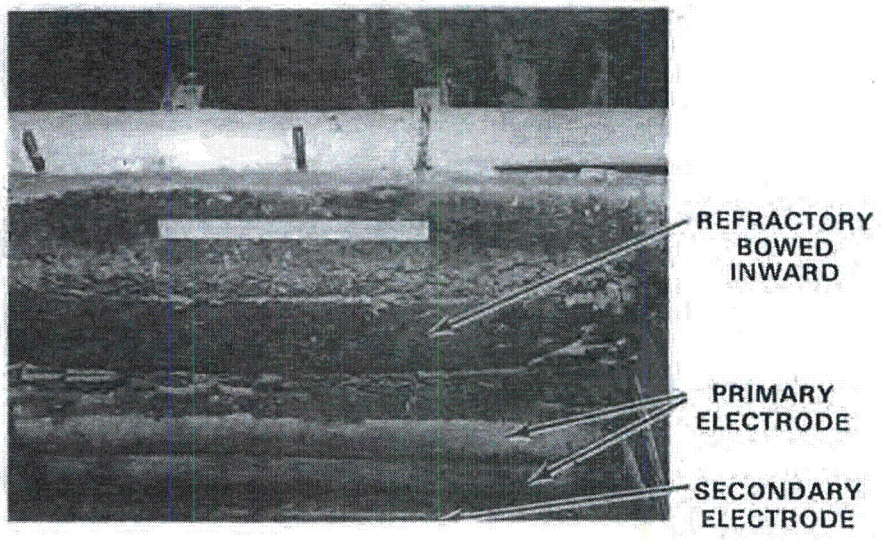

FIGURE 35. Melting Cavity East Electrode Wall

Monofrax K-3 forming the melter floor remains in nearly new condition, remaining at the original 6-in. (15.2-cm) thickness, as shown in Figure 40.

5.3.2 Alfrax 66

Alfrax 66, a high alumina castable refractory, was installed behind the Monofrax K-3 in the walls. When the melter was disassembled, the surface of the Alfrax 66 behind the Monofrax K-3 was covered with a thin glass film. The Alfrax 66 found to be largely unaffected by contact with the glass, appears well suited for the corrosive environments of this application.

As the disassembly progressed, the Alfrax 66 was found to contain many glass-filled cracks. This was especially true in the Alfrax 66 cast around the riser block, Figure 41. A significant quantity of glass penetrated the Alfrax 66 along the north wall. One of the large glass-filled cracks and the large glass pool behind the Alfrax 66 are pictured in Figure 42. This was by far the largest glass penetration found in the examination, forming a solidified layer against the containment box roughly 75-cm by 60-cm by 0.5-cm thick. Minor glass migrations were also found behind the electrodes, but the glass did not penetrate the Alfrax 66 to the containment box in this region

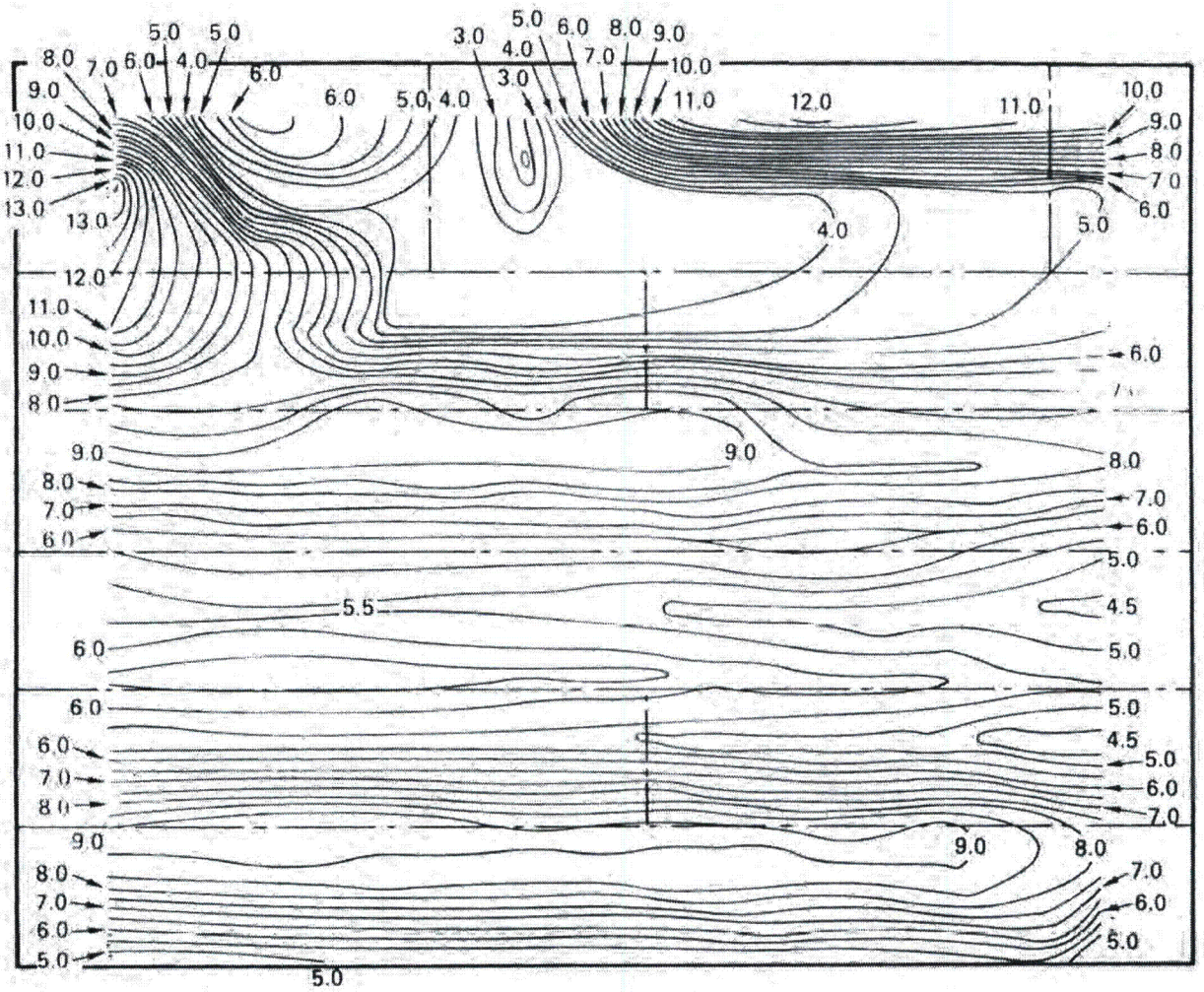

FIGURE 36. Contour Plot of East Electrode Wall

The Alfrax 66 was subjected to conditions most likely to create structural failures in the LFCM application. Alfrax 66 is a castable refractory (mixed with water and cast into place, much like concrete). The solidified Alfrax 66 contains both free water and water of hydration. As the temperature of the refractory exceeds 100°C, the free water begins to vaporize, forming microscopic steam pockets in the refractory. If this water vapor is not allowed to diffuse from the Alfrax 66 (by maintaining the refractory near

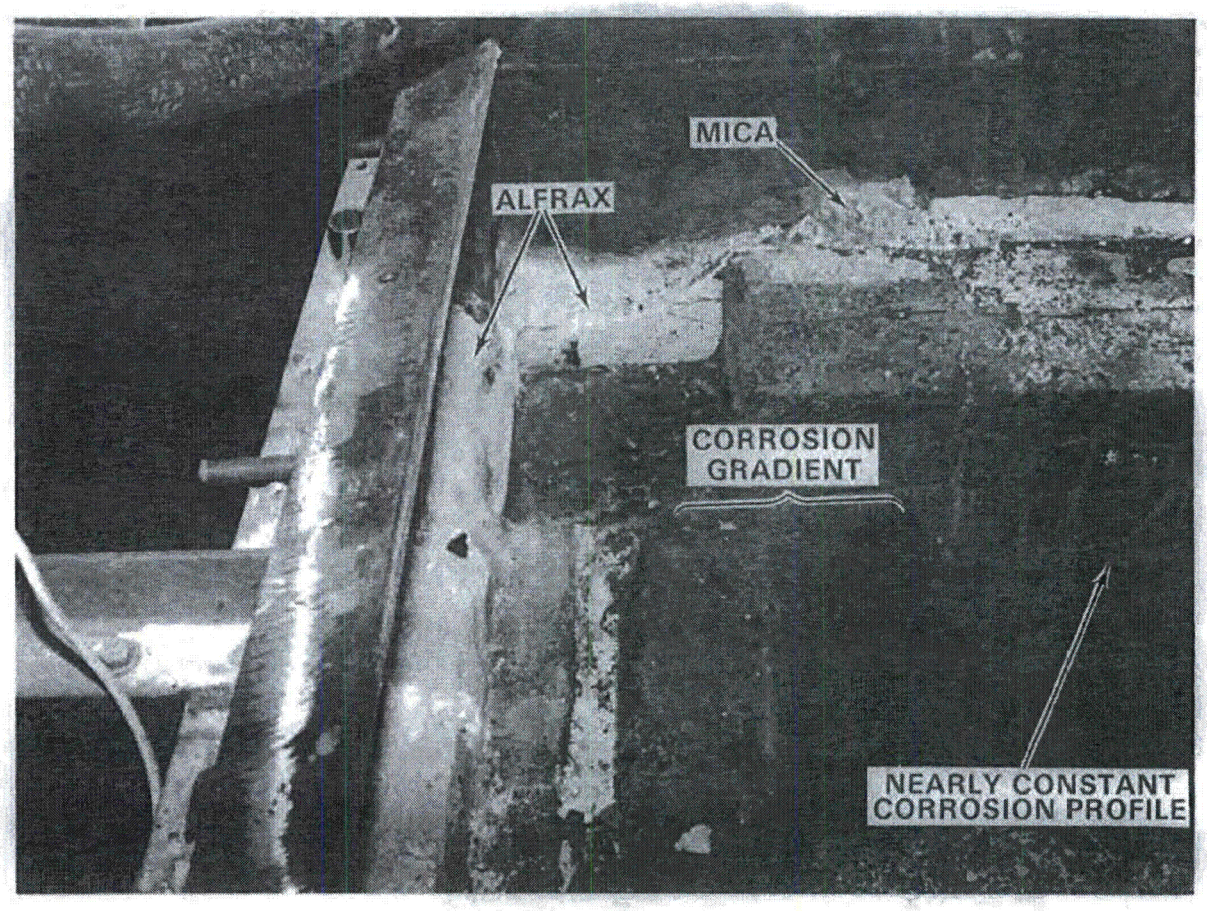

FIGURE 37. Corrosion Profile on North Wall Near Electrodes

100°C) for an extended time period, the internal steam pressure can build until refractory failure occurs. During the melter startup, the melter was heated from ambient to operating temperatures in less than 24 h. This is in sharp contrast to the Alfrax 66 curing schedule recommended by the manufacturer:

- Maintain Alfrax 66 temperatures between 95 to 120°C until visible steam condensation in the coolest melter region ceases.
- Increase the Alfrax 66 temperature (<40°C/h) to 480°C.
- Between 400 to 650°C, reduce the temperature increase to <30°C/h to permit dissipation of hydrated water released in this temperature range.

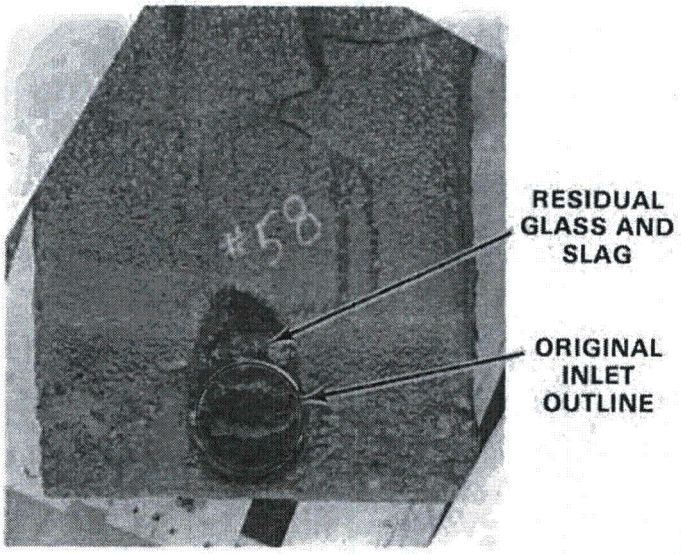

FIGURE 38. Corrosion of Riser Inlet Nozzle

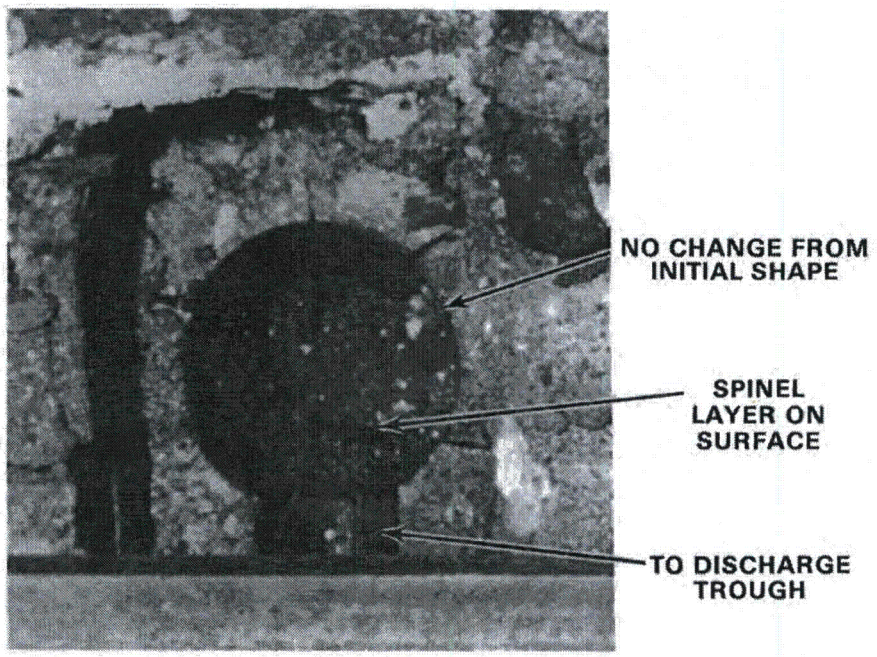

FIGURE 39. Condition of Riser Outlet Following Operating Period

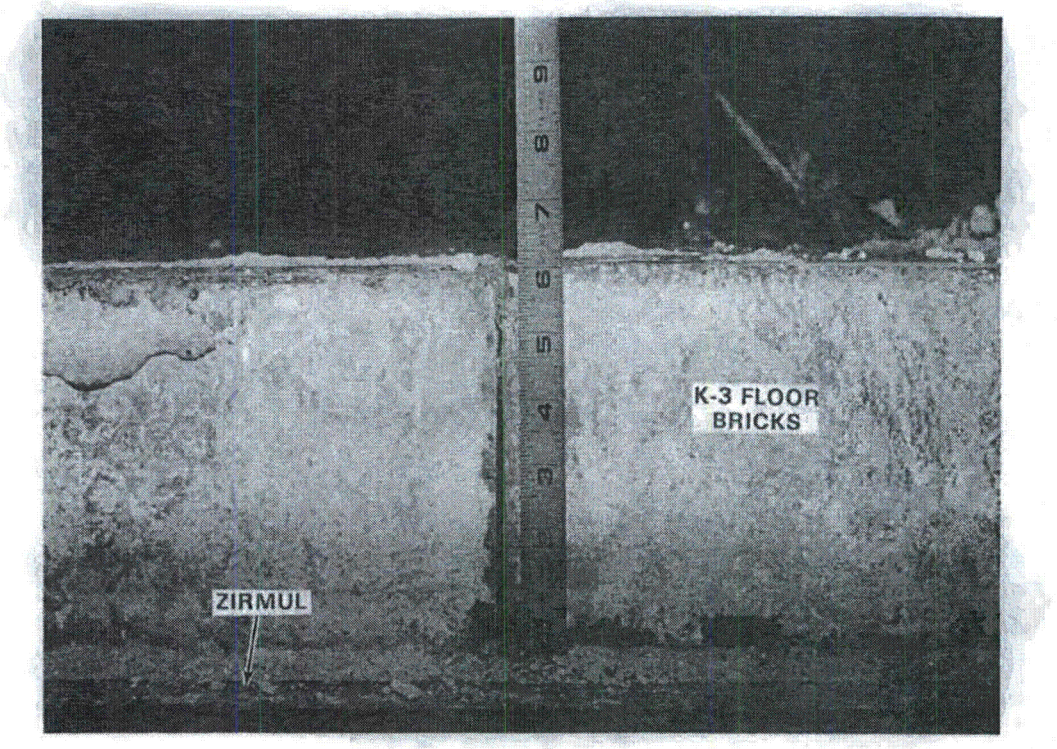

FIGURE 40. Condition of Monofrax K-3 Floor Blocks

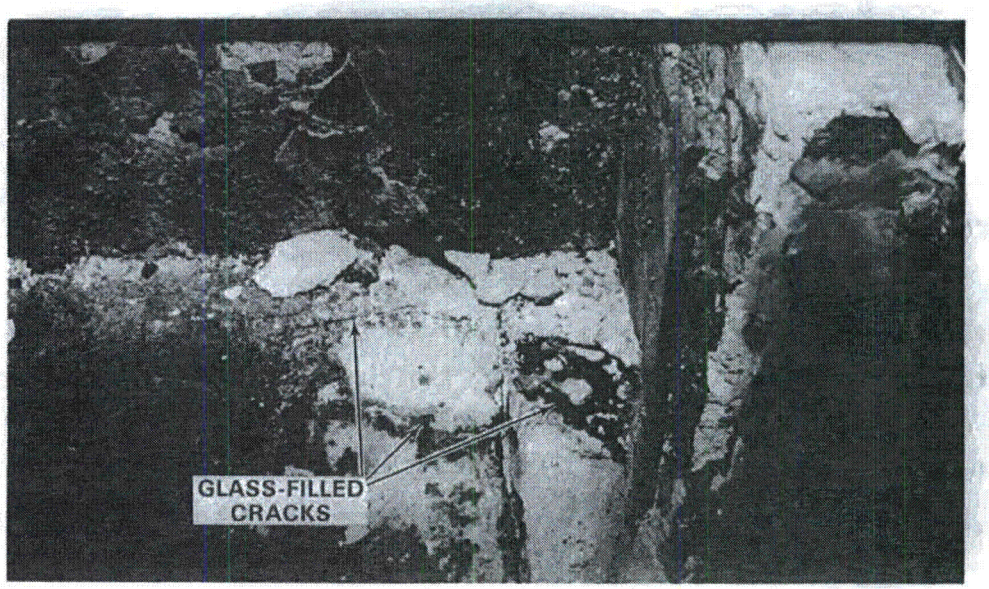

FIGURE 41. Cracking of Alfrax 66 Around Riser Block

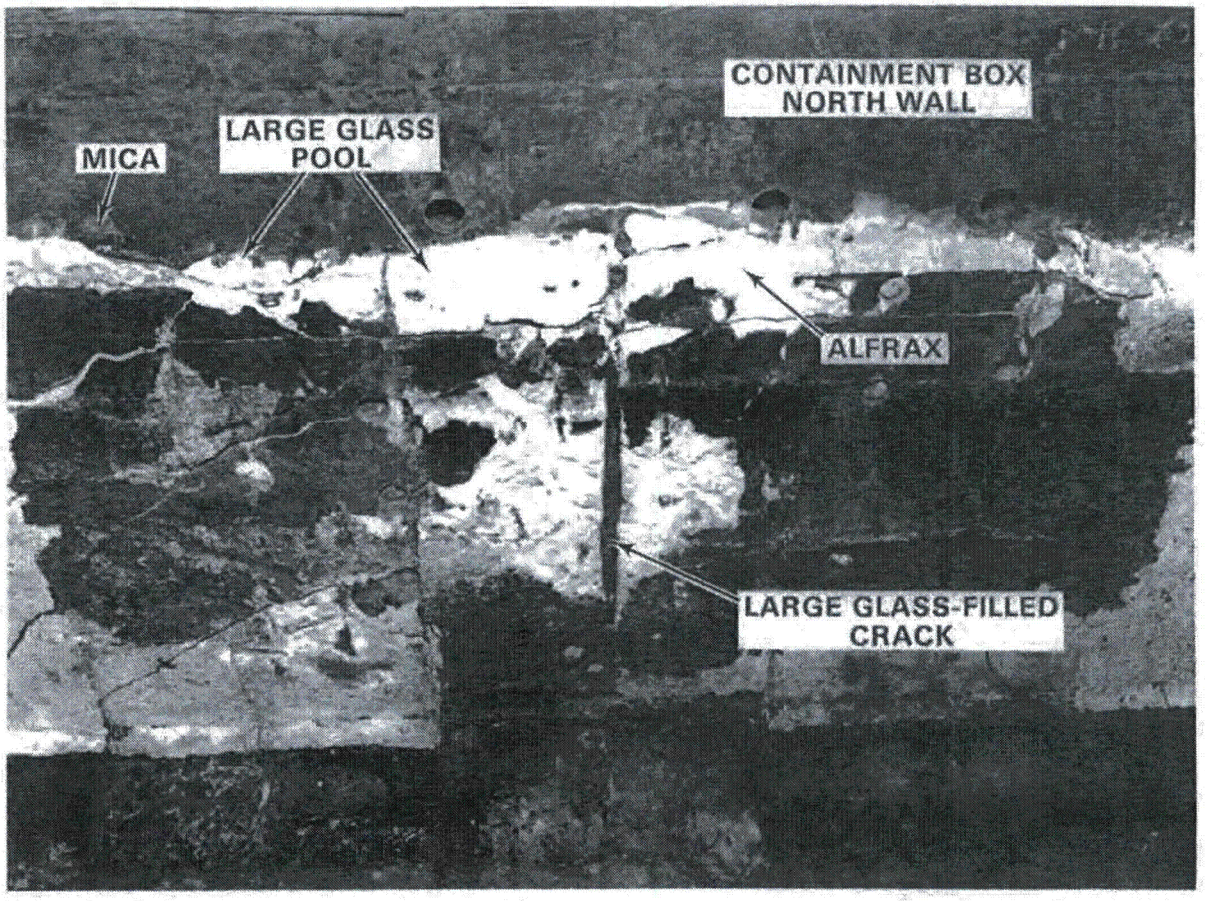

FIGURE 42. Glass Penetration Through Alfrax 66 North Wall

- Above 650°C, increase Alfrax 66 temperatures <40°C/h until the desired operating temperature is reached.

After the Alfrax is cured, temperature changes should be <40°C/h. Also, Alfrax 66 has different initial thermal expansion characteristics than the Monofrax K-3. During Alfrax 66 curing, the thermal expansion is offset by shrinkage of the refractory caused by the water loss. In this refractory installation, the Alfrax 66 was cast behind and above the Monofrax K-3. Therefore, during startup the Monofrax K-3 would expand as the temperature was increased; the Alfrax 66 would tend to retain its initial dimensions. This produces tensile stresses in the Alfrax 66, which could lead to the cracking observed.

Glass samples removed from the cracks near the large glass migration in the north wall and at the base of the riser block resemble glass formulations processed in early melter testing. This supports the conclusion that the Alfrax 66 cracking was the result of the rapid startup and thermal expansion differences between the Monofrax K-3 and the Alfrax 66 refractories. Much of the Alfrax 66 cracking discovered in the LFCM can be prevented in the future by following the recommended curing schedule and by assuring that slip planes are included in the refractory design to permit the Monofrax K-3 to expand during the Alfrax 66 curing period.

5.3.3 Zirmul

The Zirmul bricks installed beneath the Monofrax K-3 floor were in excellent condition on removal from the melter. The bricks were covered with a thin layer of glass in the center of the floor, Figure 43, and glass had

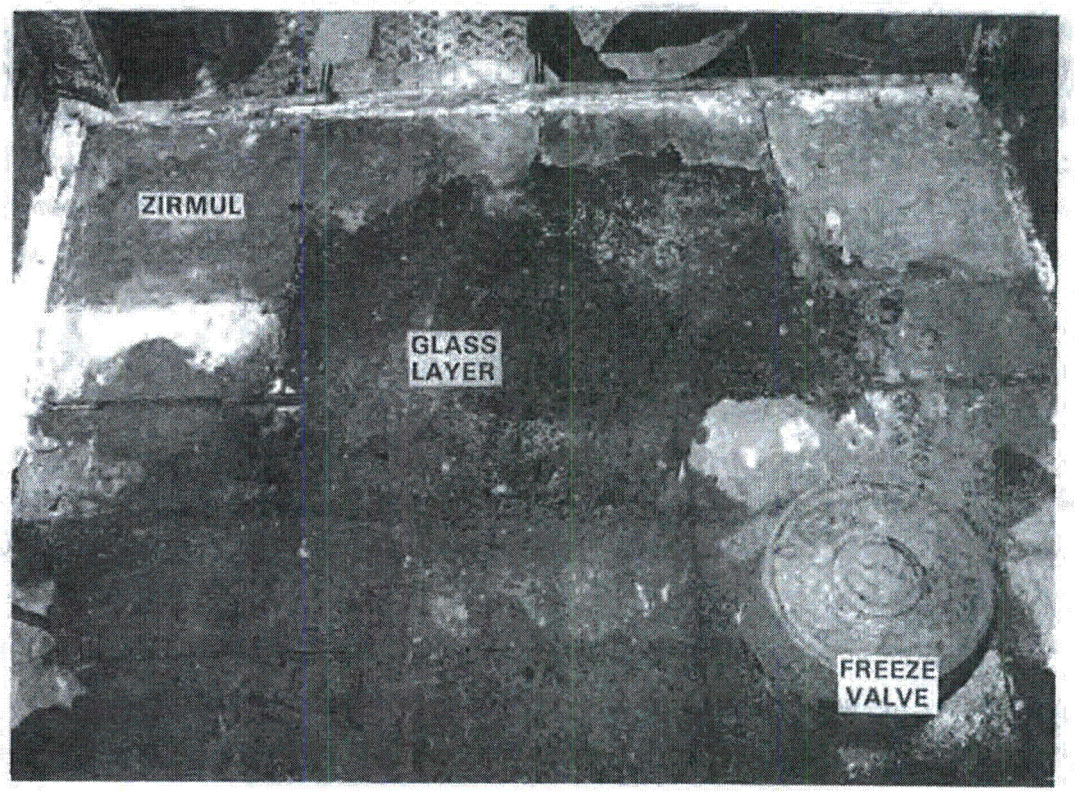

FIGURE 43. Glass Layer on the Zirmul Floor Blocks

penetrated the interbrick joints in this region. Glass was also found in Zirmul cracks near the freeze valve. Visual inspection of the Zirmul revealed no significant interaction between the glass and the refractory. The most severely affected regions were discolored up to 0.5 cm into the bricks. Other than the discoloration, no effects on the Zirmul were detected.

5.4 OVERFLOW DRAIN

The glass discharge was fabricated from Monofrax K-3, Alfrax 66, and a low-density, insulating-type brick. This region of the melter performed satisfactorily during the melter life, but two operational effects were noted during the disassembly.

The Monofrax K-3 trough block was found to be broken into two pieces, each roughly one half of the length of the original brick. The channel along the discharge face of the block also appeared to have been fractured during the operating period. This damage may have occurred as the result of thermally shocking the block during rapid overflow section heatup cycles or as the result of mechanical stresses during manual removal of solidified glass. The appearance of the the overflow drain in the new and final states is shown in Figure 44. The damage to the trough block did not affect the operation of the melter.

A more serious concern may be the corrosion of the low density bricks by glass that migrated from the drain. Figure 45 shows the glass covering these bricks. The glass easily penetrated the pores of these bricks and some rounding of the corners is apparent. Use of higher density, more corrosion-resistant bricks may be considered for future designs to prevent loss of structural integrity in this region.

The Inconel 690 pouring tip did not appear to be adversely affected by the three years of melter operation. A detailed examination of the pouring tip is included in Section 7.2.3 of this report.

5.5 ELECTRODES

The primary and secondary electrodes are pictured in Figure 46 (east electrodes) and Figure 47 (west electrodes) after the three years of exposure

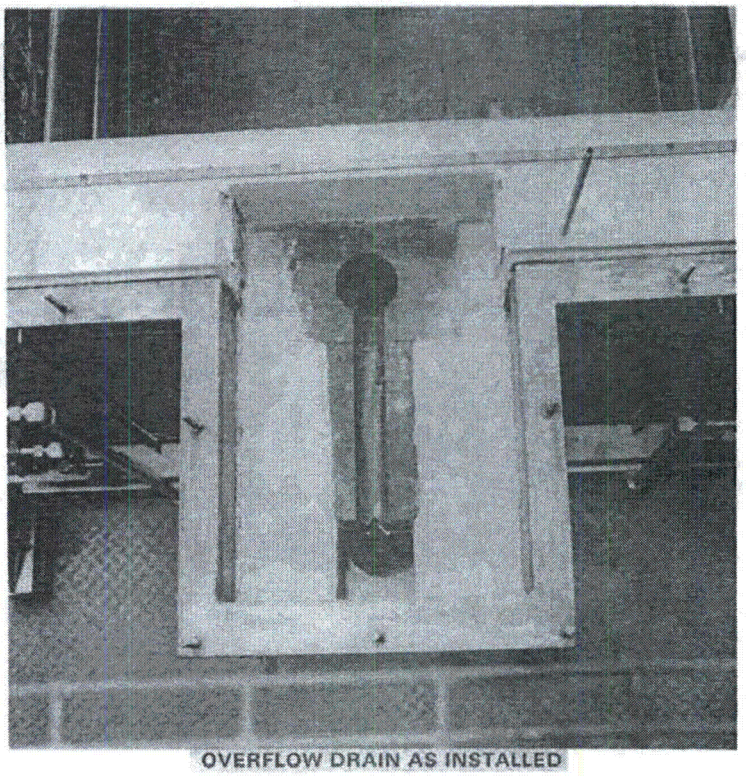

OVERFLOW DRAIN AS INSTALLED

AFTER THREE YEARS OF SERVICE

FIGURE 44. Overflow Drain as Installed and After Three Years of Service

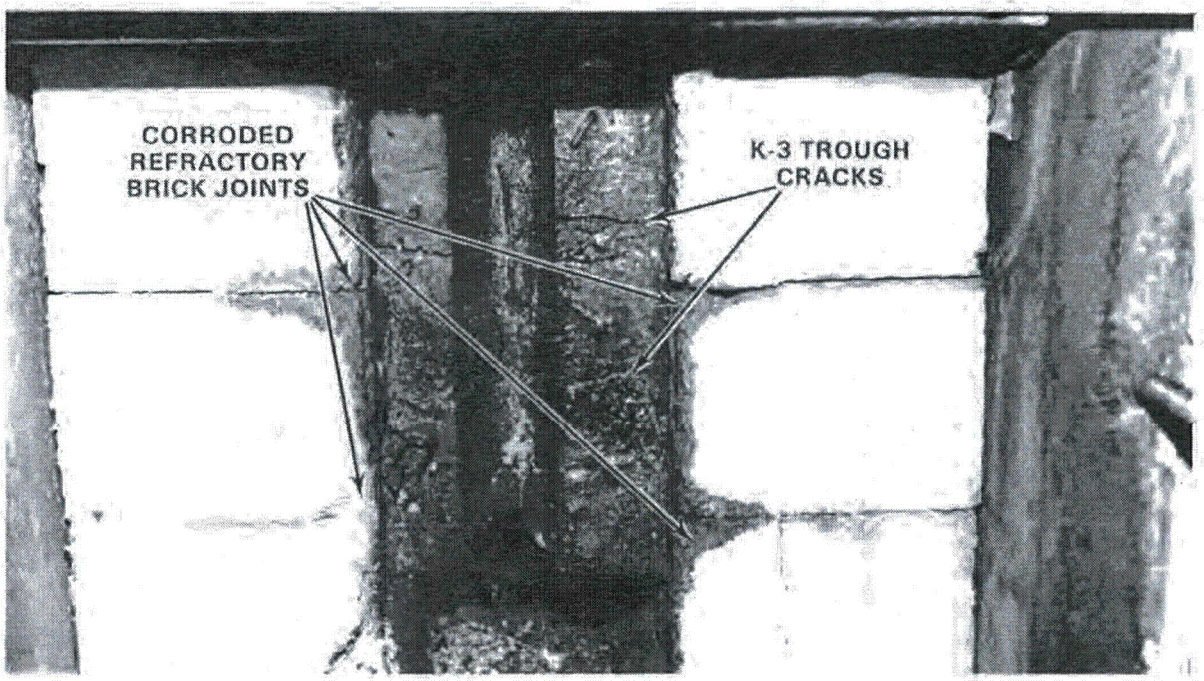

FIGURE 45. Glass Attack of Insulating Bricks in Overflow Drain

to molten glass. Remnants of the spinel crystal layer that covered the electrodes can be seen in these photographs. A similar layer of crystals can be seen adhering to the adjacent refractories. The surface of the primary electrodes appears rough (similar to the surface of sand-blasted cast iron), but the secondary electrodes appear to be in excellent shape. In fact, marks from the original machining process are still visible on the secondary electrodes. The spaces visible at the ends of the electrodes are designed to compensate for the electrode thermal expansion. Minor quantities of glass were found behind the electrodes and between the primary electrode elements.

The difference in the appearance of the primary electrodes and secondary electrodes is due to two factors. The secondary electrodes routinely operated at a lower electrical current output per square centimeter of glass contact face (0.34 to 0.68 A/cm^2 primary versus 0.23 to 0.62 A/cm^2 secondary). The secondary electrodes also operated at lower temperatures than the primary electrodes (primary operating temperature, 950 to 1100°C; secondary operating temperature, 900 to 1000°C).

FIGURE 46. East Electrodes Following Operation

The changes in dimensions of the LFCM electrodes are presented in Table 1. Based on this data and assuming that the dimensional changes are only due to material loss (i.e., the effects of high-temperature creep and volume changes related to changing solid phases in the alloy following the extended heat treatment received do not contribute to the measured dimensional changes), the metal loss from the electrodes is 3 μm/d or less.

Following removal from the melter, the east primary and secondary electrodes were sectioned near the centerline and samples were removed for detailed corrosion examination. The results of these tests are presented in Section 7.2.1 of this document.

FIGURE 47. West Electrodes Following Operation

5.6 IONIC BOOSTER ELECTRODES

The ionic booster electrodes, fabricated from 304L stainless steel, were designed to be continually water cooled. To prevent damage to the melter from water leaking into the melting chamber, the system was designed to stop the coolant flow in the event of an offgas pressure surge in the idling operation mode. On two occasions, an offgas pressure surge (unrelated to an ionic booster coolant leak) tripped the cooling system and went undetected for several days.

Following the second coolant outage, a leak in one of the electrodes developed and air cooling was used for the final three months that the

FIGURE 48. Ionic Booster Electrode After Removal from LFCM

TABLE 1. Electrode Dimensions

	Length			Height	
	Front, cm	Back, cm	Width, cm	Front, cm	Back, cm
East Primary Top	86.6	86.4	12.5	20.3	20.2
East Primary Bottom	85.6	56.4	12.5		
East Secondary	86.3	86.4	12.7	10.2	10.2
West Primary Top	85.7	86.5	12.5	20.1	20.2
West Primary Bottom	85.7	86.4	12.5		
West Secondary	86.0	86.5	12.7	10.2	10.2
Original Primary Dimensions	86.4	86.4	12.7	20.3	20.3
Original Secondary Dimensions	86.4	86.4	12.7	10.2	10.2

electrodes were installed in the LFCM. The ionic booster electrodes received a total of 25 months exposure to the melting cavity environment.

When the electrodes were removed, the welded zones had become very brittle. The metal bellows used to seal the system and permit vertical electrode motion had developed pin-hole penetrations and had lost all elasticity. Traces of glass were detected in the electrode interior. Apparently the cooling air inside the electrodes blowing past the leakage sites sucked in glass-forming materials during feeding periods. Figure 48 shows the condition of the ionic booster electrodes after removal. Figure 49 is a photograph of the corroded bellows.

Analyses of samples removed from the electrode and bellows showed that the embrittlement of the electrode was caused by sensitization (formation of chromium carbides at the grain boundaries) and that the bellows were corroded by halogens and sulfur compounds. Additional details are presented in Sections 7.2.4 and 7.2.5.

5.7 OFFGAS PIPING

The offgas piping connected to the LFCM did not experience significant visible corrosion, and was used for extended periods of time. This piping was generally a stainless steel alloy, either type 304L or 316.

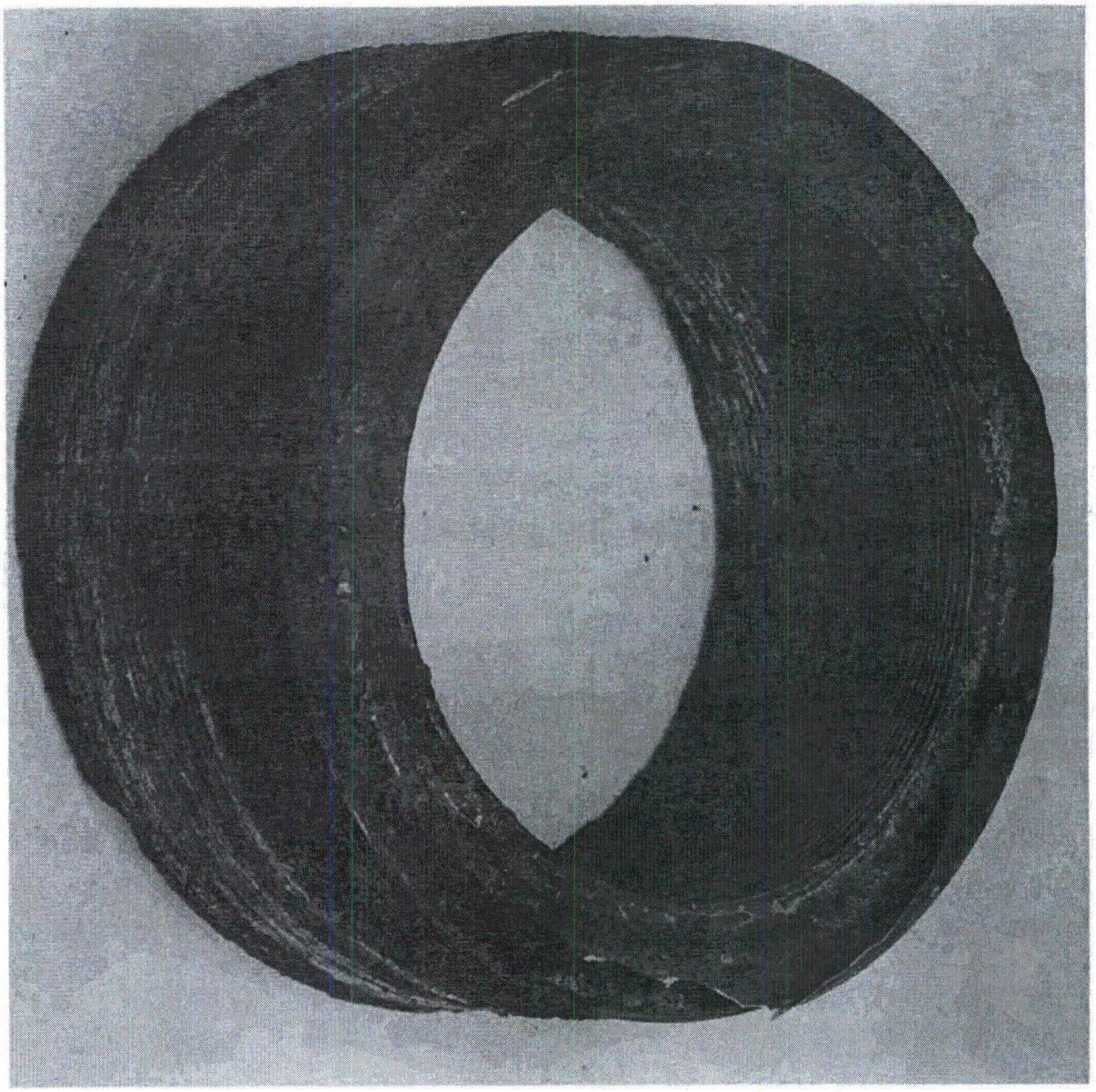

FIGURE 49. Failed Ionic Booster Bellows

Following the shutdown of the LFCM and completion of the methodical disassembly process, the LFCM was recontructed in the original containment shell. Although this document is intended to summarize the corrosion experience of

the original LFCM, the details of the corrosive attack of the initial offgas jumper between the melter and the offgas system are included because of the rapid failure encountered.

The stainless steel, convoluted piping from which the offgas connecting section immediately adjacent to the melter was fabricated, failed 106 h into the first slurry feeding test. A section of the corroded metal is pictured in Figure 50. This experiment was unique up to that point because the lid heaters were used to increase the slurry feed processing rate. This additional energy input from above the feed resulted in offgas temperatures approaching 600°C. At this temperature the type 204L, stainless steels piping was severely attacked by chlorine and sulfur compounds. The details of the particular corrosion mechanisms are presented in Section 7.2.6.

5.8 FREEZE VALVE

The LFCM freeze valve operated as designed. Following the cessation of the freeze-valve coolant flows, the freeze valve satisfactorily drained the melter. At least 2 cm of slag deposits were above the valve before the draining operation (see Figure 25).

Figure 51 is a photograph of the freeze valve following removal of the refractory. The refractories and slag deposits prevented any damage to the freeze valve during the melter operation, and it was reinstalled in the rebuilt LFCM.

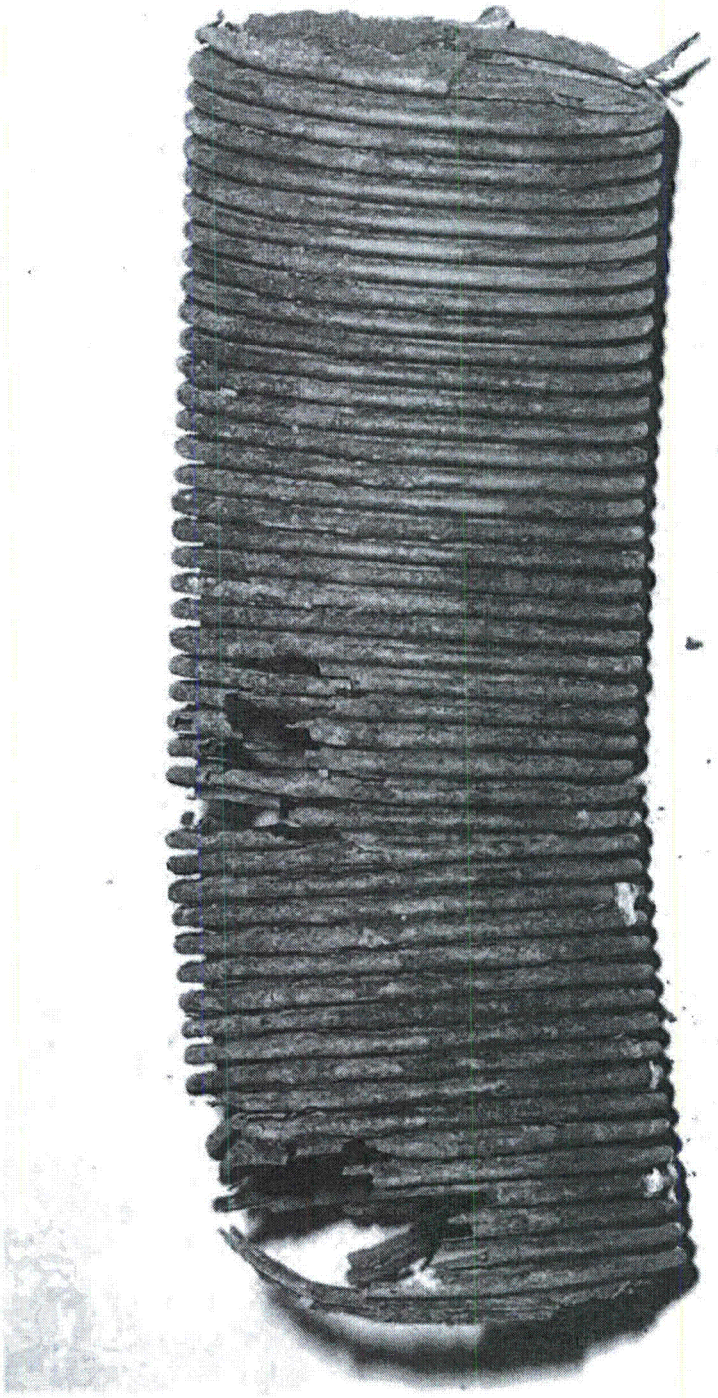

FIGURE 50. Corroded Offgas Piping

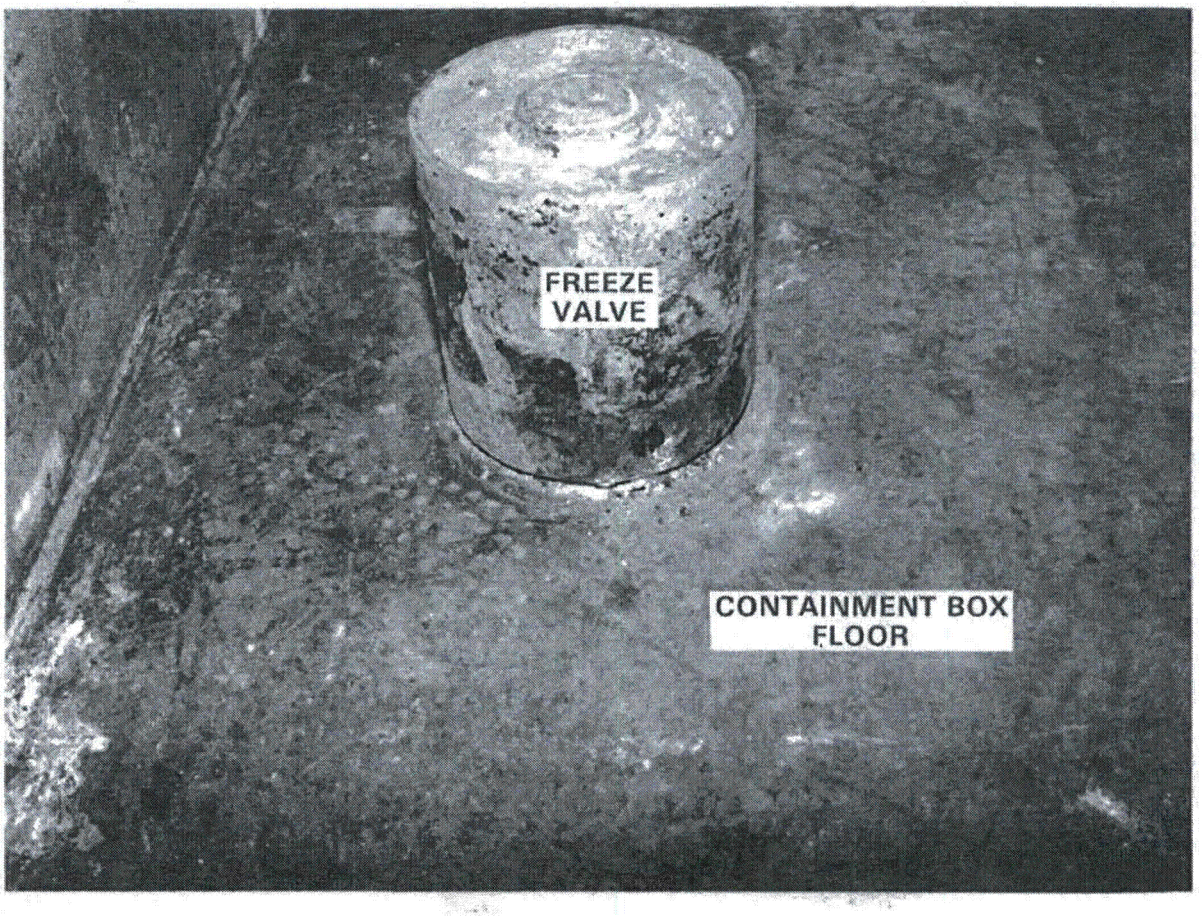

FIGURE 51. LFCM Freeze Valve

6.0 MELTER STRESS ANALYSIS

An analytical model of a ceramic-lined glass melter was developed to investigate the stress levels possible in refractory designs similar to the LFCM and to predict the effects of the different operating modes on the stress profiles. This model was based on the LFCM refractory design, temperature profiles, and containment box. The modeling was performed with a two-dimensional, finite-element code, ANSYS, with in-plane strain capabilities. The melter simplification required for a two-dimensional model implies that specific planar cuts within the refractory must be selected to investigate the local stress profiles of interest. The two-dimensional model also implies that the modeled structure is long enough in the third dimension to negate end effects, that there is no thermal gradient in the third direction, and that a stress gradient in the third dimension does not occur.

6.1 MODEL DESCRIPTION

The cuts (sections) selected for the analytical model were in the north-south direction through the LFCM refractory. This orientation was selected because of the major differences in appearance between the north and south walls after the melter was drained. These cuts meet the model restriction for length in the third direction. However, the changing geometry of the melter in the riser block region, the heating of the upper levels of the riser block from the overflow drain heaters, and the lack of containment shell cooling in the overflow drain region, all give rise to an east-west temperature, and thus stress gradient in these regions. The effects of the temperature and stress gradients in the third dimension are not included in this model.

A possible limitation of a finite-element analysis of the refractory stresses is the inherent linear elasticity assumption of this model. This assumption essentially implies that the modeled material does not fail. Ceramic materials tend to initiate cracks that propagate in a manner characteristic of brittle materials in a moderate to high tensile stress field. Little plastic strain energy is absorbed in the propagation of the crack as

the strain required to fail ceramic matrices is very small. Modeling this type of failure requires a specialized computer routine, very small finite elements, and considerable data on the structural materials being modeled. Generalized codes, such as ANSYS, will not accurately model crack development because the matrix is assumed to be continuous. In actuality, after the development of a crack, the tensile load normal to the crack must be zero and the material is no longer continuous. Also, this type of analysis requires that the refractory characteristics related to fracture failure be well defined. These data are not generally available for refractory ceramics (not available for the Monofrax K-3 and Alfrax 66 in particular) as common design practices do not employ these materials when flexure stress levels are likely to create failures.

Notwithstanding these limitations, a linear-elastic, finite-element model of the refractories will generate results that can be used to assess stress levels within the melter and to determine possible crack initiation sites. The linear-elastic analysis will also indicate the direction of crack propagation once it is initiated. Brittle materials tend to propagate cracks in the direction normal to the orientation of the maximum tensile stress in the material. If relaxation of the stress creating the crack occurs because of the crack propagation, and the direction of the maximum tensile stress changes, the crack will tend to follow the direction normal to the new maximum tensile stress.

Therefore, the constant stress contours generated by the ANSYS model should predict the initial crack direction and the nature of the resulting stress field. Additionally, the ANSYS code does not require the fracture mechanics' characteristics of the refractories. This eliminates the need to assume these values and thereby reduces the potential for modeling error.

Two models, based on the ANSYS code, were used to predict the refractory stress levels in a design similar to the LFCM with various boundary conditions. The initial, simplified model, shown in Figure 52, is based on 15.2-cm Monofrax K-3 walls and floor assuming no Alfrax 66, fiberboard, or containment box. This model was given temperature boundary conditions and allowed to expand

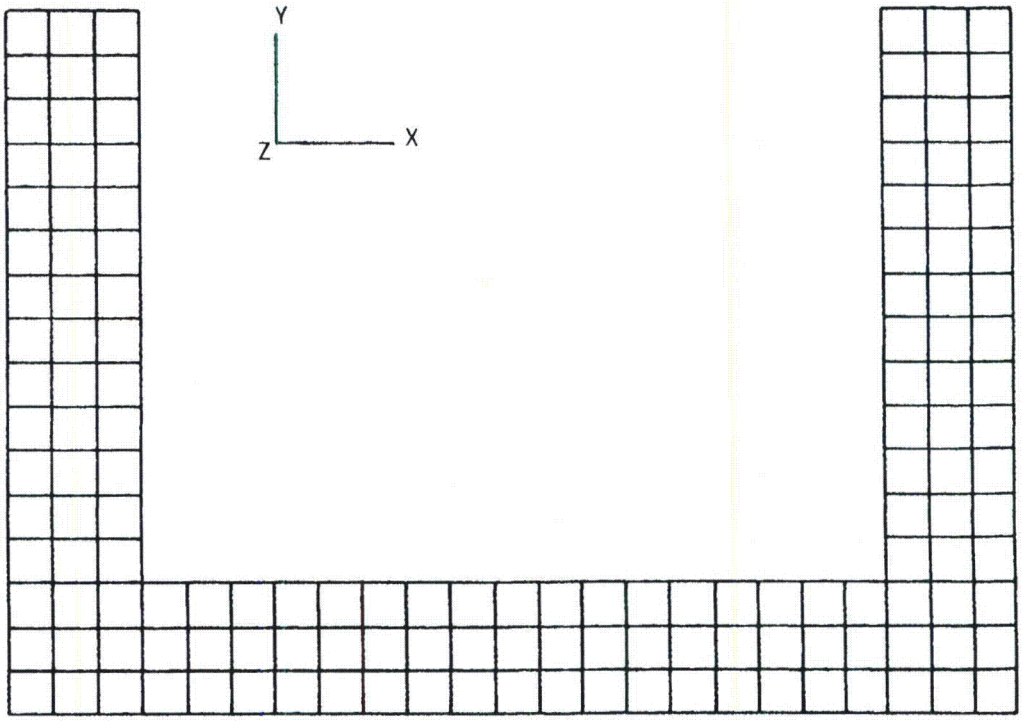

FIGURE 52. Simple Model of Melter Used in Preliminary Calculations

freely, but was not permitted translational or rotational motion. With these conditions very low refractory stresses were produced, but the upper corners of the walls were displaced outwards roughly 5 cm. In the next simulation, an additional boundary condition was added which constrained the upper refractory ends from moving. These assumptions produced stresses as high as 345 MPa. The published Monofrax K-3 ultimate compressive strength is 138 MPa (Carborundum Company 1980). The degree of thermal strain allowed in the structure, therefore, will determine the magnitude of the thermal stresses. If the refractory is allowed to expand thermally without restraint, the thermal stresses will be low. Conversely, if the refractory is constrained, the thermal stresses will be high and will generally cause failure of the material.

The second model based on the LFCM refractory design comprises elements representing the Monofrax K-3, Alfrax 66, Zirmul, and the fiberboard. In this

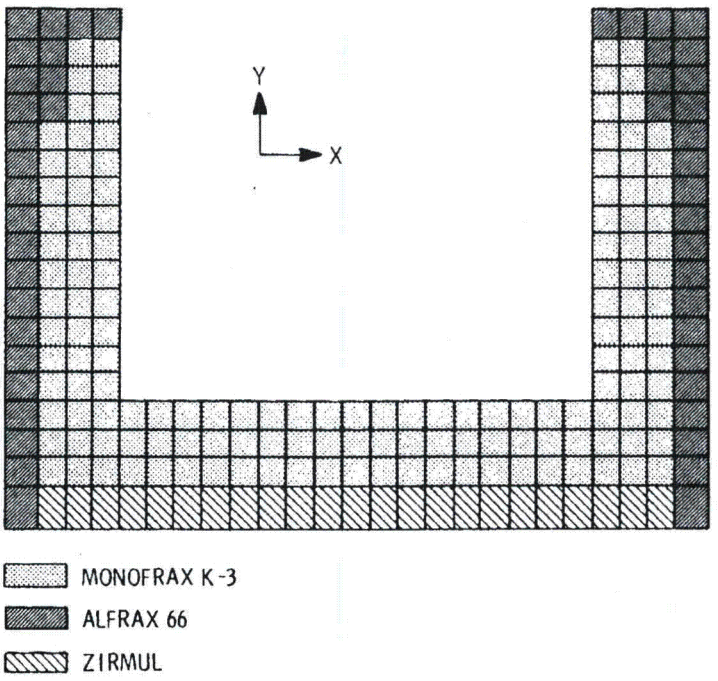

FIGURE 53. Finite-Element Model of Cut Through Melter to East (or West) of Riser Block (Cut #1)

model, three cuts through the melter were analyzed. The modeled refractory planes are depicted in Figures 53 through 55. Figure 53 is to the east or west of the riser block; Figure 54 is cut through the riser block, but to the east or west of the drain riser; and Figure 55 is a plane slicing the refractory through the riser centerline. Between the refractory layers and at the junctions of the blocks, spring or truss elements were employed to model the interaction between refractories or blocks. These trusses have a stiffness that is associated with the contact stiffness at each junction. Each refractory element, therefore, was allowed to transmit a force to the surrounding refractory elements.

Outside the insulating layer of castable Alfrax 66 in the LFCM design, a layer of crushable fiberboard was installed to accommodate thermal expansion of the refractories. This fiberboard was modeled using soft trusses of 1.3-cm length between the outer layer of the refractory and a fixed set of nodes. This fixed set of nodes models the stainless steel containment box.

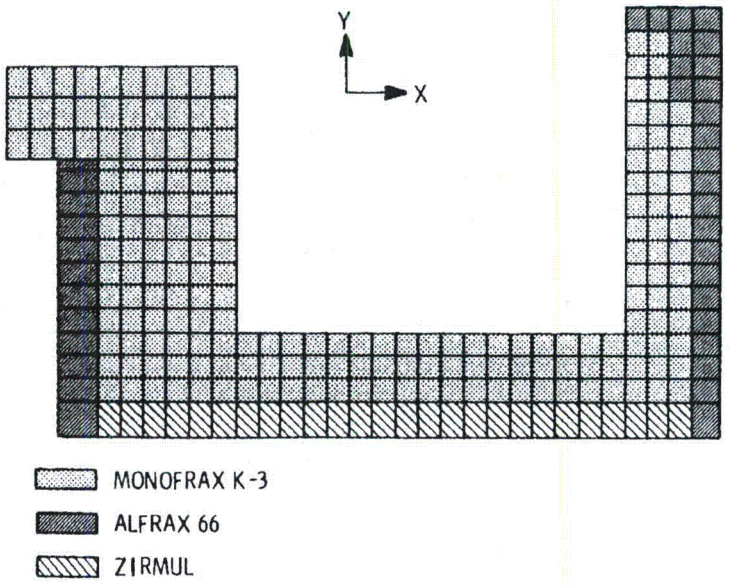

FIGURE 54. Finite-Element Model of Cut Through Melter to East (or West) of Riser Within Riser Block (Cut #2)

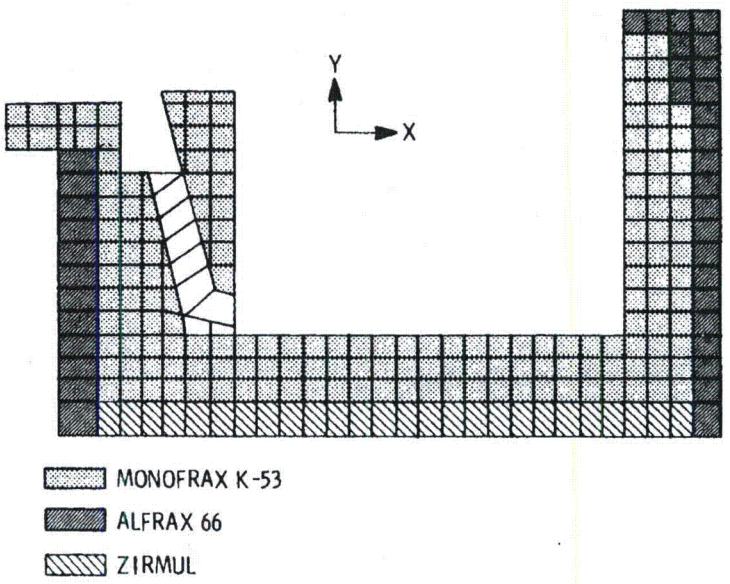

FIGURE 55. Finite-Element Model of Cut Through Melter Centerline, Including Riser (Cut #3)

The physical properties of the refractory materials required by this analysis are not readily available from the literature. The elastic constants for Monofrax K-3 (Chan and Nicholson 1978), Zirmul, and Alfrax 66 are listed in Table 2. The elastic properties of Zirmul and Alfrax 66 were estimated by the method suggested by Van Vlack (1964).

6.2 ANALYSES RESULTS

The analytical refractory model was subjected to boundary conditions representative of steady-state idling and liquid-feeding operating modes. The third operating mode, calcine feeding, was not simulated because this mode would present temperature profiles somewhere between the idling and liquid-feeding extremes. A discussion of the transient conditions present at liquid-feeding initiation is also presented.

6.2.1 Idling Mode

The first two cuts through the refractory were analyzed for temperature boundary conditions representative of idling conditions. The temperature profiles calculated for the model were obtained by performing a steady-state thermal conduction calculation based on an assumed internal face temperature of 1200°C and temperature data from LFCM thermocouples. The predicted temperature profiles are presented in Figures 56 and 57. These calculated thermal patterns were used for temperature conditions for the stress analysis.

The predicted stress contours for the two cuts are shown in Figures 58 through 61. These plots represent the locus of points with constant horizontal or vertical stresses. Tensile stresses are represented by positive numbers, compressive stresses by negative values. For these stress predictions,

TABLE 2. Material Properties of Each Refractory

Material	Young's Modulus, MPa	Poisson's Ratio	Thermal Expansion, cm/cm°K	Thermal Conductivity, W/m°K
Monofrax K-3	1.4 (10^6)	0.4	7.97 (10^{-6})	2.6 (10^{-8})
Zirmul	6.9 (10^5)	0.4	6.66 (10^{-6})	1.7 (10^{-8})
Alfrax 66 Castable	3.4 (10^5)	0.4	9.0 (10^{-6})	2.1 (10^{-8})

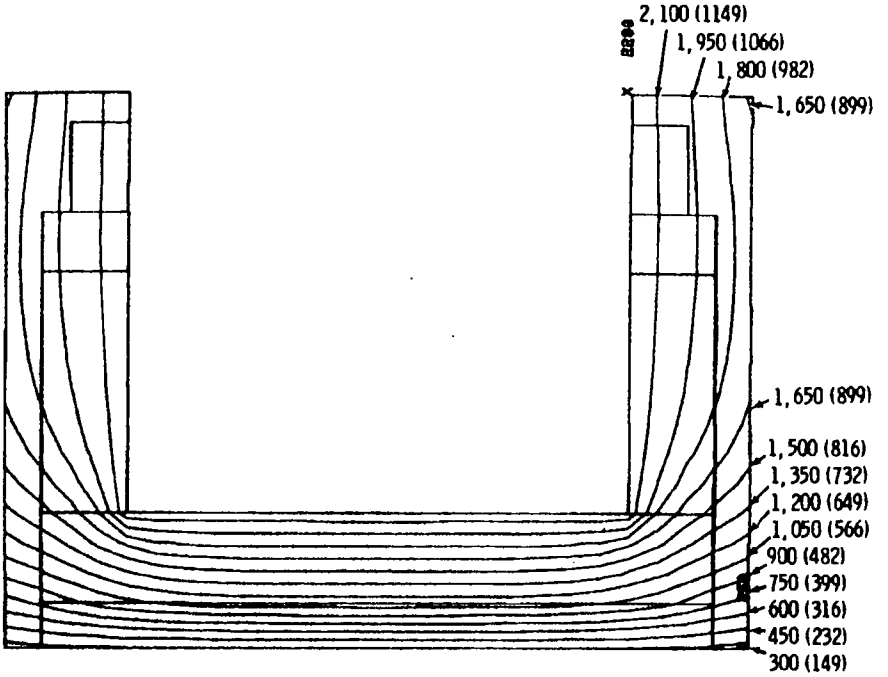

FIGURE 56. Temperature Profiles for Cut #1 Idling--^{o}F (^{o}C)

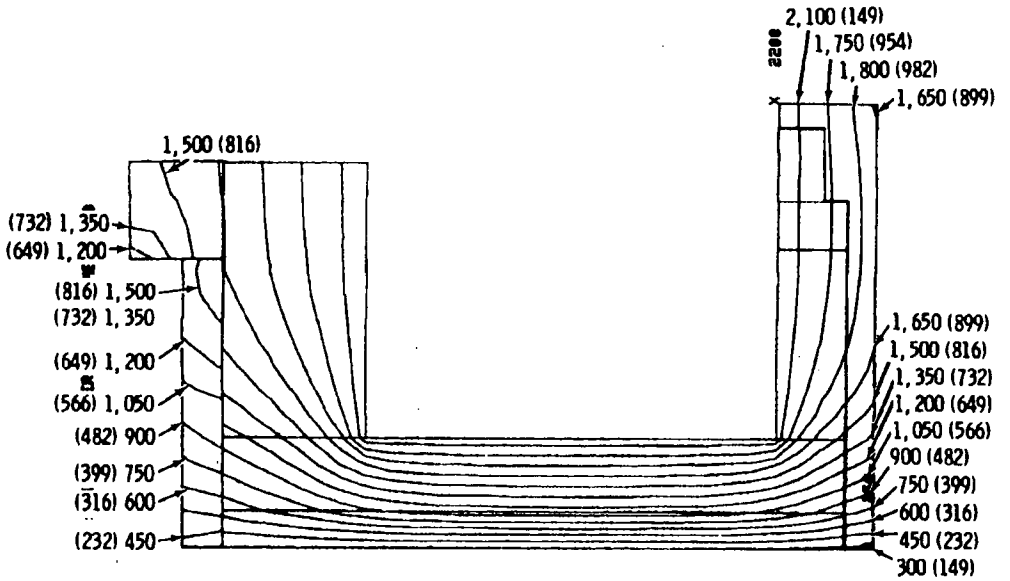

FIGURE 57. Temperature Profiles for Cut #2 Idling--^{o}F (^{o}C)

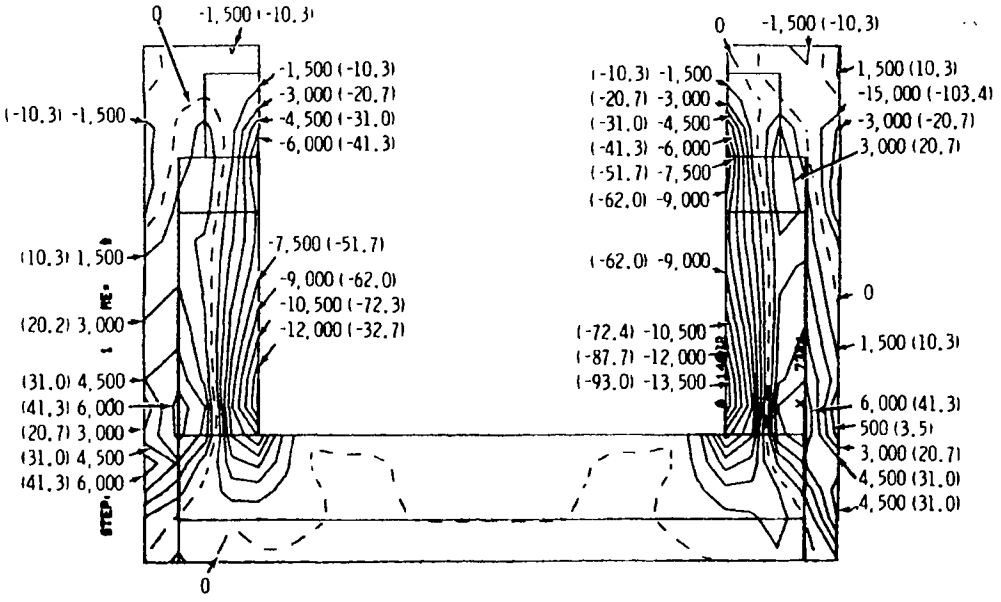

FIGURE 58. Vertical Stress Profiles for Cut #1 Idling

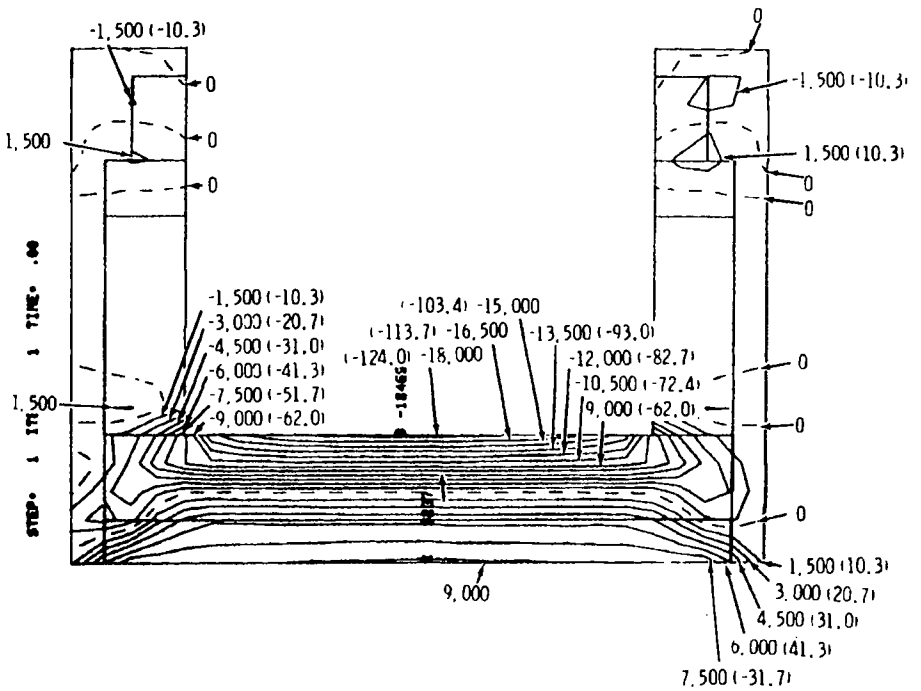

FIGURE 59. Horizontal Stress Profiles for Cut #1 Idling

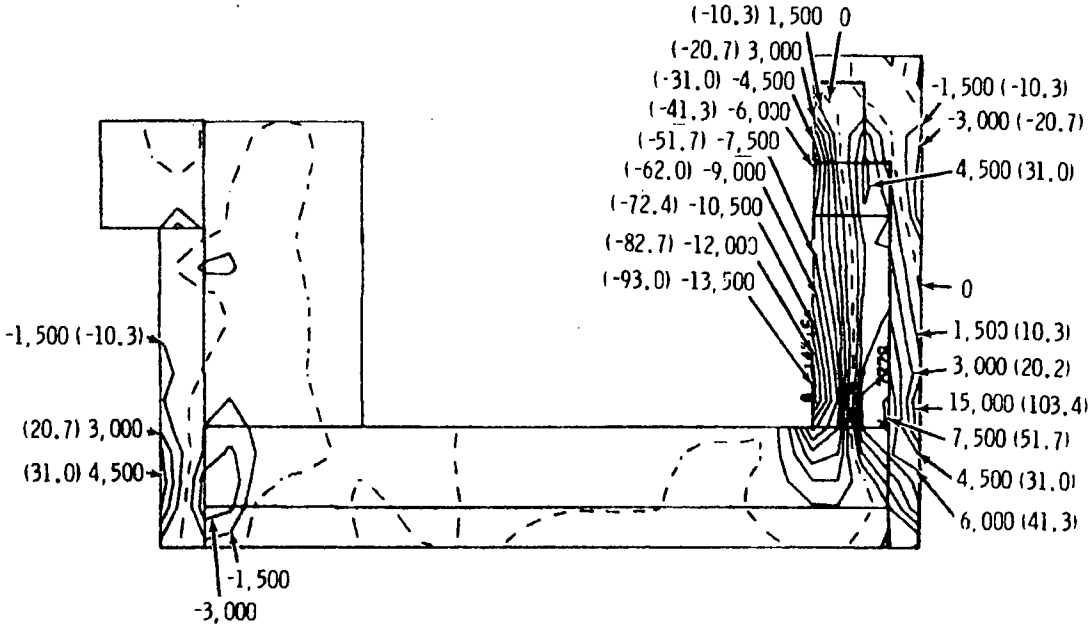

FIGURE 60. Vertical Stress Profiles for Cut #2 Idling

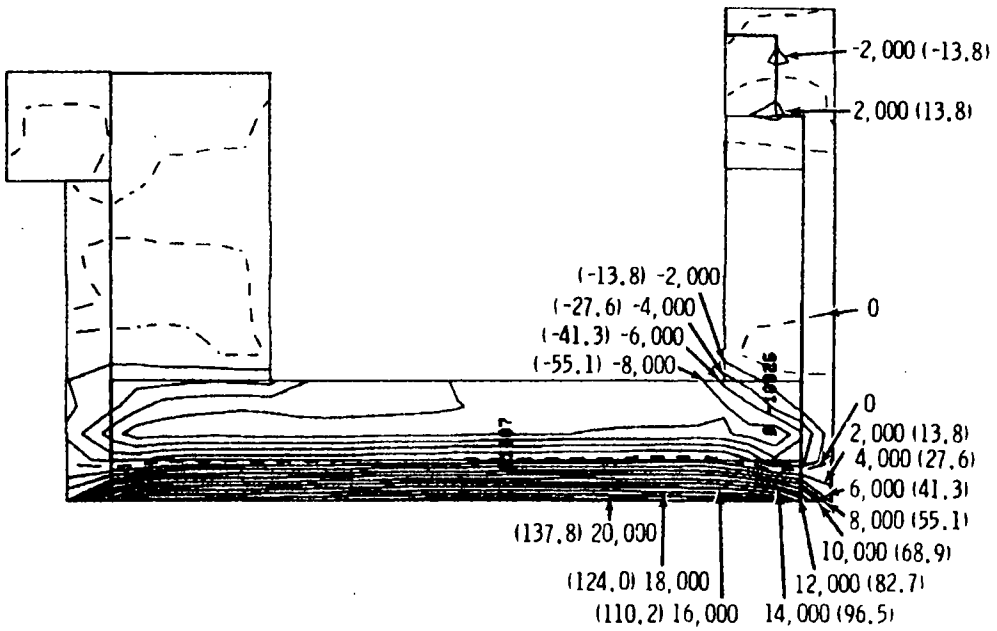

FIGURE 61. Horizontal Stress Profiles for Cut #2 Idling

the walls and floor are constrained from horizontal motion by the representation of the containment box in the model. Vertical growth is not restricted.

Several observations can be made from these predictions. Of special interest are the high compressive stresses at the inside surface of the refractory and the fairly high tensile stresses near the outside of the Monofrax K-3. These stresses are to be expected because of the restraint imposed upon the refractory by the steel jacket. The crushable fiberboard does not provide sufficient allowance at the top of the melter for the walls to freely expand. The compressive stresses predicted do not exceed the 138-MPa rupture strength of the Monofrax K-3, but the tensile stresses at the outer edge of the Monofrax K-3 are as high as 41 MPa. Although the tensile stress is relatively small, ceramic materials are notorious for failure under tension loads, and this stress level may be sufficient to nucleate cracks. The horizontal stress contours of Figure 60 are also relatively high. They are again compressive at the inside surface and tensile at the outside surface. This indicates that the center of the floor atempted to bow upwards but was constrained by the refractory walls.

The north wall of the second cut through the melter displays temperature and stress patterns similar to the first cut. Note, however, that the south wall has fairly low stress levels. The refractory is free to move upward in the model, relieving any thermal stresses in that direction. In the actual melter, the lid contacts the upper surface of this refractory. This interaction was neglected because of the difficulties in accurately modeling the force transmitted at the interface between lid and refractory block.

The effect of restraining the thermal expansion of the riser block on the refractory stress levels is graphically shown in Figure 62. The magnitude of the stresses predicted with this additional boundary condition are nearly twice the rupture strenth of Monofrax K-3 and reach 551 MPa in the Zirmul flooring. Neither of these two boundary conditions (total or no restraint from vertical expansion) are likely to represent the actual conditions present in a melter of the LFCM design. The actual stress level is probably a transient function

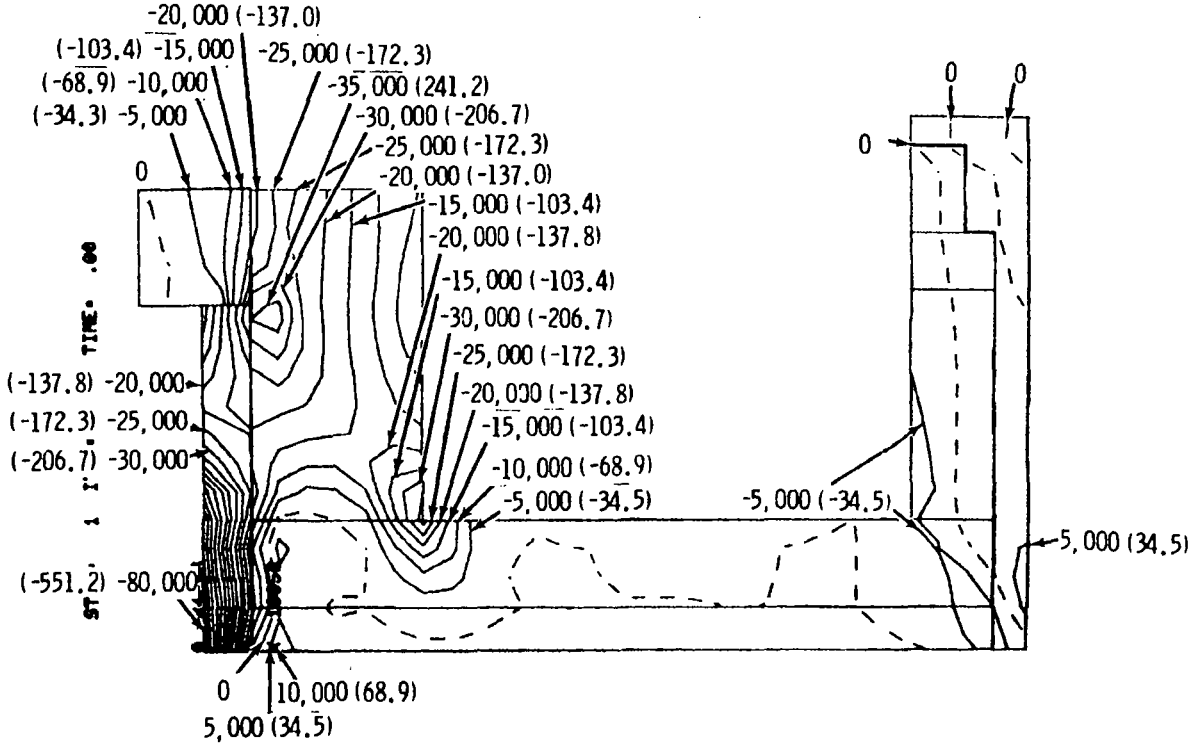

FIGURE 62. Vertical Stress Profiles for Cut #2 Idling with Upper Portion of Riser Block Constrained

of the lid and refractory temperatures. Clearly, the magnitude of the refractory stresses is directly related to the degree of restraint from free thermal expansion.

6.2.2 Steady-State Liquid-Feeding Mode

The liquid-feeding analysis was based on the temperature assumptions of 1200°C below 48 cm (nominal glass level) and 149°C above the 48-cm level. These temperature conditions are due to the presence of the cold cap on the glass surface and are the values assumed for earlier LFCM numerical modeling efforts (Hjelm and Donovan 1979). As in the idling simulations, the refractory walls are restrained from north-south expansion, but no vertical expansion constraint was included.

The effect of the change in temperature boundary conditions from the idling mode is readily apparent in Figures 63 through 65. The constant stress contours for this combination of conditions are plotted in Figures 66 through 71.

The thermal stress output by the model for the first two cuts are not significantly different from those in the idling mode. The thermal strains, however, are significantly different. These quantities, unfortunately, are not output by ANSYS, but a short analysis of the thermal strains during the transition to the liquid-feeding mode is presented in Section 6.2.3.

The vertical stress profile predicted in the analysis model for Cut #3 through the riser is of particular interest. The section of Monofrax K-3 that appears to be separated from the rest of the structure is actually tied to the melter through a series of trusses (see Figure 55). The rigidity of these trusses is related to the stiffness of the Monofrax K-3 that surrounds the riser channel. This is the best modeling technique to simulate the modeled melter geometry and stiffness with a two dimensional model. The high compressive stresses on the inside surface of both sides of the riser channel and the tensile stresses on the glass-contact surface of the riser block indicate that the inside portion of the riser block is attempting to bow toward the center of the melter at the top (to the right in Figure 70), but is restrained by the surrounding refractory. This stress pattern, assumably, is created because the surface of the riser is at glass temperature ($\sim$1200^{o}C), whereas all but the lower tip of the discontinuous refractory section is at 149^{o}C. This is another possible source of fracture in the inside surface of the Monofrax K-3.

6.2.3 Transition to Liquid-Feeding Mode

Performing a transient, finite-element analysis of a refractory model based on the LFCM design was not within the scope of this study. Analytical modeling of these effects requires an iterative solution for each of the elements and thus was prohibitively expensive. Along with the reduction of the surface refractory temperature, the major effect of the cold cap is the establishment the local heat flux from the refractory. This heat flux is a

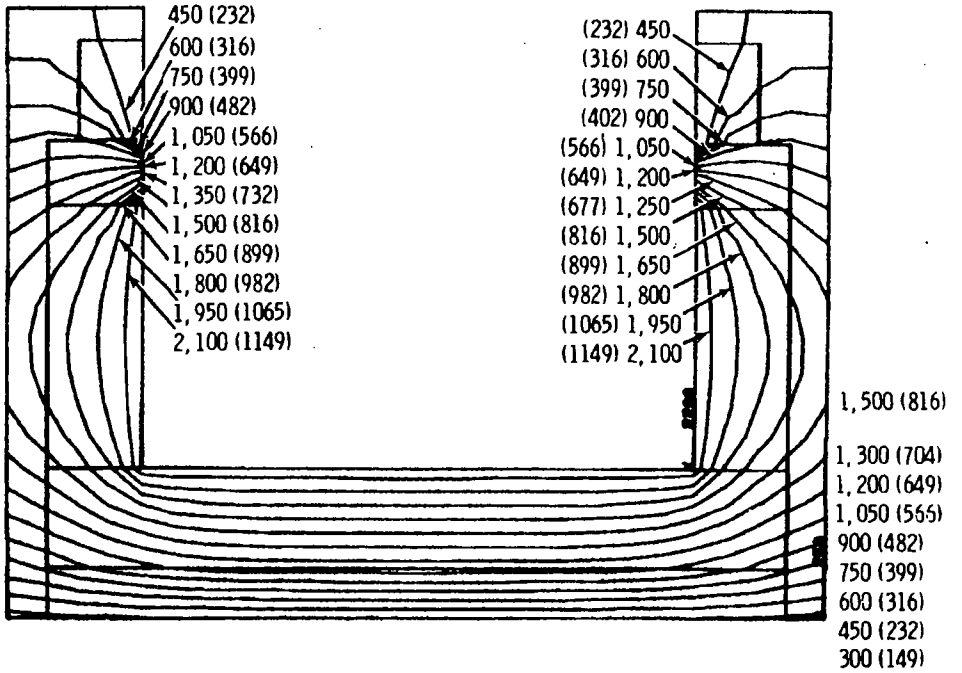

FIGURE 63. Temperature Profiles for Cut #1 Liquid Feed--^{o}F (^{o}C)

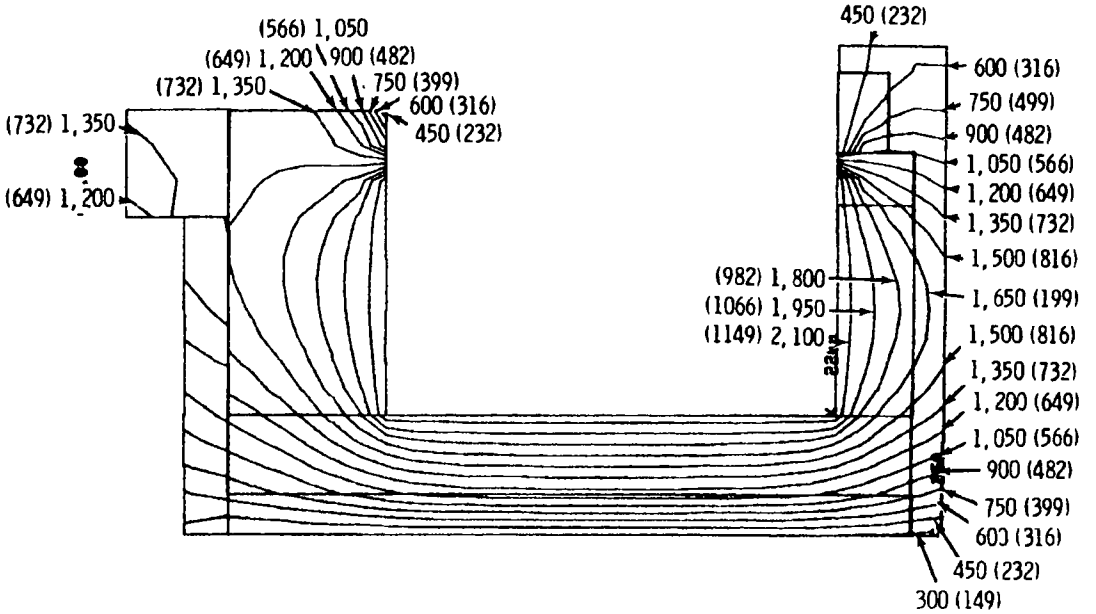

FIGURE 64. Temperature Profiles for Cut #2 Liquid Feed--^{o}F (^{o}C)

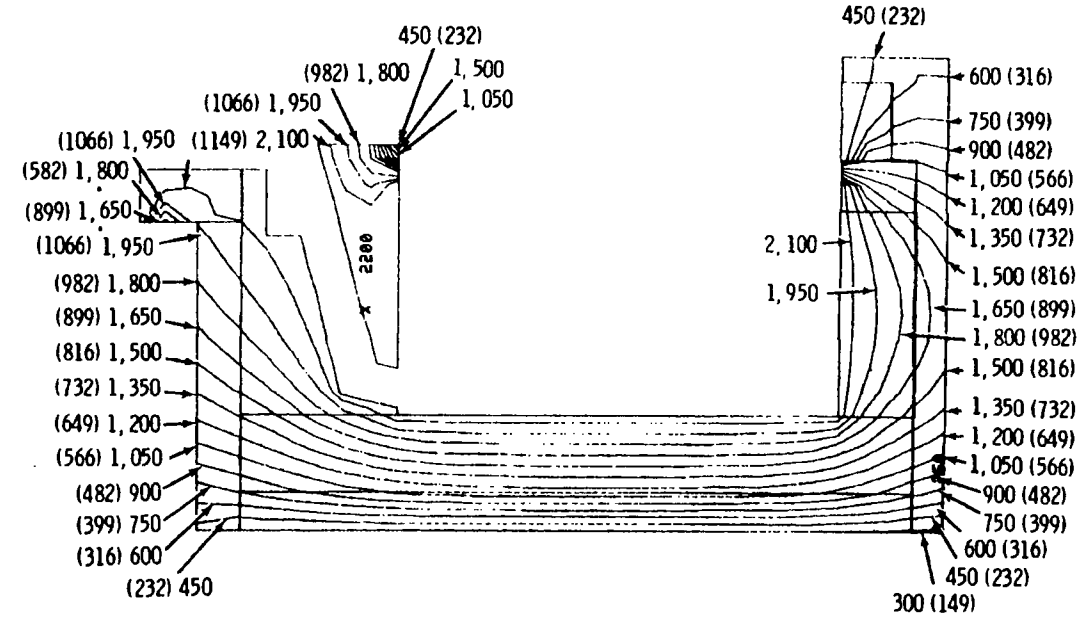

FIGURE 65. Temperature Profiles for Cut #3 Liquid Feed--^{o}F (^{o}C)

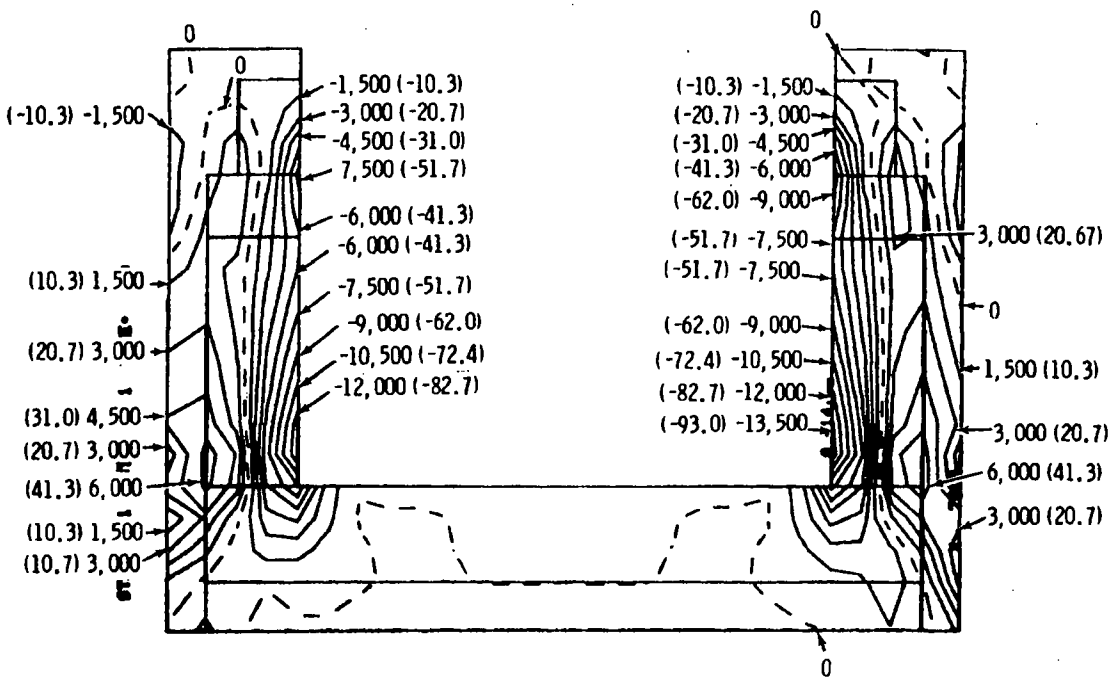

FIGURE 66. Vertical Stress Profiles for Cut #1 Liquid Feed

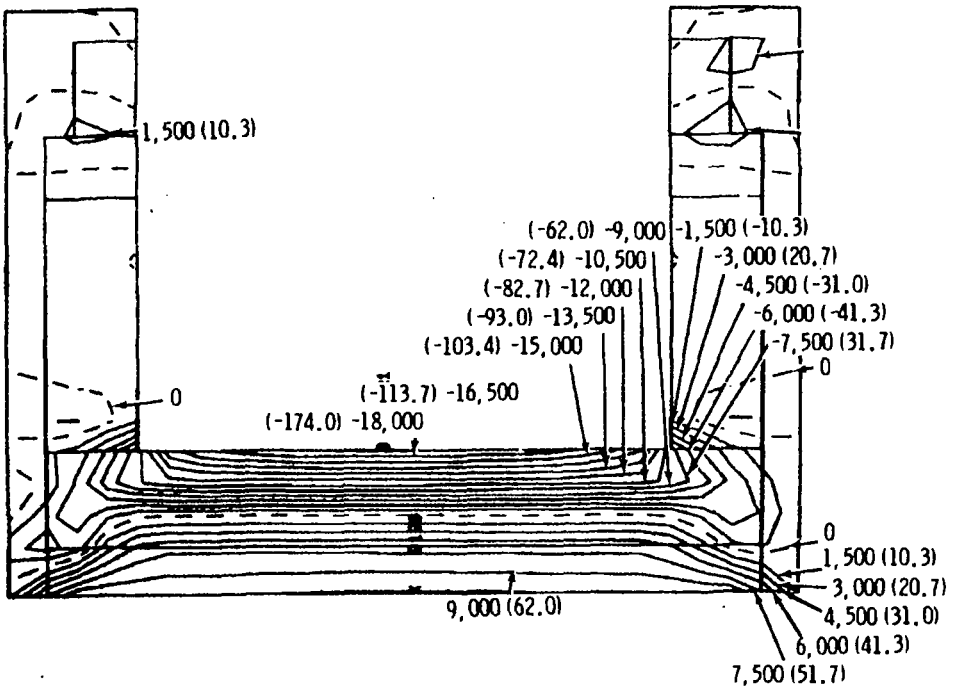

FIGURE 67. Horizontal Stress Profiles for Cut #1 Liquid Feed

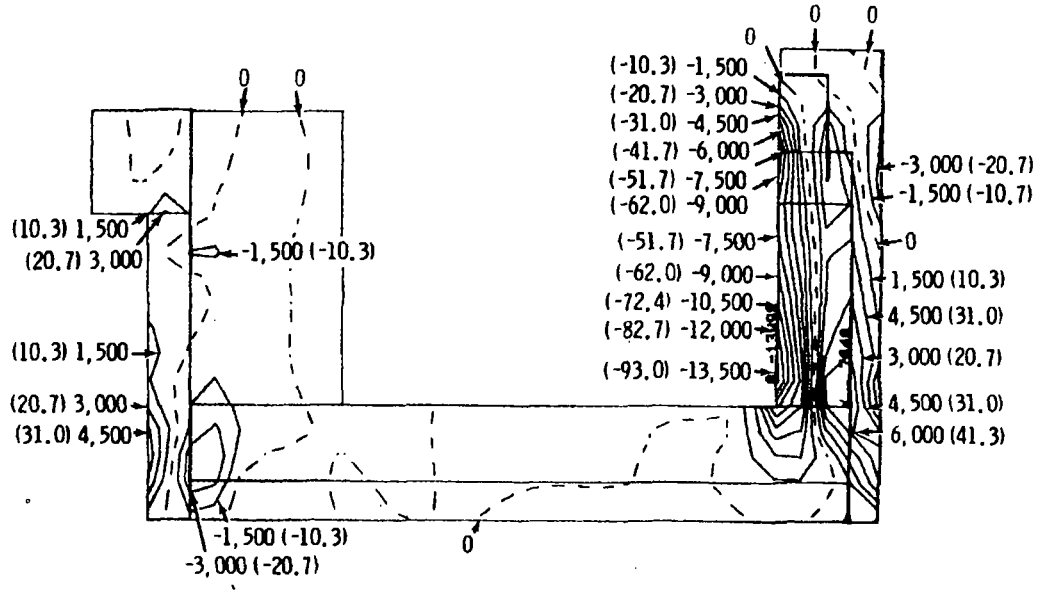

FIGURE 68. Vertical Stress Profiles for Cut #2 Liquid Feed

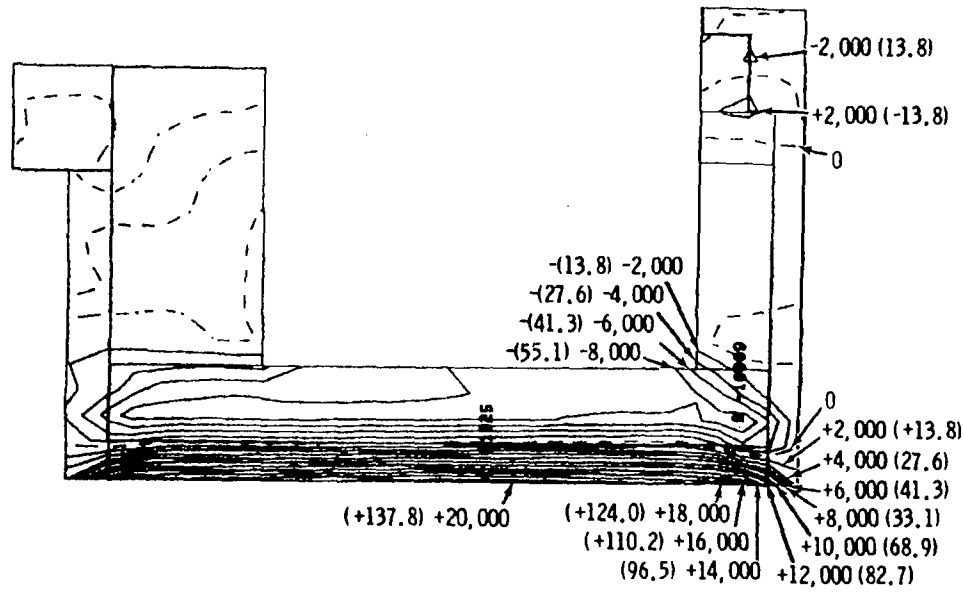

FIGURE 69. Horizontal Stress Profiles for Cut #2 Liquid Feed

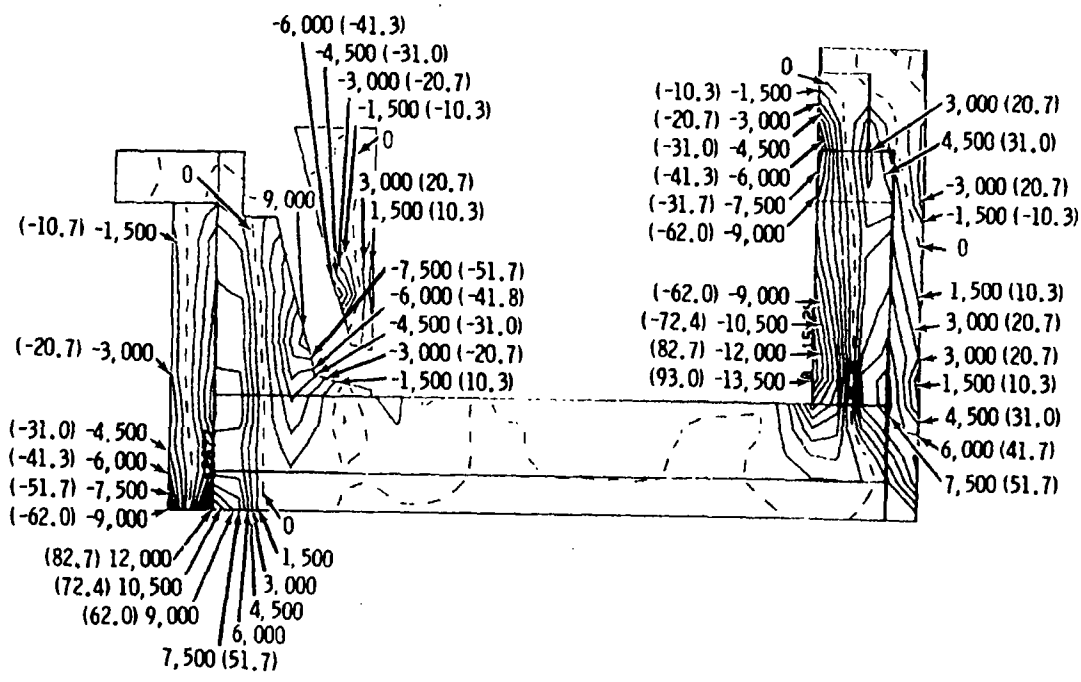

FIGURE 70. Vertical Stress Profiles for Cut #3 Liquid Feed

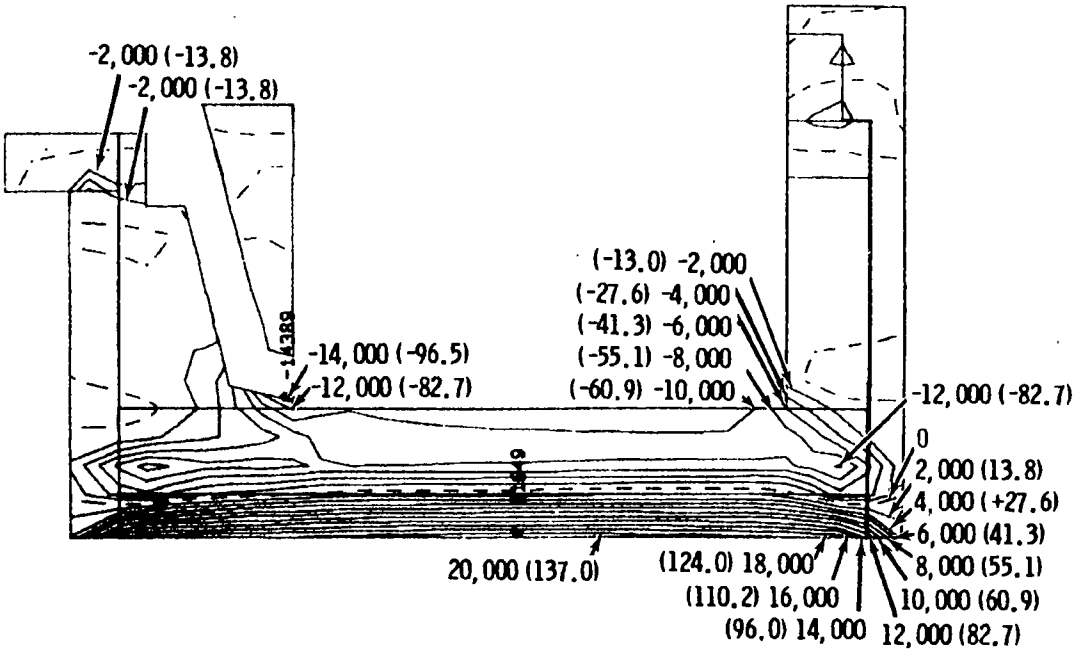

FIGURE 71. Horizontal Stress Profiles for Cut #3 Liquid Feed

function of the cold cap depth, the vaporation rate of the refactory surface, the refactory/cold cap thermal contact resistance, the cold cap thermal conductivity, and the porosity of the cold cap. Currently, these cold cap properties are not well defined. However, simplified calculations were performed to predict the probable upper limit of the transient thermal stress and strains.

When a hot material is cooled rapidly from its outside surface, the outside surface will attempt to shrink. The hot interior resists this shrinkage and surface tensile stresses are created, which can initiate cracks. For example, if a heated marble is plunged into ice water, cracks form at the surface of the marble as the surface shrinks against the hot interior. This effect is the most probable source of cracking in the Monofrax K-3 at the level of the cold cap.

Calculation of the surface tensile-stress upper limit is fairly straight forward. The maximum stress, caused by thermal loading of a member constrained from thermal expansion or contraction can be calculated by:

$$\sigma = E\ (\alpha)\ \Delta T$$

where

σ = thermal stress

α = thermal expansion coefficient

E = Young's modulus

ΔT = difference in temperature between the cool outside and hot inside of the refractory.

The thermal stress can be calculated using this equation if a temperature gradient into the refractory is assumed. In this case, the solution assumes an infinite solid initially at 1200°C and an instantaneously applied surface temperature boundary condition of 150°C. Using a one-dimensional, heat-transfer solution, the temperature gradient 5 cm into the refractory is calculated, as well as the thermal stress developed between the surface and this depth. The results are presented in Table 3.

The thermal stress calculations indicate that a sudden temperature change of as little as 115°C exceeds the rupture strength of the Monofrax K-3. This demonstrates the necessity of slow temperature changes within the refractory to prevent excessive thermal-shock tensile stresses.

Another calculation producing similar results is the thermal strain in the Monofrax K-3 created by changing temperatures. The thermal strain is calculated by:

$E = \alpha\ (\Delta T)$ (E = thermal strain)

$= (7.92\ cm/^{o}C)\ \ (1056^{o}C)$

$= 0.84\%$ strain

In contrast, the strain induced in a ceramic at failure in a standard compression test is defined as:

$$E\ (\text{at failure}) = \frac{\text{ultimate stress}}{E} \qquad E = \text{Young's modulus}$$

$= 0.1\%$ strain

TABLE 3. Temperatures and Upper Bound Thermal Stresses at Varying Times at a 5 cm Depth into the Refractory

t (minutes)	T (^{o}C)	(MPa)
0	1204	1152
0.25	1089	1026
0.5	1029	960
0.75	970	896
1	914	836
5	263	146
10	159	11

This quantity is significantly smaller than the strain the refractory undergoes in the transition from idling to liquid feeding. This does not mean that heating or cooling the ceramic will cause it to fail. A rapid change in temperature will, however, cause a rapid strain rate. Ceramic materials are inherently susceptible to fracture at high strain rates. Thus, the high strain rate in the transition from idling to liquid feeding is the probable source of the fractures and perhaps of the spalling of the Monofrax K-3 seen in the LFCM when it was disassembled.

6.3 MELTER LID

Cracks were discovered in each of the four corners of the melter lid following removal from the LFCM. The positions of these cracks are shown in Figure 72. The lid was fabricated from 0.5 cm Inconel 601 plate with 2.5-cm by 5-cm-type 304L stainless steel stiffeners welded to the exterior to increase the materials resistance to bending moments. These stiffeners (strongbacks) run along all four sides of the vertical box portion of the lid and extend to the edges of the lid. The long-side strongbacks are continuous bars, but the shorter side strongbacks are welded to the long stifteners in sections. It is at these welds that the melter lid developed cracks.

The failures were the result of diffential thermal expansion and excessive thermal stresses in the stiffening members. Because the melter lid was

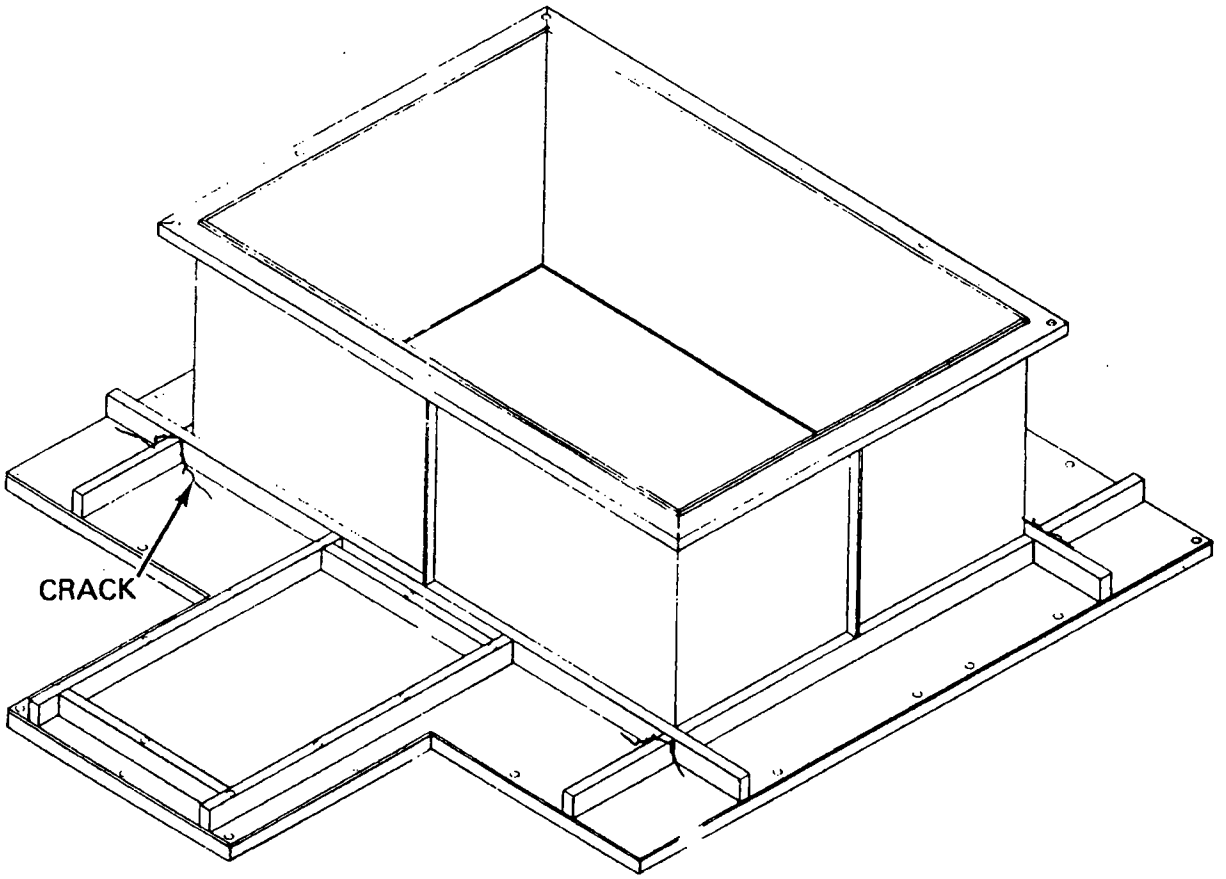

FIGURE 72. Melter Lid Indicating Position of Strongback Weld Cracks

externally insulated, the lid temperature would approach the glass temperature during idling conditions. Assuming that the stainless steel strongback is at approximately the same temperature as the Inconel plate, the total length change required in the short-side strongback for it to be stress-free can be calculated as follows:

$$\Delta L = L\alpha\Delta T$$
$$= 0.72 \text{ in.}$$

where

ΔL = length change due to temperature increase

L = length of heated portion of strongback = 91.4 cm

α = thermal expansion coefficient of 304 stainless = 18×10^{-6}/cm/cm^{o}C

T = temperature change from room temperature to 1094^{o}C.

The strongback obviously cannot freely expand as it is constrained by the Inconel vertical plate (which has a lower expansion coefficient), and by the outside walls of the melter. These walls are held at a much lower temperature than the lid by the water-cooling jackets. Compressive stresses will, therefore, develop in the strongbacks during idling periods. Assuming that 75% of the thermal expansion can be accommodated by the structure, the magnitude of the compression stress in the strongback can be estimated as follows:

$$\sigma = E \alpha T$$
$$\cong 1034 \text{ MPa}$$

The magnitude of this compressive stress indicates that some active plastic flow must occur in the strongback. As metals are heated, they tend to be able to accommodate more of this type of plasticity and also to creep rapidly. Essentially, this strongback will deform plastically and creep to relieve the compression stress. When the melter is placed in the liquid-fed mode and a cold cap develops, the lid cools to roughly 150^{o}C. The strongback will tend to contract as it has already relieved the high compression stresses by creep and deformation. Therefore, tensile stresses will be developed in the strongback of the same order of magnitude as the original compressive stresses. These tensile stresses will produce the weld failures observed in the short-side strongback.

As Inconel 601 has a lower thermal expansion coefficient than type 304L stainless steel, welds between these materials will result in a similar situation as the strongback problem just discussed. During heating to idling temperature, the Inconel will expand less than the stainless steel and will develop tensile stresses (or compression stresses in the steel). The load transfer between the Inconel plate and the stainless steel must occur at the weld joint along the strongback. As such, this weld joint is also suspect and could fail in a melter lid.

The gross deformation and warping of the lid was due to thermal, plastic, and high-temperature creep-related deformations and residual stresses, as discussed above.